SPACE STATION TRACKING REQUIREMENTS FEASIBILITY STUDY

Final Report
Volume II

Contract No. NAS9–17414

Prepared for

NASA Lyndon B. Johnson Space Center
Houston, TX 77058

Technical Monitor: Sid Novosad

Prepared by

Sergei Udalov
James Dodds

Contributions by

Dr. Gaylord K. Huth
Dr. K. T. Woo
Dr. Robert Scholtz
Dr. Unjeng Cheng
Richard Austin

Axiomatix
9841 Airport Boulevard
Suite 1130
Los Angeles, CA 90045

Axiomatix Report No. R8807-3
July 27, 1988

TABLE OF CONTENTS

VOLUME II

APPENDIX K	Design Considerations for Links between Shuttler Orbiter and Space Station
APPENDIX L	Shuttle Ku-Band Radar Interference to Space Station Links
APPENDIX M	Preliminary Considerations for Antenna Switching, Power Control, and AGC Functions for Space Station Multiple Access System
APPENDIX N	Power Control for Space Station Multiple Access System
APPENDIX O	Design Considerations for a Universal Multi-Channel Modem for Space Station Ku-Band Links
APPENDIX P	Coding for the Space Station Information System
APPENDIX Q	SSIS Header Code
APPENDIX R	SSIS SM Codes
APPENDIX S	A Critique of the Schilling-Manela Codes
APPENDIX T	Wanderer Tracker Performance Goals
APPENDIX U	Simulation Models for Optical Communication Systems Analysis

APPENDIX K

DESIGN CONDERATIONS FOR LINKS BETWEEN SHUTTLE ORBITER AND SPACE STATION

DESIGN CONSIDERATIONS FOR LINKS BETWEEN SHUTTLE ORBITER AND SPACE STATION

Contract No. NAS9-17414

Interim Report

Prepared for

NASA Lyndon B. Johnson Space Center
Houston, TX 77058

Prepared by

Sergei Udalov

Axiomatix
9841 Airport Boulevard
Suite 912
Los Angeles, CA 90045

Axiomatix Report No. R8607-3
July 22, 1986

Table of Contents

	Page
List of Figures	i
List of Tables	ii
1.0 Introduction and Summary	1
2.0 Requirements	4
3.0 Implementation Possibility and Trade-offs	6
3.1 Shuttle Orbiter/Space Station Link	6
3.1.1 Shuttle Orbiter/Space Station Link at S-Band	6
3.1.1.1 Possible Implementation at S-Band	6
3.1.1.2 Link Budget for SO/SS at S-Band	11
3.1.2 Shuttle Orbiter/Space Station Link at Ku-Band	14
3.1.2.1 Implementation Consideration	14
3.1.2.2 Link Budget for SO/SS Link at Ku-Band	16
3.1.3 Hybrid S-Band/Ku-Band Implementation	16
4.0 Discussion of Trade-offs	21
5.0 References	24

List of Figures

		Page
Figure 3-1	Orbiter/Space Station Link at S-Band	7
Figure 3-2	Functional Diagram for Orbiter Equipment for Implementing Orbiter/Space Station Link at S-Band	8
Figure 3-3	Modification of CIE to Multiplex Command Voice on Forward Link	10
Figure 3-4	Orbiter/Space Station Link at Ku-Band	15
Figure 3-5	Orbiter/Space Station Links at S-Band and Ku-Band	19

List of Tables

		Page
Table 1-1	Link Margin Summary for Shuttle Orbiter/Space Station S-Band and Ku-Band Link at 37 km	2
Table 2-1	Requirement for Orbiter/Space Station RF Links (Reference 1)	5
Table 3-1	S-Band Link, Shuttle Orbiter to Space Station	12
Table 3-2	S-Band Link, Space Station to Shuttle Orbiter	13
Table 3-3	Shuttle Orbiter/Space Station Link at Ku-Band for Command and Voice	17
Table 3-4	Space Station/Shuttle Orbiter Link at Ku-Band for Telemetry and Voice	18

1.0 INTRODUCTION AND SUMMARY

This report considers possible implementations of the RF links for command, telemetry, and voice communication between the Shuttle Orbiter (SO) and the Space Station (SS). For these links, there are three implementable and realistic candidates. These are:

1) All S-band link
2) All Ku-band link

and

3) Hydrid S-band/Ku-band Link

Another possibility would involve the use of UHF for voice communication, but this approach was not considered here because of potential frequency utilization problem.

Table 1-1 shows link margin summary for Shuttle/Orbiter RF link implementations at either S-band or Ku-band.* The table indicates that the Ku-band implementation has significantly higher margins than the S-band implementation. This is due primarily to the use of high gain (24 dB) antennas on the Space Station end of the link.

The advantage of larger antenna appertures provided by S-band is offset by the fact that only 0 dB antenna gain is assumed at the Space Station end for the S-band operation. This assumption is very conservative and it results rather low margins for the S-band link which carries the telemetry and voice from the Space Station to the Orbiter. If the Space Station antenna gain at S-band is increased to 3 dB, then the margins improve accordingly. At this point, we do not see any reasons why such antenna gain increase could not be acceptable if the decision is made to operate at S-band.

The unique feature of the S-band implementation considered in this report is technique for transmitting two-way 16 kbps delta-modulation voice between the Shuttle and the Space Station at the maximum range of 37 km. This approach, as proposed by Axiomatix, uses the existing standard subcarriers for communicating digital voice. For the

*Hybrid use of S- and Ku-bands would involve same link margins, therefore, no listing is given for a "hybrid" approach.

Link	Band	Signal Transmitted	Origin	Destination	Rate	EIRP (dBm)	Link Margin (dB)	Comments
Shuttle Orbiter (SO) to Space Station (SS)	S	CMD	SO	SS	2 kbps	30.7	7.9	PI Link
		VOICE			16 kbps		7.8	PI Link
	Ku	CMD			2 kbps	28	16.4	Ku-band MA Link
		VOICE			16 kbps		16.4	Ku-band MA Link
Space Station (SS) to Shuttle Oribter(SO)	S	TLM	SS	SO	16 kbps	33	3.4	PI/Transponder link
		VOICE			16 kbps		2.5	PI/Transponder link
	Ku	TLM			16 kbps	52.4	13.9	Ku-band MA Link
		VOICE			16 kbps		13.9	Ku-band MA Link

Table 1-1. Link Margin Summary for Shuttle Orbiter/Space Station S-Band and Ku-Band Link at 37 Km

Shuttle/Space Station link, the subcarriers in the range from 65 KHz to 95 KHz are considered as possible candidates. These subcarriers are typical of CIE and/or CIU equipment and are readily handled by the payload interrogator (PI). For the Space Station/Shuttle link, the standard 1.7 MHz subcarrier can be used for digital (16 kbps) voice. Consequently, by modulating the appropriate subcarriers at both ends of the S-band link a viable method for a two-way voice communication can be provided.

From the S-band and Ku-band link budgets considered, it appears that either implementation alone or the combination of the two can meet the requirements for the Shuttle Orbiter/Space Station link. Furthermore, as described in this report, there appears to be a possibility of adapting some of the existing S-band payload link equipment for providing two-way voice capability to the link. This capability will permit the Orbiter to satisfy the voice link requirements without actually using the Ku-band MA system.

From the standpoint of the Orbiter, this appears to be relatively low cost solution, requiring only minor baseband modifications to CIE or similar equipment and the corresponding transponder. Neither RF nor any antenna modifications will be required. However, remaining at S-band beyond the IOC capability will impose dual-band (S- and Ku-bands) operation requirement on the Space Station. The impact of the latter requirement remains to be addressed.

The reference made above to the CIE is not to the actual CIE which is a part of DOD's SGLS network. What is meant here is simply an equipment which is "CIE-like" in design, i.e., it has more than one subcarrier on the link to the payload. In fact, it could possible be a modified PSP. Whatever equipment it may be, the main requirement is that the 16 kbps digital voice can be "patched in" into it at the Orbiter and also be recovered and separated from telemetry for on-board use. Commands, however, could originate either on the ground or on-board.

2.0 REQUIREMENTS

Table 2-1 shows the requirements for the Orbiter/Space Station links as defined in Reference [1]. The requirements listed in this table can be interpreted to mean that (1) the commands and telemetry link can be satisfied by the present S-band Orbiter capability and (2) the two-way voice capability will be added when the Shuttle Orbiter EVA communication system is upgraded to be compatible with Space Station's multiple-access (MA) system. The table can be also interpreted that the S-band and Ku-band communication links can be used simultaneously to satisfy both the commands/telemetry and the voice link requirements.

As explained in the subsequent sections of this report, however, there is a possibility to implement the addition of voice capability at S-band with minor modifications of the existing Orbiter's S-band equipment. Specifically, Axiomatix has come up with techniques for such an S-band implementation which will provide simultaneous transmission of commands and voice on the Orbiter/Space Station link and telemetry and voice on the Space Station/Orbiter link.

The advantage of this approach is that it provides the voice capability for the Oribter/Space Station link during the early stages of Space Station operations. In principle, this S-band capability could be retained indefinitely without ultimately converting to Ku-band MA operation. But, the continuing utilization of S-band will necessitate additional equipment and antennas on the Space Station. Thus, the current thinking among Phase B contractors is to satisfy most of the space-to-space link requirements with the Ku-band MA system including the Orbiter/Space Station link. If such an approach is adopted, then the Orbiter/Space Station and the Space Station/Orbiter link can be implemented with the Ku-band MA link. This will eliminate the requirements for separate commands and telemetry link at S-band.

Frequency Band		Capability		Data Rate (Max)		Number of Simult. Vehicles	Max Range Km (nm)	Comments
Xmt*	Rcv*	Xmt*	Rcv*	Xmt*	Rcv*			
S	S	TLM	CMD	16 kbps	2 kbps	1	37 (20)	See Note 1
Ku	Ku	VOICE	VOICE	16 kbps	16 kbps	1	37 (20)	See Note 2

*Referenced to Space Station

Note 1: Orbiter compatible Link

Note 2: Upgraded Orbiter EVA Link

Table 2-1. Requirement for Orbiter/Space Station RF Links (Reference 1)

3.0 IMPLEMENTATION POSSIBILITY AND TRADE-OFFS

3.1 Shuttle Orbiter/Space Station Link

For this link there are following three (3) possible realizations:

(1) All S-band link

(2) All K-band link

and

(3) Hybrid S-band/K-band link.

The pros and cons of each of these implementations are discussed below.

3.1.1 Shuttle Orbiter/Space Station Link at S-Band

3.1.1.1 *Possible Implementation at S-Band*

Figure 3-1 shows functionally an all S-band implementation of Shuttle/Space Station link. The important feature of the implementation shown is that the CIE (Communication Inferface Equipment) may be used as an interface between the baseband signals and the PI at the Orbiter end of the link. The CIE equipment was developed by Rockwell for use with DOD payloads, but it has certain features which make it suitable, with some modifications, for this link.*

Specifically, the existence of more than one subcarrier on the forward and return links provide for transmission of both commands and voice on the forward link and reception of telemetry and voice on the return link.

The return link implementation is based on the availability of two simultaneous subcarries, i.e., 1,024 MHz and 1.7 MHz which can be phase-shift-keyed (PSK) at the Space Station transponder (Xponder) with telemetry (16 kbps) and digital voice (16 kbps), respectively.

The payload interrogation (PI) can demodulate these subcarries and the data streams can subsequently be recovered by CIE. Figure 3-2 shows the functional diagram

*Here we do not imply the actual CIE equipment as part of SGLS network. What we mean here is simply an equipment which is based on CIE design with modification.

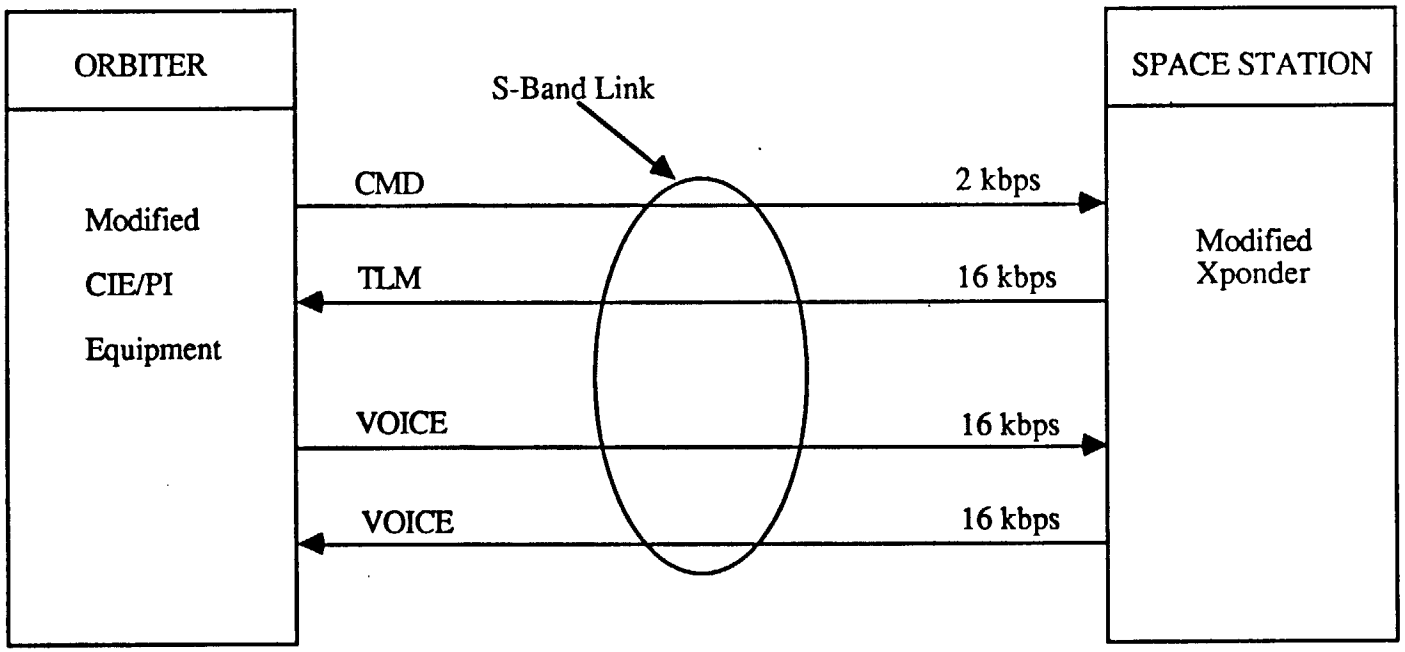

Figure 3-1. Orbiter/Space Station Link at S-Band

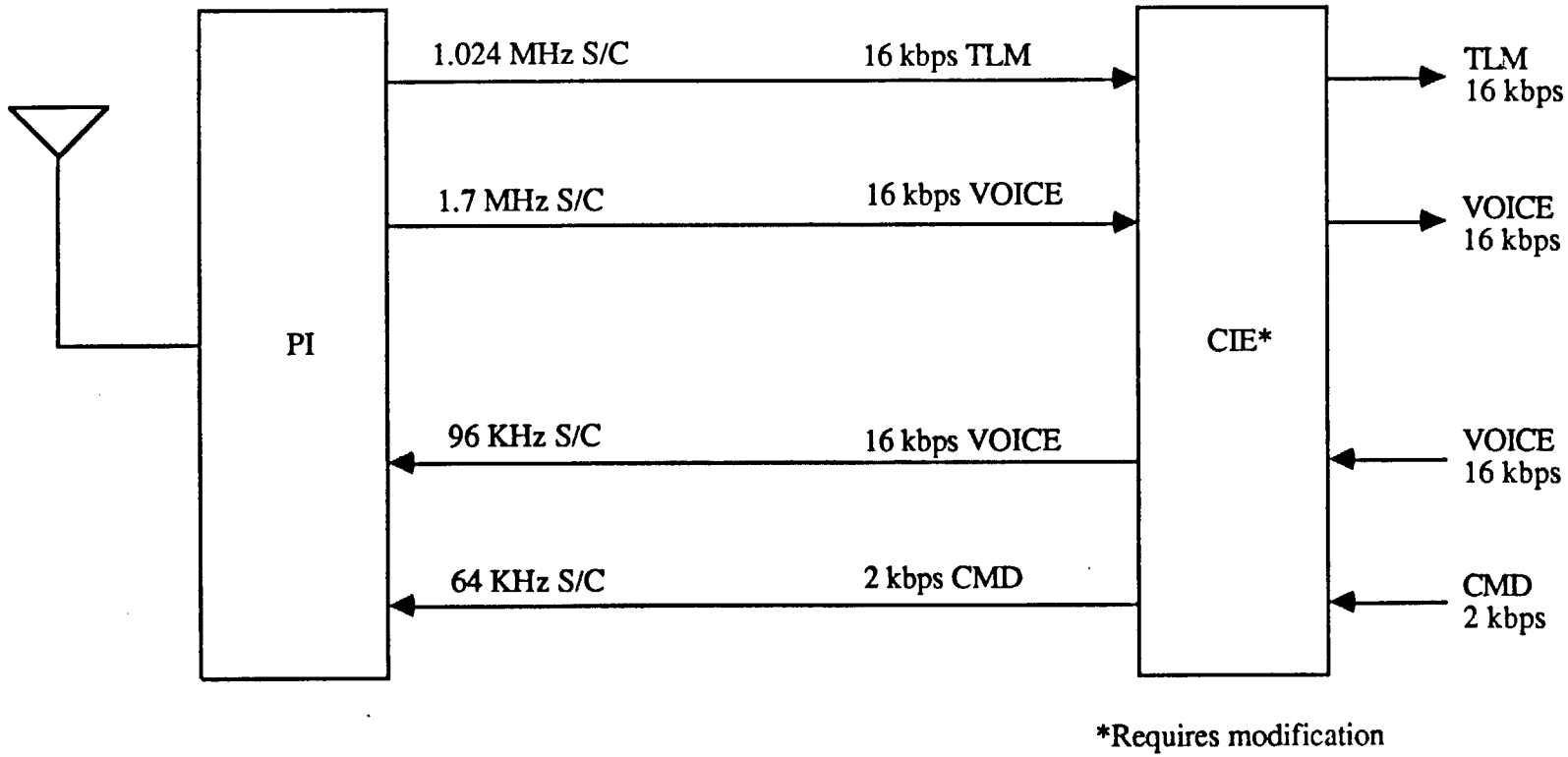

Figure 3-2. Functional Diagram for Orbiter Equipment for Implementing Orbiter/Space Station Link at S-Band

of this implementation. It is important to note that the return link does not require considerable CIE modification because the CIE already has the features which permit such operation.

The forward link, however, requires modification of the frequency-shift keying (FSK) scheme used for DOD payloads. Specifically, three tones ,i.e., 65 KHz, 76 KHz and 95 KHz are used to transmit symbol rates up to 2000 symbols/second. The low symbol rate of the current system is not a limitation of PI modulation capability. This is because the PI modulator on the forward link responds primarily to the tone frequency and only in a second order fashion to the tone's fine modulation structure. Consequently, several methods for transmitting both 2 kbps command and 16 kbps voice are available. Figure 3-3 shows the modification for the CIE which will provide this simultaneous capability. Part (a) of Figure 3-3 shows the frequency division multiplexing implementation (FDM) of command (CMD) and voice data for input to the payload interrogator (PI). As shown in the figure, the two tones, i.e., 65 KHz and 95 KHz, have been replaced by two subcarriers at 64 KHz and 96 KHz, respectively. These subcarriers are bi-phase modulated with the respective binary data streams 2 kbps (CMD) and 16 kbps (VOICE).

The reason for changing each of the S/C frequencies by 1 KHz (95 KHz to 96 KHz and 65 KHz to 94 KHz) is to place the CMD subcarrier in the null of modulation spectra of the 94 KHz subcarrier. To further prevent the frequency interaction between the two S/C modulation streams bandpass/ filters (BPF) may be required for each modulated subcarrier prior to summing. The detailed requirements for these filters have to be determined in the future if this approach is adopted.

Another method of implementing combined transmission of commands and voice is shown in part (b) of Figure 3-3. In this approach straight forward time-division multiplexing can be used. The maximum combinded data rate will be 18 kbps, plus some overhead to accommodate frame synchronization. This combined data stream is then bi-phase modulated on a 96 KHz subcarrier and delivered to PI.

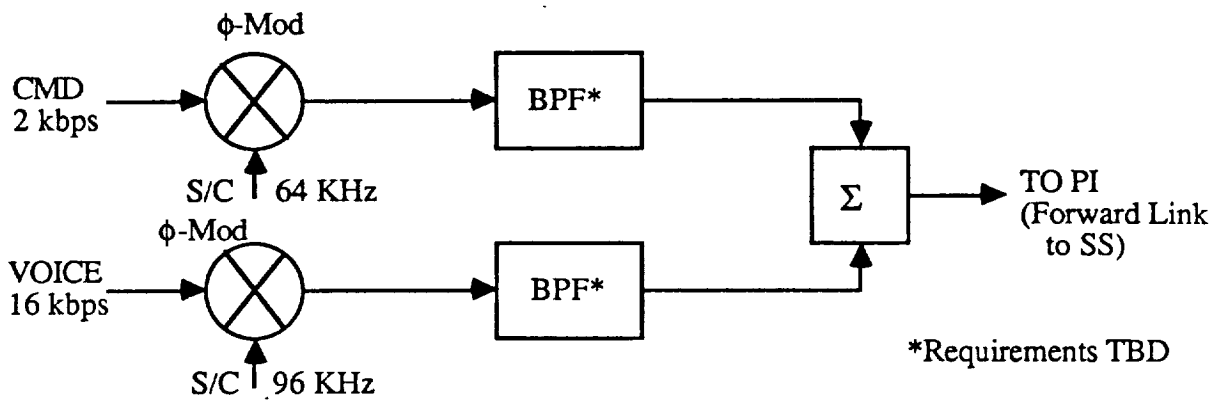

(a) Frequency Division Multiplexing Implementation of CMD and VOICE Data for Forward Link

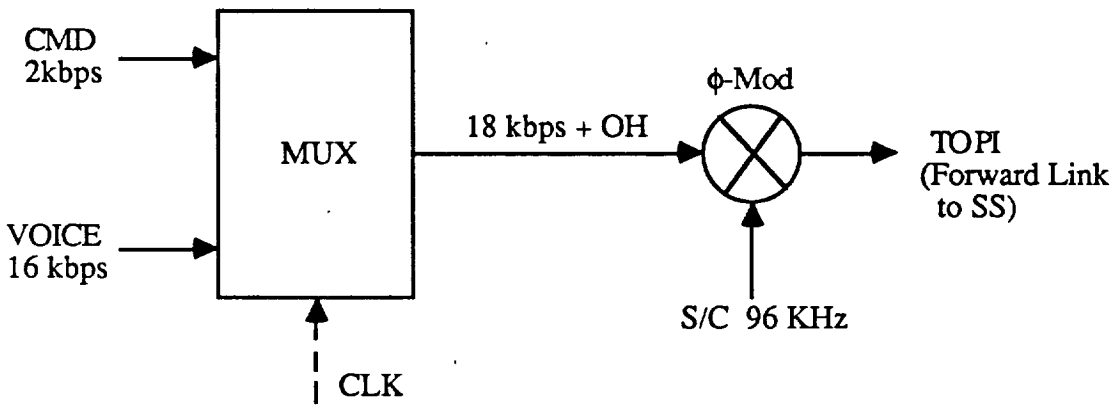

(b) Time Division MUX of CMD and VOICE on a Bi-Phase Modulated S/C

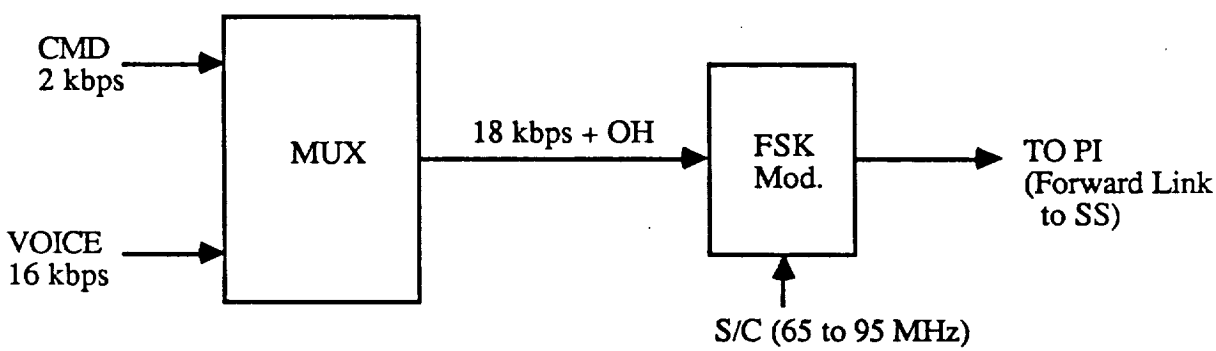

(c) Time Division MUX of CMD and VOICE on an FSK S/C

Figure 3-3. Modification of CIE to Multiplex Command Voice on Forward Link

The advantage of the TDM is that it conserves baseband spectrum. On the other hand, it requires multiplexing/demultiplexing equipment.

Part (c) of Figure 3-3 shows another implementation of TDM, this time with a frequency-shift keyed (FSK) modulator. The detailed trade-offs of PSK versus FSK modulation are not critical at this point in time. Both approaches, i.e., PSK and FSK, are discussed here for the purpose of demonstrating the alternatives available.

Moderate modifications of CIE may be required to implement either one of the schemes shown in Figure 3-3. However, these modifications are only at baseband and should affect the RF portions of the PI. Neither will they affect the antenna system.

Baseband modifications of the transponder* are also required in order to work with the modified Orbiter equipments. Again, these modifications are not considered severe, compared to modifications which would be required if RF modification were found necessary.

3.1.1.2 *Link Budget for SO/SS Link at S-Band*

To get a better quantitative idea of the performance of an S-band communication between the Orbiter and the Space Station baseline link budgets have been derived. These are shown in Tables 3-1 and 3-2.

The Shuttle Orbiter to Space Station budget is shown in Table 3-1. For this budget it is assumed that PI/CIE equiment is used such as shown in Figure 3-2. It is also assumed that a linear phase modulation of PI carrier is implemented such as shown in (a) of Figure 3-3.

In one of the versions of the link budget, approximately equal modulation indexes are assumed for the command subcarrier (β_1 = 1.1 radian) and the voice subcarrier (β_2 = 1.0 radian). With such a power division, however, the command channel carries

*Here we imply either a modified network transponder or a transponder similar to those used by the payloads.

	CMD 2 kbps $\beta_1 = 1.1$ rad	VOICE 16 kbps $\beta_2 = 0.5$ rad	CMD 2 kbps $\beta_1 = 0.5$ rad	VOICE 16 kbps $\beta_2 = 1.2$ rad	COMMENTS
Transmitter power (dBm)	37		37		5 w
Transmit circuit loss (dB)	–8.1		–8.1		
Transmit antenna gain (dB)	2.5		2.5		
Transmit pointing loss (dB)	–1		–1		
EIRP (dBm)	30.4		30.4		
Path Loss (dB)	–130.4		–130.4		D = 37 km F = 2.125 GHz
Received antenna gain (dB)	0		0		
Received pointing loss (dB)	–1		–1		
Polarization loss (dB)	–0.3		–0.3		
Received circuit loss (dB)	–3		–3		
Received signal power (dBm)	–104.3		–104.3		
System noise density (dBm/Hz)	–170		–170		NF = 4 dB for SS
Carrier to noise density (dB-Hz)	65.7		65.7		
Modulation loss (dB)	–6.1	–7.0	–13.2	–4.3	
Data rate (dB-Hz)	33(a)	42(b)	33(a)	42(b)	
Receive E_b/N_0 (dB)	26.6	16.7	19.5	19.4	
Theoretical E_b/N_0 (dB)	9.6	9.6	9.6	9.6	
Implementation loss (dB)	2	2	2	2	
Required E_b/N_0 (dB)	11.6	11.6	11.6	11.6	
Link Margin (dB)	15.0	5.1	7.9	7.8	

(a) = 2 kbps CMDS
(b) = 16 kbps VOICE

Table 3-1. S-Band Link, Shuttle Orbiter to Space Station

	TLM 16 kbps	VOICE 16 kbps	TLM ONLY 16 kbps	COMMENTS
Transmitter power (dBm)	37		37	5w
Transmit circuit loss (dB)	–3		–3	
Transmit antenna gain (dB)	0		0	
Transmit pointing loss (dB)	-1		–3*	
EIRP (dBm)	33		31	
Path Loss (dB)	-131		–131	D = 37 km, F = 2.29 GHz
Received antenna gain (dB)	2.5		2.5	
Received pointing loss (dB)	–1		–3	
Polarization loss (dB)	–0.3		–0.3	Rockwell Value
Received circuit loss (dB)	–8.1		–8.1	
Received signal power (dBm)	–104.9		–108.9	Rockwell Value NF = 6 dB
System noise density (dBm/Hz)	–168		–168	
Carrier to noise density (dB-Hz)	63.1		59.1	β_1 =1.1rads, β_2 =1.0rad, TLM only β_1 =1.1 rads
Modulation loss (dB)	–6.1	–7.0	–3.4*	
Data rate (dB-Hz)	42	42	42	
Receive E_b/N_0 (dB)	15.0	14.1	13.7	
Theoretical E_b/N_0 (dB)	9.6	9.6	9.6	
Implementation loss (dB)	2	2	2	
Required E_b/N_0 (dB)	11.6	11.6	11.6	
Link Margin (dB)	3.4	2.5	2.1	

*Voice Subcarrier Modulation is removed to allow for more TLM power when receive and transmit pointing losses increase from 1 to 3 dB.

Table 3-2 S-band Link, Space Station to Shuttle Orbiter

about 10 dB more margin than the voice channel, although both channels show adequate margins.

To provide for more even distribution of link margins, the modulation indexes can be readjusted as shown in Table 3-1. With such power division link margins are about 8 dB for both channels. With such margins a total pointing loss can increase by as much as 6 dB with the links still being operational.

Table 3-2 shows the Space Station to Shuttle Orbiter link budget. From the table, it is evident that this link has much less margin than the forward link. This is due to the fact the data rate is 16 kbps on both links. Because of the relatively low margins, a total increase of 3dB in pointing loss may "wipe out" the voice link. Thus, a budget for a contingency operation link with telemetry only going from Space Station to Orbiter is shown.

The consideration of such a contingency depends on the performance of the S-band antennas at the Space Station. If such antennas have adequate coverage, then our concern for the voice link failing at 37 km is not valid. Thus, a better understanding of the antenna coverage of the S-band at the Space Station is in order before the final conclusion can be drawn. Another possibility is to consider the use of steered beam S-band antennas on the Shuttle. Such possibility is being considered as a possible upgrade of Shuttle avionics.

3.1.2 Shuttle Orbiter/Space Station Link at Ku-Band

3.1.2.1. *Implementation Consideration*

Figure 3-4 shows the functional representation of an all Ku-band link between the Orbiter and the Space Station. The implementation shown is based on utilization of the Ku-band multiple access (MA) system which is planned for the Space Station. Thus, at the Space Station end the Orbiter is handled as one of the multiple users of the RF resources assigned to the Station. Such handling, therefore, does not present additional burded to the Station.

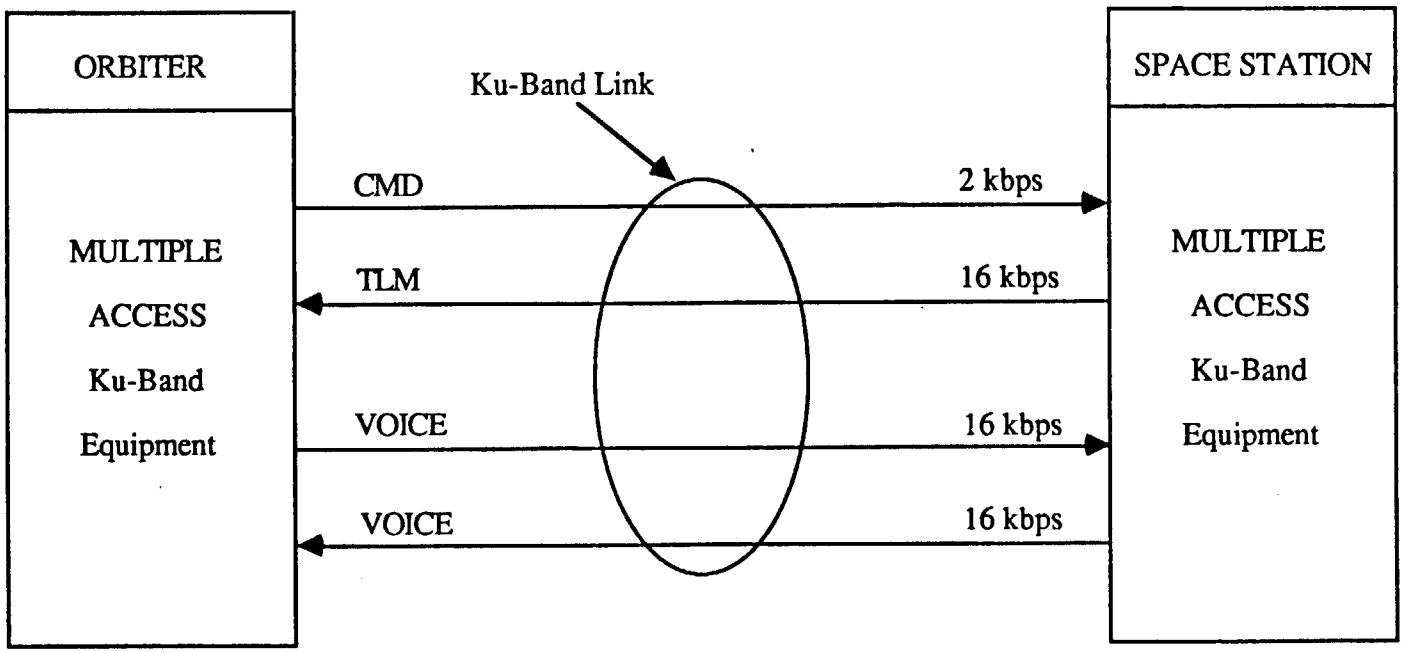

Figure 3-4. Orbiter/Space Station Link at Ku-Band

On the Orbiter end, however, Ku-band equipment identical, or similar to that employed by Station's user space vehicles (S/V) must be utilized. For the Orbiter this may involve considerable amount of new equipment installation and integration. Of particular, concern may be the integration of Ku-band antennas into the Orbiter's antenna systems ensemble. The exact nature of such an impact requires further, more detailed study of all of the factors involved. More information for such a study will become available when the configuration for the Space Station is better defined.

3.1.2.2 *Link Budget for SO/SS Link at Ku-Band*

Table 3-3 shows a link budget for a Ku-band implementation of the command and voice communication links between Shuttle Orbiter and the Space Station. Table 3-4 shows the corresponding return link between the SS and SO. The power division is assumed to be proportional to the data rates.

In all, it appears that within the assumptions used in Tables 3-3 and 3-4, the Ku-band implementation of the SO/SS link has a relatively good margin.

3.1.3 Hybrid S-Band/Ku-Band Implementation

Figure 3-5 shows a functional representation of a hybrid link which utilizes both the S-band and Ku-band equipment. As indicated in the figure, the S-band link is used only for the commands and telemetry interchange between the Orbiter and the Space Station. In this case, the Space Station is treated as a payload. Voice communication takes place via a Ku-band link, such as the MA link used by the Space Station to communicate with other space vehicles.

These appears to be no obvious advantage to this type of operation for the following reason: If the Ku-band MA system is installed into the Orbiter, then this system should be utilizable for all of the communication interchange between the Orbiter and Space Station. The only possible utilization of the S-band link may be in the earlier phases of the assembly of the Space Station. Once the Ku-band system is installed on the Orbiter then S-

	SO/SS		COMMENTS
	CMD 2 kbps	VOICE 16 kbps	
Transmitter power (dBm)	30		1 watt
Transmit circuit loss (dB)	–2		
Transmit antenna gain (dB)	3		
Transmit pointing loss (dB)	–3		
EIRP (dBm)	28		
Path Loss (dB)	–146.5		R = 37 km @ 13.67 GHz
Received antenna gain (dB)	24		High gain antenna at SS
Received pointing loss (dB)	–0.2		
Polarization loss (dB)	–1.8		
Received circuit loss (dB)	–2		
Received signal power (dBm)	98.5		
System noise density (dBm/Hz)	–169		NF = 5 dB at both ends
Carrier to noise density (dB-Hz)	70.5		
Powever Division loss (dB)	–9.5	0.5	Power division set by data rate
Data rate (dB-Hz)	33	42	
Receive E_b/N_0 (dB)	28	28	
Theoretical E_b/N_0 (dB)	9.6	9.6	
Implementation loss (dB)	2	2	
Required E_b/N_0 (dB)	11.6	11.6	
Link Margin (dB)	16.4	16.4	

Table 3-3. Shuttle Orbiter/Space Station Link at Ku-band for Command and Voice

	SO/SS		COMMENTS
	CMD 2 kbps	VOICE 16 kbps	
Transmitter power (dBm)	30		1 watt
Transmit circuit loss (dB)	–2		
Transmit antenna gain (dB)	24.6		High gain antenna at SS
Transmit pointing loss (dB)	–0.2		
EIRP (dBm)	52.4		
Path Loss (dB)	–147.1		
Received antenna gain (dB)	3		
Received pointing loss (dB)	–3		
Polarization loss (dB)	–1.8		
Received circuit loss (dB)	–2		
Received signal power (dBm)	–98.5		
System noise density (dBm/Hz)	–169		
Carrier to noise density (dB-Hz)	70.5		NF = 5 dB at both ends
Powever Division loss (dB)	-3	-3	Power division set by rate
Data rate (dB-Hz)	42	42	
Receive E_b/N_0 (dB)	25.5	25.5	
Theoretical E_b/N_0 (dB)	9.6	9.6	
Implementation loss (dB)	2	2	
Required E_b/N_0 (dB)	11.6	11.6	
Link Margin (dB)	13.9	13.9	

Table 3-4. Space Station/Shuttle Orbiter Link at Ku-Band for Telemetry and Voice

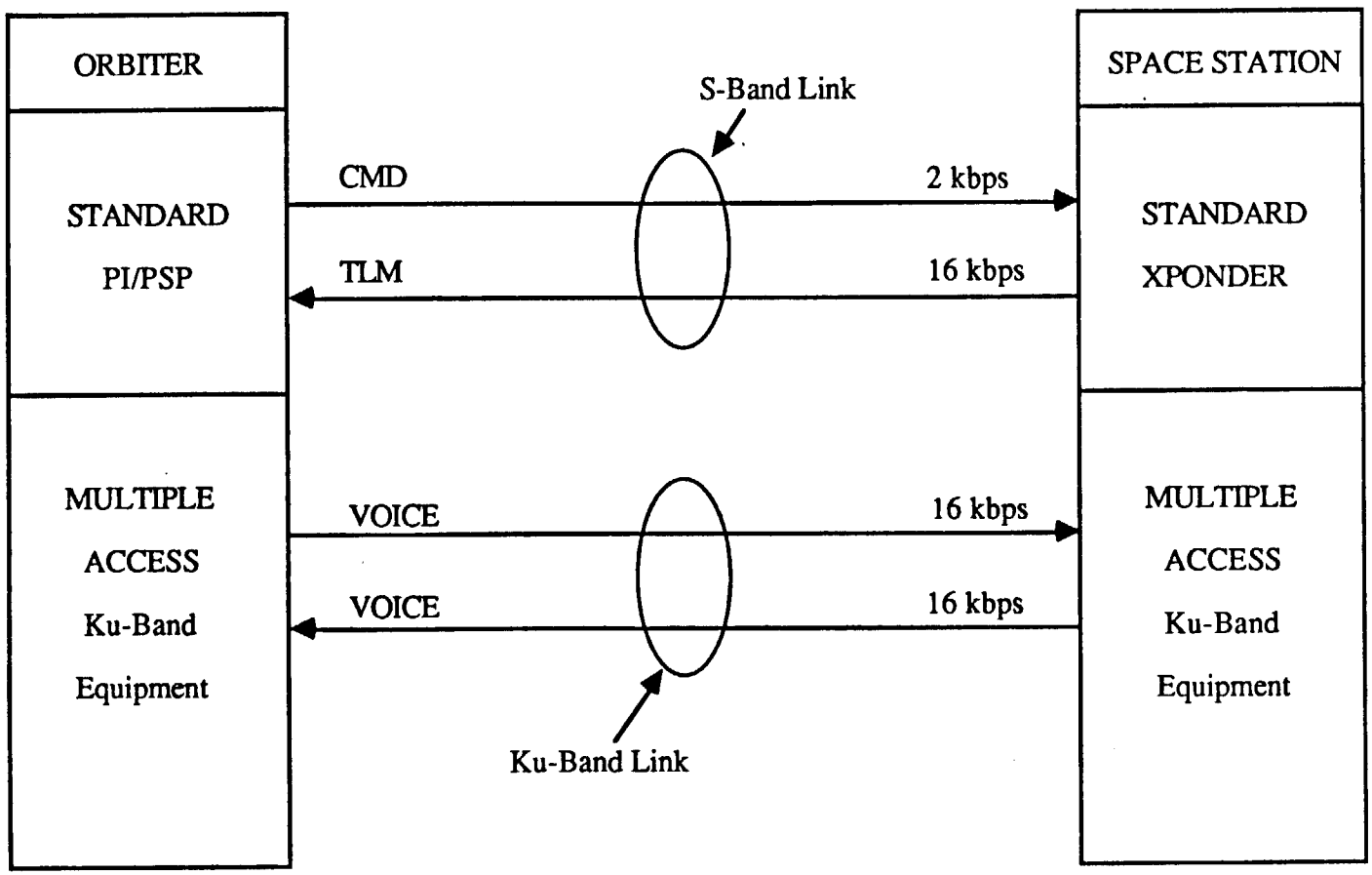

Figure 3-5. Orbiter/Space Station Links at S-Band and Ku-Band

band system use to the communicate with the Station will only impose the requirement of carrying S-band equipment on the latter beyond the IOC phase.

4.0 DISCUSSION OF TRADE-OFFS

From the S-band and Ku-band link budgets presented above, it appears that either implementation alone can meet the requirements for the Shuttle Orbiter/Space Station link. Specifically, as described in Section 3.1.1.1, there is a possibility of adapting some of the exsiting S-band payload link equipment for providing a two-way voice capability to the link. This capability will permit the Orbiter to satisfy the voice link requirements without actually using the Ku-band MA system.

From the standpoint of the Orbiter, this appears to be a relatively low-cost solution, requiring only minor baseband modifications to CIE or similar equipment and the corresponding transponder. Neither RF nor any antenna modifications will be required. However, remaining at S-band beyond the IOC capability will impose dual-band (S and Ku-bands) operation requirement on the Space Station. The impact of the latter requirement remains to be assessed.

Among the factors to be used in the evaluation process are the following criteria:

- Authorized Frequency Band(s)
- Sufficient Bandwidth
- Minimum Interference
- Development Risk
- User Impact
- Growth Potential
- IOC cost.

Explanation of these criteria is presented below:

<u>Authorized Frequency Band(s)</u>

This refers to exclusion of UHF bands from use in future NASA space programs. In the future this way change, but for the purpose of this report, UHF was not considered.

Sufficient Bandwidth

To accommodating simultaneous users, Space Station communication link require considerable amount of RF bandwidth. This is particularly true when MSC operates with multiple video channels. Bandwidth at S-band is limited. Ku-band is much more acceptable from this standpoint.

Minimum Interference

This implies both the effect of our links (i.e., space links) on other users as well as the effect of other emitters on our links. There is considerable history of ground-based interference on UHF and S-band links. In comparison, Ku-band looks promising from the standpoint of minimum interference.

Development Risk

This criterion is based on the technology state and the amount of available design history. From this standpoint, an all S-band implementation rates high.

User Impact

The amount of modifications required by Orbiter equipment can be considered as user impact. For S-band operation, this impact is minimal. For Ku-band, the impact is high, but the fact that MA Ku-band system will be developed from other users can reduce the cost of the impact.

Growth Potential

From this standpoint of the Space Station, the Ku-band system appears to be most desirable because it can accommodate more users in the future. Use of specialized S-band equipment on the Space Station limits growth.

IOC Cost

This criterion needs analytical modeling based on the experience and projections of Phase B contractors for the Space Station. From the point of view of the Shuttle Orbiter, the S-band approach appears to be most cost effective for the IOC. For the

long term considerations, this may not be true and the Ku-band approach may be more desirable.

The criteria listed above indicate that the process of evaluating various approaches is rather complex. The current, on-going Space Station programs and design definitions will provide more data for carrying out a more accurate assessment.

5.0 REFERENCES

[1] "Space Station Reference Configuration Description," NASA/JSC, Document No. JSC-19989, August 1984.

APPENDIX L

SHUTTLE KU-BAND RADAR INTERFERENCE TO SPACE STATION LINKS

SHUTTLE KU-BAND RADAR INTERFERENCE TO SPACE STATION LINKS

Contract No. NA9-17414

Interim Report

Prepared for

NASA Lyndon B. Johnson Space Center
Houston, Texas 77058

Technical Monitor: Dean Bratton

Prepared by

Sergei Udalov
James Dodds

Axiomatix
9841 Airport Blvd., Suite 912
Los Angeles, CA 90045

Axiomatix Report No. R8609-2
September 26, 1986

Table of Contents

	Page
Overview and Summary	1
Shuttle Ku-Band Radar Interference to Space Station Links	
Shuttle Ku-Band Radar Interference to Space Station Receive Links	3
Ku Radar Frequencies and Related Interference	4
Determining Ku Radar Power at Space Station Receivers	5
Ku Radar Power at Space Station Receivers	6
Relative Spectral Density of Ku-Radar and SS Communication Links	7
Ku Radar Interference to SGL	
Radar Power Level Greatly Exceeds Received SGL Forward Link Power	8
Ku Radar Interference Spectral Density	9
Spectral Representation of Radar Interference to Forward Link — High Rate Data	10
Potential Fixes for Ku Radar Interference to SGL	11
Operational Fix	
Operational Fix Using Ku Radar in Beacon Mode	12
Ku-Radar Interference to SGL When Radar Is in Beacon Mode at 13.883 GHz	13
RF and Receiver Fix	
Antenna Sidelobe Canceller	
Antenna Sidelobe Pulse Canceller Functional Block Diagram	14
Sidelobe Pulse Canceller Operation Description	15
Sidelobe Pulse Canceller — Pros and Cons	16
Pulse Estimator Canceller	
RF Pulse Canceller Using PLL/CAD Pulse Estimator (Ref. 2)	17
PLL/CAD RF Pulse Canceller Operation Description	18

PLL/CAD RF Pulse Canceller — Pros and Cons 19

Hard Limiter Pulse Canceller

RF Pulse Canceller Using Hard Limiter 20

Hard Limiter Canceller Operation Description 21

Hard Limiter Canceller Demonstrated Performance (Ref. 3) 22

Hard Limiter RF Pulse Canceller — Pros and Cons 23

Baseband Canceller

Pulse Cancelling at Baseband with Costas Loop 24

Ku Band Radar Interference to SGL — Conclusions 25

Ku Radar Interference to Space Station MA Links

Ku Radar Interference to Space Station MA Links — Sample Calculation 26

Ku-Band Radar Interference to Space Station MA Links 27

Ku Radar Interference to MA Links — Summary 28

Appendix A — MA Link Budgets

Table A-1: MA Link Budgets 29

References 30

OVERVIEW AND SUMMARY

The problem of radar interference arises when the shuttle rendezvous with the Space Station using its Ku-band radar which freqeuncy hops between five frequencies in the range from about 13.8 GHz to 14.0 GHz.

Of particular concern is the radar frequency (out of five) at 13.779 GHz. This frequency is only 4 MHz away from the 13.775 GHz Space Ground Link (SGL) received by the Space Station from TDRS. The Ku-band radar signal enters Space Station's SGL receiver via sidelobes of the high gain antenna pointed to TDRS.

The estimates indicate that the peak Ku-band radar power intercepted by sidelobes of SGL receiver when shuttle is 10 km away may be in the order of – 40 dBm (peak) for a sidelobe level of – 30 dB. In contrast, the nominal value of SGL signal at the Space Station receiver may be about – 80 dBm. This presents interference-to-signal ratio of about 40 dB.

Several technical as well operational "work-arounds" to solve the interference problem have been considered by Rockwell Space Station study team. In principle, we agree with these findings within the scope of "pros and cons" defined by Rockwell team. In addition, however, we are considering such possibilities as:

1) **Operational fix**

Use only a single radar frequency for Space Station rendezvous taking advantage of station's large radar cross section which may be also enchanced by a suitable reflector. In this case the radar frequency will be in the middle of the radar band, i.e., around 13.88 GHz, which is the frequency for beacon mode. The reflector must be optimized for returning circularly-polarzied (CP) RF pulses such as used in beacon mode.

2) **RF and Receiver Fixes**

Use of cancellation techniques such as:

a) antenna sidelobe cancellation

b) precision pulse cancellation based on accurate amplitude and phase information with respect to the received radar pulse.

The operational fix appears to be most desirable from standpoint of requiring minimum amount of new hardware for either Space Station or TDRSS. However, feasibility of precision approach and rendezvous using the beacon mode for skin return from Space Station remains to be established.

RF and receiver fixes using cancellation techniques are still available if operational fixes are not accepted. The advantage of these technquies for solving SGL interference is that they do not require any operational coordination. In other words, these techniques belong into "set them and forget them" category. Moderate hardware development is required, however, at the Space Station receiver.

We have also examined the Ku-band radar interference level to the reception by the Space Station MA receiver of the signals transmitted by users such FF, OMV, EMU and the NSTS itself. These signals arrive at SS in 13.64 – 13.70 GHz NB return band and in 14.00 – 14.30 GHz WB return band. These signals may potentially be interfered with the extreme lower and upper radar transmission frequencies, respectively.

Our analysis, however, indicates that with the exception of OMV and FF wideband return at maximum ranges, the radar interference is below thermal noise even when the users are at their respective maximum ranges.

Link margin degradation to OMV and FF video WB return links is only about 1.5 dB leaving margins of 2.6 dB and 4.3 dB, respectively. Furthermore, the estimated 1.5 dB degradation is based on a worst case assumption that the Orbiter is approaching the Space Station along the axis of the high gain (46.3 dB) antennas used for communication with FF and OMV at long ranges. Operationally, this may not be the case.

Thus, it appears that the major remaining problem is to deal with Ku radar interference to the reception of the SGL.

The material that follows represents our analysis and other support data dealing with Ku radar interference to Space Station communications.

SHUTTLE KU-BAND RADAR INTERFERENCE TO SPACE STATION LINKS

BY

SERGEI UDALOV
JAMES DODDS

AXIOMATIX

SEPTEMBER 1986

SHUTTLE KU-BAND RADAR INTERFERENCE TO SPACE STATION RECEIVE LINKS

Axiomatix

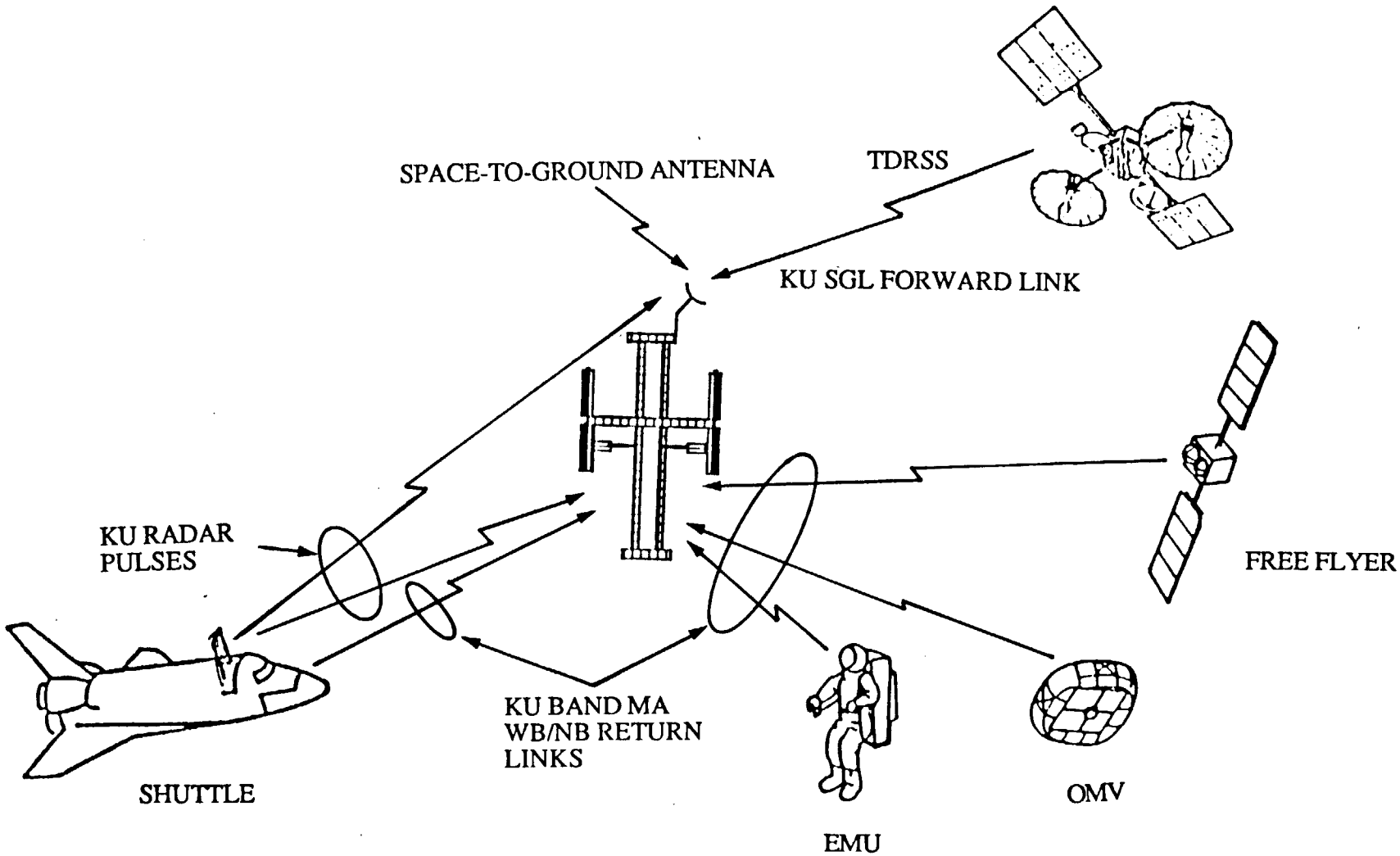

PRECEDING PAGE BLANK NOT FILMED

KU RADAR FREQUENCIES AND RELATED INTERFERENCE

Axiomatix

FREQUENCIES	COMMENTS
f_1 = 13.779 GHz	• Direct inband interference to SGL 12.5 Mbps link to Space Station • May potentially interfere with NB MA return links in the 13.64 GHz to 13.70 GHz range
f_2 = 13.831 GHz	
f_3 = 13.883 GHz	• Beacon mode frequency (fixed frequency mode)
f_4 = 13.935 GHz	
f_5 = 13.987 GHz	• Potential interference to WB user return at 14.15 GHz

DETERMINING KU RADAR POWER AT SPACE STATION RECEIVERS

Axiomatix

- COMPUTE KU RADAR POWER IMPINGING UPON THE SPACE STATION
- TO FIND RADAR POWER WHICH ACTUALLY REACHES INPUTS OF VARIOUS COMMUNICATION RECEIVERS MODIFY RADAR POWER OBTAINED IN STEP ABOVE BY ANTENNA GAINS AND RECEIVER LOSSES OF THE APPROPRIATE LINKS
- ANTENNA GAINS FOR VARIOUS LINKS ARE ASSUMED AS FOLLOWS:

<u>TDRS SGL</u> G_A = 49.4 DB SIDELOBES GAINS G(–30) = 19.4 DB
G(–40) = 9.4 DB
G(–50) = –0.6 DB

<u>MA USERS</u>

HIGH GAIN	G = 46.3 DB	[G(–30) = 16.3 DB]
MEDIUM GAIN	G = 24 DB	
OMNI	G = 3 DB	

- TABLE THAT FOLLOWS USES THESE GAINS FOR RADAR POWER CALCULATIONS

TABLE 1

	LINKS AFFECTED BY RADAR								
	TDRS FWD SGL			WB RET. VIDEO			NB RET. TLM		COMMENTS
	SIDELOBES			FF/OMV		EMU	FF, OMV, NSTS	EMU	
	– 50	– 40	– 30	HGA	HGA/SL	MGA	MGA	OMNI	
Ku Radar Peak power (dBm)	47			47			47		50 watts
Transmit circuit loss (dB)	– 3			– 3			– 3		
Radar antenna gain (dB)	37.7			37.7			37.7		
Radar pointing loss (dB)	N/A			N/A			N/A		
EIRP (dBm)	81.7			81.7			81.7		
Path Loss (dB)	– 135.2			– 135.2			– 135.2		10 km
Received Signal at SS (dBm)	– 53.5			– 53.5			– 53.5		
Receiver antenna gain (dB)	– 0.6	9.4	19.4	46.3	16.3	24	24	3	
Polarization loss (dB)	– 3.5			– 4		– 4	– 4	– 4	LP to CP*
Received circuit loss (dB)	–1.5			– 2		- 2	– 2	– 2	
Radar Power at SS Receiver (dBm)	– 19.1	– 29.1	– 39.1	– 13.2	– 43.2	– 35.5	– 35.5	– 56.5	Peak Power

*Radar is LP, Communication is CP

Notes:

Shuttle at 10 km

Radar Pulse Width = 66.3 sec

Radar PRF = 3 KHz

HGA = MA High Gain Antenna (46.3 dB)

MGA = MA Medium Gain Antenna (24dB)

HGA/SL = MA High Gain Antenna Sidelobe (– 30 dB)

RELATIVE SPECTRAL DENSITY OF KU-RADAR AND SS COMMUNICATION LINKS

Axiomatix

Conditions: Shuttle at 10 km
Radar Pulse width = 66.3 μsec
Radar PRF = 3 KHz

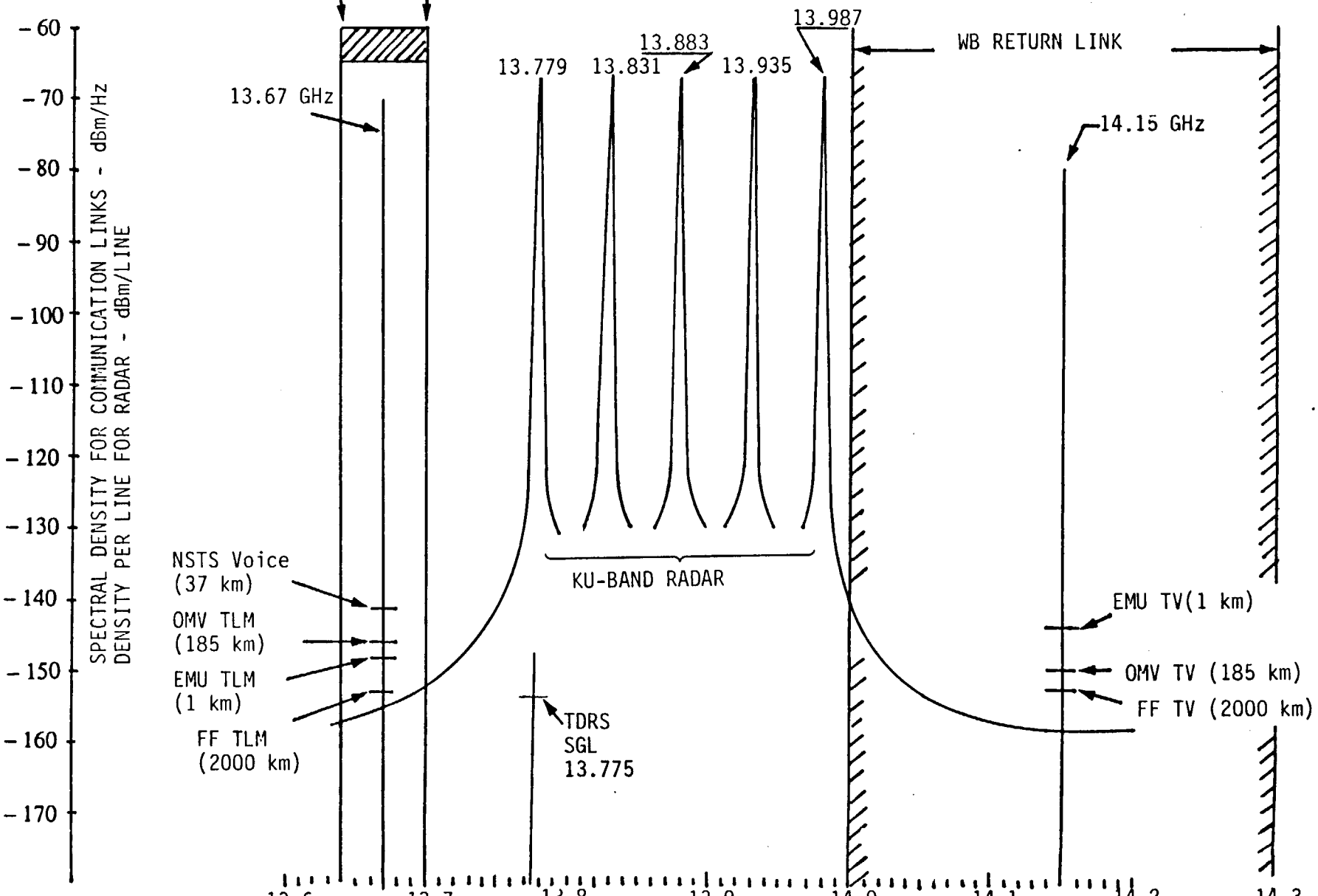

KU RADAR INTERFERENCE TO SGL

RADAR POWER LEVEL GREATLY EXCEEDS RECEIVED SGL FORWARD LINK POWER

Axiomatix

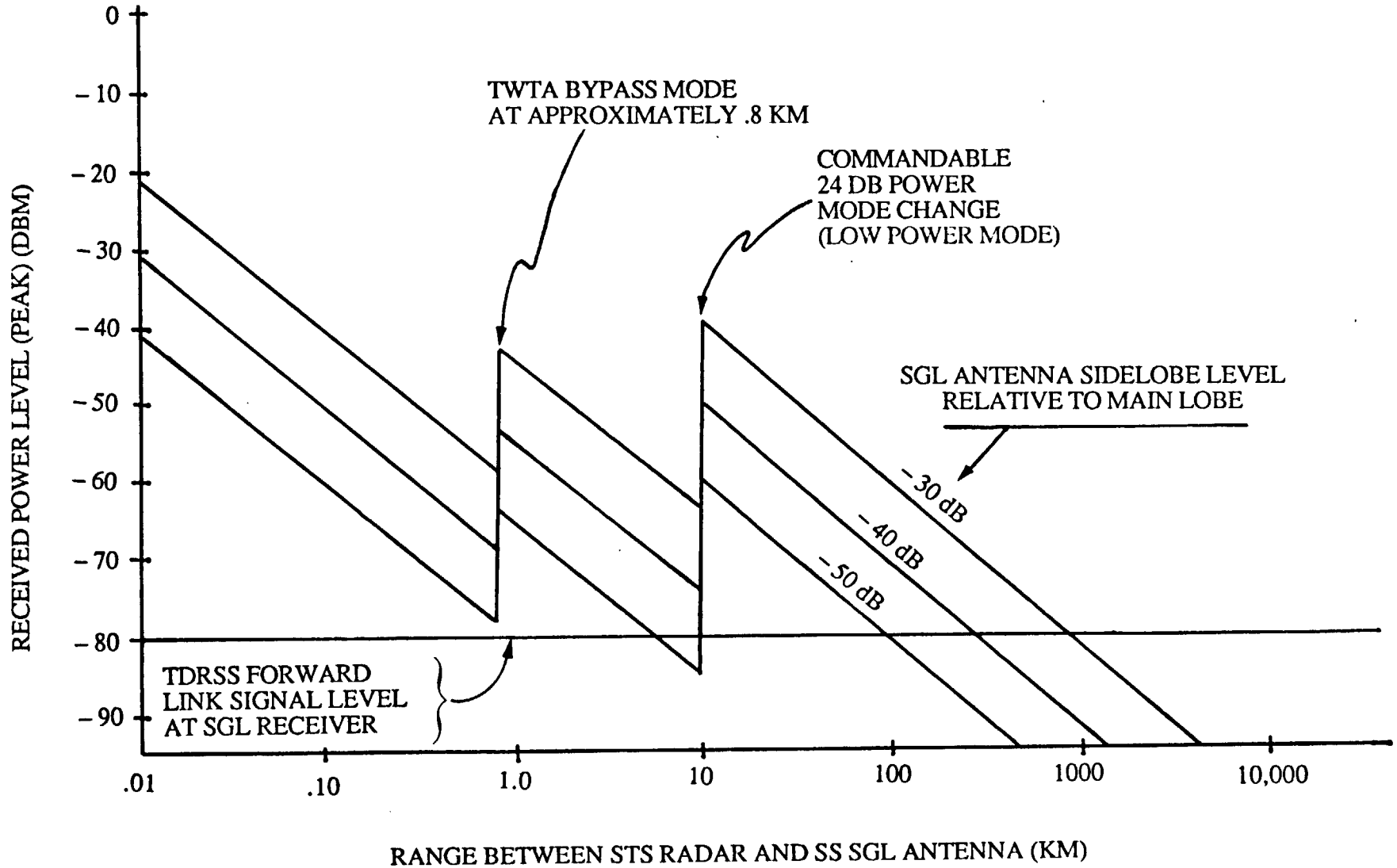

Ku radar at 10 km in acquisition mode:

τ (pulse width) = 66.4 μsec

τ (interpulse period) = 333.3 μsec (PRF = 3 KHz)

$$d_1 \text{ (pulse duty factor)} = \frac{66.4\ \mu\text{sec}}{333.3\ \mu\text{sec}} = 0.2$$

d_2 (frequency dwell duty factor) = 0.2 (one frequency out of five)

Power in center line of radar = $P_{peak} \times d_1^2 \times d_2^2$

or in dB $\quad P = P_{peak}(\text{dBm}) + 20 \log (0.2) + 20 \log (0.2)$

$= P_{peak} - 14\text{ dB} - 14\text{ dB}$

$= P_{peak} - 28\text{ dB}$

Example: For SGL receiver (–30 dB SL) peak radar power is –39.1 dBm. Thus

Center Spectral Line Power = –39.1 dBm – 28 dB = – 67.1 dBm.

Plot of corresponding spectral envelope is shown on next page.

SPECTRAL REPRESENTATION OF RADAR INTERFERENCE TO FORWARD LINK—HIGH DATA RATE

Axiomatix

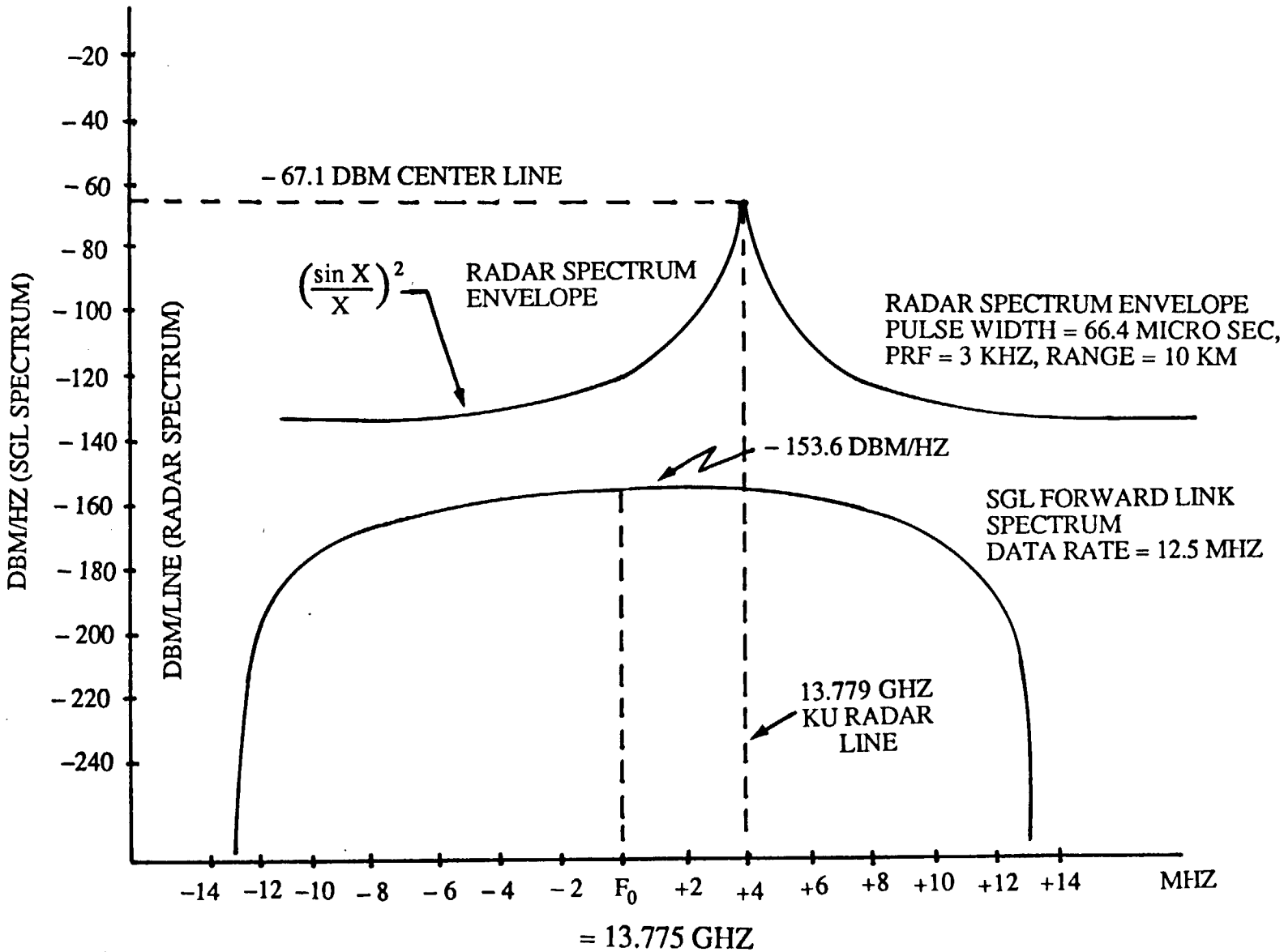

FOLLOWING FIXES WERE CONSIDED BY AXIOMATIX IN ADDITION TO FIXES ALREADY CONSIDERED BY OTHER SPACE STATION CONTRACTORS:

OPERATIONAL FIX

- USE KU BAND RADAR BEACON MODE AT UNHOPPED FREQUENCY OF 13.883 GHz WITH APPROPRIATE PASSIVE RELECTOR AT SS TO PROVIDE FOR CP RETURN.

RF AND RECEIVER FIXES

- ANTENNA SIDELOBE CANCELLER
- PULSE ESTIMATOR CANCELLER
- HARD LIMITER CANCELLER
- BASEBAND CANCELLER

OPERATIONAL FIX

OPERATIONAL FIX USING KU RADAR IN BEACON MODE

GENERAL PRINCIPLE

USE ONLY A SINGLE RADAR FREQUENCY FOR SPACE STATION RENDEZVOUS TAKING ADVANTAGE OF STATION'S LARGE RADAR CROSS SECTION WHICH MAY BE ALSO ENHANCED BY A SUITABLE REFLECTOR. IN THIS CASE THE RADAR FREQUENCY WILL BE IN THE MIDDLE OF THE RADAR BAND, I.E., AROUND 13.88 GHZ, WHICH IS THE FREQUENCY FOR BEACON MODE. THE REFLECTOR MUST BE OPTIMIZED FOR RETURNING CIRCULARLY-POLARIZED (CP) RF PULSES SUCH AS USED IN BEACON MODE.

ESTIMATED EFFECTIVENESS

KU RADAR INTERFERENCE IN SGL BANDWIDTH REDUCED TO ABOUT 20 DB BELOW SGL SIGNAL.

REMAINING ISSUES

- ACTIVE MODE IS RHCP TRANSMIT AND RECEIVE, BUT SINGLE BOUNCE WILL RETURN LHCP. HOWEVER, DATA FROM SKOLNIK (REF 1) INDICATES MINIMAL DEGRADATION WITH COMPLEX TARGET. DOUBLE BOUNCE REFLECTOR MAY NOT BE NEEDED.

- KU BAND ACTIVE MODE NOT ADEQUATELY TESTED FOR ACQUISITION PERFORMANCES AND TRACK AT ALL RANGES.

KU-RADAR INTERFERENCE TO SGL WHEN RADAR IS IN BEACON MODE AT 13.883 GHZ

Axiomatix

	Units	Wide Pulse	Narrow Pulse	Comments
1) Beacon Mode Pulse Width	μsec	4.15*	0.122**	*Initial track, **Final track
2) Pulse BW	MHz	0.248	8.2	
3) Interpulse Period	μsec	142.8	142.8	PRF ≈ 7 KHz
4) Radar Duty Cycle		0.029	8.54×10^{-4}	d_1
5) Duty Cycle Squared		0.000841	7.3×10^{-7}	$(d_1)^2$
6) Peak pwr/Line Ratio	dB	– 30.7	– 61.4	$10 \log (d_1)^2$
7) Radar Peak Power at SS	dBm	– 39.1	– 39.1	From Table 1 (– 30 dB SL)
8) Power in Center Line	dBm	– 69.8	– 100.5	(6) + (7)
9) Frequency Separation (Δf)	MHz	108	108	13.883 GHz (Radar) –13.775 GHz (TDRS)
10) Number of Sidelobes in Δf	lobes	444	13	In terms of pulse bandwidth (2)
11) Envelope of Line Density	dB	– 63	– 32	$(\sin X/X)^2$ maximum envelope w/r to (8)
12) Line Density Envelope	dBm/line	– 132.8	– 132.5	(8) + (11)
13) Lines in SGL BW (12.5 MHz)	dB	32.5	32.5	1785.7 lines for PRF of 7 KHz
14) Peak/Null Averaging	dB	– 3	– 3	Not all lines are on maximum envelope
15) Polarization Gain/Loss	dB	+3.5	+ 3.5	With respect to Table 1
16) Interference Power in BW	dBm	– 99.8	– 99.5	(12) + (13) + (14) + (15)
17) SGL Signal	dBm	– 80	– 80	
18) S/I Ratio	dB	– 19.8	– 19.5	See note

Note: This ratio is for Shuttle at 10 km. Radar power must be reduced as Shuttle approaches Space Station. Means are available to do so manually on Shuttle.

RF AND RECEIVER FIXES

ANTENNA SIDELOBE CANCELLER

ANTENNA SIDELOBE PULSE CANCELLER FUNTIONAL BLOCK DIAGRAM

Axiomatix

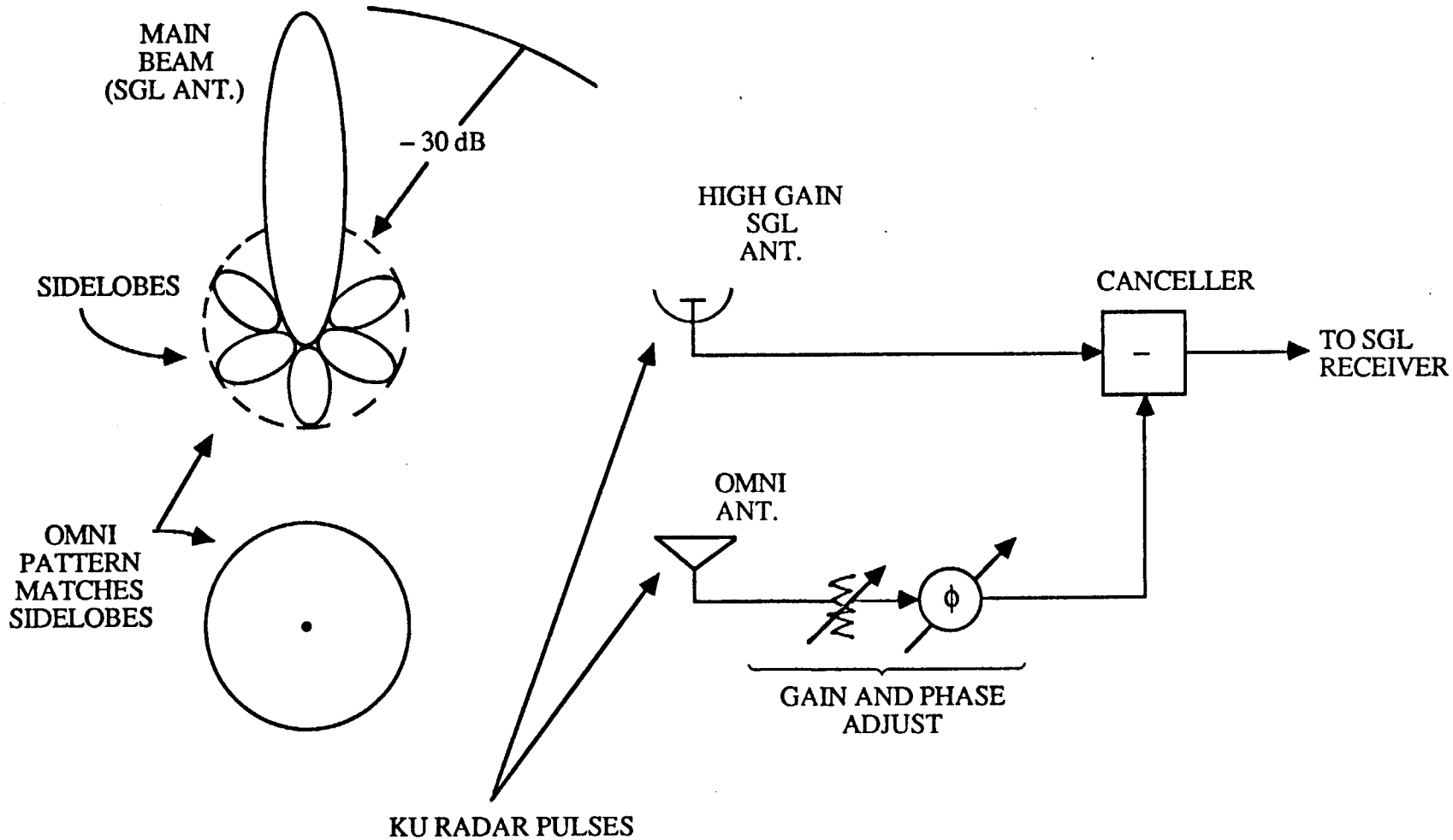

SIDELOBE PULSE CANCELLER OPERATION DESCRIPTION

Axiomatix

1) RADAR PULSES ENTER SPACE STATION SGL RECEIVER VIA SIDELOBES

2) OMNI ANTENNA GAIN IS MATCHED APPROXIMATELY TO SIDELOBES OF HIGH GAIN SGL ANTENNA

3) ADDITIONAL GAIN AND PHASE ADJUSTMENT IS PERFORMED ON OMNI ATTENNA SIGNAL

4) SIGNAL PICKED UP BY OMNI CONTAINS PRIMARILY THE INTERFERENCE, THUS SUBTRACTING THE AMPLITUDE AND PHASE ADJUSTED SIGNAL FROM MAIN ANTENNA SIGNAL CANCELS PULSE INTERFERENCE.

SIDELOBE PULSE CANCELLER – PROS AND CONS

Axiomatix

ADVANTAGES

1) RELATIVELY SIMPLE DESIGN.

2) PULSE CANCELLED AT FRONT END THUS RECEIVER OVERLOAD IS PREVENTED.

DISADVANTAGES

1) OMNI PATTERN MATCHES SIDELOBES ONLY ALONG FEW DIRECTIONS. AT OTHER DIRECTIONS CANCELLATION IS NOT EFFECTIVE.

2) REQUIRES CONTINUOUS READJUSTMENT OF PHASE AND AMPLITUDE OF OMNI SIGNAL AS SGL ANTENNA FOLLOWS TDRS.

PULSE ESTIMATOR CANCELLER

RF PULSE CANCELLER USING PLL/CAD PULSE ESTIMATOR (REF. 2)

Axiomatix

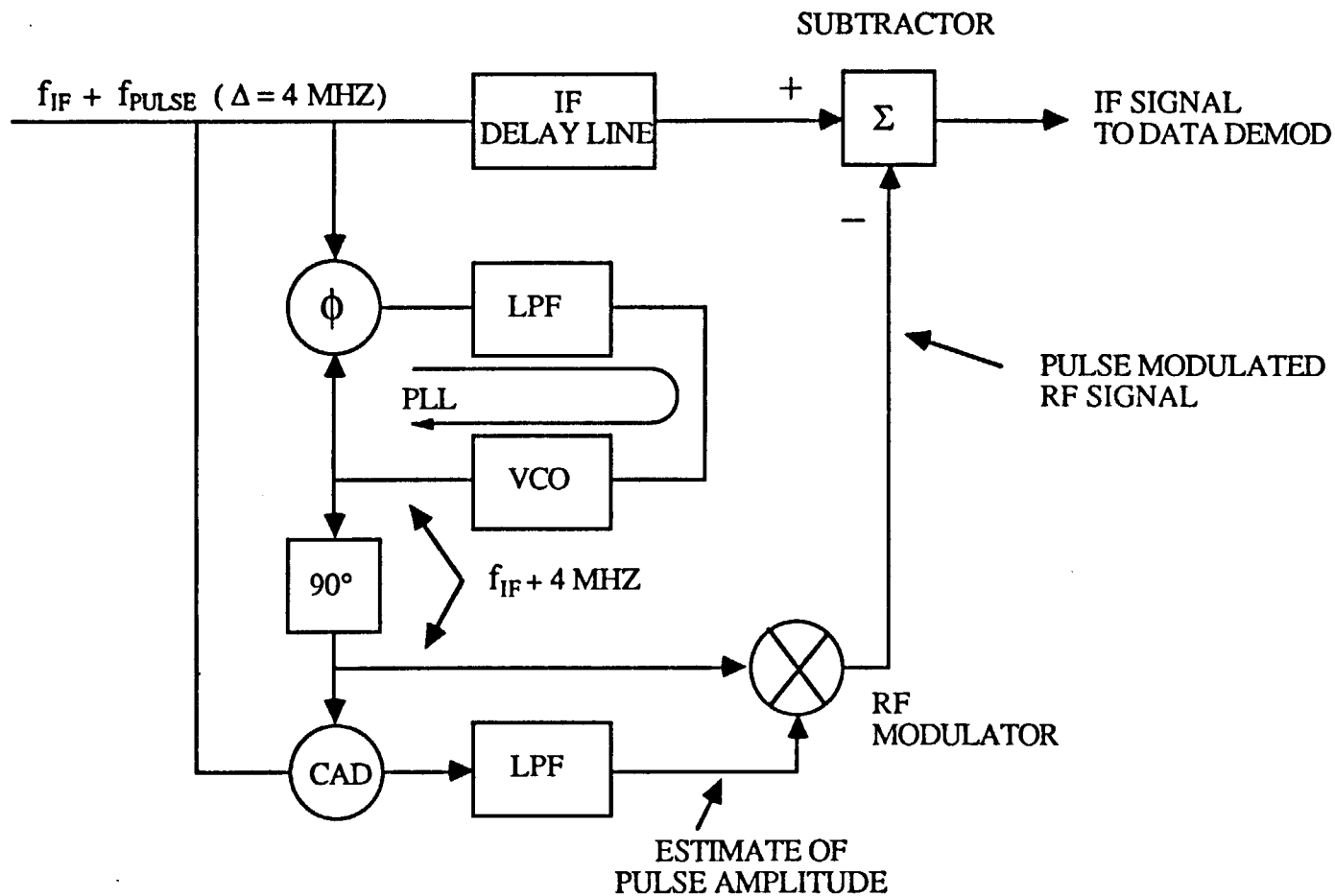

CAD = COHERENT AMPLITUDE DETECTOR

PLL/CAD RF PULSE CANCELLER OPERATION DESCRIPTION

Axiomatix

- SGL IF AND KU RADAR PULSE ARE APPLIED TO IF DELAY LINE AND TO PLL TUNED TO PULSE FREQUENCY (4 MHz ABOVE IF)
- PLL LOCKS ON TO RADAR PULSE AND COHERENT AMPLITUDE DETECTOR (CAD) RECOVERS AMPLITUDE INFORMATION
- OUTPUT OF CAD IS FILTERED IN LPF AND IS USED AS AN "ESTIMATE" OF RADAR PULSE AMPLITUDE
- ESTIMATE SIGNAL OUT OF LPF DRIVES RF MODULATOR WHICH THUS RECONSTRUCTS THE RADAR PULSE WITH HIGH DEGREE OF ACCURACY
- RECONSTRUCTED RADAR PULSE (AN ESTIMATE) IS SUBTRACTED FROM DELAYED IF SIGNAL THUS "CANCELLING" THE INTERFERRING RADAR PULSE AT IF LEVEL

PLL/CAD RF PULSE CANCELLER—PROS AND CONS

Axiomatix

ADVANTAGES

1) CANCELLER FUNCTIONS REGARDLESS OF SGL ANTENNA ORIENTATION

2) INTERFERENCE IS REMOVED PRIOR TO DATA DEMODULATOR

3) USE OF AMPLITUDE ESTIMATOR MAKES CANCELLER "SELF-ADJUSTING"

DISADVANTAGES

1) CANCELLATION WORKS BEST IF INTERFERENCE IS MUCH GREATER THAN SIGNAL

2) PERFORMANCE DEGRADES WHEN INTERFERENCE AND SIGNAL ARE ABOUT SAME ORDER OF MAGNITUDE

HARD LIMITER PULSE CANCELLER

RF PULSE CANCELLER USING HARD LIMITER

Axiomatix

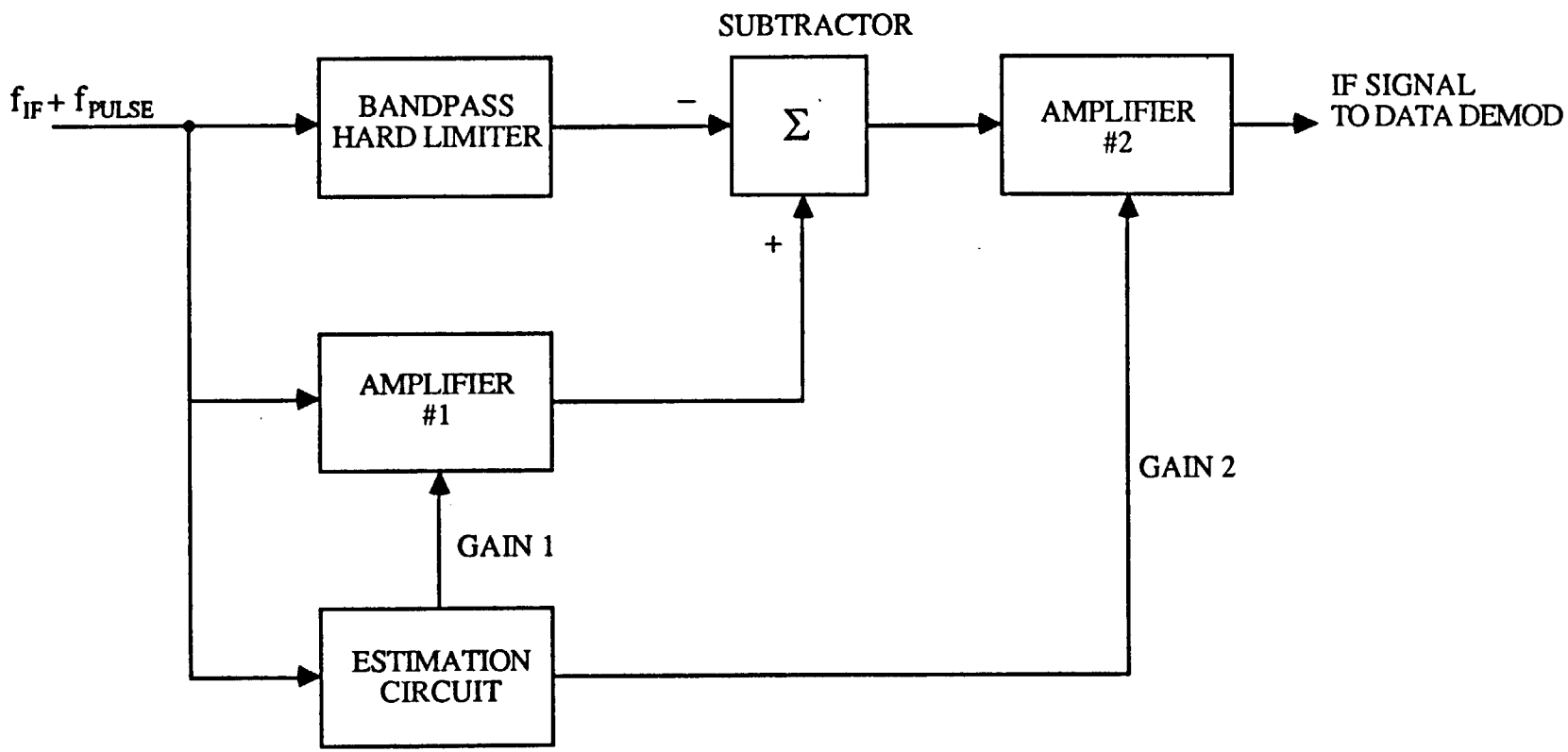

HARD LIMITER CANCELLER OPERATION DESCRIPTION

Axiomatix

- SGL IF AND RADAR PULSE ARE APPLIED TO BANDPASS HARD LIMITER, AMPLIFIER #1 AND ESTIMATION CIRCUIT.
- ESTIMATION CIRCUIT CONTROLS GAIN OF AMPLIFIER #1 TO MAKE ITS OUTPUT EQUAL THE OUTPUT OF HARD LIMITER.
- OUTPUT OF LIMITER CONTAINS MAINLY THE PULSE SIGNAL BECAUSE WEAK SGL SIGNAL IS HIGHLY SUPPRESSED.
- OUTPUT OF ESTIMATOR CONTAINS BOTH THE PULSE AND THE DESIRED SGL SIGNAL
- SUBTRACTOR THUS CANCELS THE STRONG INTERFERING SIGNAL.
- GAIN OF AMPLIFIER 2 IS CONTROLLED BY ESTIMATOR TO BRING UP THE CLEANED UP WEAK SIGNAL TO LEVEL REQUIRED BY DATA DEMODUALTOR.

HARD LIMITER CANCELLER DEMONSTRATED PERFORMANCE (REF. 3)

Axiomatix

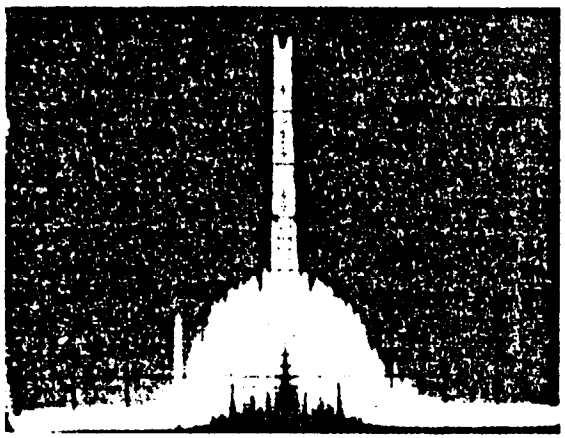

a) input

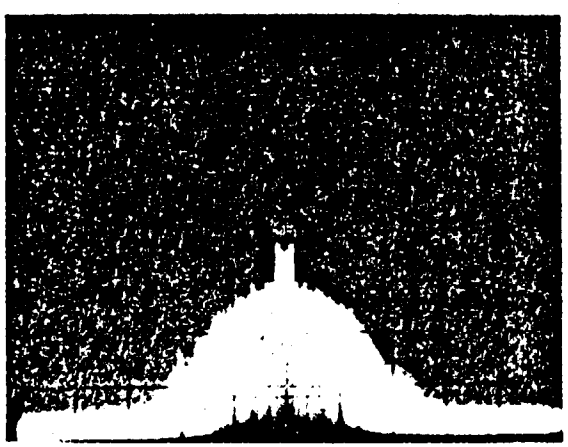

b) output

Amplitude spectra of band limited direct sequence spread-spectrum signal plus FM interferer (vertical axis 10 dB/div; horiz. axis 5 Mhz/div)

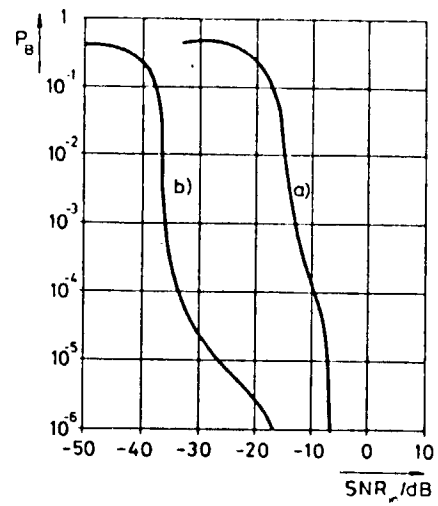

Bit error probability p_B in a spread-spectrum receiver

a) without interferer suppression

b) with interferer suppression

Note: Although performance demonstrated here is for a spread spectrum signal, it is quite impressive. Interference to SGL is a similar case where data is wideband compared to interfering signal

ORIGINAL PAGE IS OF POOR QUALITY

HARD LIMITER RF PULSE CANCELLER—PROS AND CONS

Axiomatix

ADVANTAGES

1) CANCELLER FUNCTIONS REGARDLESS OF SGL ANTENNA ORIENTATION

2) INTERFERENCE IS REMOVED PRIOR TO DATA DEMODULATOR

3) USE OF LIMITER AND ESTIMATOR MAKES CANCELLER "SELF-ADJUSTING"

4) CANCELLER WORKS OVER A WIDE RANGE OF INTERFERENCE SIGNAL FREQUENCY OFFSETS.

DISADVANTAGES

1) CANCELLATION WORKS BEST IF INTERFERENCE IS MUCH GREATER THAN SIGNAL

2) PERFORMANCE DEGRADES WHEN INTERFERENCE AND SIGNAL ARE ABOUT SAME ORDER OF MAGNITUDE

BASEBAND CANCELLER

PULSE CANCELLING AT BASEBAND WITH COSTAS LOOP

Axiomatix

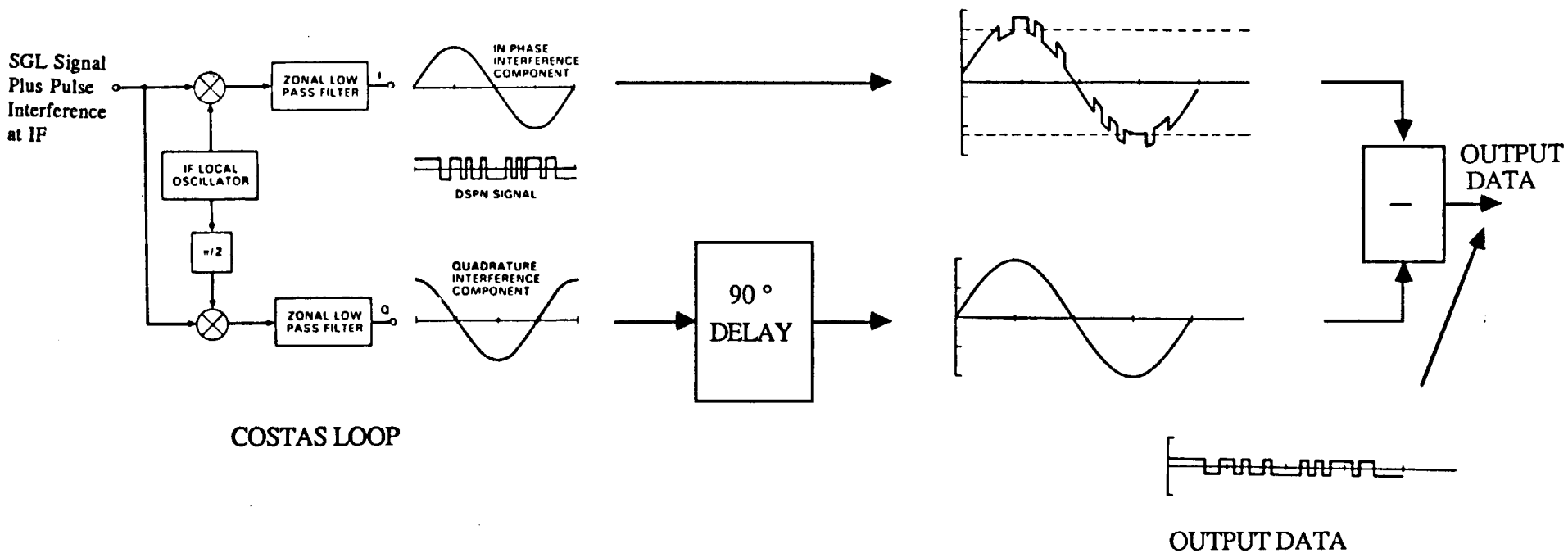

COSTAS LOOP

- RADAR PULSE APPEARS IN Q-CHANNEL OF COSTAS LOOP
- PULSE WAVEFORM IS DELAYED BY 90° AND SUBTRACTED FROM I-CHANNEL
- SUBTRACTION SEPARATES INTERFERENCE FROM DATA

<u>NOTE:</u> THIS IS APPLICABLE TO BI-PHASE MODULATION ONLY

FOR QPSK MORE ELABORATE METHODS MAY BE USED.

KU BAND RADAR INTERFERENCE TO SGL — CONCLUSIONS

PREFERRED APPROACH

- USE OF ACTIVE MODE CENTER FREQUENCY (WITHOUT BEACON) PROVIDES LOWEST COST SOLUTION — NO MODIFICATIONS TO SPACE STATION SYSTEMS.
- REQUIRES INVESTIGATION OF SPACE STATION RADAR CROSS SECTION WITH CP WAVES.
- REQUIRES MORE THOROUGH TEST OF KU-BAND RADAR ACTIVE MODE PERFORMANCE
- MAY REQUIRE PASSIVE RADAR ENHANCEMENT DEVICE.
- MAY RESTRICT SHUTTLE APPROACH VECTORS IF DIRECTIONAL RADAR ENCHANCEMENT DEVICE IS REQUIRED.

ALTERNATE APPROACHES

- CANCELLATION METHODS PROVIDE ALTERNATE SOLUTION BUT THEY REQUIRE DEVELOPMENT OF ADDITIONAL HARDWARE.
- CANCELLATION MAY PROVIDE FOR UNRESTRICTED APPROACH DIRECTIONS.

KU RADAR INTERFERENCE TO SPACE STATION MA LINKS

SAMPLE CALCULATION FOR FLYER (FF) AT 2000 KM:

PARAMETER	VALUE	VALUE IN DB	COMMENTS
1) Ku Radar Frequency	13,987 MHz		
2) FF Frequency	14,150 MHz		
3) Number of 15 KHz Sidelobe Separation	10,867		
4) Spectrum Envelope Att.		– 91 dB	$(\sin X/X)^2$ Maximum Envelope
5) FF Signal Bandwidth	25,000 KHz		Digital Video
6) Number of Sidelobes in Signal Bandwidth	1,667	32.2 dB	Sidelobe is 15 KHz wide (66.3 μsec pulse)
7) Number of PRF Lines in One Sidelobe	4	6 dB	3 KHz PRF
8) Duty Cycle Squared	0.0016	– 28 dB	$d_1^2\ d_2^2$ where $d_1 = d_2 = 0.2$
9) Center Line Radar Power		–13.2 dBm	Via FF HGA (See Table 1)
10) Sidelobe Peak/Null Averaging		– 3 dB	Not all lines are on maximum envelope
11) Radar Power in FF BW		– 97 dBm	Sum of (4), (6), (7), (8), (9) and (10)
12) Thermal Noise in FF BW		– 95 dBm	Table A-1, Appendix A
13) FF Signal Power		– 79.4 dBm	Table A-1, Appendix A
14) Thermal Noise SNR		15.6 dB	(13) minus (12)
15) Interference Noise SNR		17.6 dB	(13) minus (11)
16) Thermal Noise Link Margin		5.8 dB	Table A-1, Appendix A
17) Margin Loss Due to Data		–1.5 dB	Radar interference adds to thermal noise
18) Modified Margin		4.3 dB	

KU-BAND RADAR INTERFERENCE TO SPACE STATION MA LINKS

Axiomatix

	NB RETURN				WB RETURN			COMMENTS
	FF	OMV	EMV	NSTS	FF	OMV	EMU	
Max Range (km)	2000	185	1	37	2000	185	1	THESE VALUES ARE TAKEN FROM TABLE A-1 OF APPENDIX A
Signal	TLM			VOICE	VIDEO			
Link Frequency (GHz)	13.67				14.5			
Received Power (dBm)	– 104.8	– 98.0	– 99.6	– 98.5	– 79.4	– 75.7	– 70.2	
Noise BW (KHz)	64			16	25,000			
Noise BW (dB-Hz)	48			42	74			
Thermal Noise Power (dBm)	– 120.9			– 127	– 95			
Thermal Noise SNR (dB)	16.1	22.9	21.4	28.4	15.6	19.3	24.8	
ΔF from nearest radar Frequency (KHz)	109,000 from 13.779 GHz				163,000 FROM 13.987 GHz			
Approx. No. of 15 KHz Sidelobe Separation	7267				10867			
Max Line Density in Noise BW (dBm/line)	– 151.5		– 172	– 151.5	–132.2 (HGA)			
Lines in Noise BW	16			4	6667			
Radar Interference Power in Noise BW (dBm)	– 142.5		– 163.5	– 148.5	– 97.0 dBm			Includes – 3dB Sidelobe Peak/Null Averaging
Signal/Interference Ratio in Noise BW (dB)	37.7	44.5	63.9	50.0	17.6	21.3	49.1	
Interference Below Thermal Noise (dB)	– 21.6	– 21.6	– 42.5	– 21.6	– 2	– 2	– 24.3	
Link Margin Degrad. (dB)	NEGLIGIBLE				1.5	1.5	NEGLIGIBLE	For FF and OMV Orbiter in main beam of HGA
Remaining Margin (dB)	6.3*	7.7*	6.2*	13.2*	4.3	2.6	9.7*	*UNAFFECTED MARGINS

KU RADAR INTERFERENCE TO MA LINKS—SUMMARY

Axiomatix

- ANALYSIS INDICATES THAT THERE MAY BE ABOUT 1.5 dB MARGIN DEGRADATION TO RECEPTION OF WIDEBAND VIDEO SIGNALS FROM FF AND OMV WHEN THESE VEHICLES ARE AT THEIR MAXIMUM RANGES OF 2000 KM AND 185 KM, RESPECTIVELY.

- THE MARGIN DEGRADATION OF 1.5 dB IS BASED ON WORST CASE ASSUMPTION OF KU RADAR BEING IN THE BEAM OF HIGH GAIN ANTENNAS SERVICING FF AND OMV VIDEO LINKS. NEVERTHELESS, THERE STILL IS A REMAINING MARGIN FOR THESE LINKS.

- OTHER LINKS DO NOT EXHIBIT DEGRADATION NEITHER IN THE NB NOR IN THE WB RETURN LINKS.

APPENDIX A

MA LINK BUDGETS

TABLE A-1 MA LINK BUDGETS*

Parameter	FF to SS Video	FF to SS TLM	SS to FF CMD	OMV to SS TLM	OMV to SS TLM	OMV to SS Video	SS to OMV CMD	SS to OMV CMD	NSTS to SS Voice	SS to NSTS Voice	EMU to SS Video	EMU to SS TLM	SS to EMU Video	SS to EMU CMD
Frequency (GHz)	14.15	13.67	14.63	13.67	13.67	14.15	14.63	14.63	13.67	14.63	14.15	13.67	14.63	14.43
Range (km)	2000	2000	2000	185	1	185	185	1	37	37	1	1	1	1
Tx power (dBm)	30	30	30	30	30	30	30	30	30	30	27	27	30	30
Tx loss (dB)	2	2	2	2	2	2	2	2	2	2	2	2	2	2
Ptng loss (dB)	0.2	0.2	3.3	0.2	0.2	0.2	0.2	3	3	0.2	3	3	0.2	3
Tx gain (dB)	30.3	30	24.6	13	13	13.3	24.6	3	3	24.6	3	3	24.6	3
EIRP (dBm)	58.1	57.8	49.3	40.8	40.8	41.1	52.4	28.0	28.0	52.4	25.0	25.0	52.4	28.0
Path loss (dB)	181.5	181.2	181.8	160.5	115.2	160.8	161.1	115.7	146.5	147.1	115.5	115.2	115.7	115.6
Pol loss (dB)	0.1	0.2	0.2	0.1	1.8	0.1	0.1	1.8	1.8	1.8	1.8	7.4	1.8	7.4
Prop loss (dB)	181.6	181.4	182.0	160.6	117.0	160.9	161.2	117.5	148.3	148.9	117.3	122.6	117.5	123.0
Rx gain (dB)	46.3	24	30.6	24	3	46.3	13.6	13.6	24	3	24.3	3	3	3
Ptng loss (dB)	0.2	3.3	0.2	0.2	3	0.2	0.2	0.2	0.2	3	0.2	3	3	3
Rx loss (db)	2	2	2	2	2	2	2	2	2	2	2	2	2	2
Rcv power (dBm)	-79.4	-104.9	-104.3	-98.0	-78.2	-75.7	-97.4	-78.1	-98.5	-98.5	-70.2	-99.6	-67.1	-97.0
KTo	-174	-174	-174	-174	-174	-174	-174	-174	-174	-174	-174	-174	-174	-174
Noise fig (dB)	5	5	5	5	5	5	5	5	5	5	5	5	5	5
Noise BW (kHz)	25000	64	48	64	64	25000	48	48	16	16	25000	64	400	48
Noise power (dBm)	-95.0	-120.9	-122.2	-120.9	-120.9	-95.0	-122.2	-122.2	-127.0	-127.0	-95.0	-120.9	-113.0	-122.2
SNR (dB)	15.6	16.1	17.9	22.9	42.8	18.3	24.8	44.0	28.4	28.4	24.9	21.4	45.8	25.2
Ideal SNR (dB)	9.6	9.6	10.2	9.6	9.6	9.6	10.2	10.2	9.6	10.2	9.6	9.6	10.2	10.2
Code gain (dB)	5	5	5	0	0	0	0	0	0	0	0	0	0	0
Proc loss (dB)	4	4	4	4	4	4	4	4	4	4	4	4	4	4
Des loss (dB)	1.2	1.2	1.2	1.6	1.6	1.6	1.6	1.6	1.6	1.6	1.6	1.6	1.6	1.6
Req'd SNR (dB)	9.8	9.8	10.4	15.2	15.2	15.2	15.8	15.8	15.2	15.8	15.2	15.2	15.8	15.8
Margin (dB)	5.8	6.3	7.5	7.7	27.6	4.1	9.0	28.2	13.2	12.6	9.7	6.2	30.0	9.4

* Rockwell International, Space Station Work Package 2, Definition and Preliminary Design Phase, Communication and Tracking Report, SSS-85191, Volume III, p. B-14, Table B-1.1.2-1.

REFERENCES

[1] M. I. Skolnik, "Radar Handbook," McGraw Hill, 1970 Edition, p. 28-16.

[2] M. J. Bouvier, Jr., "The Rejection of Large CW Interferers in Spread Spectrum Systems," IEEE Transactions on Communications, Vol. COM-26, No. 2, February 1978, pp. 254-256.

[3] K. J. Friederichs, "A Novel Canceller for Strong CW and Angle Modulated Interferers in Spread-Spectrum Receivers," Milcom, Los Angeles, California, October 21-24, 1984, Volume 3, pp. 32.4.1—32.4.4.

APPENDIX M

PRELIMINARY CONSIDERATIONS FOR ANTENNA SWITCHING, POWER CONTROL, AND AGC FUNCTIONS FOR SPACE STATION MULTIPLE ACCESS SYSTEM

PRELIMINARY CONSIDERATIONS FOR ANTENNA SWITCHING, POWER CONTROL, AND AGC FUNCTIONS FOR SPACE STATION MULTIPLE ACCESS SYSTEM

Interim Report

Contract No. NAS9-17414

Prepared for

NASA Lyndon B. Johnson Space Center
Houston, TX 77058

Technical Monitor: Dean Bratton

Prepared by

Sergei Udalov

Axiomatix
9841 Airport Boulevard
Suite 912
Los Angeles, CA 90045

Axiomatix Report No. R8701-2
January 29, 1987

1.0 INTRODUCTION

This interim report includes some preliminary considerations for antenna switching, power control, and AGC functions for the Space Station's multiple-access (MA) system. The background for the general requirements for these functions is given below.

Antenna Switching

Antenna switching will be required to provide for optimum link conditions despite the relative movement of the MA system users with respect to the Space Station (SS). For movement within the proximity operations zone, several omni atnennas located at various points of the Space Station will provide for near-spherical coverage, but some criteria for selecting the proper antenna are required. Also, the quality of the received signal must be sampled to determine when to switch from an omni to a medium gain antenna and vice versa, the latter scenario being a part of power control.

Power Control

The users of the Space Station's MA system transmit signals at two widely separated rates. For example, the telemetry rate is about 100 Kbps and the video rate is about 22 Mbps. Also, the range to a user may be from about a few meters (EMU) to about 37 km (OMV, NSTS). This creates a potential problem of interchannel interference and receiver overloading. Thus, means of controlling EIRP of users to reduce the Min/Max signal differential at Space Station's receivers is required.

AGC Function

The multiple access system of the Space Station receives Ku-band signals from several users. These signals are picked up by antennas placed at various locations of the SS. The signals are amplified, filtered and supplied via a bus (IF or Fiber-Optical) to the

programmable signal processors (PSP) for data demodulation. The type and distribution of the AGC function has to be identified.

The role of Axiomatix in dealing with these requirements can be summarized as follows:

1) Identify key issue in each of these tasks,
2) Analyze tradeoffs between available alternatives,

and

3) Recommend baseline approaches.

As the title of this report indicates, the material presented here is only of a preliminary nature. The report addresses primarily the issues as we see them now. It also lists additional tasks to be carried out by us towards the recommendation of a baseline design for each of the functions specified. In some cases we also identify the approaches which appear promising at this point. In arriving at the material presented in this report we had to examine the technical material contained in the reports prepared by the Phase B contractors. Not all of the aspects of the MA system design are finalized in these reports. Thus, we had to assume certain baseline approaches which were rated in these reports as most promising candidates. In other cases, we had to apply our best engineering judgement and expertise to identify the issues.

The material which follows is presented in a vu-graph form to simplify the process of communicating our ideas. As concepts and baselines will evolve and grow in complexity, a conventional format of the report will be utilized.

ANTENNA SWITCHING

ANTENNA SWITCHING SCENARIOS TASK REQUIREMENTS

Axiomatix

REQUIREMENT

Identify and analyze candidate Space Station multiple access (MA) antenna switching scenarios, i.e., use of a spare receiver to scan all antennas for best signal, perform BER estimates, etc.

- Identify key issues of each scheme considered
- Recommend a baseline design

BACKGROUND

Antenna switching will be required to provide for optimum link conditions despite the relative movement of the MA system users with respect to the Space Station. For movement within the the proximity operations zone, several omni antennas located at various points of the Space Station will provide for near-spherical coverage, but some criteria for selecting the proper antenna are required. Also, the quality of the received signal must be sampled to determine when to switch from an omni to a medium gain antenna and vice versa, the latter scenario being a part of power control.

ANTENNA SELECTION CRITERION ALTERNATIVES

Axiomatix

ALTERNATIVE	COMMENT
1) Received Power	Absolute received power is measured in a bandwidth matched to signal rate. Assuming good calibration and good receiver gain stability, the decision is made based on signal level.
2) SNR	Signal-to-noise ratio is measured by comparing signal strength in a matched bandwidth to a noise level in another bandwidth. What is really measured is S+N/N ratio.
3) Variance of Measurement	Some parameter of signal quality such as jitter, autocorrelation function or some other indicator of signal "noisiness" is used to determine the status of the link.
4) BER	BER is monitored and when it increases above a preset level, the receiver is switched to a different antenna. (See next chart for comments regarding BER measurement).

COMMENTARIES REGARDING BER MEASUREMENTS

Axiomatix

STATEMENT

BER testing requires a known bit stream pattern (non-corrupted by noise) to indicate the error rate.

PROBLEM

What is to be used as a "known pattern" in a return link data stream?

SOME ALTERNATIVES ARE

(a) Sync words which have known bit sequence patterns

Adv. Frame sync words are always present in the telemetry data.

Disadv. Sync words constitute a small fraction of the return link data stream. This slows down the response of a BER test.

(b) Errors detected in the error correction code decoding.

Adv. BER detection response may be faster than that using sync words

Disadv. Not all links are coded to allow for this feature.

Following issues still remain to be addressed:

- Determine optimum method and/or criterion for antenna selection. Additional investigation is still required in this area.

- Investigate best method for connecting a signal sampling receiver to various antennas. One approach is to use a spare receiver that continuously scans and samples all channels on all antennas. Signal strength data obtained this way can be used by <u>any</u> channel when the need arises. An alternate way would be to use the spare receiver on a demand assignment basis only by a channel which is losing the signal strength. The tradeoffs between these two approaches need to be investigated.

- Interaction between the antenna selection/switching function and the closely associated functions of power control and AGC requires careful examination.

POWER CONTROL CONSIDERATIONS

REQUIREMENT

Determine realistic power control window considering hardware restrictions and algorithm complexity.

- Recommend baseline scheme and window.

BACKGROUND

The users of the Space Station's multiple access (MA) system transmit signals at two widely separated rates. For example, the telemetry rate is about 100 Kbps and the video rate is about 22 Mbps. Also, the range to a user may be from about few meters (EMU) to about 37 km (OMV, NSTS). This creates a potential problem of interchannel interference and receiver overloading. Thus, means of controlling EIRP of users to reduce the Min/Max signal differential at Space Station's receivers is required.

FACTORS TO CONSIDER:

GENERAL

- Range variation (near/far)
- Antenna directivity considerations
- Ground irradiation (is it a problem?)

USER

- EIRP levels at user end
- EIRP control methods (steps vs. continuous)

SPACE STATION

- Required realistic power window
- Received power sensing methods
- Interfaces with other related functions at the Space Station (i.e., antenna selection, AGC)

USER POWER CONTROL BY RELATIVE AGC COMPARISON

Axiomatix

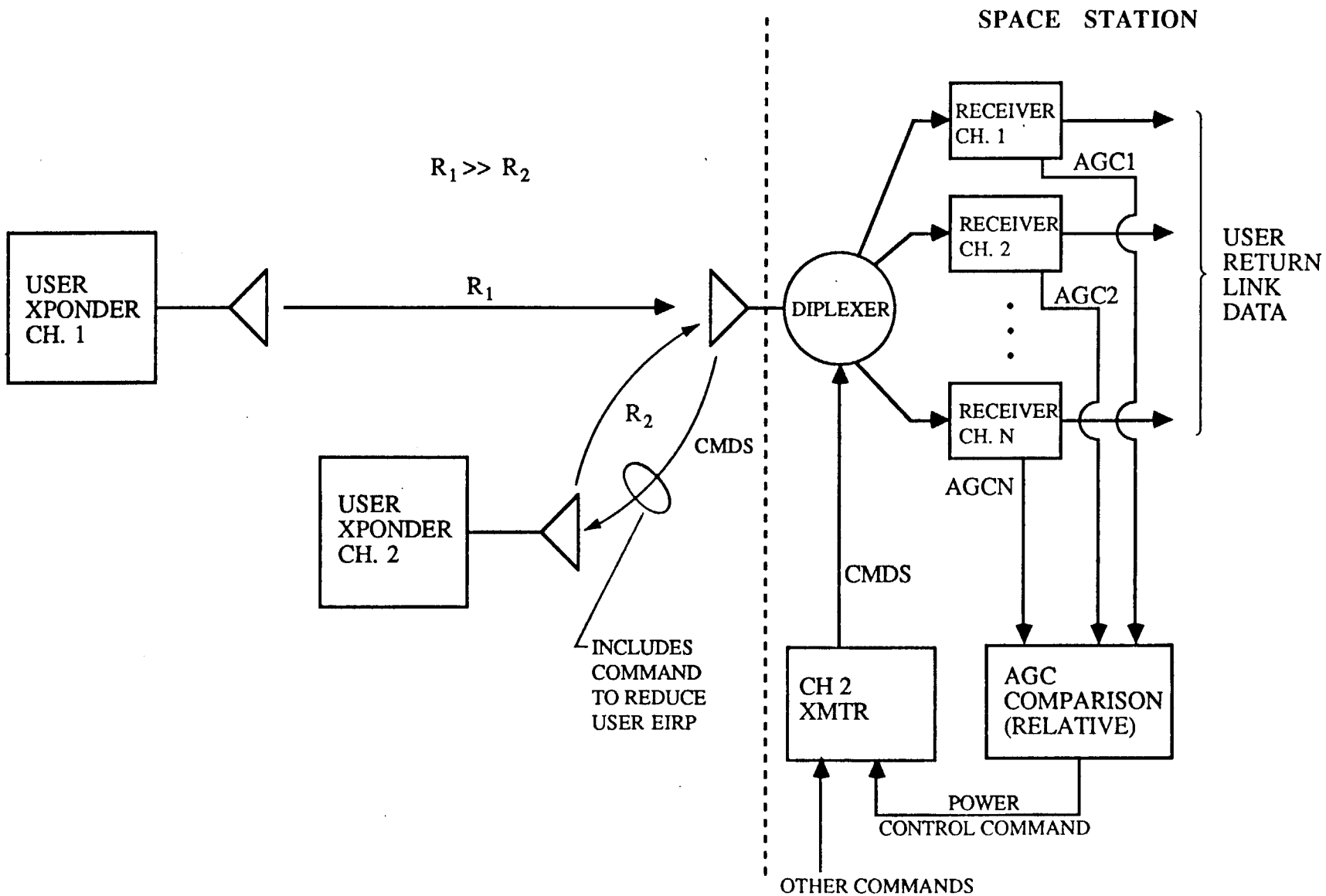

USER POWER CONTROL BY RELATIVE AGC COMPARISON—CONT.

Axiomatix

FUNTION: To prevent adjacent channel interference degradation to a weak signal from a stronger signal.

SCENARIO: User at close range generates adjacent channel interference to a signal received from another user at a longer range. Primary mode of interference is via insufficient filtering of spectral sidelobes in the adjacent channel.

IMPLEMENTATION:

- Levels of AGC signals are sampled and levels from adjacent channels are compared.
- When a difference exceeding a preset level is detected, a power control command is generated.
- Power control command is transmitted to the close range user via a standard command link.
- User reduces EIRP by either transmitter power control, or antenna switching, or both.

METHODS FOR USER EIRP CONTROL

Axiomatix

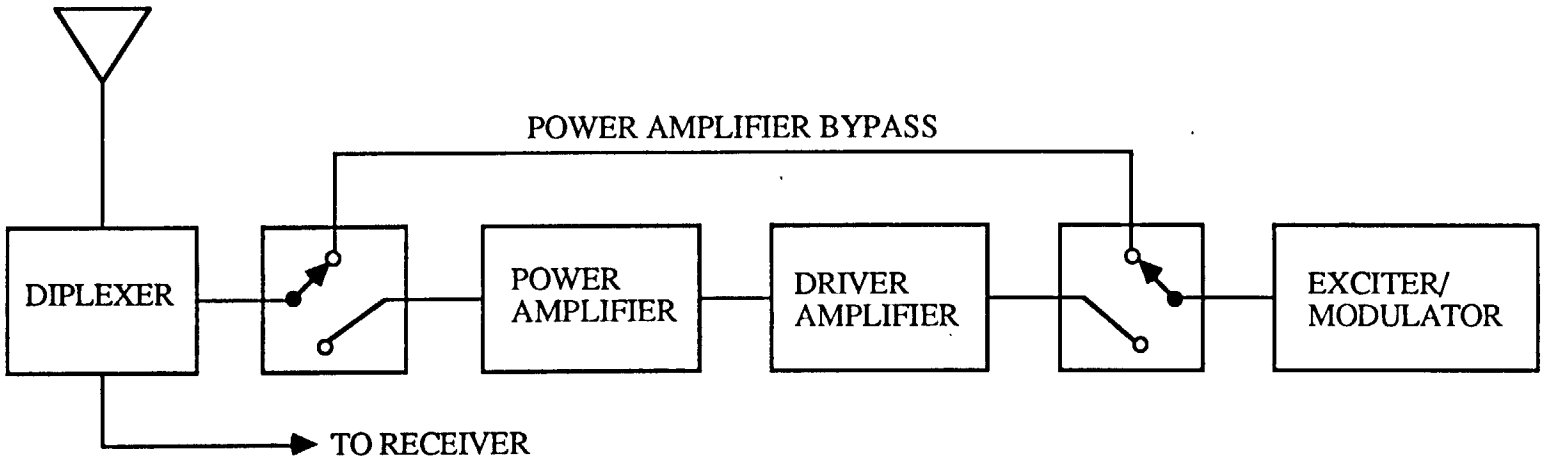

(a) Amplifier Bypass Switching

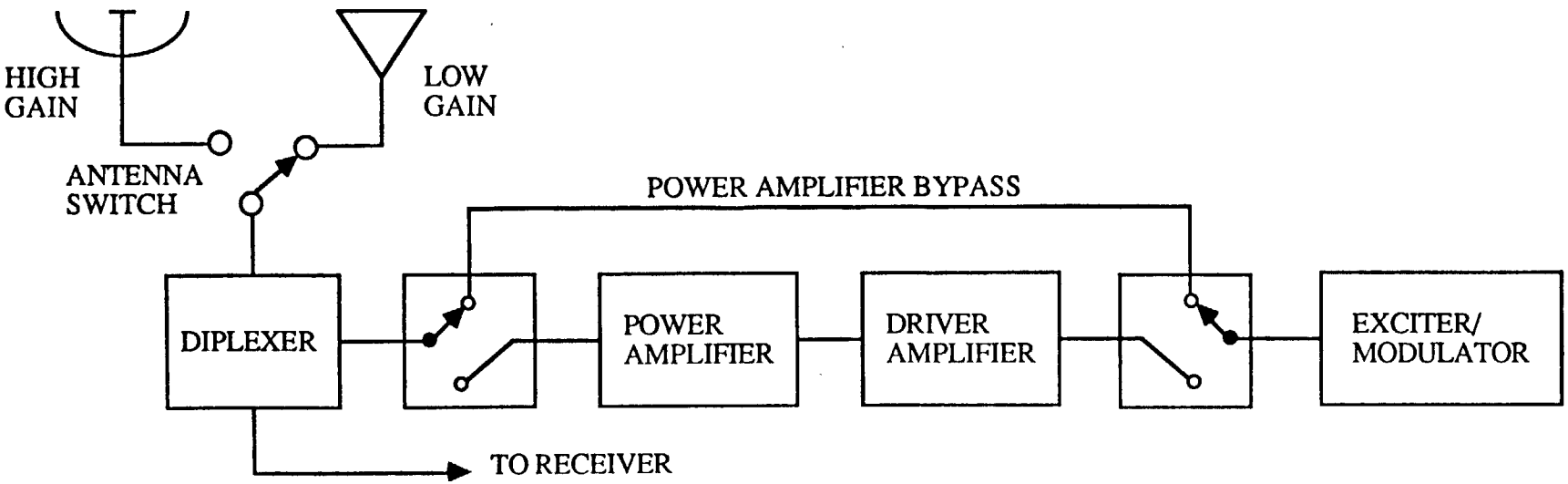

(b) Amplifier Bypass and Antenna Switching

POWER CONTROL — REMAINING ISSUES

Axiomatix

In the area of the power control, the following tasks/issues remain to be addressed:

- Based on available link budget information establish the min/max values of the Ku-band signal received by the Space Station from various users.

- Identify users which may have switchable antennas.

- Consider a baseline configuration for a typical user transmitter and make reasonable assumptions of how much of transmitter power control can be accomplished. Do same for a user which can have both transmitter power and antenna switching.

- Identify factors which determine the power control window from a standpoint of:
    - Interchannel interference
    - Equipment functions at SS (front end, bus system, etc.)

- Consider the interaction between the power control function and the related functions of antenna switching and AGC.

AGC FUNCTION CONSIDERATIONS

REQUIREMENTS

Analyze approaches to performing AGC function at receiver front end, i.e., coherent versus non-coherent, etc.

- Identify key issues in tradeoff of approaches
- Make recommendations.

BACKGROUND

The multiple access (MA) system of the Space Station (SS) receives Ku-band signals from multiple users. These signals are picked up by several antennas placed at various locations of the SS. The signals are amplified, filtered and supplied via a bus (IF or Fiber-Optical) to the programmable signal processors (PSP) for data demodulation. The type and distribution of the AGC function has to be identified.

AGC FUNCTION ALTERNATIVES

Axiomatix

OPTION A: Non-coherent AGC at the Antenna Group Receiver

OPTION B: Coherent AGC at the Antenna Group Receiver with AGC control signal supplied by PSP

OPTION C: Non-coherent AGC at the Antenna Group Receiver and an additional coherent AGC at PSP.

NON-COHERENT AGC AT ANTENNA GROUP RECEIVER (OPTION A)

Axiomatix

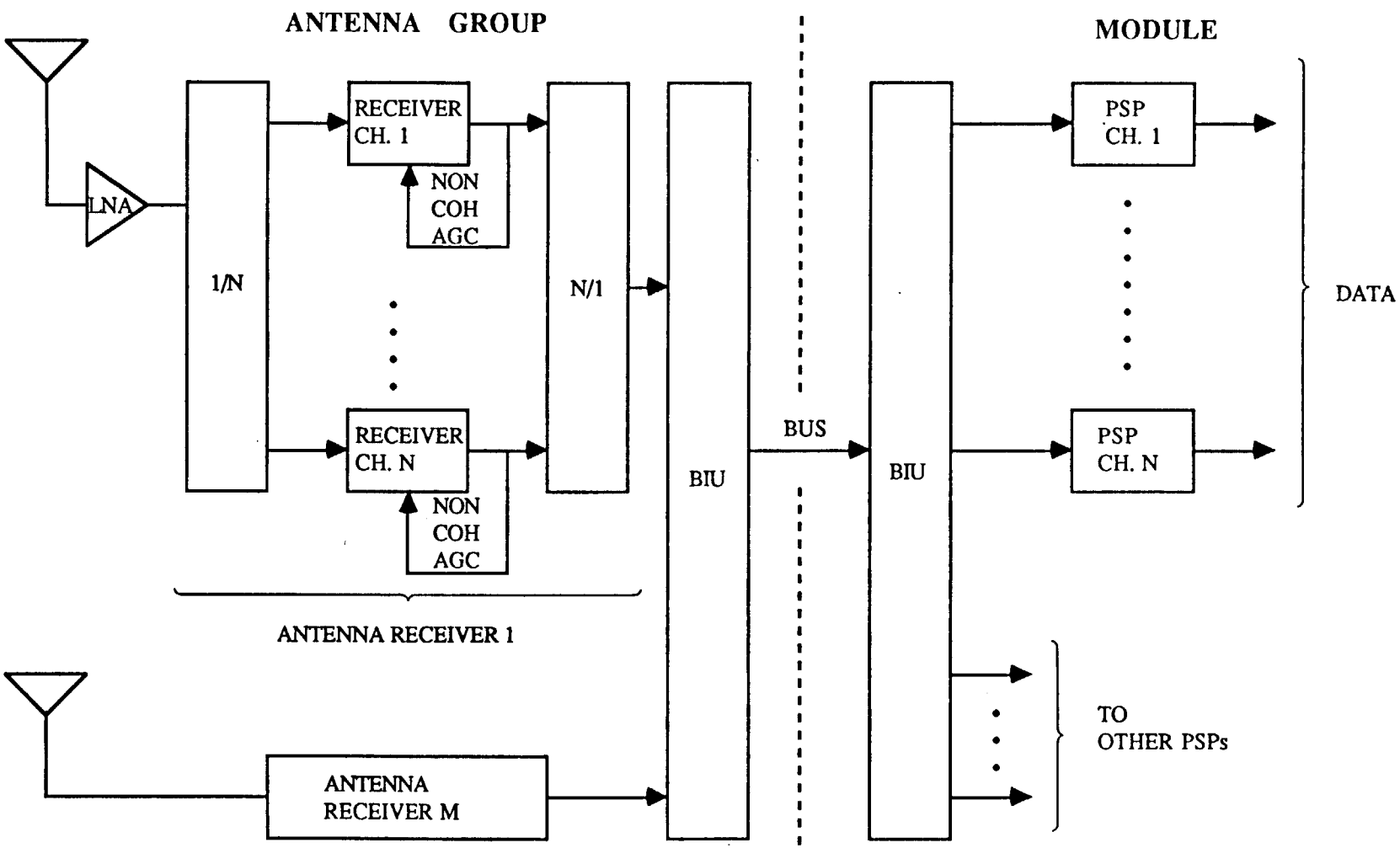

N = NUMBER OF RF CHANNELS PER ANTENNA
M = NUMBER OF ANTENNAS PER GROUP
BIU = BUS INTERFACE UNIT

1/N = N-WAY POWER DIVIDER
N/1 = N-WAY POWER COMBINER

IMPLEMENTATION

Non-coherent AGC is applied at the antenna group receiver. There is no other AGC beyond the front end receiver.

ADVANTAGES

- Dynamic range of received signals is compressed prior to the bus, thus minimizing the crossmodulation in the bus driver and the interface units.
- Relative simplicity.

DISADVANTAGES

- Considerable RF/IF gain (80 to 100 dB) is required from the RF/IF segments of the antenna group receiver to develop non-coherent AGC for the weak signals.
- Strong signals primarily are affected by the noncoherent AGC unless additional gain is provided prior to BIU.

COHERENT AGC AT ANTENNA GROUP RECEIVER SUPPLIED BY PSP (OPTION B)

Axiomatix

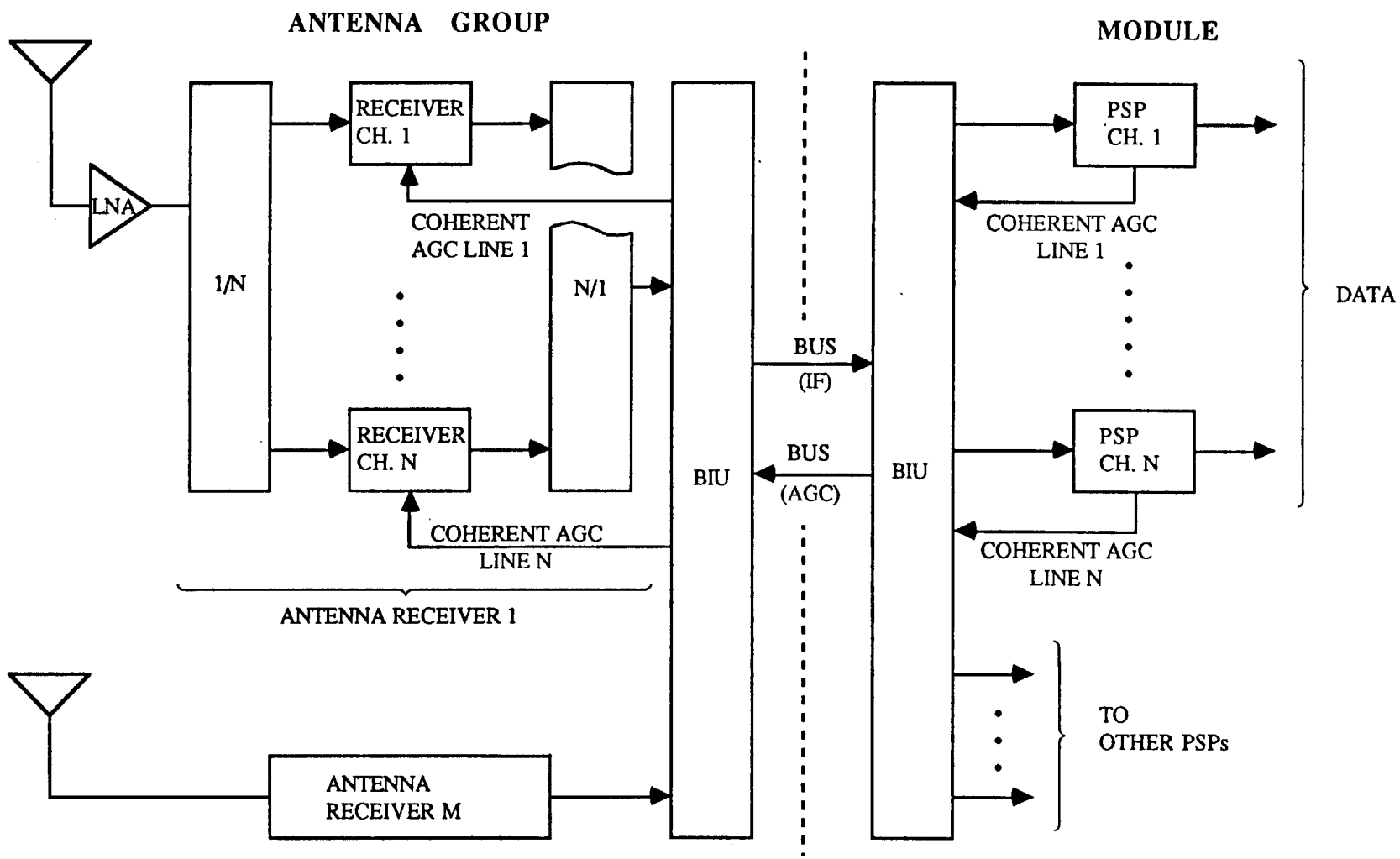

N = NUMBER OF RF CHANNELS PER ANTENNA
M = NUMBER OF ANTENNAS PER GROUP
BIU = BUS INTERFACE UNIT

1/N = N-WAY POWER DIVIDER
N/1 = N-WAY POWER COMBINER

IMPLEMENTATION

Coherent AGC is developed by a PSP and the AGC signal is fed back to the antenna group receiver(s) via a bus.

ADVANTAGES

- AGC function is provided for the weak signals.
- Optimum receiver gain can be accomplished at various IF frequencies eliminating requirement for excessive gain within any one receiver segment.

DISADVANTAGES

- Two way bus must be provided to carry the AGC signal from the PSP back to the antenna group receiver.
- Receiver and PSP selector matrices must handle additional signals (i.e., the AGC signals).
- Relative complexity of AGC function implementation with physically separated front end/receiver/PSP units.

NON-COHERENT AGC AT ANTENNA GROUP RECEIVER AND COHERENT AGC AT PSP (OPTION C)

Axiomatix

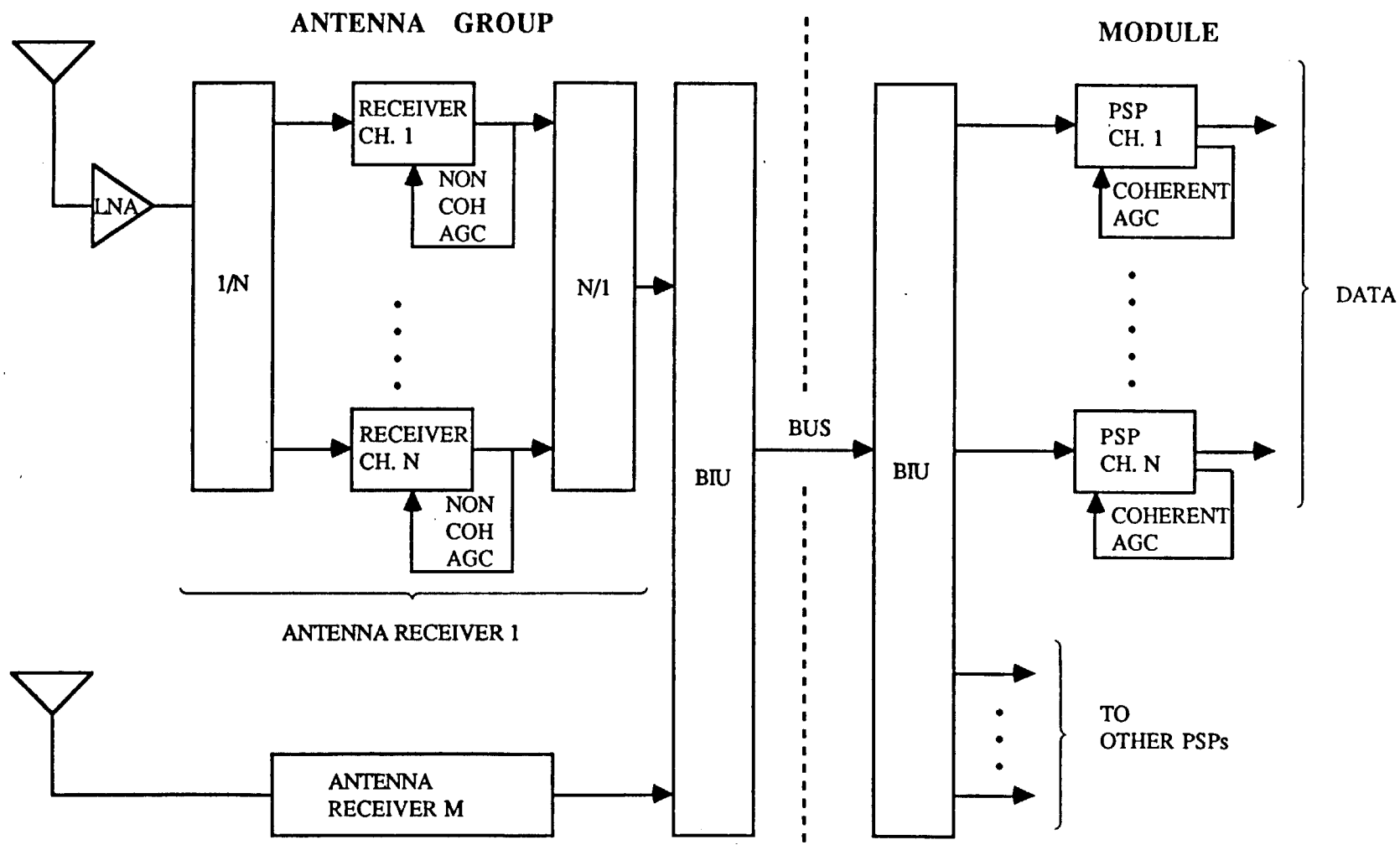

N = NUMBER OF RF CHANNELS PER ANTENNA
M = NUMBER OF ANTENNAS PER GROUP
BIU = BUS INTERFACE UNIT

1/N = N-WAY POWER DIVIDER
N/1 = N-WAY POWER COMBINER

IMPLEMENTATION

Non-coherent AGC is applied at the antenna group receiver level. Additional coherent AGC is provided at the PSP level.

ADVANTAGES

- No AGC signal path is required between the PSPs and the antenna group receivers.
- Non-coherent AGC prior to BIU reduces the dynamic range which the BIU's have to handle.
- Coherent AGC at PSP level provides AGC function for weak signal.

DISADVANTAGES

- Complicates PSP design by requiring an AGC function within the PSP units.

SUMMARY(Preliminary)

- Option C which provides non-coherent AGC at the antenna receiver and coherent AGC at the PSP looks attractive from a preliminary point of view.

- Quantitative analysis has to be applied to verify the tradeoffs involved.

- Axiomatix will base this analysis of information available to us from Phase B contractors reports and on best engineering judgement.

REMAINING ISSUES

- MA receiver(s) and bus architectures are not finalized yet in detail by Phase B constractors. Thus, some assumptions on our part will have to be made.

- The interaction between the AGC function and the associated functions of power control and antenna switching must be defined in quantitative terms.

APPENDIX N

POWER CONTROL FOR SPACE STATION MULTIPLE ACCESS SYSTEM

POWER CONTROL FOR SPACE STATION MULTIPLE ACCESS SYSTEM

Contract No. NAS-17414
Interim Report

Prepared for

NASA Lyndon B. Johnson Space Center
Houston, TX 77058

Technical Monitor: Dean Bratton

Prepared by
Sergei Udalov

Contributions by
Richard Austin

Axiomatix
9841 Airport Boulevard
Suite 912
Los Angeles, CA 90045

Axiomatix Report No. R8704-2
August 27, 1987

TABLE OF CONTENTS

	Page
List of Figures	i
List of Tables	iii
EXECUTIVE SUMMARY	1
1.0 INTRODUCTION	8
2.0 TECHNICAL CONSIDERATIONS	12
2.1 Received Signal Spread	12
2.2 The Effect of Receiver Implementation on System Intermods	15
2.2.1 Wideband Ku-Band Receiver	15
2.2.2 Channelized Ku-Band Receiver Implementation	20
2.3 Cable Driver Considerations	25
2.3.1 FO Cable Driver Functional Diagram Description	26
2.3.2 Optimizing System Gain Ahead of the FO Line Driver	29
2.4 Power Control	32
2.4.1 Power Control for a Wideband Receiver	32
2.4.2 Power Control with a Channelized Receiver and AGC	37
2.4.2.1 General Consideration	37
2.4.2.2 Example of a 3 dB Power Window	42
2.4.2.3 Possibilities and Limitations of Wider Power Windows	44
2.4.2.4 Power Control Algorithm for a Channelized Receiver	55
2.4.2.5 The SNR Estimation	57
2.4.3 User Power Control	59
3.0 CONCLUSIONS	60
4.0 RECOMMENDATIONS	61
APPENDIX A	A-1
APPENDIX B	B-1
APPENDIX C	C-1

LIST OF FIGURES

		Page
Figure 1	Power Control Function Scenario	2
Figure 2	Third Order Intermods for (a) Wideband Receiver and (b) Channelized Receiver	3
Figure 3	System SNR Transfer Curve as Function of FO Cable Loss (EMU and MSC-3 Power Control Window of 10 dB)	5
Figure 4	System SNR Transfer Curve as Function of FO Cable Loss (FF and OMV Power Control Window of 15 dB)	6
Figure 5	Functional Block Diagram for User Power Control	7
Figure 1-1	Power Control Functional Scenario	9
Figure 1-2	Power Received at Space Station from Various Users as Function of Range	10
Figure 2.1-1	Video Link Signal Levels and Margins as Function of Range	14
Figure 2.2.1-1	Configuration with One Wideband Receiver and FO Cable per Antenna	16
Figure 2.2.1-2	Wideband Receiver Third Order Intermodulation as Function of Input Signal	17
Figure 2.2.1-3	Channel Degradation Due to Third Order Intermodulation in the Wideband Receiver	19
Figure 2.2.2-1	Channelized AGC Equalizes Signal Levels into Cable Driver	21
Figure 2.2.2-2	Channelized Receiver Front End Third Order Intermodulation as Function of Input Signal	23
Figure 2.2.2-3	Channel Degradation Due to Third Order Intermodulation in Front End LNA as Function of Signal Input to a Channelized Receiver	24
Figure 2.3.1-1	FO Cable Driver Functional Block Diagram	27
Figure 2.3.2-1	Optical Driver Output as Function of System Gain Preceding the Driver	30
Figure 2.3.2-2	Link Degradation Due to FO Driver Optical Noise as Function of System Gain Preceding the Driver	31
Figure 2.4.1-1	Min/Max Received Power Spread for a 3 dB Window Power	34

	Control	
Figure 2.4.1-2	Optical Cable Driver Output Levels for 3 dB Window Power Control	35
Figure 2.4.2.1-1	Effect of Channelized AGC on Relative Signal and Noise Levels at the Output of FO Cable Driver	38
Figure 2.4.2.1-2	FO Cable Driver Output SNR vs. System Input Thermal	41
Figure 2.4.2.2-1	Optical Driver Output Levels for 3 dB Power Control Window (channelized received with AGC)	43
Figure 2.4.2.3-1	FO Cable Link Noise Sources	46
Figure 2.4.2.3-2	Carrier/Noise versus Received Optical Power	47
Figure 2.4.2.3-3	System SNR Transfer Curve as Function of FO Cable Loss (EMU and MSC-3 Power Control Window of 10 dB)	49
Figure 2.4.2.3-4	System SNR Transfer Curve as Function of FO Cable Loss (FF and OMV Power Control Window of 15 dB)	50
Figure 2.4.2.3-5	Effect of FO Cable Loss on Power Control Decision (MSC-3 User)	51
Figure 2.4.2.3-6	A Loose Power Control Decision Tolerance May Push Control into the Margin Region	53
Figure 2.4.2.3-7	Excessive Power Window is Vulnerable to Decision Tolerance	54
Figure 2.4.2.4-1	Power Control Algorithm for a Channelized Receiver	56
Figure 2.4.2.5-1	QPSK Costas Loop Signals for SNR Estimation	58
Figure A-1	FO Cable Link Noise Sources	A-2
Figure A-2	Carrier/Noise versus Received Optical Power	A-3
Figure A-3	Carrier/Noise Ratio per Channel as Function of FO Cable Loss	A-8
Figure C-1	Functional Block Diagram for User Power Control	C-2'

LIST OF TABLES

		Page
Table 2.1-1	Signal Level Characteristics of Ku-Band Video Return Links	13

EXECUTIVE SUMMARY

In this report various technical aspects of implementing the power control for the Space Station Multiple Access (MA) system are addressed. Particular emphasis is placed on the RF/IF processing of the Ku-Band MA signals received by the station. A fiber optic (FO) cable link is assumed to be carrying the IF signals between the boom locations of the receiver/transmitter (R/T) units and the central processing unit located in the habitat module. Capabilities and limitations of using an FO cable link as a subunit of the power control function are examined.

The motivation for the power control arises due to the following three factors: (1) the FDMA configuration of the return links, (2) the near/far problem, and (3) the dynamic range limitation of the Space Station's RF receiving and the IF distribution components. Figure 1 shows the power control function scenario.

Two receiver architectures were examined for their ability to handle the FDMA signals. These architectures are: (1) a wideband receiver proposed by the McDonnel Douglas team and (2) a channelized receiver proposed by the Rockwell International team.

The salient feature of the first approach is a single wideband downconversion of the entire return link band (300 MHz wide) to a wideband IF. Thus, each antenna of an antenna group is connected to a separate receiver which then connects to its own FO cable driver. The main advantage of this approach is the simplicity of the Ku-Band receivers. With a channelized approach a group of antenna receivers have a capability to amplify selectively the individual channels of the return link band. Although this approach is more complicated than the wideband approach it provides for a channel-dedicated AGC function within each receiver.

Figure 2 presents a side by side comparison of our estimates for the third order intermodulation behavior of the two receiver architectures. The bandwidth assumed is that of a digital video link, i.e., 25 MHz. As indicated in the figure, the origins of the third

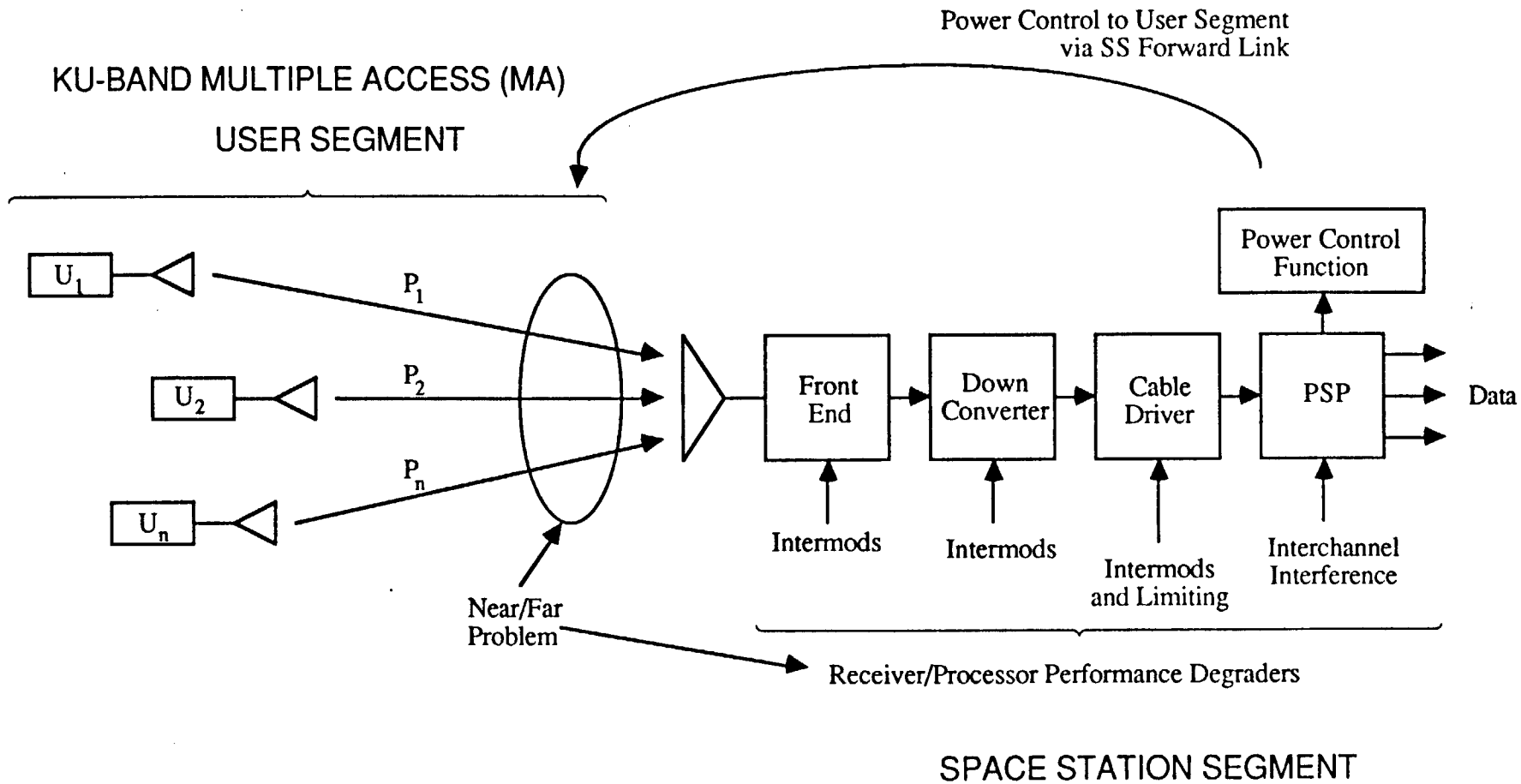

Figure 1. Power Control Functional Scenario.

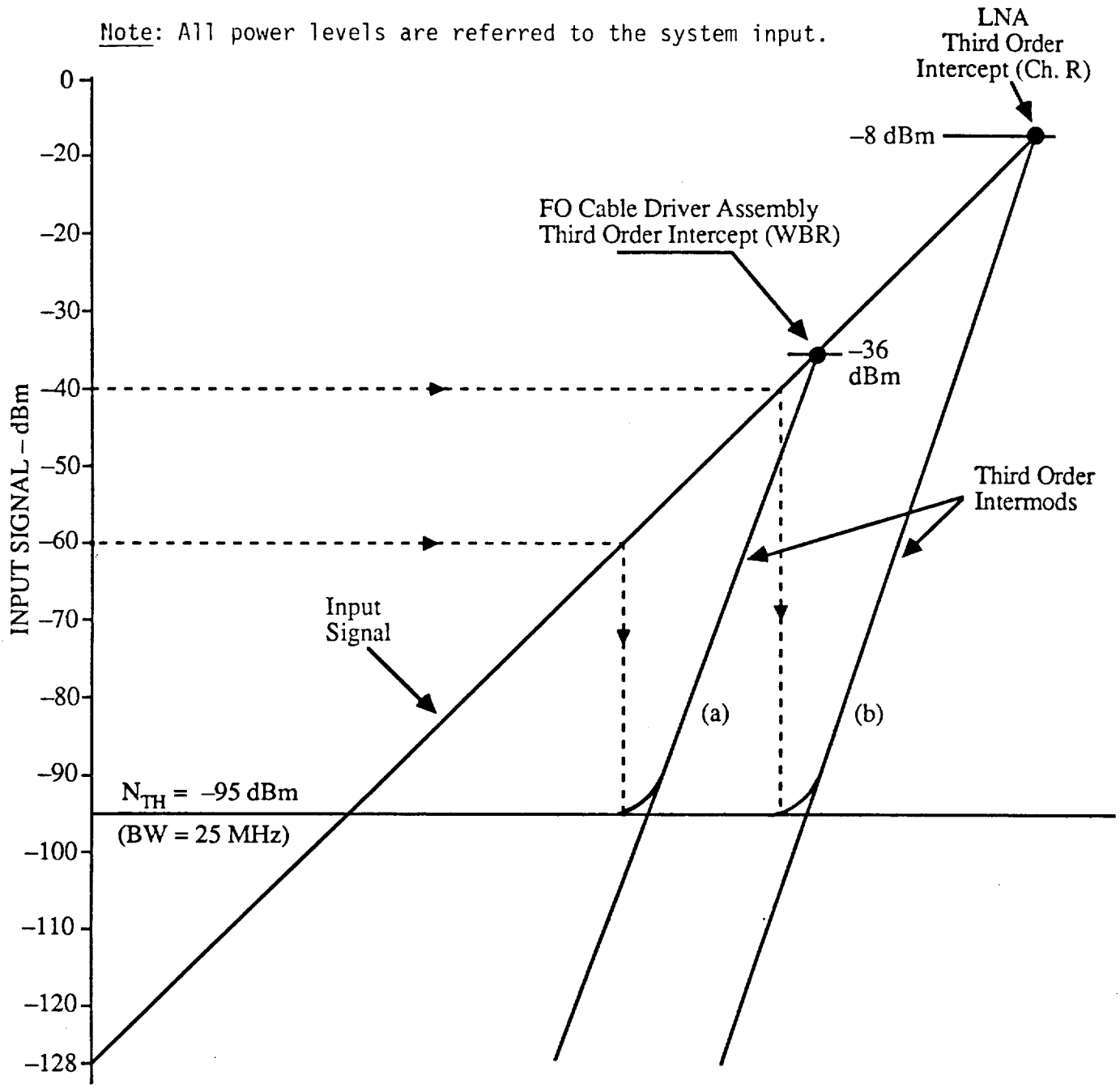

Figure 2. Third Order Intermods for (a) Wideband Receiver and (b) Channelized Receiver.

order intercepts are different for the two receiver architectures. It can also be seen from this figure that a channelized receiver can, at least in principle, accommodate a 20 dB higher level of the input signals before the internal generation of the third-order intermods. This capability is due to the channelized AGC available with a channelized receiver.

Because of the potential advantages of the channelized receiver, this configuration was adapted as a baseline for subsequent analysis to determine the power control window capabilities and limitations of the Space Station receiving system. Of particular significance was the analysis of the FO cable link capabilities.

Based on a practical model of an FO cable link, it was established that the basic limitation for the power control window is the FO cable loss which causes the degradation in the system SNR at the optical receiver. In view of this degradation, it is estimated that a power window for the high SNR users, such as EMU and MSC-3,* may be limited to 10 dB. For the lower SNR users, such as FF and OMV, the power control window of up to 15 dB appears feasible. Figures 3 and 4 show how the FO cable loss affects the system SNR transfer curve.

However, a conservative recommendation is a 6 dB ± 3 dB power control window with a channelized receiver. The "flattening" of the curve at the higher input SNR means that it is more difficult to estimate with accuracy the large SNR values which are the result of the increasing signals due to the range closure. This is based on a baseline assumption that the power control signal is developed at the coherent demodulators located at the receiving end of the FO cable link.

The possibility of using a PIN diode to control the power input to the user's transmitter, and thus control the output EIRP, was examined. It was determined that 60 dB of power control can be obtained in this manner without antenna switching. Figure 5 shows a functional block diagram for this viable concept.

* A three channel 8-PSK system.

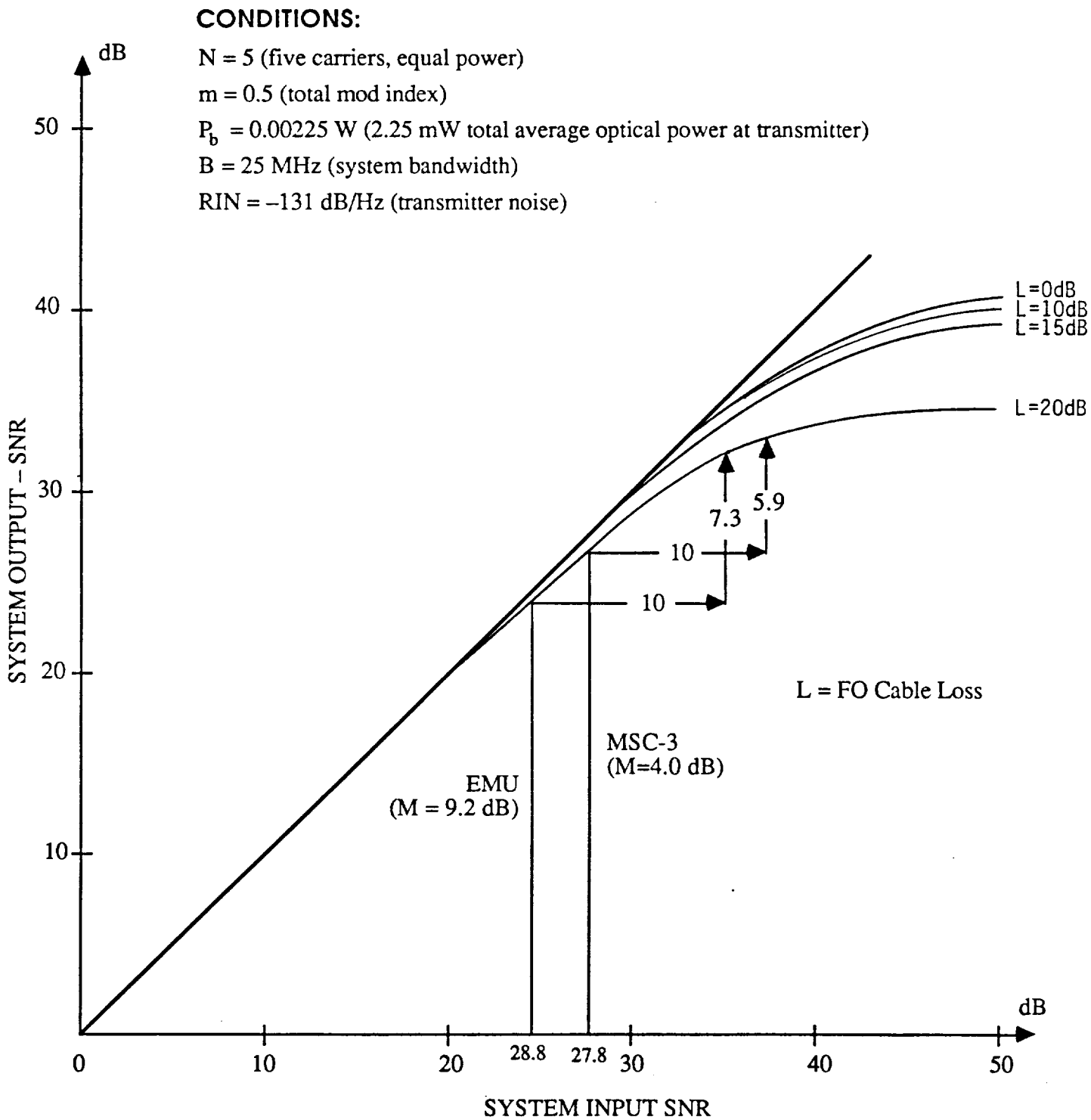

Figure 3. System SNR Transfer Curve as Function of FO Cable Loss (EMU and MSC-3 Power Control Window of 10 dB).

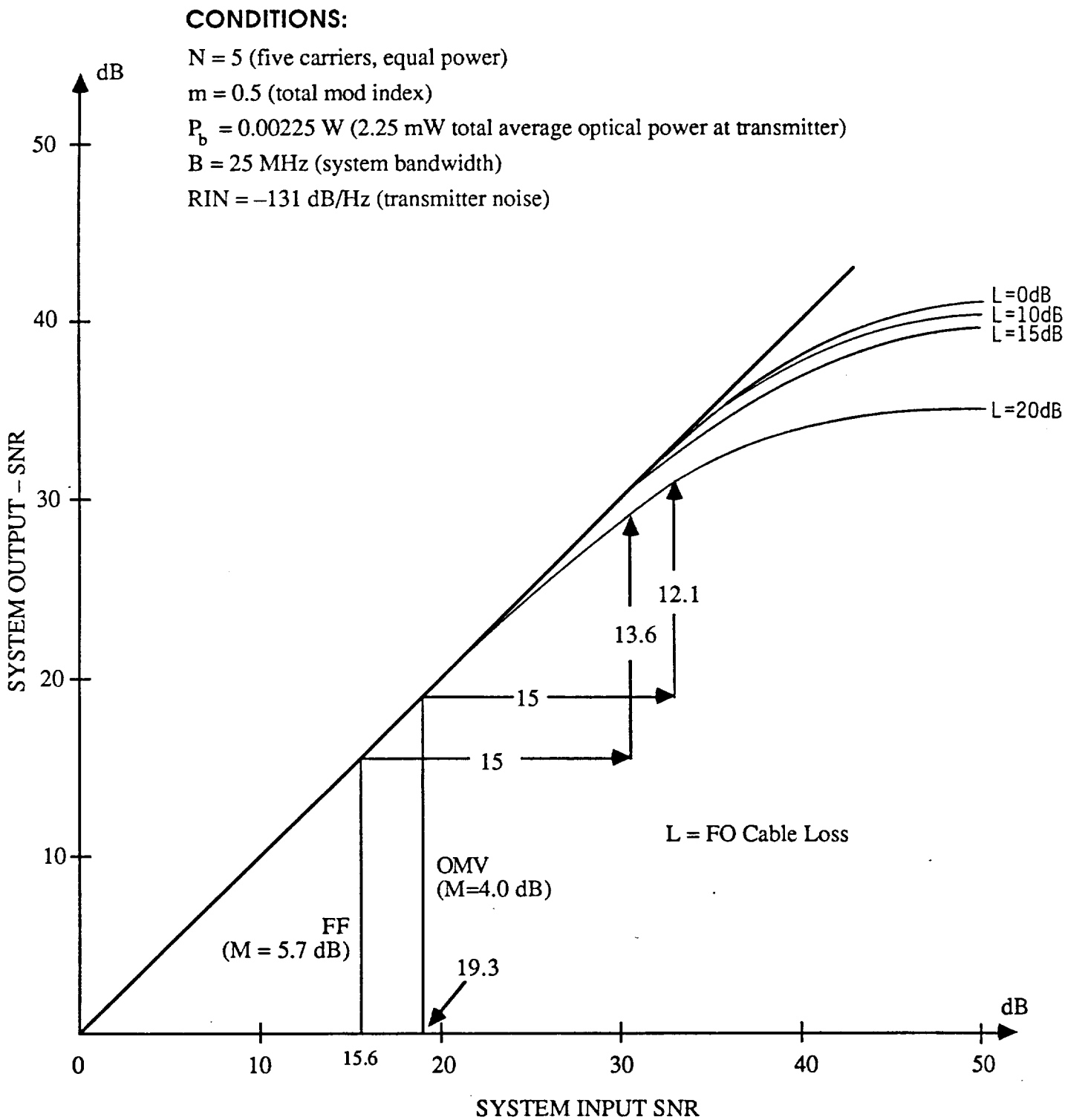

Figure 4. System SNR Transfer Curve as Function of FO Cable Loss (FF and OMV Power Control Window of 15 dB).

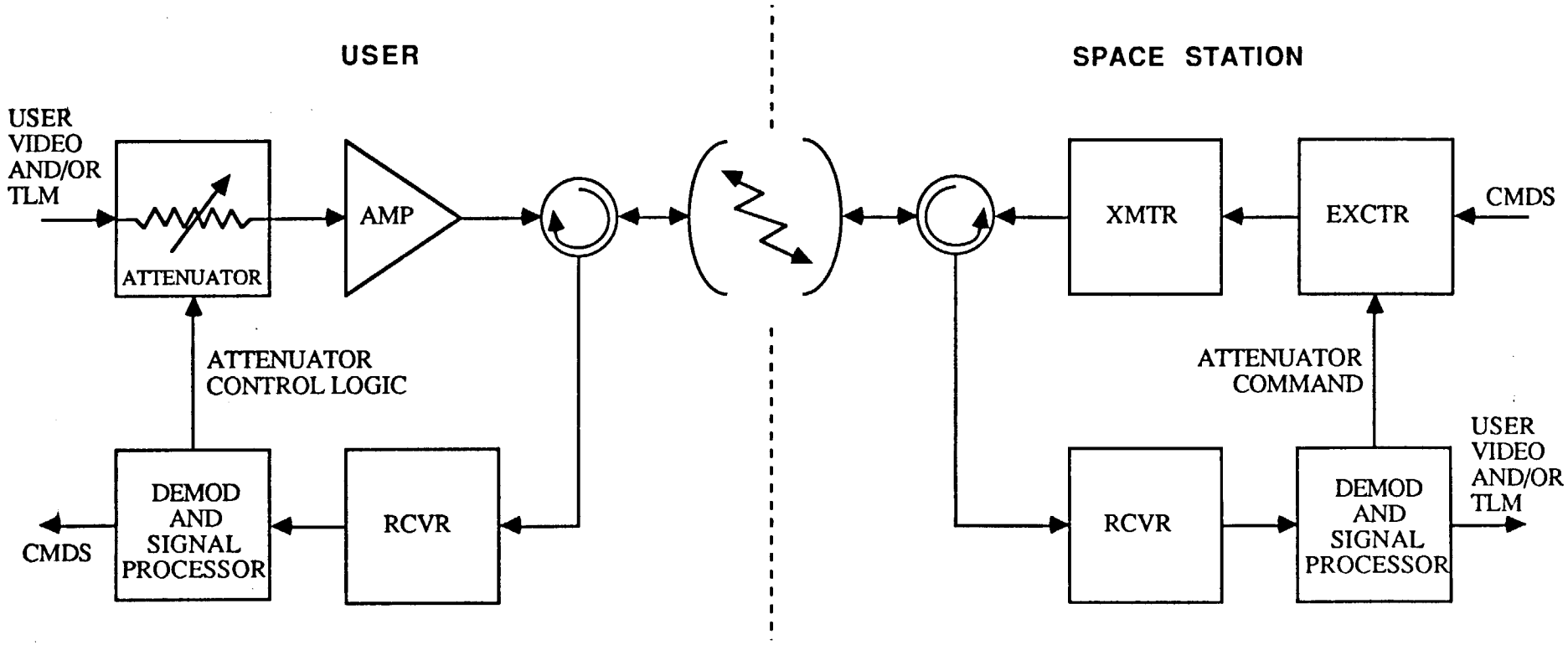

AMPLIFIER:

- Solid State
- 1 watt @ 14.5 — 15 GHz
- Gain = 30 dB
- NF = 10 dB
- SNR_{max} = 77 dB
- SNR_{min} = 17 dB

ATTENUATOR:

- PIN Diode
- 0 — 60 dB
- Continuous

Figure 5. Functional Block Diagram for User Power Control.

1.0 INTRODUCTION

The subject of this report is the return link power control for the user segment of the Space Station's Ku-band multiple access (MA) system. The motivation for the power control is due to the following factors:

(1) the baseline configuration for the return link(s) is the frequency division multiplexing (FDMA),

(2) there is a large spread between the signal levels received by the Space Station from the users at the maximum and the minimum ranges,

and (3) the limitations of the dynamic range capabilities of the Space Station's RF receiving and the IF distribution components.

Figure 1-1 illustrates a functional scenario for the Ku-band MA system's return link power control. As shown in the figure, a number of users may be transmitting to the Space Station simultaneously from different ranges. In some cases, they may be transmitting to a common antenna. In other cases, they may be transmitting to different antennas and yet their signals may be combined in either a common RF or a common IF equipment.

Figure 1-2 shows the signal power received at the Space Station from various users as a function of user range and signal modulation. From the figure it is evident that a power differences of as much as 90 dB may exist. For example, a telemetry received signal from a free flyer (FF) at 2000 km may be at about –105 dBm while a video signals received from another FF at 1 km may be at about –14 dBm.

It must be pointed out, however, that just because one signal is far above the other, it does not mean that there will be an interference to the weaker signal. A great deal depends on such factors as the return link frequency plan, adjacent channel filtering at the user transmitter and the receiver configuration at the Space Station. Of more direct concern is the near/far problem which may exist for the users within the same transmission band and serviced by the same antenna.

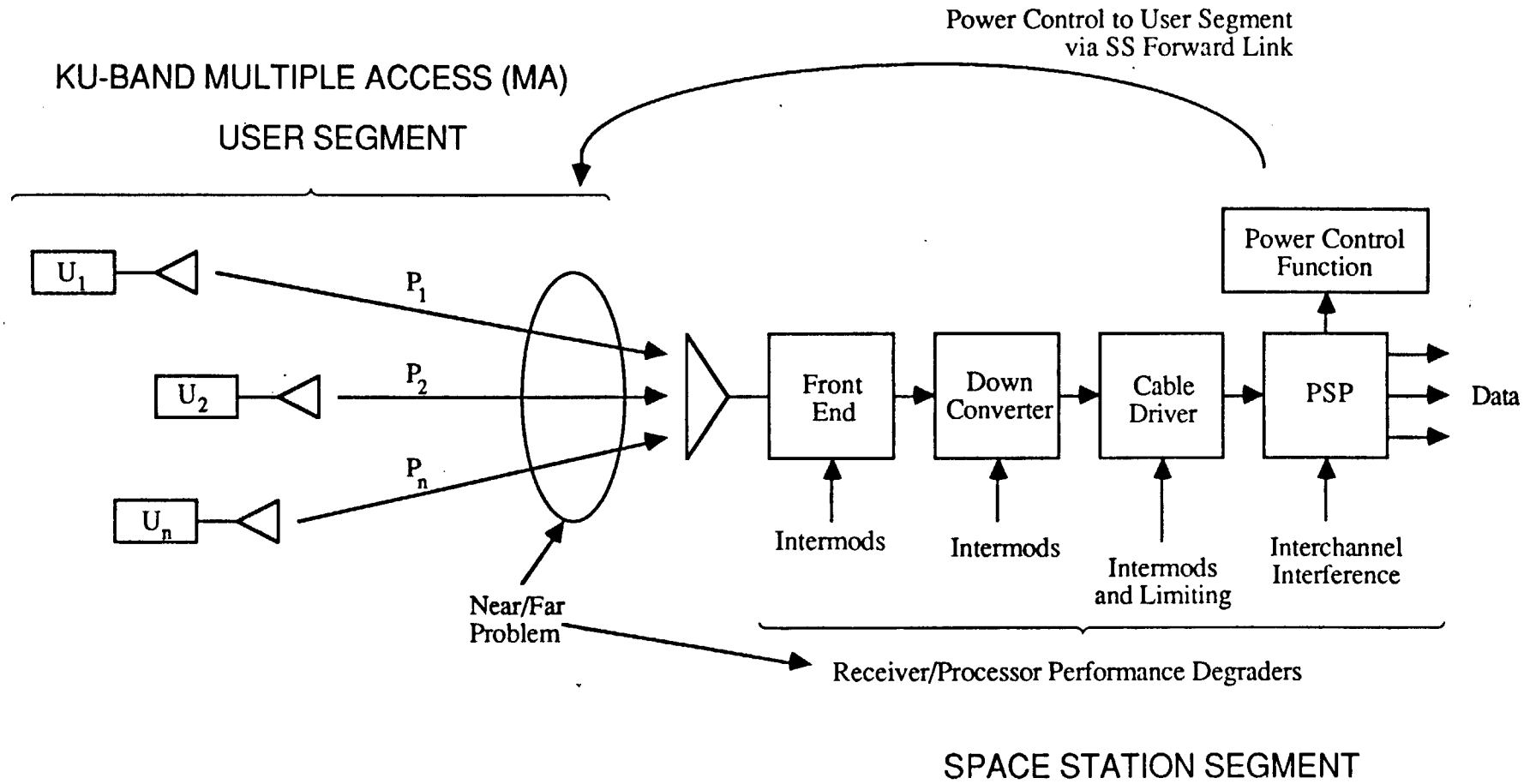

Figure 1-1. Power Control Functional Scenario.

Figure 1-2. Power Received at Space Station from Various Users as Function of Range.

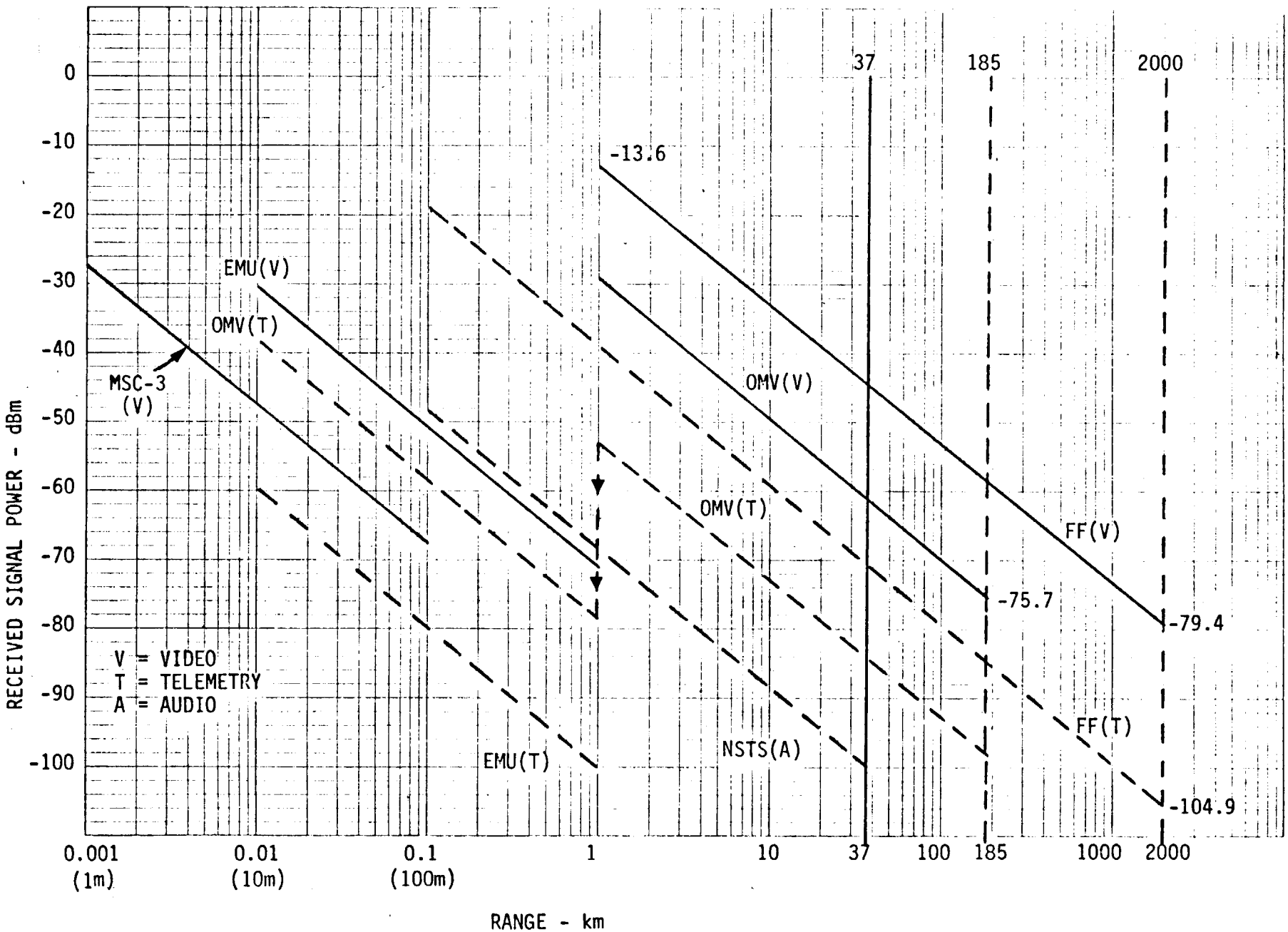

ORIGINAL PAGE IS
OF POOR QUALITY

The near/far problem, if not alleviated by the user power control, may lead to a performance degradation of the Space Station's receiving and signal processing equipment. This degradation may be in the form of:

(1) intermodulation products generated in such receiver elements as the front end, the down converter and the cable driver.

(2) interchannel interference in both the receiving and the signal processing equipment,

and (3) signal limiting in various element of the receiving equipment, particularly the drivers which feed either the RF/IF or the optical signal distribution cables.

The power control function can be implemented by sensing either the power levels of the received signals or their signal-to-noise ratio (SNR) and then using this information to send the power control commands to the users via the forward link. The required information can be obtained from the received signals on either an absolute basis, or a relative basis, or some combination of both. In this report we baseline a method for measuring the SNR of the received signals and using this information to implement the power control.

The degree to which the power, or more generally the EIRP, is to be controlled depends on a tolerable "power window" at the Space Station. Different criteria influence the power window in a different way. The criteria for the interchannel interference may be different from the criterion dictated by a limitation in the dynamic range of an optical cable driver. For example, a 2 or 3 dB power window may satisfy most of the criteria and thus eliminate most of the performance degraders. On the other hand, imposing on the users a power control within such narrow limits will increase the complexity of user's transmitting equipment.

In the material which follows various criteria for the power window are examined and various implementation tradeoffs are discussed.

2.0 TECHNICAL CONSIDERATIONS

2.1 Received Signal Spread

In this section we take a closer look at the significance of the signal level spread due to the near/far problem. For the purpose of discussion, we will consider primarily the video link signals and we will assume that a similar argument holds for the narrowband signals, i.e., the telemetry and the digital audio.

Table 2.1-1 summarizes the signal level characteristics of the Ku-band video return links. Of particular note in this table are the minimum signal-to-noise ratios of the different users. It must be noted that the spread in SNRs ranges from 15.6 dB (FF) to 27.8 dB (MSC-3). This represents a spread of about 12 dB. The spread of the margins, however, extends only from 4.8 dB (MSC-3) to 9.6 dB (EMU), i.e., a difference of less than 5 dB. If the margins are reduced to zero, then there is a spread in SNR of 13.2 dB.

The point that we are making here is that because of the nature of the links, it is not possible to equalize the working SNRs of these different signals. Neither is it possible to equalize the margins. This means that when a combination of signals from various users appear at the same antenna, there will be an unavoidable spread in signal levels which is not a function of range. Also, the criteria for power control may have to be different for different links because of this intrinsic difference. As a result, the power control algorithm may have to be tailored to each user.

Figure 2.1-1 shows video link signal levels and the corresponding margins as the function of the range.

USER	R_{max} (km)	R_{min} (km)	P_{min} (dBm)	P_{max} (dBm)	ΔP (dB)	SNR (min) (dB)	Margin (min) (dB)	User G_A (dB)	Station G_A (dB)	Zero Margin Min. SNR (dB)	Zero Margin C/N_0 (dB)
FF	2000	1	–79.4	–13.6	66	15.6	5.8	30.3	46.3	9.8	83.8
OMV	185	0.1	–75.7	–10.4	65.3	19.3	4.1	13.3	46.3	15.2	89.2
EMU	1	0.01	–70.2	–30.2	40	24.8	9.6	3	24.3	15.2	89.2
MSC–3	0.1	0.001	–67.2	–27.2	40	27.8	4.8	3	3	23.0	97

Table 2.1-1. Signal Level Characteristics of Ku-Band Video Return Links.

Figure 2.1-1. Video Link Signal Levels and Margins as Function of Range.

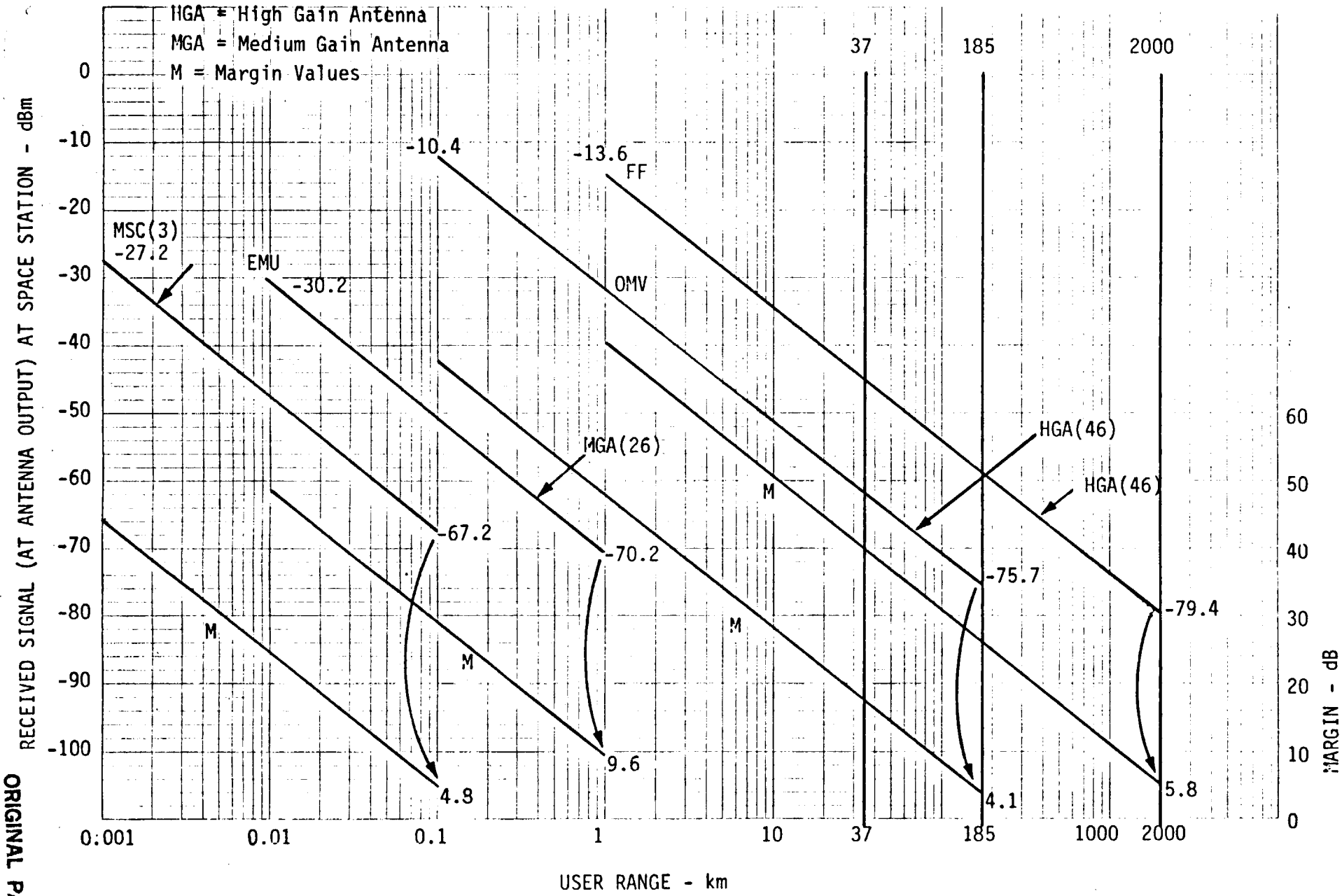

ORIGINAL PAGE IS
OF POOR QUALITY

2.2 The Effect of Receiver Implementation on System Intermods

2.2.1 Wideband Ku-Band Receiver

Figure 2.2.1-1 shows a wideband Ku-band receiver implementation.* The salient feature of this implementation is a single wideband downconversion of the entire return link band (300 MHz wide) to a wideband IF. As shown, the output of the downconverter extends over a bandwidth of 450 to 750 MHz. Each antenna of an antenna group is connected to a separate receiver which in turn connects to its own FO cable driver.

The main advantage of this approach is the simplicity of the Ku-band receivers. Each receiver consists of a wideband (300 Mhz) bandpass filter, followed by a low noise amplifier (LNA), which in turn is followed by a wideband downconverter. The function of the bandpass filter is to restrict the signals applied to the LNA to only those within the MA return link band and to provide the image rejection. The low noise amplifier provides the gain required to maintain a low noise figure despite the downconverter loss. The output of the downconverter is then increased by a fixed gain which is tailored to provide the required input level to the cable driver.

At the other end of the FO cables, the signals are detected by FO receivers and applied to an IF switch matrix. This matrix permits any antenna to be connected to any PSP unit. Channel separation and bandpass filtering takes place in the PSP units. Thus, the intermodulation can occur at any point within the receiver/FO cable driver chain. Because there may be several signals received simultaneously by any one antenna at any time, it is important to maintain a high degree of linearity in this receiver in order to keep the IM interference at tolerable levels.

Of specific concern is the effect of the third order intercept which is due to the FO cable driver assembly. This intercept is reflected to the system input at a level of about –36 dBm. The effect is shown in Figure 2.2.1-2. In this figure all of the levels have been

* This approach is being considered by the McDonnell Douglas team.

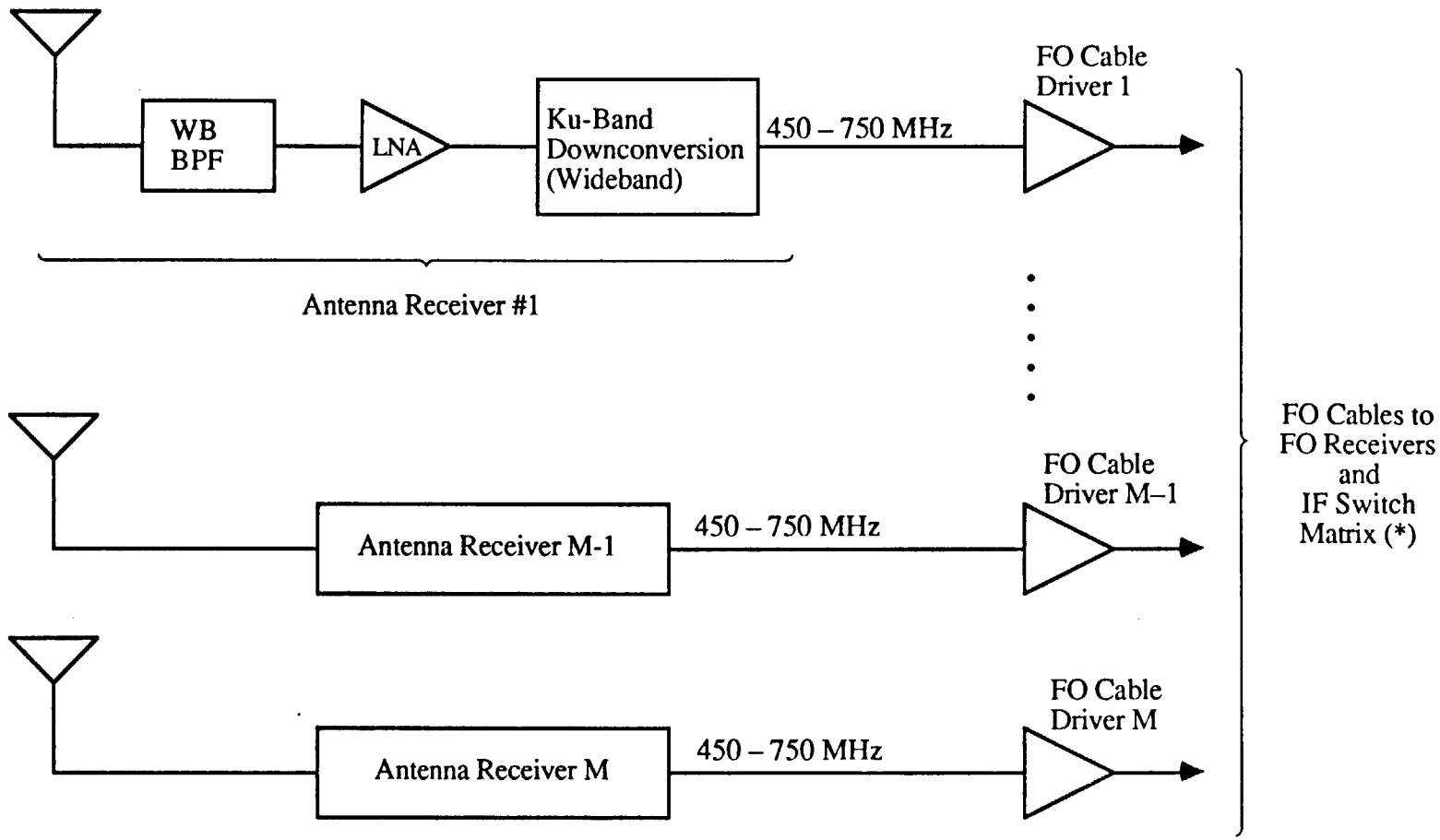

*IF switch matrix cross-connects receivers and PSPs.

Figure 2.2.1-1. Configuration with One Wideband Receiver and FO Cable per Antenna.

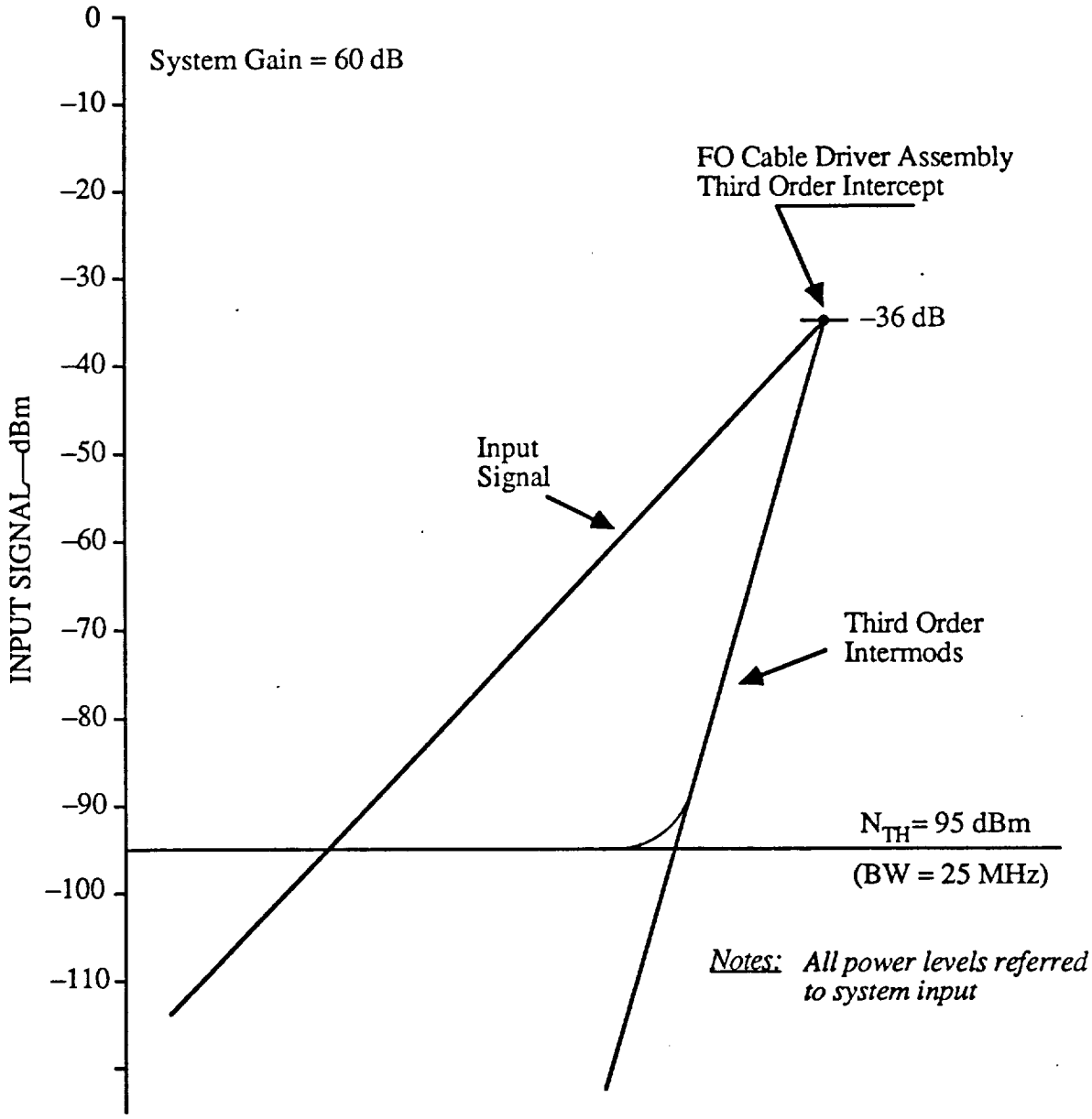

Figure 2.2.1-2. Wideband Receiver Third Order Intermodulation as Function of Input Signal.

normalized to a bandwidth of 25 MHz which is typical of a digital video link. From the figure it is evident that as the input signals increase above –60 dBm, the intermodulation products begin to rise above the thermal noise in the 25 MHz bandwidth.

Figure 2.2.1-3 shows the channel degradation due to the third order intermodulation as the function of the input signal level. This figure shows that to keep the degradation below 0.5 dB, the received input signal level should not exceed –59 to –60 dBm. This requirement places a rather stringent demand on the user power control.

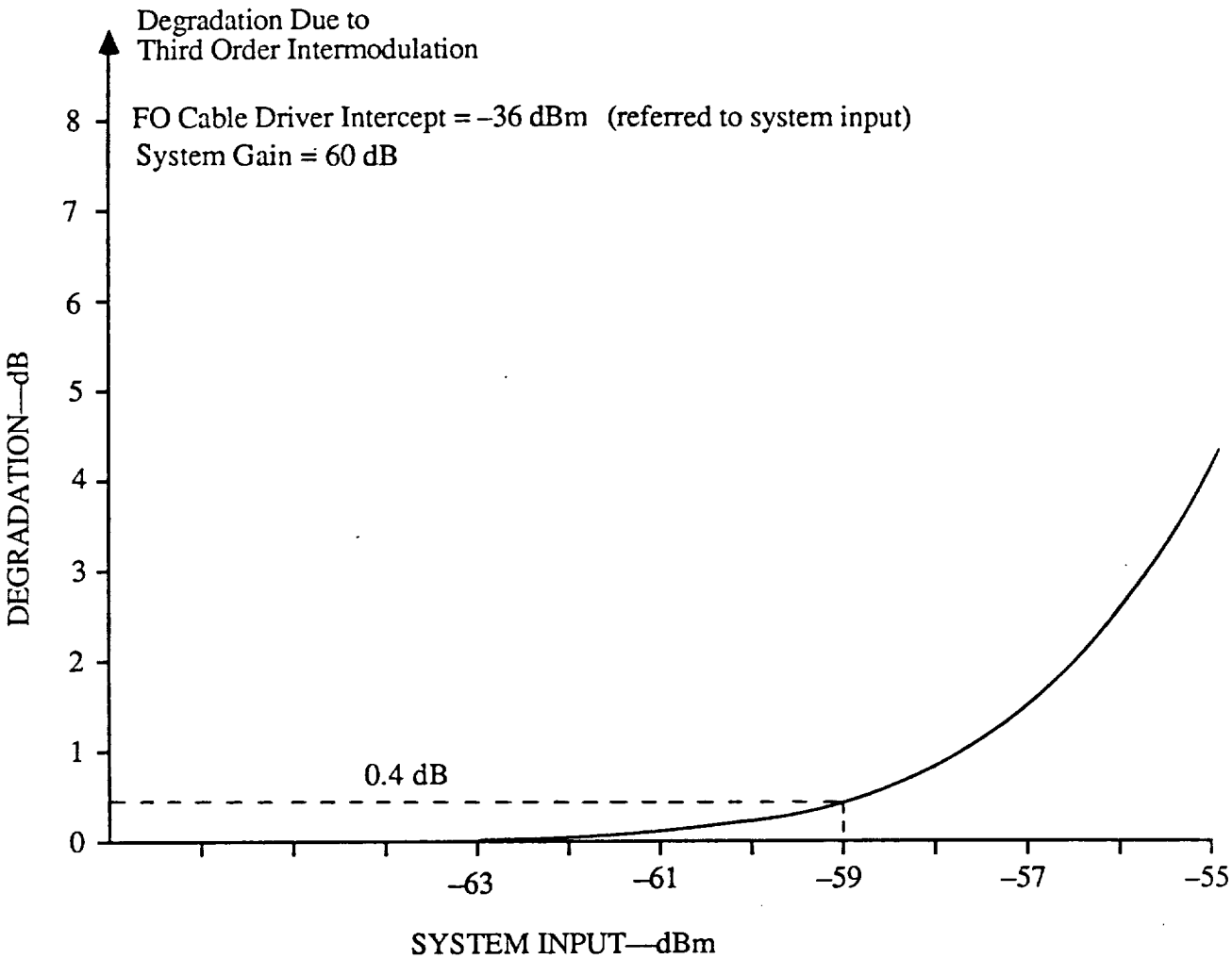

Figure 2.2.1-3. Channel Degradation Due to Third Order Intermodulation in the Wideband Receiver.

2.2.2 Channelized Ku-Band Receiver Implementation

Figure 2.2.2-1 shows a group of antenna receivers which have a capability to amplify selectively the individual channels of the return link band.* This capability is provided by implementing each antenna receiver with several parallel receivers. The number of parallel channel receivers in each antenna receiver is equal to the total number of channels in the return link band (or bands).

As shown in the figure, each antenna is connected to a wideband bandpass filter followed by an LNA. The LNA is connected to an N-way power divider. The N output ports of the divider feed N channel receivers. Each channel receiver has its own downconverter (not shown) and at least one, or possible two, IF amplifiers.** Thus, the channel receivers can be tuned to the signals picked up by a particular antenna. Similarly, the return channels picked up by other antennas are applied to their respective channel receivers. The outputs of all M antenna receivers are then combined and applied to the cable driver.

The advantage of this receiver implementation is that once the received signals are separated into the individual frequency-selective channels, the levels of these signals can be controlled by AGC prior to the summation at the input to the cable driver. Such control provides two following features: (1) the levels of different received signals can be "equalized" at the input to FO cable driver and (2) the signal levels can be held at a relatively constant level despite signal increase due to range closure.

The availability of a channelized AGC prior to the FO cable driver implies that, at least in principle, the input signals can vary over a wide range of power levels, before the intermodulation becomes a problem.

---

* This approach is being considered by the Rockwell International team.

** The detailed architecture of the channel receivers is not addressed here. These receivers may be either single conversion or double conversion type.

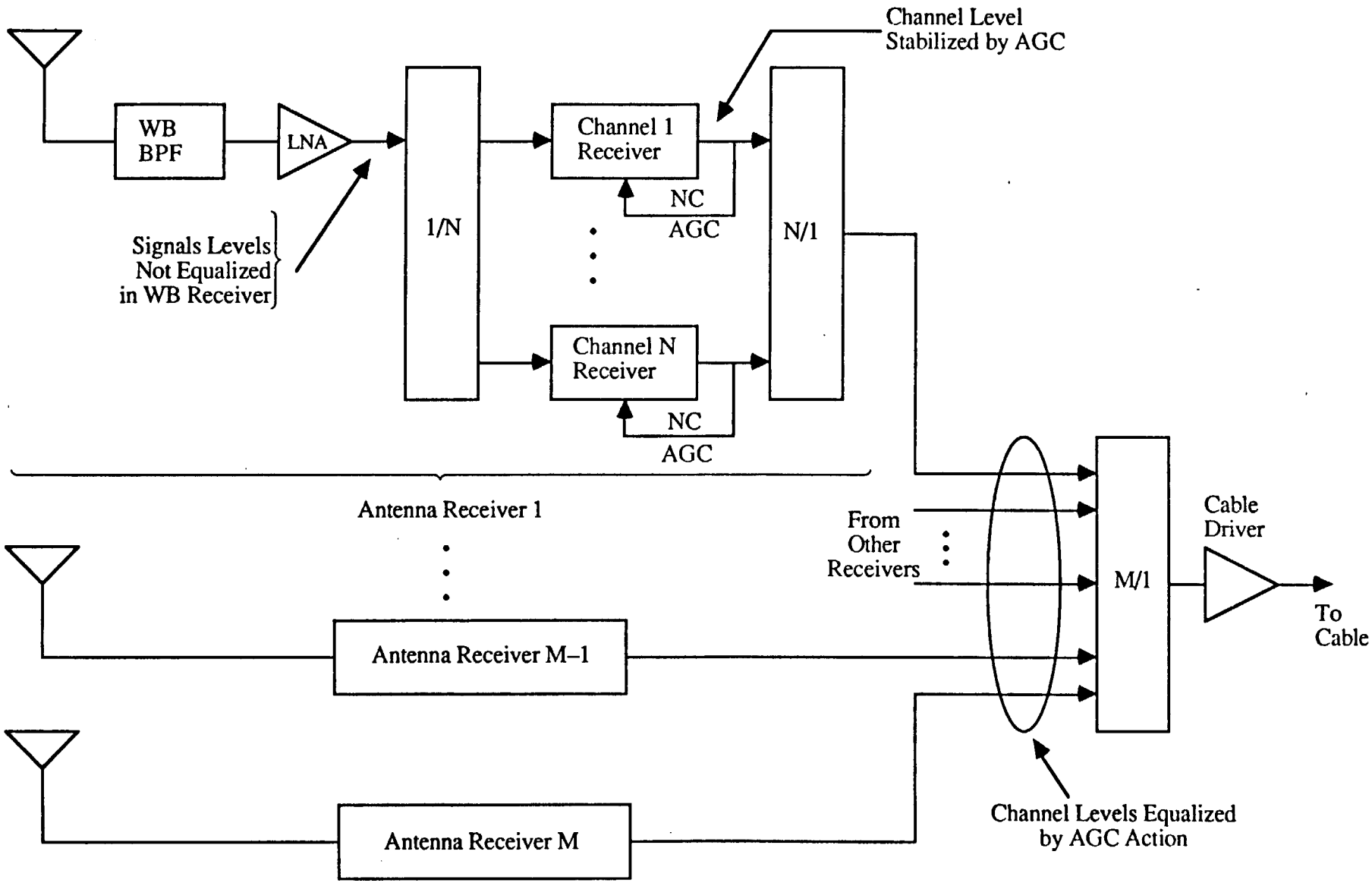

Figure 2.2.2-1. Channelized AGC Equalizes Signal Levels into the Cable Driver.

It is important, however, that the circuitry preceding the line driver is not overloaded by the received signals prior to the frequency selective channelization. This requirement is due to the fact that the LNA and the downconverters of the channel receivers are wideband and thus have a limited dynamic range compared to the channel receivers. Consequently, the power control is still required but its function is primarily to reduce the interchannel interference due to spectrum sidelobes and to prevent intermodulation in the wideband LNA and the downconverters.

With the channelized receiver, it is reasonable to assume that the primary source of the intermodulation distortion is the LNA unit where all the channels are amplified on a broadband basis. Figure 2.2.2-2 shows the third order intermodulation level originating in the front end (LNA) portion of a channelized Ku-band receiver. Figure 2.2.2-3 shows the degradation, on a channel basis as function of the input signal level. Comparing this figure to 2.2.1-3, we can see that the channelized receiver can accommodate about 20 dB more input signal level than the wideband receiver. This means that, at least in principle, a wider power control window can be tolerated with a channelized receiver. This, of course, is based on the assumption that a channelized power level equalization takes place ahead of the FO line driver.

The disadvantage of the channelized approach is the relative complexity of the antenna receivers. This disadvantage may be offset by the intrinsic component redundancy provided by the availability of several channel receivers within each antenna receiver. Thus, if one channel receiver fails, another may be used in its place.

Although a noncoherent AGC is shown in Figure 2.2.2-1 for the purpose of functional clarity, such AGC may not necessarily be the final choice, and a coherent AGC may be called for this application.

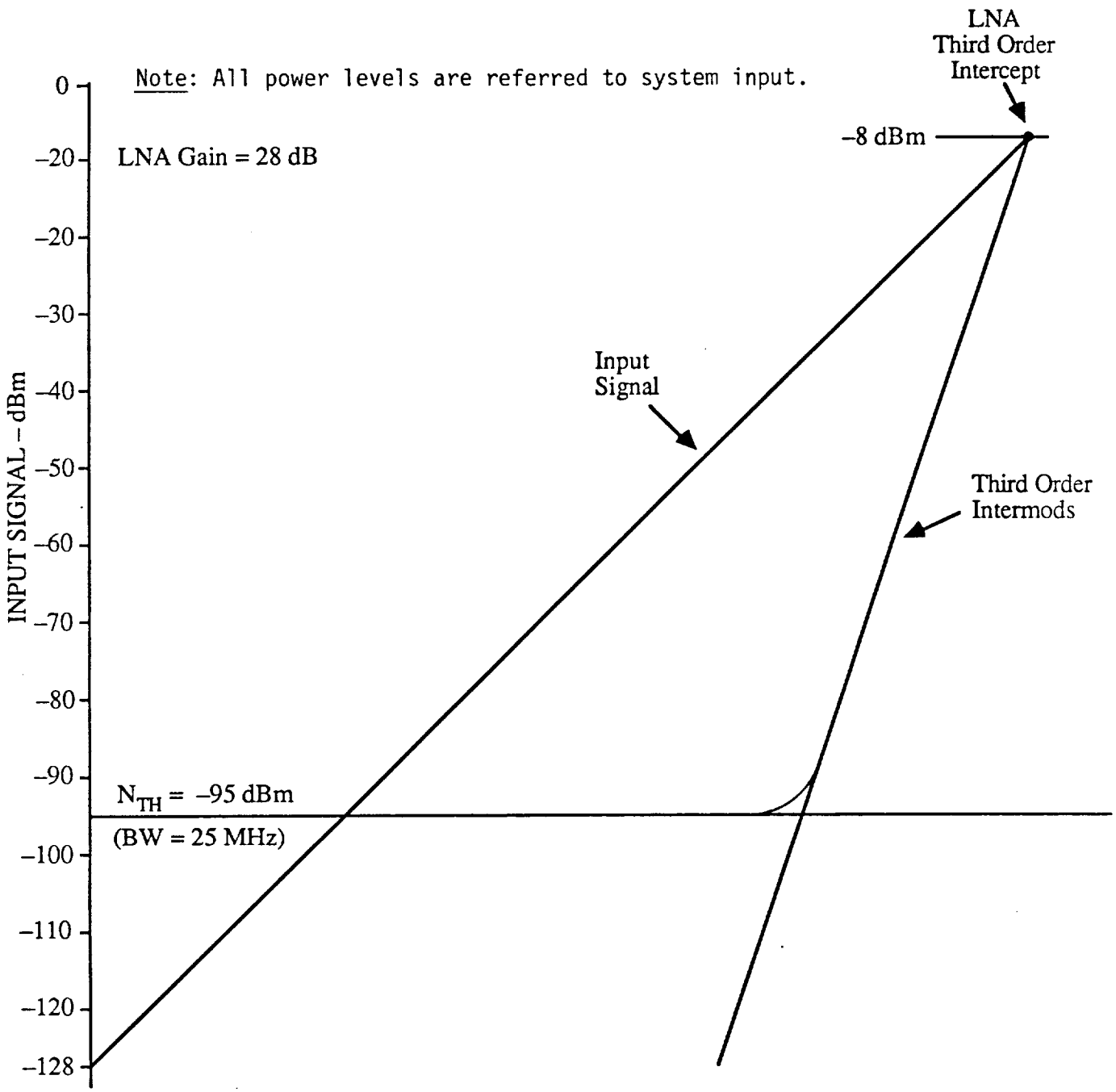

Figure 2.2.2-2. Channelized Receiver Front End Third Order Intermodulation as Function of Input Signal.

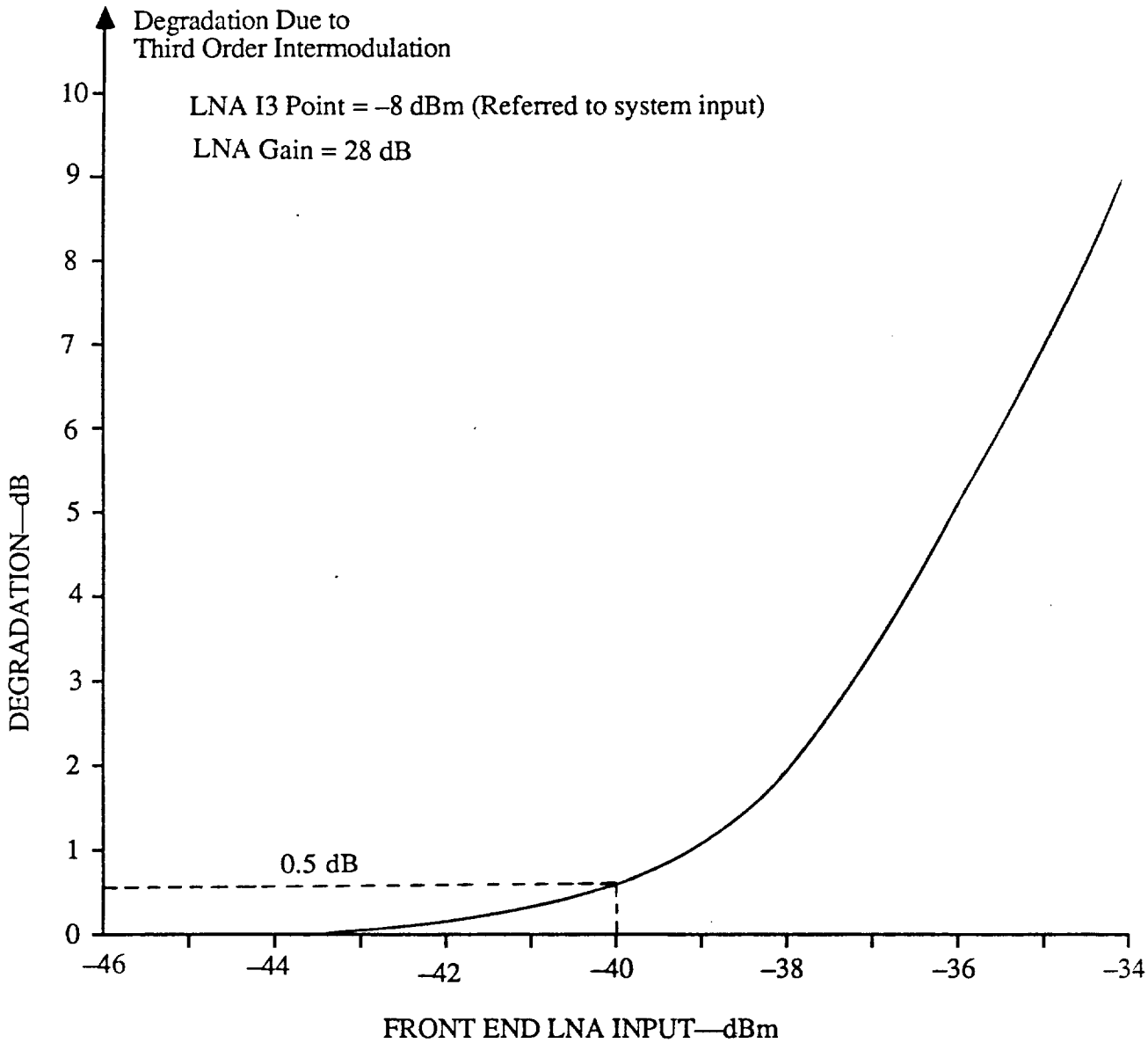

Figure 2.2.2-3. Channel Degradation Due to Third Order Intermodulation in Front End LNA as Function of Signal Input to a Channelized Receiver.

2.3 Cable Driver Considerations

The dynamic range of signals applied to either an RF/IF or a FO cable driver is among the factors, which must be taken into account when specifying the degree of power control. The specific effects to consider in this case are the intermodulation products and a limited dynamic range of practical cable drivers. However, as explained in the preceding sections, the architecture of the Ku-band receiver ahead of the cable driver influences to a great degree the interaction between the capabilities of the driver and the power control requirement. For example, if channel separation is provided prior to the cable driver, then such means as AGC can be used to equalize the levels of different channels at the input to the driver. With the spread in signal levels reduced in this manner, the requirements for the power control can be relaxed somewhat without seriously impacting the performance of the cable driver unit.

In this report we are baselining an FO cable driver such as General Optronics Corp. Model GO DIP 1000 or equivalent. Presented below are the factors which determine the tradeoffs between the drivers capability and the power control requirements.

2.3.1 FO Cable Driver Functional Diagram Description

Figure 2.3.1-1 shows a functional diagram of an FO cable driver. We constructed this diagram based on the information available to us from the data sheets on the GO DIP 1000 laser module. As shown in the figure, an RF/IF amplifier supplies RF power to an RF to optical power converter which in this case is an injection laser diode. The laser diode is biased into the conduction region by the bias current. In the absence of the RF modulation, the laser diode emits an optical power which is proportional to the bias current. When the RF power developed by the driver amplifier is applied to the laser diode, the bias current following through the diode is amplitude-modulated at the RF/IF rate. This results in an intensity modulation which is propagated along the FO cable and is detected at the other end by an appropriate photo-detector. The optical limitations of the FO cable driver shown arise from the following:

(1) Third order intermodulation

(2) Maximum power clipping

and (3) Optical noise.

In addition to these optical limitations, there is a limitation contributed by the 3rd order intermodulation generated in the RF driver amplifier.

The optical limitations are functions of the bias current. If the bias current is increased, the allowable optical modulation is reduced, but the optical noise is also reduced, which is a desirable factor. Also, when the allowable modulation is decreased, the maximum clipping can be reached with a smaller RF signal, a result which is undesirable from the standpoint of obtaining a maximum dynamic range out of the optical power converter (i.e., laser diode). Thus, finding an optimum operating print for a laser diode becomes an important consideration.

Furthermore, the intermodulation contributed by the driver amplifier is an important factor. In most cases it is this intermodulation which limits to the dynamic range of an FO driver. For example, if the third order intercept of the driver amplifier is at 24 dBm and the

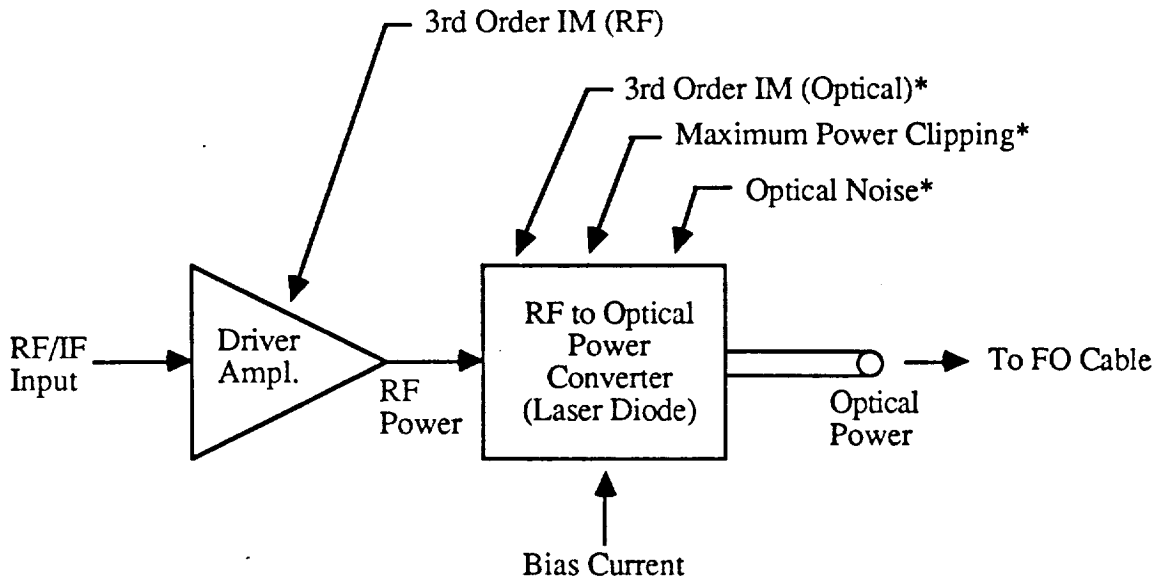

*Function of Bias Current

Figure 2.3.1-1. FO Cable Driver Functional Block Diagram.

system gain, including the gain of the driver amplifier, is about 60 dB, this third order intercept is reflected to the system input as a –36 dBm intercept. Consequently, it becomes evident that such factors as laser diode bias current and the system gain are some of the parameters which have to be optimized before the actual capabilities of an FO line driver are established.

2.3.2 Optimizing System Gain Ahead of the FO Line Driver

Figure 2.3.2-1 shows the optical driver output as the function of the system gain preceding the optical driver. As is shown in the figure, there is a certain fixed level of the optical noise which is delivered by the optical driver to the optical cable. This level (–51 dBm) is based on the optical noise density of –125 dBm/Hz in a 25 MHz bandwidth. This noise is the relative intensity noise (RIN) and is a function of the laser diode.

On the upper end, the maximum modulated signal out of the optical element is limited at about –2.7 dBm which corresponds to 50% modulation with respect to the 3mw peak unmodulated output of the laser diode. The maximum modulated signal is the function of the bias current, which in this case is assumed to be set to allow for 50% optical modulation.

For low values of system gain, the desired signals are degraded by the optical noise (i.e., RIN) of the laser diode. As the system gain is increased, the received signals and the thermal noise are amplified until the thermal noise exceeds the RIN. At about 60 dB of system gain, the degradation due to the RIN is only 0.1 dB. From this point on any additional gain reduces the dynamic range of the optical driver.

Thus, from Figure 2.3.2-1, it is evident that the dynamic range of the optical driver can be traded off for some degradation in the link margin. This degradation would come from operating the system at some lower gain, say 50 dB, where the degradation due to the contribution from the RIN is about 1 dB. At system gain below 40 dB, the margin degradation increased inversely proportional to system gain as the received signals get buried in the RIN. This is shown in Figure 2.3.2-2.

The SNR of the received signal must be also considered when determining the system gain. As shown in the figure, the SNR of 15.6 dB (FF) can be handled by a gain of about 76 dB while that of 27.8 dB (MSC-3) needs a reduced gain of about 64 dB to avoid clipping. But, as has been said earlier, there is a need to increase the system gain above the point at which the optical noise contribution is negligible. Thus, the discussions that follow will assume a baseline minimum value of system gain of about 60 dB.

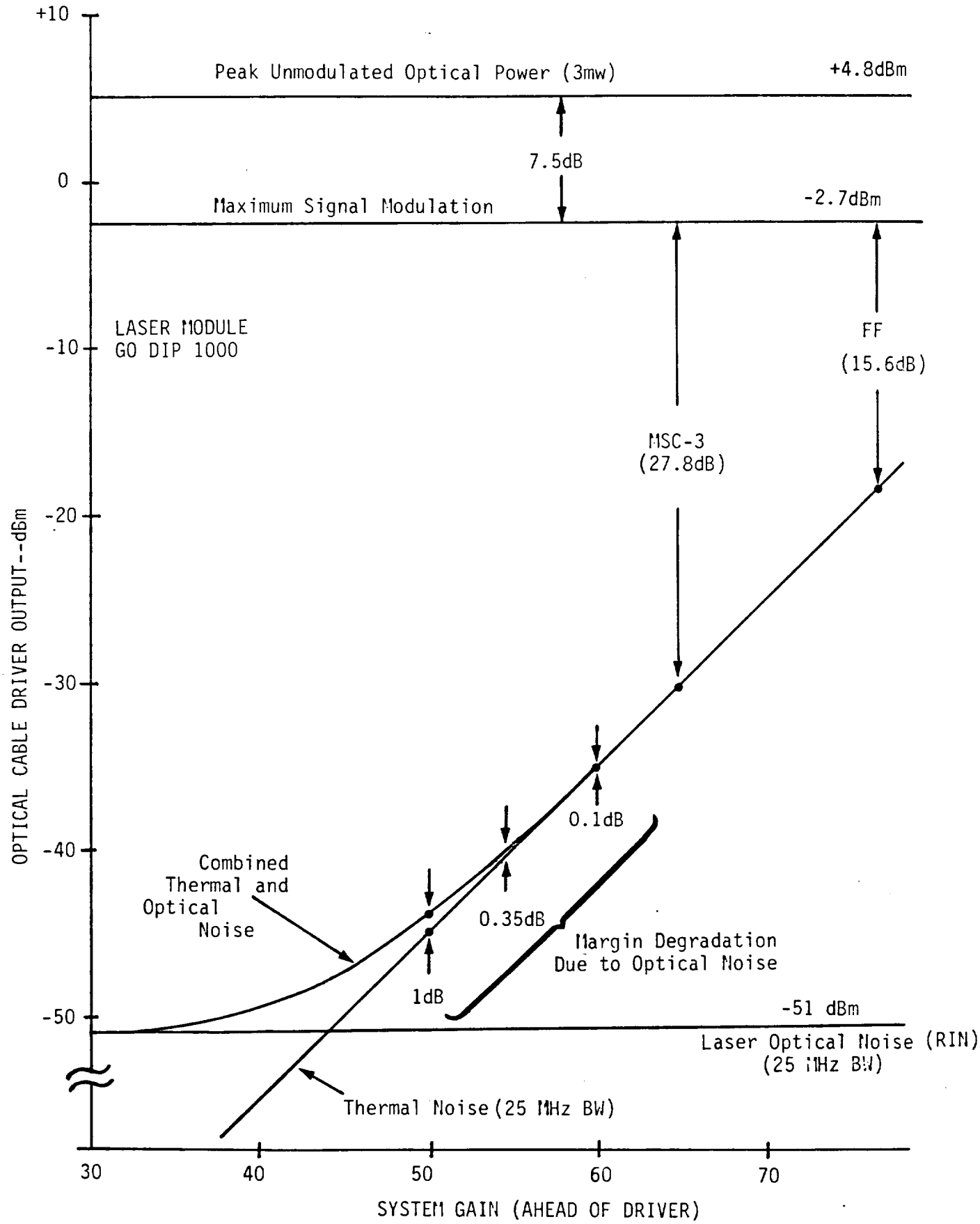

Figure 2.3.2-1. Optical Driver Output as Function of System Gain Preceding the Driver.

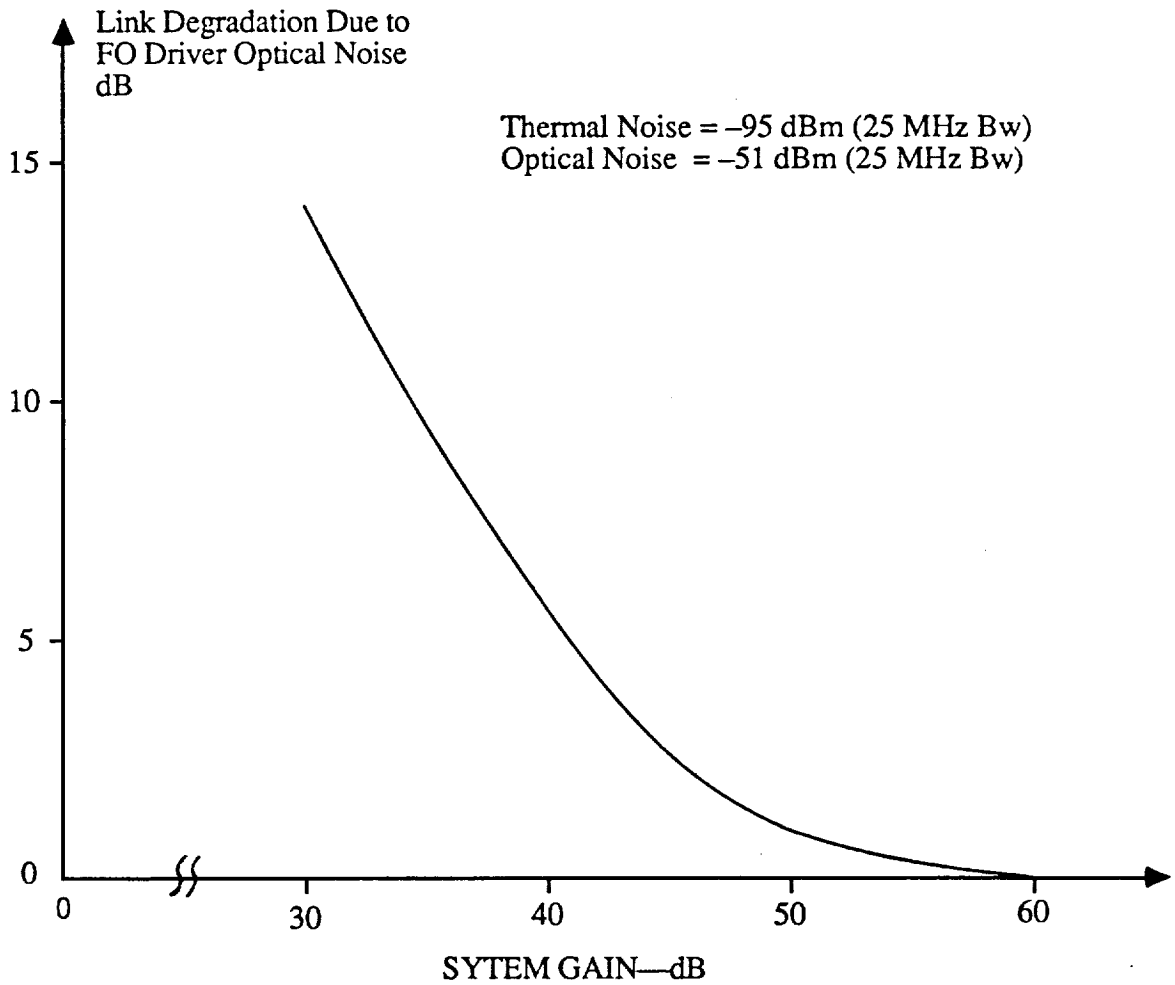

Figure 2.3.2-2. Link Degradation Due to FO Driver Optical Noise (RIN) as Function of System Gain Preceding the Driver.

2.4 Power Control

In this section we explore the various aspects of the power control. Specifically, we consider how the receiver implementation at the Space Station impacts the power control "window".

2.4.1 Power Control for a Wideband Receiver

In this section we will consider a baseline power control window for a wideband receiver such as shown in Figure 2.2.1-1. We will consider the effect of a particular power control window on the operation of the FO cable driver as it is influenced by the wideband nature of the receiver preceding the driver.

As shown in Figure 2.2.1-1, each wideband receiver is dedicated to a single antenna and it feeds a single cable driver. Thus, only the signals picked up by a particular antenna are applied to a related FO cable driver. However, an antenna may be receiving signals from different users at different ranges. For example, signals from OMV and FF may be picked up by the same high gain (46.3 dB) antenna at their extreme ranges. Thus, they will appear together at the output of the same FO line driver. Also, signals from an MSC-3 and an EMU may be picked up by the same hemi antenna. This may happen when the reception from an EMU is switched from the medium gain (24.3 dB) antenna to the reception by a hemi (3 dB) to permit a close-in operation. If this switch-over occurs at a range of about 60 meters, the margin for the reception from the EMU will be about the same as the margin for the reception at 1 km.

At this point let us baseline a 3 dB power control window and determine what effect this window has on the system operation. First, we must consider the third order intermodulation intercept referenced to the system input. As shown in Figure 2.2.1-2, this intercept is at –36 dBm, and the performance degradation resulting from this intercept is shown in Figure 2.2.1-3. From that figure we conclude that to keep the performance degradation at less than 0.5 dB the input signals should not exceed about –59 dBm.

Figure 2.4.1-1 shows the effect of a 3 dB power control on the video links received from the FF, OMV, EMU and MSC-3. As can be seen from this figure, the power control keeps all signals below the –59 dBm level with a margin of about 5 dB. Thus, there are no significant intermods due to the RF/IF circuitry of the wideband receiver. The signal level spread is 15.2 dB between the minimum (FF at 2000 km) and the maximum (MSC-3 at 1 meter) signals. This corresponds to the existing link budget spread in SNRs of these different users, i.e., 12.2 dB plus the power control window of 3 dB

Figure 2.4.1-2 shows the four received signals as they may appear at the output of the FO cable driver. In this figure all of the signals pertaining to the output of the cable driver have been referred to the system input by subtracting 60.5 dB of the system gain.* Thus, the +4.8 dBm (3 mw) value of the peak modulated optical power appears as –55.7 dBm in Figure 2.4.1-2. Other output-referenced signals are also reduced accordingly. Both the thermal and the optical noise are based on a channel equivalent noise bandwidth of 25 MHz (i.e., 74 dB-Hz).

From Figure 2.4.1-2, it is evident that even with a relatively narrow power control window of 3 dB, there is not much operating margin at the output of the optical cable driver. This is due to the fact that the SNRs of the four signals differ by about 12 dB in the 25 MHz bandwidth.

Of particular concern is the fact that the maximum signal of the MSC-3 is only one dB away from the level of the maximum signal modulation. This means that any drift in gain in the portion of the receiver which precedes the optical driver may drive the MSC-3 signal into limiting along with the other signals which may be present at the same antenna output. In fact, the RMS addition of the highest MSC-3 signal (–64.2 dBm) and the highest EMU signal (–67.2 dBm) will make the combined signal exceed the –63.2 dBm

* At this system gain the degradation due to the optical noise does not exceed 0.1 dB

Figure 2.4.1-1. Min/Max Received Power Spread for a 3 dB Window Power Control

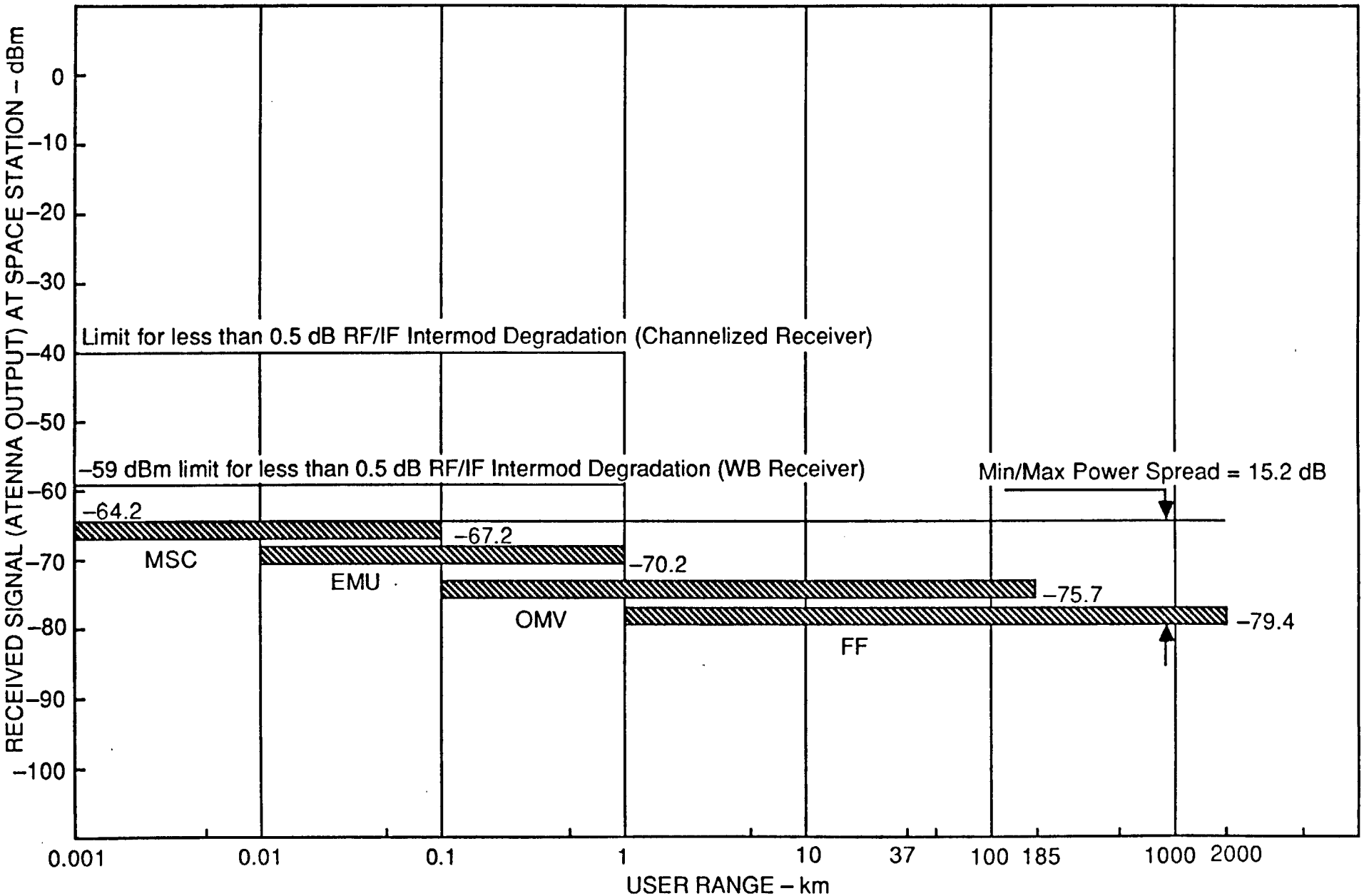

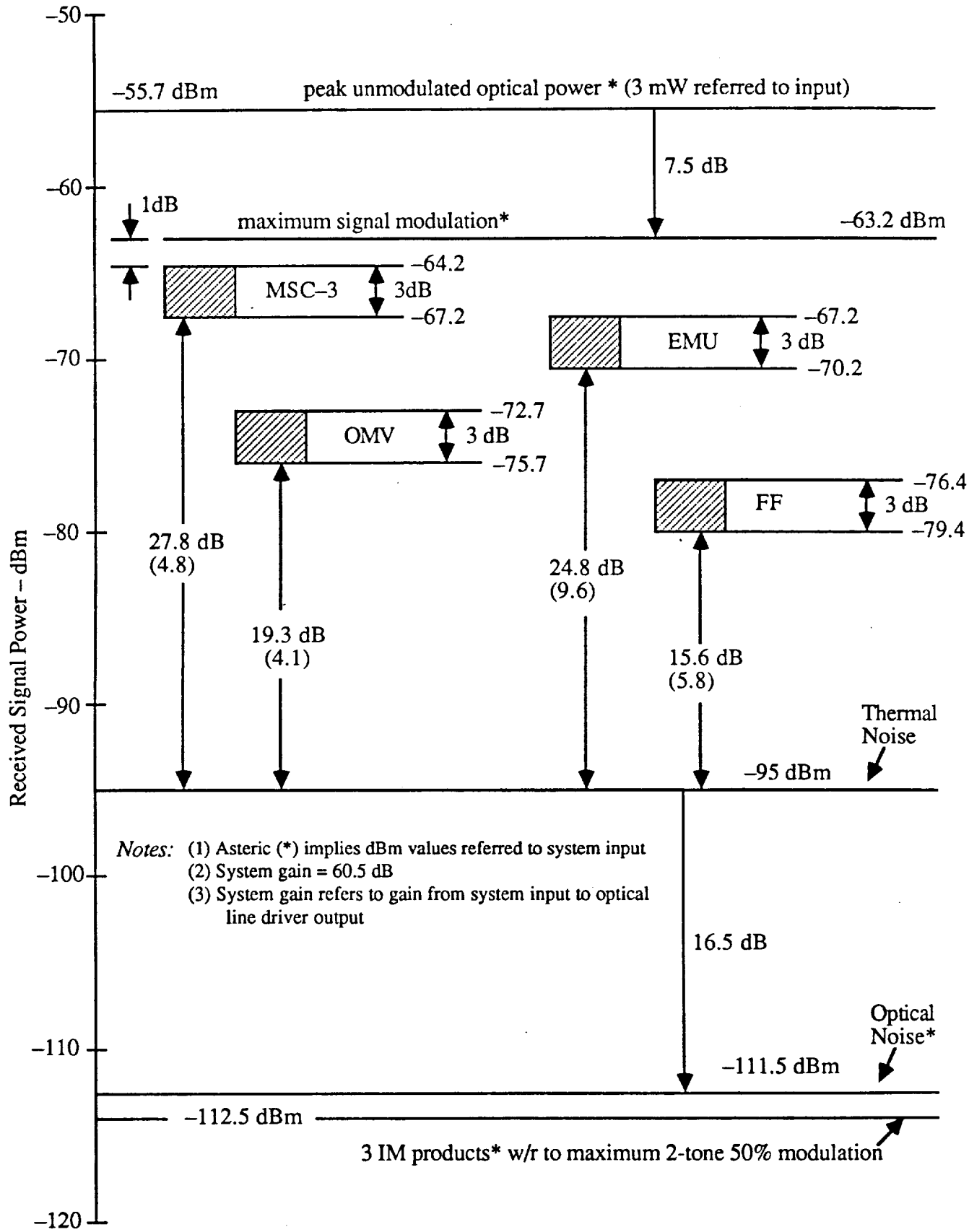

Figure 2.4.1-2. Optical Cable Driver Output Levels for 3 dB Window Power Control (Wideband Receiver).

threshold by about 0.5 dB. And this does not even include the secondary effect of adding other lower level signals.

One of the solutions to this problem is to narrow the power control window to 2 dB or less. However, in view of the added complexity to the power control function necessitated by such a "tight" window this approach does not look attractive, particularly within the user segment. Instead, one may consider operating the system with a reduced margin by lowering the gain prior to the optical driver. The margin degradation in this case will then by due the increased level of RIN relative to the system thermal noise. Another alternative would be to lower the bias on the FO driver and thus allow more modulation range on the cable driver.

Perhaps the most technically workable alternative, although a more expensive one, may be to increase the power handling capability of the laser diode used for the FO cable driver. The trade-offs in this area are, however, beyond the scope of this report.

2.4.2 Power Control with a Channelized Receiver and AGC

2.4.2.1 General Consideration

As was explained in Section 2.2.2, the advantage of a channelized receiver is that the received signals can be separated (i.e., bandpass filtered) according to their channel frequencies prior to being applied to an FO cable driver. Such separation permits AGC to be applied to the individual channels to achieve some degree of signal level equalization at the input to the FO cable driver. In this section we consider various aspects of the interaction between the power control requirement and the channelized AGC function. For the purpose of comparison with the broadband receiver, it is initially assumed here that a 3 dB power control window is implemented. The effect of using wider power windows is then considered in view of the AGC capability inherent with a channelized receiver approach.

Before considering quantitatively a specific situation, the effect of the channelized AGC prior to the FO cable driver needs to be discussed. Figure 2.4.2.1-1 shows, in a qualitative way, the effect of a channelized AGC on the signal and noise levels at the output of the FO cable driver. As shown in that figure, the dynamic range of the FO cable driver is limited at the upper end (2) by the maximum signal modulation (MSM) level and at the lower end by the optical noise (6).

Consider first what happens to the signal (1) when the input signal increases due to a decrease in range. At the initial acquisition, the signal will be at an SNR determined by the thermal noise. Without the AGC the signal will increase due to a closer range as shown by the dotted line (1) until it reaches the maximum signal modulation level (2). At this point the clipping will occur in the optical transmitter and the signal will be distorted. The level of the thermal noise, however, will remain at a constant level (4) regardless of the increase in the signal level.

When the AGC is activated, the signal will be kept at a nearly constant level (3) despite an increase in signal strength. At the same time the AGC action will, due to the

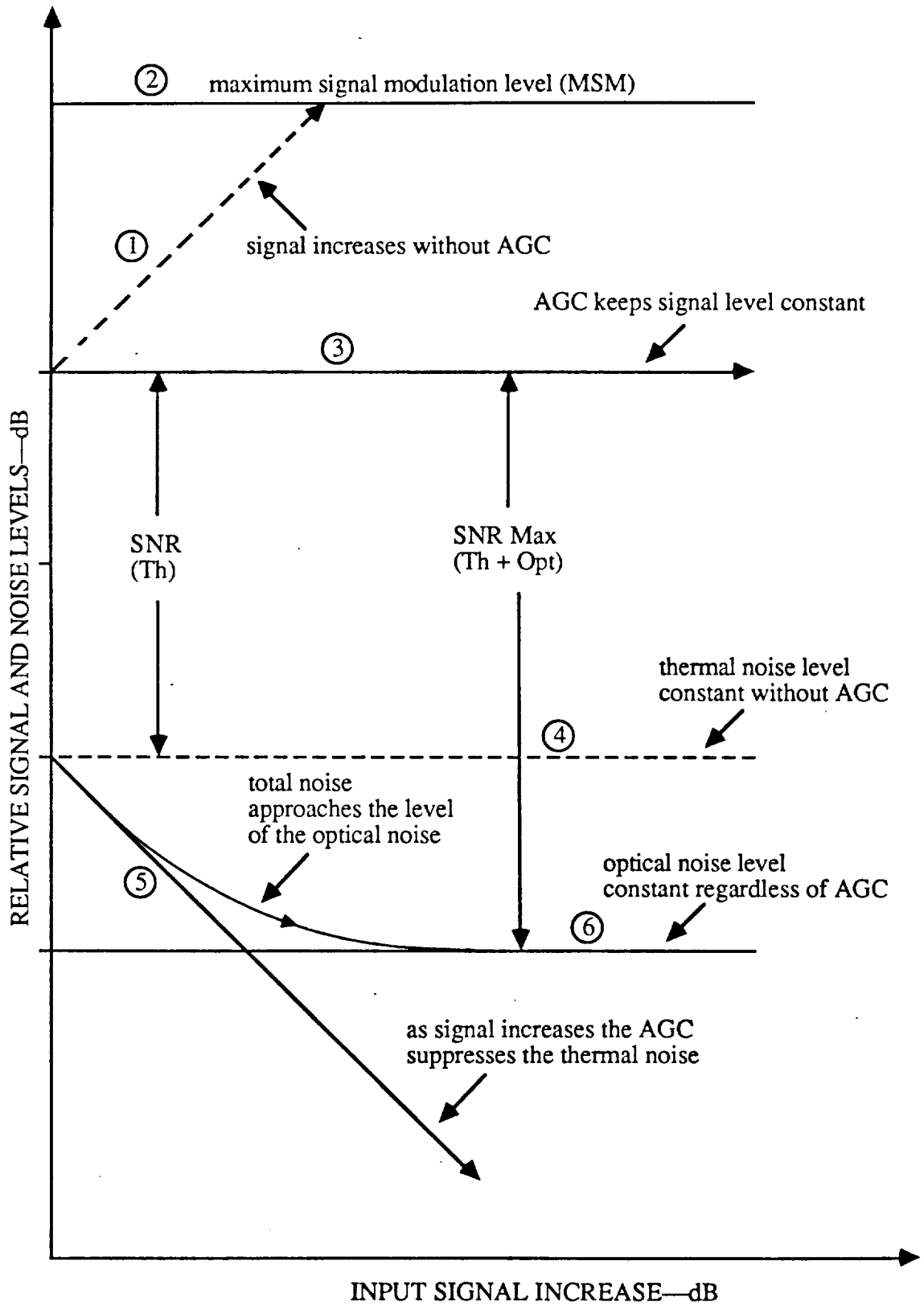

Figure 2.4.2.1-1. Effect of Channelized AGC on Relative Signal and Noise Levels at the Output of FO Cable Driver.

reduction in gain, lower the level of the thermal noise reaching the FO cable driver. This is shown by (5). At some point, however, the front end thermal noise will be at the same level as the optical noise, and thus both noises will be contributing to the total noise at the output of the FO cable driver. As the signal strength continues to increase further, the AGC action will push the thermal noise below the level of the optical noise. Beyond this point the output signal-to-noise ratio will remain constant and it will be limited by the optical noise.

Figure 2.4.2.1-2 shows FO cable driver output SNR vs. system input thermal SNR. The curves presented there demonstrate the effect of the AGC upon pushing the thermal noise below the optical noise. In this case the optical output noise consists of both the random noise and of third-order intermods due to the optical driver per se, i.e., exclusive of the RF/IF driver amplifier circuitry. The initial ratio of the thermal to the combined optical noise is 14 dB for the assumed model of the cable driver.

The curves show different behavior as the function of the AGC threshold above the thermal noise. The important common feature of the three curves shown is the leveling off of the output SNR as function of the increasing input SNR. Curve (1) is for the AGC threshold set at 26.7 dB above their thermal noise. This AGC setting keeps the maximum level of any signal at a level 6 dB below the peak optical modulation level of –2.7 dBm. Curve (2) corresponds to an AGC threshold of 19.3 dB which is the minimum SNR for the OMV signal. Curve (3) corresponds to a threshold setting of 10 dB and its purpose is to provide additional information on the behavior of the output SNR.

From Figure 2.4.2.1-2, it is evident that the output SNR ratios level off at their respective asymptotes which are equal to the respective AGC threshold setting plus 14 dB. The effective degradation in the output SNR w/r to the input SNR is also represented by a set of respective curves. Although not necessary detrimental to the link margins, the leveling of the output SNR curves presents a limitation on the accuracy with which the output SNR can be measured. Specifically, if the AGC threshold is located beyond the FO

driver, the leveling reduces the accuracy with which the power control decision can be made. We will address this subject in more detail elsewhere.

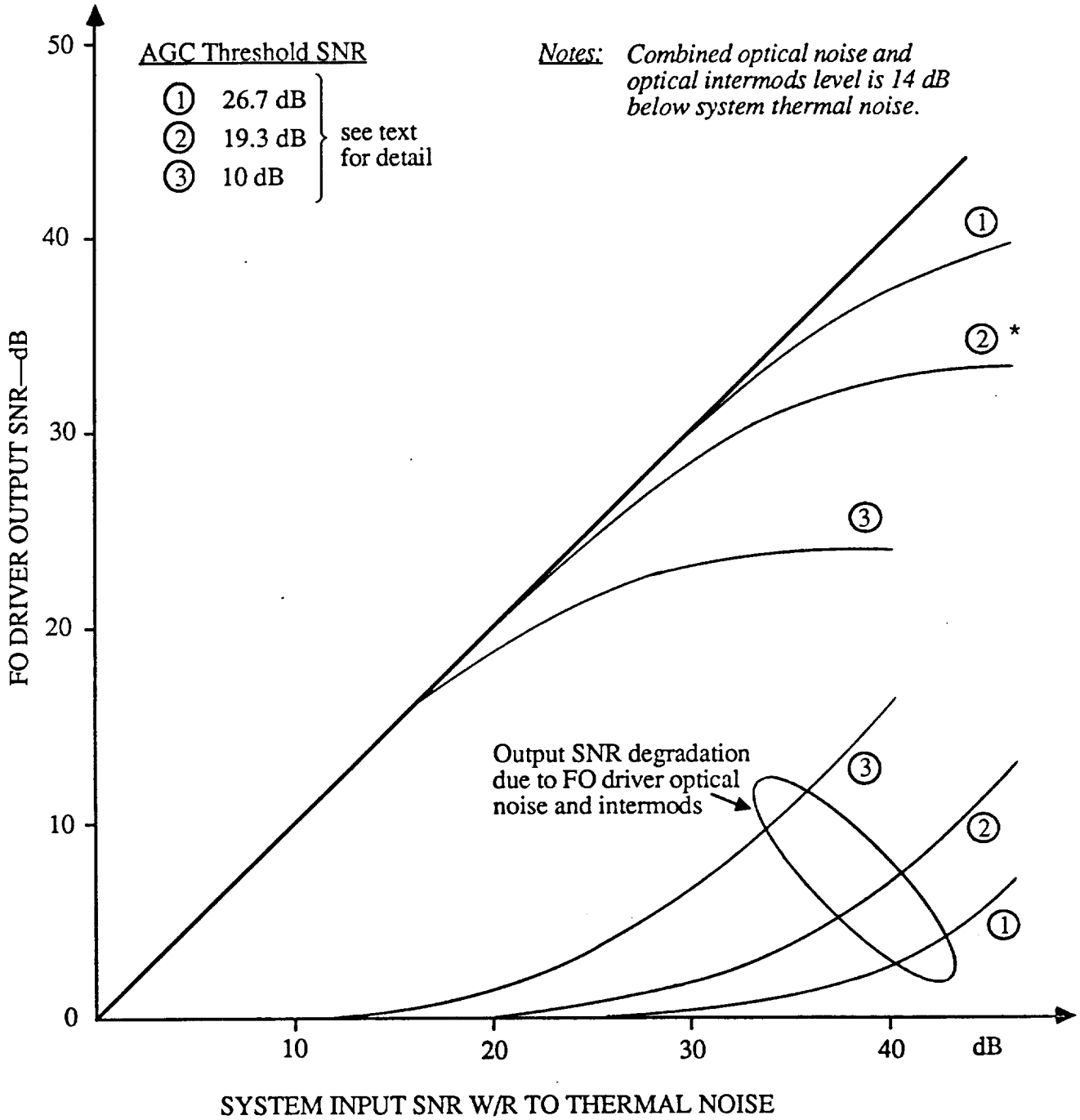

*Operating Curve for data in Figure 2.4.2.2-1

Figure 2.4.2.1-2. FO Cable Driver Output SNR vs. System Input Thermal Noise SNR.

2.4.2.2 Example of a 3 db Power Window

Figure 2.4.2.2-1 illustrates the effect of a 3 dB power control window on the FO line driver output. This figure is similar to Figure 2.4.1-2 except that all signal levels are referenced to the FO cable driver output instead of the system input.

For the example shown in Figure 2.4.2.2-1, it is assumed that the AGC threshold is set at a level equal to the signal received from an OMV. In other words, the AGC action prevents all other signals from exceeding the nominal level of an OMV signal. As shown in the figure, this level is 12.5 dB below the maximum signal modulation level (–2.7 dBm) of the FO driver. The absolute level of this AGC threshold is –15.2 dBm.

From Figure 2.4.2.2-1, the following can be observed:

(1) Signals from an FF are below the AGC threshold level and, therefore, they are not affected by the AGC action.

(2) Maximum signals from an OMV remain at the level of the AGC threshold. However, as the received OMV signal increases within a 3 dB power window the AGC reduces the channel gain accordingly. This pushes the thermal noise down by 3 dB.

(3) Maximum signals from an EMU and the MSC-3 are affected by the AGC even outside of the power control range. Specifically, this means that the AGC reduces the channel gain for these signals even at their nominal link budget values. AGC then provides further gain reduction as these signals increase within their respective 3 dB power windows. Furthermore, because the MSC-3 and the EMU signals have relatively high initial SNRs the AGC action forces the thermal noise levels closer to the optical noise, thus degrading the margins of these signals by 0.8 and 0.2 dB, respectively.

The scenario represented by Figure 2.4.2.2-1 is conservative from the standpoint of providing 12.5 dB of margin between the AGC threshold and the maximum signal modulation level (–2.7 dBm) of the FO driver. In an actual situation the 12.5 dB margin can probably be reduced to 10 dB or perhaps even to lower value. The actual margin value will depend on the number of simultaneous signals handled by the FO cable driver and on the relative magnitudes of these signals.

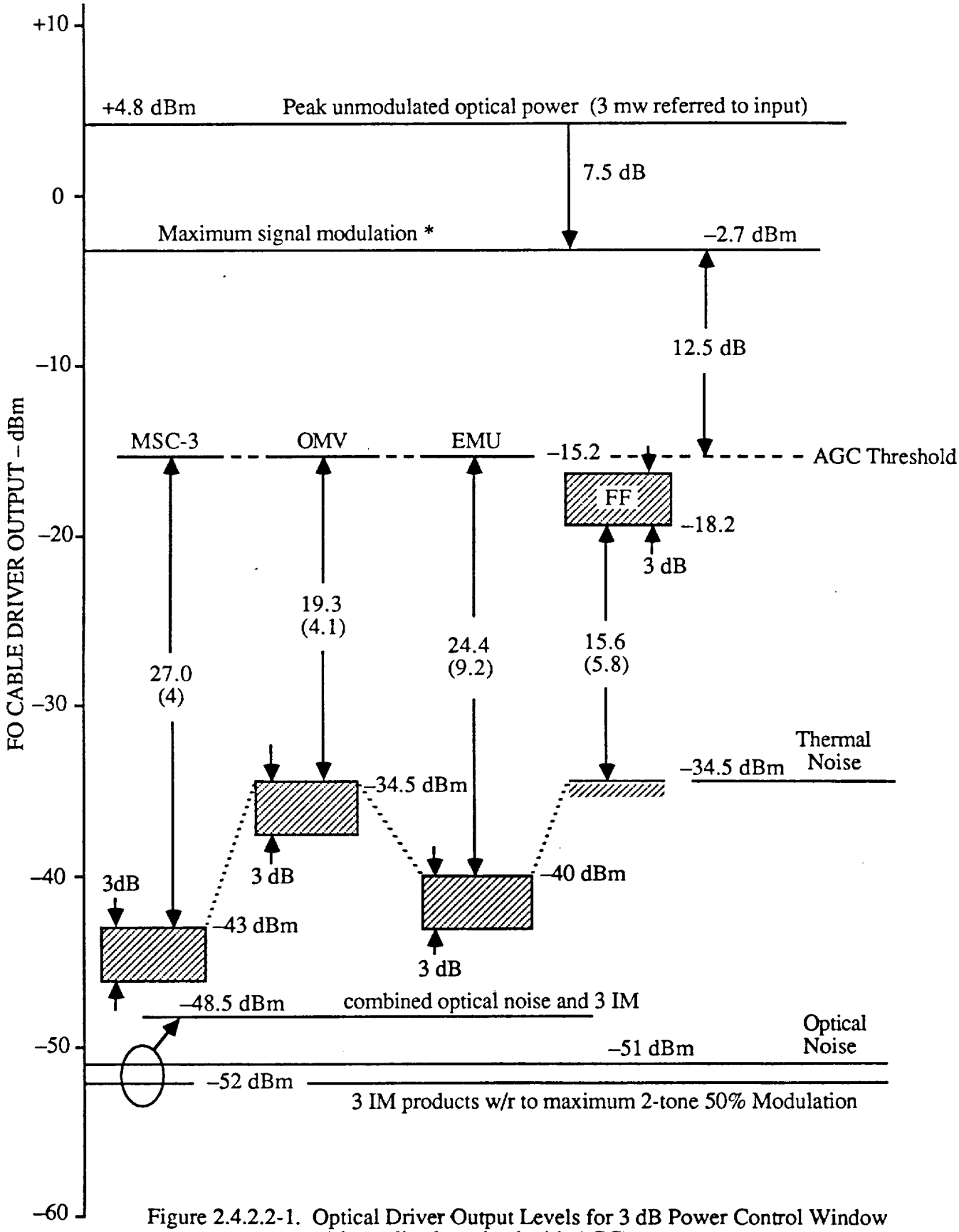

Figure 2.4.2.2-1. Optical Driver Output Levels for 3 dB Power Control Window (channelized received with AGC).

2.4.2.3 Possibilities and Limitations of Wider Power Windows

In the preceding section, a 3 dB power window was assumed and the effect of such power window on a channelized receiver was considered. It was shown that with the AGC threshold set at 12.5 dB below the MSM level the FF and the OMV signals can be received without any margin degradation. It was also shown that the EMU and the MSC-3 signals can be received with 0.8 dB and 0.2 dB margin degradation, respectively.

A power window wider than 3 dB can alleviate the power control requirements imposed on the user. It can also loosen the tolerances required of the AGC at the Space Station end of the link. Thus, the channelized architecture of the receiver and the availability of a channelized AGC naturally raise a question of whether a power window wider than 3 dB can be specified for this case.

Providing for an operation with a wide power window can be obtained by a combination of the two following conditions:

(1) moving the AGC threshold level closer to the MSM level

and

(2) allowing the AGC action to move the thermal noise level closer to the level of the optical noise.

Neither one of these conditions, however, can be realized without paying a penalty. Raising the AGC threshold level may result in amplitude clipping, particularly with multiple signals being applied to the FO cable driver. On the other hand, allowing more gain reduction with the AGC decreases system output signal-to-noise ratio due to a higher level of the optical noise. Consequently, a wider power window must be a compromise between these two limitations.

In considering the possibilities of using wider power control windows, we must also take closer look at the effect of the FO cable loss on the system output SNR. Depending on the magnitude of the FO cable loss various noise sources play the predominant roles.

As shown in Figure 2.4.2.3-1, there are three basic sources of the optical noise. One source is at the transmitter and two are at the receiver. At the transmitter the source is due to the relative intensity noise (RIN). RIN is inversely proportional to the cube of the transmitted power. However, once a given optical transmitted power is selected, RIN does not affect the C/N_0 at the receiving end of the link. This noise was already mentioned in Section 2.3.2.

The noise sources which do affect the C/N_0 value at the receiver are the quantum noise and the thermal noise of the receiving device. The quantum noise degrades the receive C/N_0 ratio at the rate of 1 dB/1 dB of received power reduction, but the thermal noise provides a corresponding C/N_0 reduction at the rate of 2 dB/1 dB. The role which these noise sources play in degrading the C/N_0 ratio depends on the level of the optical signal impinging on the optical receiver.

Figure 2.4.2.3-2 shows a typical behavior of the C/N_0 ratio for an optical link as the function of the received optical power (References [1] and [2]). As shown in this figure, for the received power levels in the 0 to –10 dBm, the RIN dominates the C/N_0 ratio. In the region extending from –10 dBm to –20 dBm, the quantum noise determines the received C/N_0. Below –20 dBm the optical receiver's thermal noise determines the performance of an FO link. Thus, depending on the transmitted optical power and the FO cable loss different noise sources determine the system performance.

It must be pointed out that the trend shown in Figure 2.4.2.3-2 is only a generalized trend, and that for each particular link, an analysis has to be performed to determine the actual performance. Based on the data obtained from the manufacturers of the optical and FO equipment, we have performed an analysis using a specific model of our link. Appendix A contains this analysis. Based on this analysis we have determined that at the maximum estimated FO cable loss of about 20 dB, the receiver thermal noise will dominate the link performance, but that at losses of 15 dB or less, the link performance will be dominated by RIN.

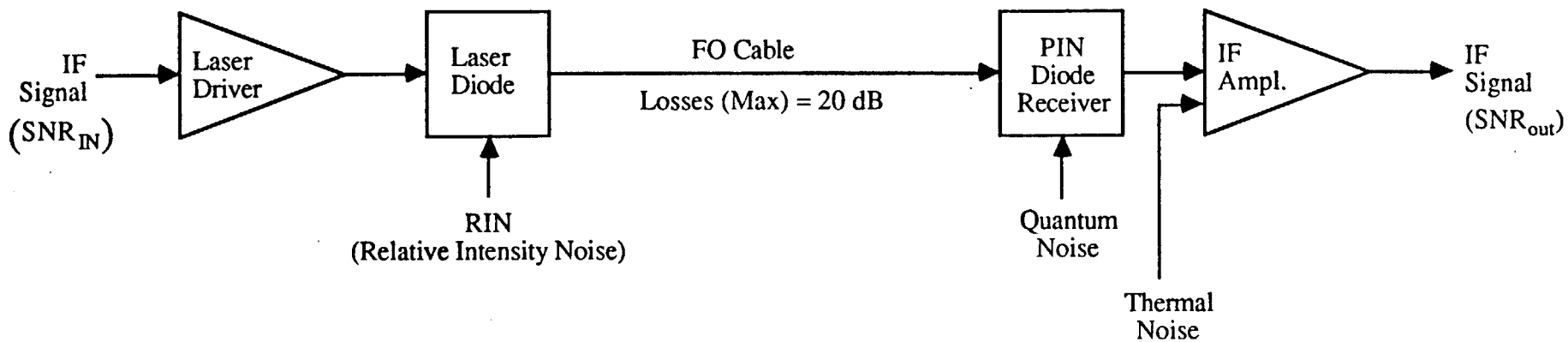

Figure 2.4.2.3-1. FO Cable Link Noise Sources.

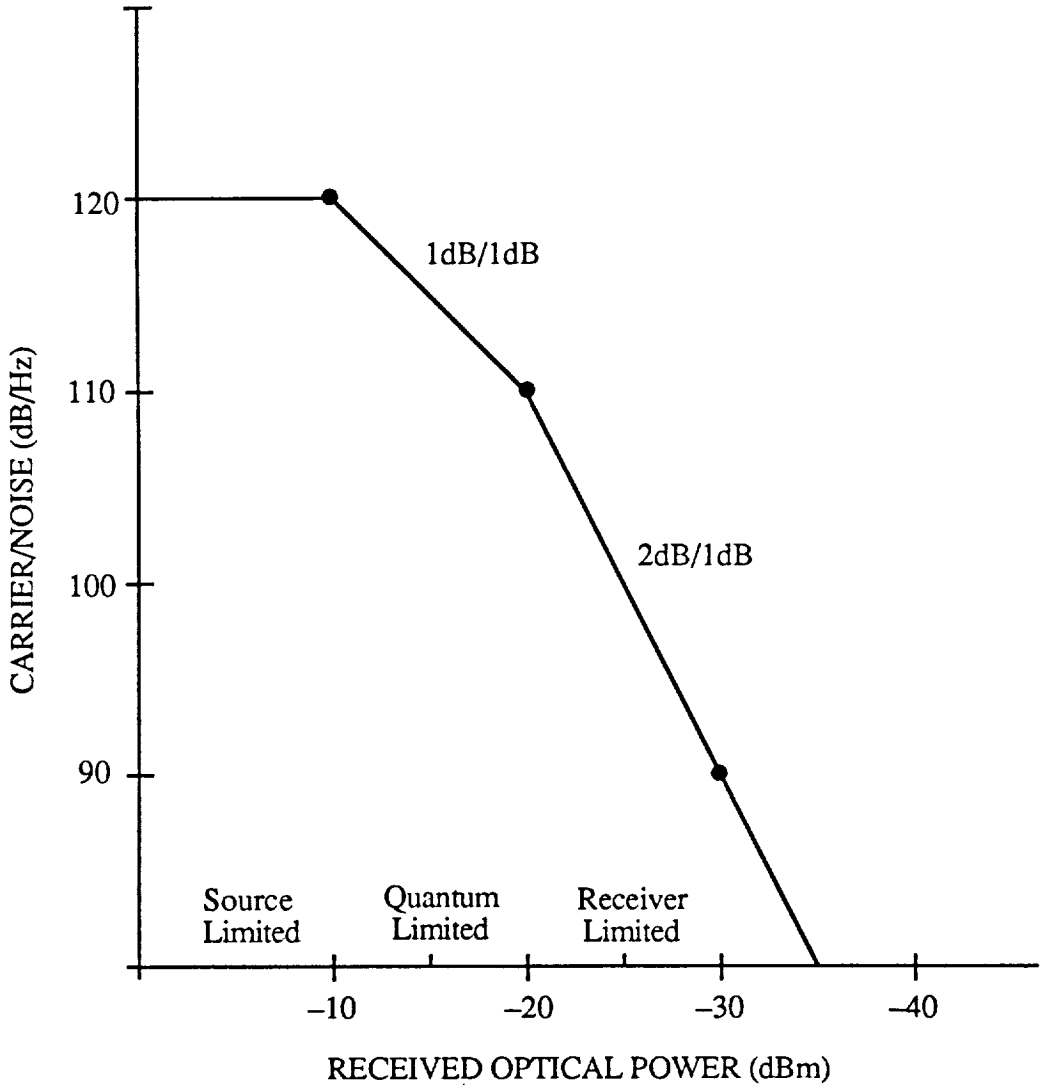

Figure 2.4.2.3-2. Carrier/Noise versus Received Optical Power.

Figure 2.4.2.3-3 shows the system SNR transfer curve as a function of the FO cable loss. From this curve we can see that for the maximum loss of 20 dB the "flattening" occurs at output SNR of about 35 dB. This, however, appears to be sufficient to receive the MSC-3 and the EMU signals with some link margins. It also appears that on top of this a 10 dB power control window may be implemented with some reasonable degree of accuracy for these high SNR users.

Figure 2.4.2.3-4 shows the same system SNR transfer curve in conjunction with the low SNR users such as an FF and an OMV. From this figure it is evident that for these low SNR users a power control window of up to 15 dB can be implemented with a reasonable accuracy and for the maximum cable loss of 20 dB. Also, these users are accommodated with some margin by the FO link.

Consider now some of the limitations which may arise as the result of striving for wide power control windows. These limitations are particularly pronounced for the high SNR users such as the EMU and the MSC-3. From Figure 2.4.2.3-3 it evident that a 10 dB increase in the received power moves the output SNR curve into a relatively flat, compressed region. Also, it can be seen that the flatness of the SNR curve is more pronounced for the case of the maximum FO cable loss of 20 dB. Thus, as the cable loss increases with time from say 10 dB to 20 dB a power increase of 10 dB at the system input will be detected as an increase in output SNR of only 5.9 dB instead of 9 dB. This fact is illustrated in Figure 2.4.2.3-5. As shown there, the SNR threshold Th(10) set at a level when the cable loss is 10 dB will not be exceed when the cable loss increases with time.

To alleviate this problem the algorithm for the power control must include provisions for compensating for such variation. The data for the compensation can be derived from an AGC amplifier placed after the photo diode at the receiver end of the FO link. The purpose for this amplifier is strictly to compensate for the gradual losses in the FO cable. Thus, this amplifier is not to be confused with other AGC amplifiers which form the conventional (i.e., the RF and the IF) portions of each Ku-Band channel receiver.

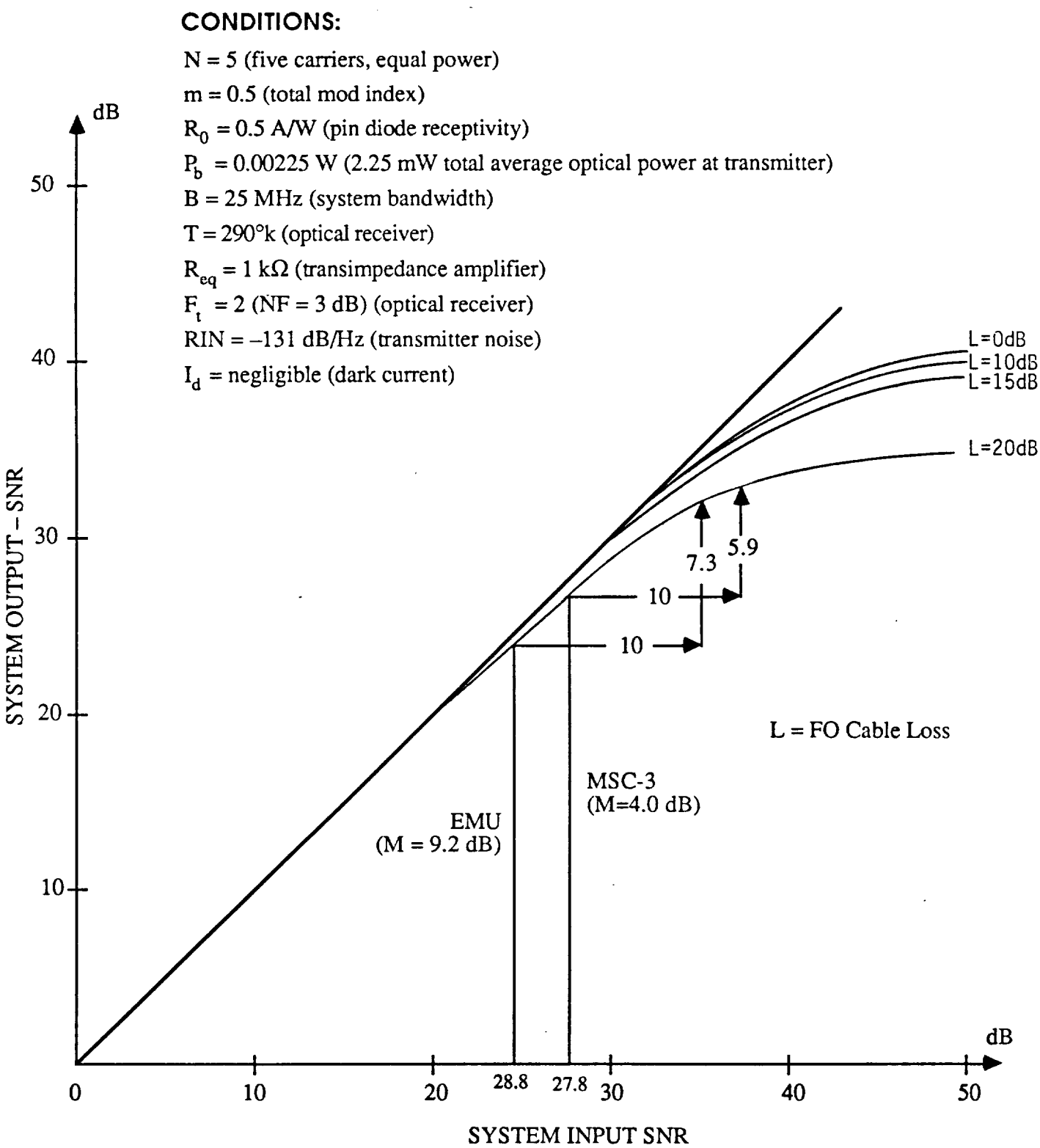

Figure 2.4.2.3-3. System SNR Transfer Curve as Function of FO Cable Loss (EMU and MSC-3 Power Control Window of 10 dB).

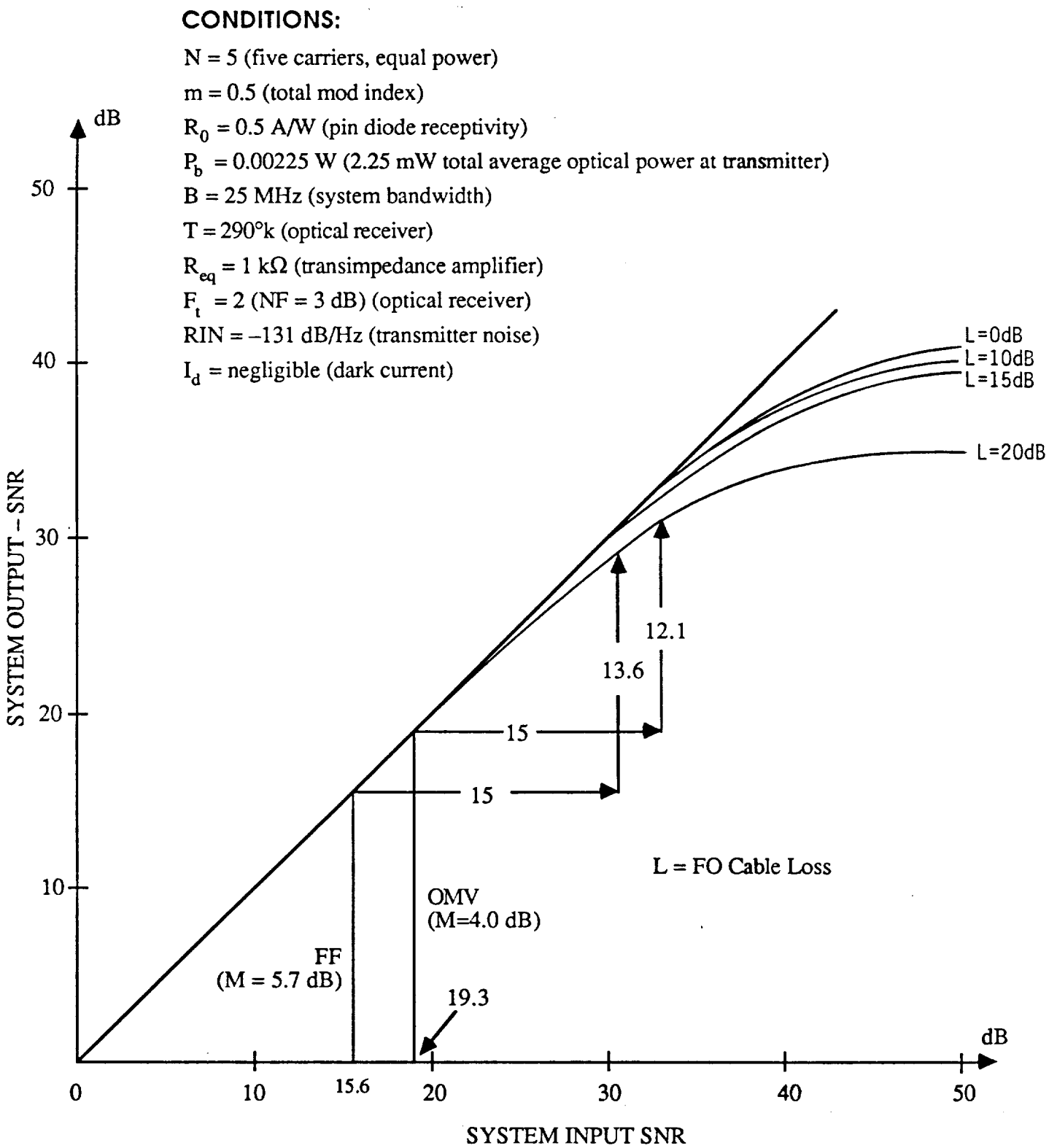

Figure 2.4.2.3-4. System SNR Transfer Curve as Function of FO Cable Loss (FF and OMV Power Control Window of 15 dB).

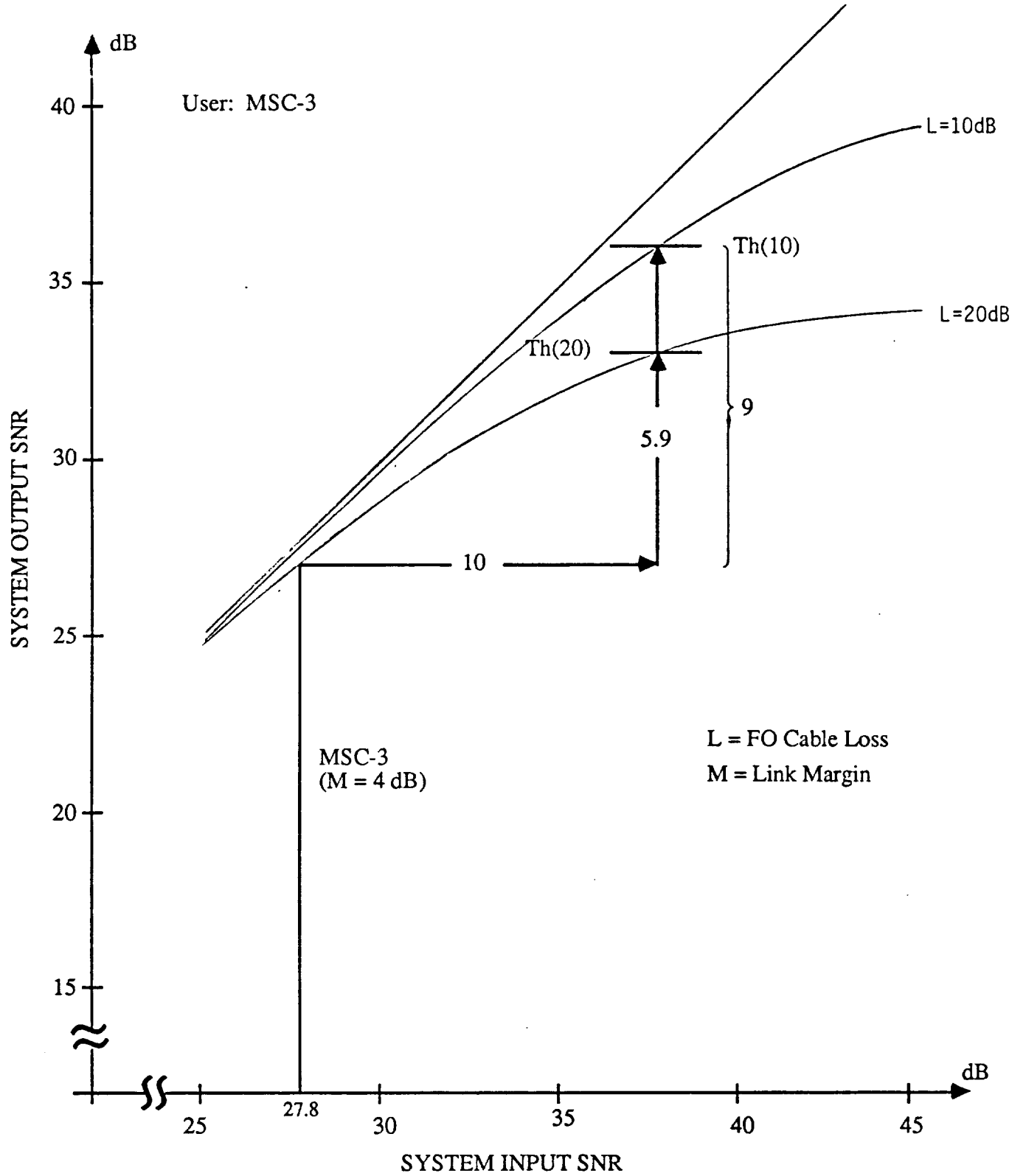

Figure 2.4.2.3-5. Effect of FO Cable Loss on Power Control Dicision (MSC-3 User).

Another significant issue encountered with large power control windows arises due to finite tolerances on the power control decision threshold. This is illustrated in Figure 2.4.2.3-6. As shown there, the normal operating point for an MSC-3 user output SNR of 27.0 dB. The corresponding margin at this SNR is 4 dB. As the signal power increases, the decision to command a 10 dB power reduction may occur at either a 6 dB power increase or at a 10 dB power increase depending on whether the threshold has moved by –2 dB or has remained at its proper value. If the decision is at the correct value, the power reduction will bring the link to its original operating point, i.e., SNR (in) = 27.8 dB and SNR (out) = 27 dB. If, however, the decision is made at the Th(–2 dB) point then the link is brought back to a much lower operating point which is still within the margin region but is dangerously close to the lower end of the margin zone.

The situation is worse if the power control window for the MSC-3 is 15 dB. Figure 2.4.2.3-7 illustrates this point. Here we see that if the decision is made at the Th(–2 dB) point, the power control command may force the link to operate below the margin.

Based on the examples presented, one can, therefore, conclude that power control windows over 10 dB should be used with caution for the high SNR users which operate in the "flattened" portion of the output SNR curve. This, however, does not preclude the lower SNR users (see Figure 2.4.2.3-4) from utilizing 15 dB windows provided that the decision threshold tolerances are set properly.

User: MSC-3
FO Cable Loss = 20 dB
Power Window = 10 dB

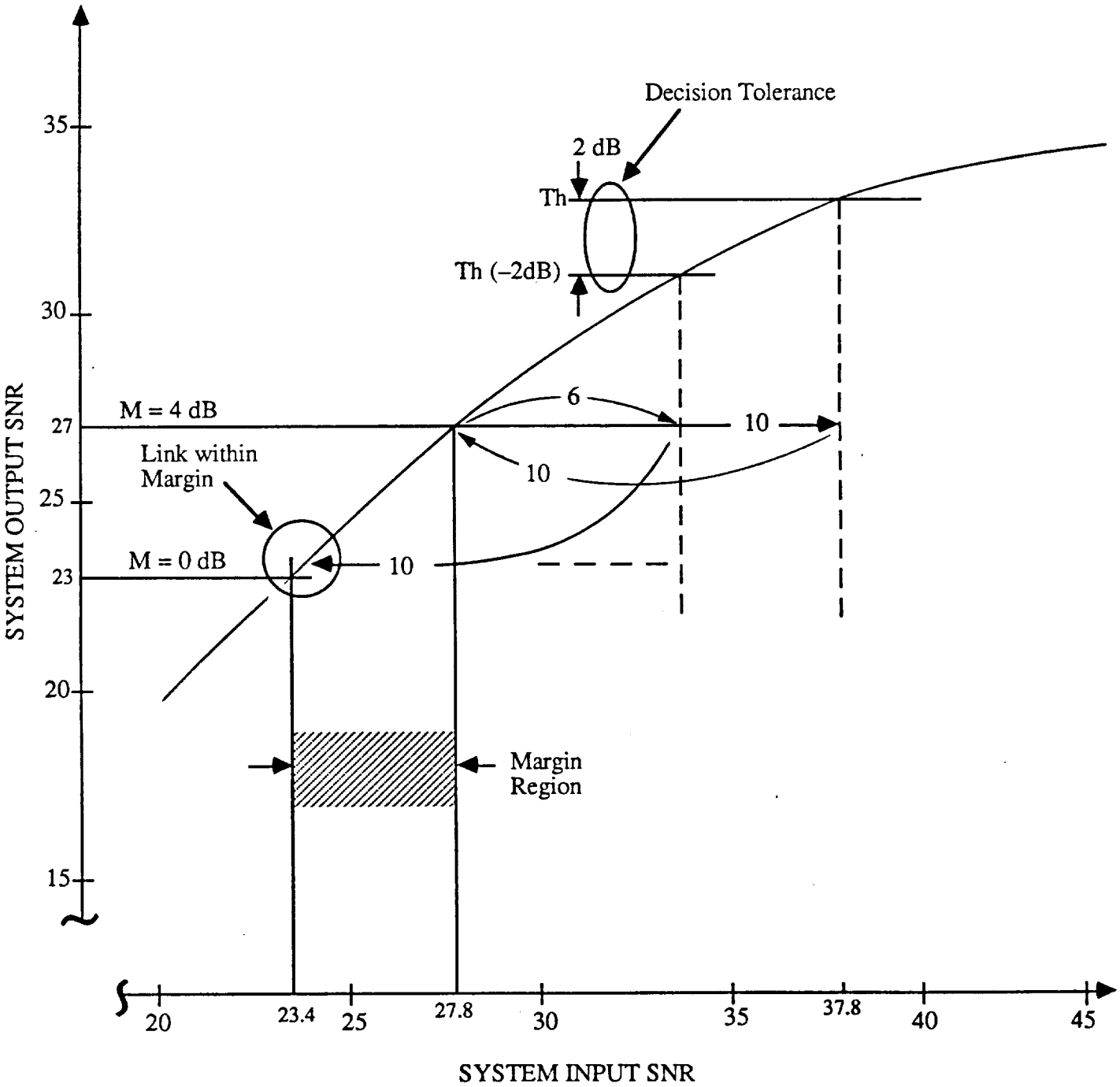

Figure 2.4.2.3-6. A Loose Power Control Decision Tolerance May Push Control into the Margin Region

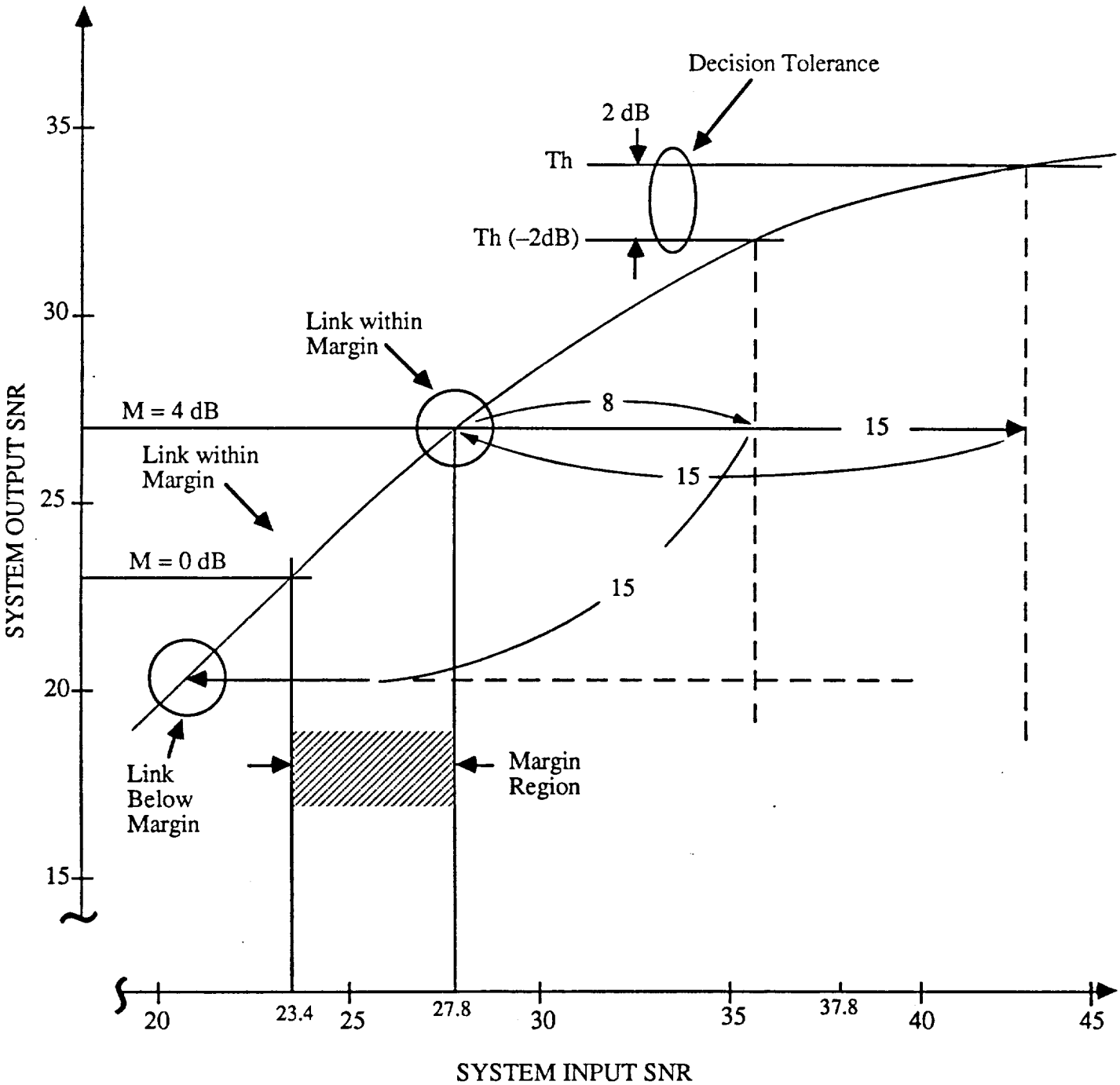

Figure 2.4.2.3-7. Excessive Power Window is Vulnerable to Decision Tolerance.

2.4.2.4 Power Control Algorithm for a Channelized Receiver

The proposed algorithm for the power control is based on the measurement of the output signal-to-noise ratio (SNR) of the controlled channel. Such measurement does not depend on the absolute signal level and thus it is less sensitive to the residual inaccuracies of the AGC.

Figure 2.4.2.4-1 shows a flow chart for implementing such algorithm for a channelized receiver. As shown in the figure, the first step is to decode the user's ID, i.e., FF, OMV, EMU, etc. The user ID permits the algorithm program to look up such user-related parameters as the SNR(min), the margin and the power control (PC) window. This data may be stored in an EPROM to permit changes in the user-related parameters. The assigned user PC threshold, i.e., the value of the SNR(out) at which the power control is activated is also obtained from the EPROM. Based on the measured FO cable loss the PC threshold is adjusted accordingly as described in Section 2.4.2.3.

The steps described above should take place prior to the actual user acquisition by the Space Station. After these steps are completed, the PC program awaits the carrier lock flag.

Once the carrier lock flag is received, the program begins to test the link SNR of the received signal. The test is based on comparing the pertinent signals at the output of the link demodulator. If the SNR falls below the SNR(min) value, the program alerts the antenna switching algorithm. But, if the SNR is within the acceptable limits, the program continues to measure the link SNR.

When the link SNR exceeds the preset PC threshold, i.e., the SNR becomes high, a command is sent to the user to reduce the power level by the appropriate power window. The program then returns to the testing for the carrier flag.

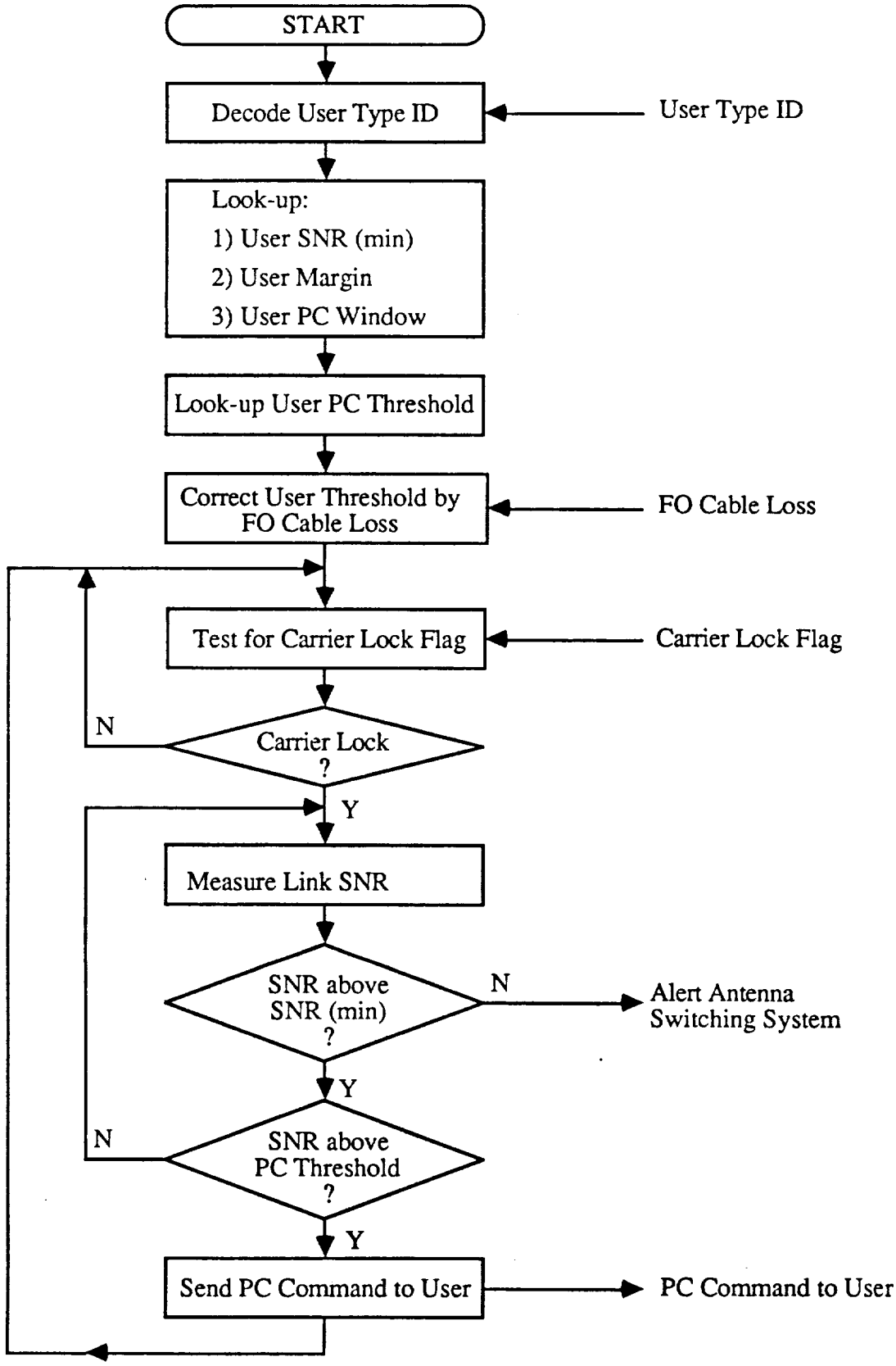

Figure 2.4.2.4-1. Power Control Algorithm for a Channelized Receiver.

2.4.2.5 The SNR Estimation

Figure 2.4.2.5-1 shows a circuit for deriving the signals for the estimation of the channel SNR. The particular circuit shown is for a QPSK Costas loop, but a similar technique can be applied to higher order modulations such as 8-PSK. As shown, the actual measurement performed is that of (S+N)/N which is a close approximation to S/N for large values of SNR.

The (S+N)/N component is derived by averaging the absolute values of the a(t) and b(t) data streams. The estimate of the N-component is obtained by taking the RMS value of the link noise in the carrier error track channel. The bandwidth of the latter channel is approximately equal to the bandwidth of the "sidearm" lowpass (LPF) filters. Furthermore, the highpass filtering eliminates the carrier tracking error component from the N-term. The SNR estimation can be performed by digital signal processing circuitry after quantizing the S+N and N signals to the required degree of accuracy.

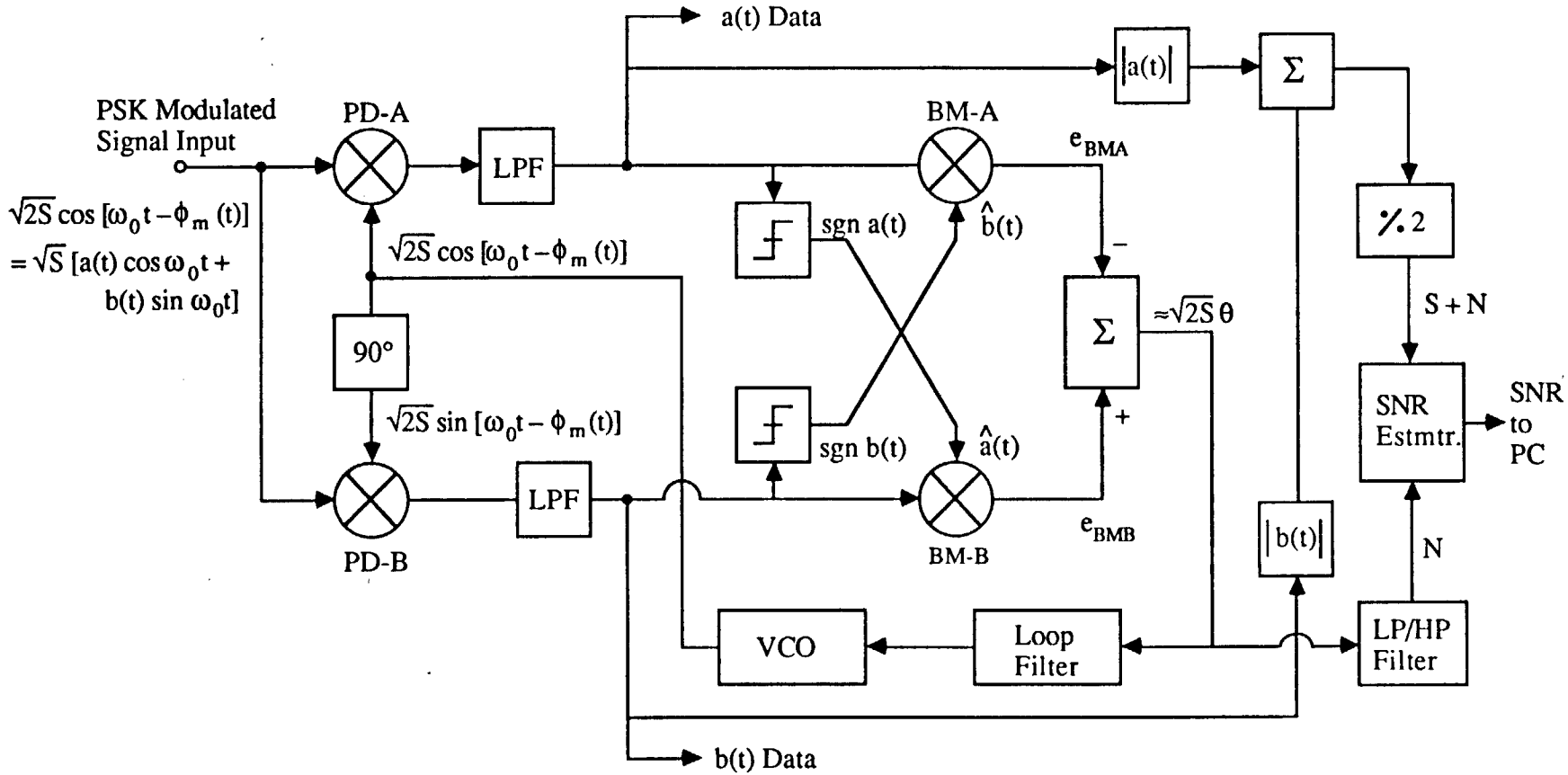

Figure 2.4.2.5-1. QPSK Costas Loop Signals for SNR Estimation.

2.4.3 User Power Control

The commands sent to the user can alter user's EIRP by either reducing the transmitter power, or the antenna gain or both. The simplest method is to control the transmitter power over a wide range of levels.

The power amplifier baselined for the MA Ku-Band system users may be a 1 watt cw solid state amplifier. The power output of such amplifier may be controlled by varying the RF input drive by means of a PIN diode. As shown in Appendix C, the input power, and hence the transmitter output of the user, can be controlled over a range of 60 dB by means of a PIN diode. Appendix C contains the support material for defining the user transmitter configuration.

3.0 CONCLUSIONS

In this report we have examined various aspects of establishing the requirements and the limitations for the power control for the Space Station Multiple Access System Users. Particular emphasis was placed on the performance of the fiber optic (FO) cable link which is currently baselined for connecting the Ku-Band receiver/transmitter units with the modem/processing equipment. Two receiver architectures were examined. These are: (1) a wideband receiver and (2) a channelized receiver. It was determined that a channelized receiver can, at least in principle, accommodate a 20 dB higher level of the input signals before the internal generation of the third-order intermodulation products. This capability is due to the channelized AGC available with the channelized receiver. Thus, we have assumed a channelized receiver as a desirable baseline for our system model.

It was also determined that, based on practical model of an FO cable link, the basic limitation for the power control window is the FO cable loss which causes the degradation in the system SNR at the optical receiver. In view of this degradation, it is estimated that a power window for the high SNR users, such as EMU and MSC-3, may be limited to 10 dB, at best. For the lower SNR users, such as FF and OMV, the power control window of up to 15 dB appears feasible. A prudent approach, however, is to set a 6 dB power control window as a design goal and allow a ±3 dB tolerance.

The possibility of using a PIN diode to control the power input to the user's transmitter, and thus control the output power, was also examined. It was determined that 60 dB of power control can be obtained in this manner without antenna switching.

4.0 RECOMMENDATIONS

Based on the findings reported in this document, it appears that a channelized receiver system with channelized AGC can provide significant advantages over a wideband receiver which amplifies all of the received signals by means of a single IF. Thus, a channelized receiver is recommended.

To allow for implementation tolerances, it is recommended that a power control window be kept below 10 dB, although some users can work with wider windows. A conservative baseline is 6 dB ± 3 dB window. Because the SNR performance of the FO cable link is limited by the optical receiver sensitivity when large (≈ 20 dB) FO cable losses are encountered a low noise optical receiver design is recommended. The receiver model used in this report is based on a PIN optical diode and a transimpedance amplifier. It is suggested that the use of an avalanche photo-diode (APD) receiver be investigated during the design phases of the MA link system. The use of an APD receiver may improve the noise performance at the receiving end of an optical FO cable link.

APPENDIX A

FIBER OPTIC CABLE LINK PERFORMANCE ESTIMATE

APPENDIX A

FIBER OPTIC CABLE LINK PERFORMANCE ESTIMATES

1.0 INTRODUCTION

In this appendix we provide a quantitative estimate of the FO cable link performance. The particular emphasis is placed on determining the effect of the noise sources which affect the performance of the link.

As shown in Figure A-1, there are three basic sources of the optical noise. One source is at the transmitter and two are at the receiver. At the transmitter the source is due to the relative intensity noise (RIN). RIN is inversely proportional to the cube of the transmitted power. However, once a given optical transmitted power is selected, RIN does not change at the receiving end of the link.

The noise sources which do affect the C/N_0 value at the receiver are the quantum noise and the thermal noise of the receiving device. The quantum noise degrades the receive C/N_0 ratio at the rate of 1 dB/1 dB of the received power reduction, but the thermal noise provides a corresponding C/N_0 reduction at the rate of 2 dB/1 dB. The role which these noise sources play in degrading the C/N_0 ratio depends on the level of the optical signal impinging on the optical receiver.

Figure A-2 shows a typical behavior of the C/N_0 ratio for an optical link as the function of the received optical power (References [1] and [2]). As shown in this figure, for the received power levels in the 0 to –10 dBm, the RIN dominates the C/N_0 ratio. In the region extending from –10 dBm to –20 dBm, the quantum noise determines the received C/N_0. Below –20 dBm the optical receiver's thermal noise determines the performance of an FO link. Thus, depending on the transmitted optical power and the FO cable loss different noise sources determine the system performance.

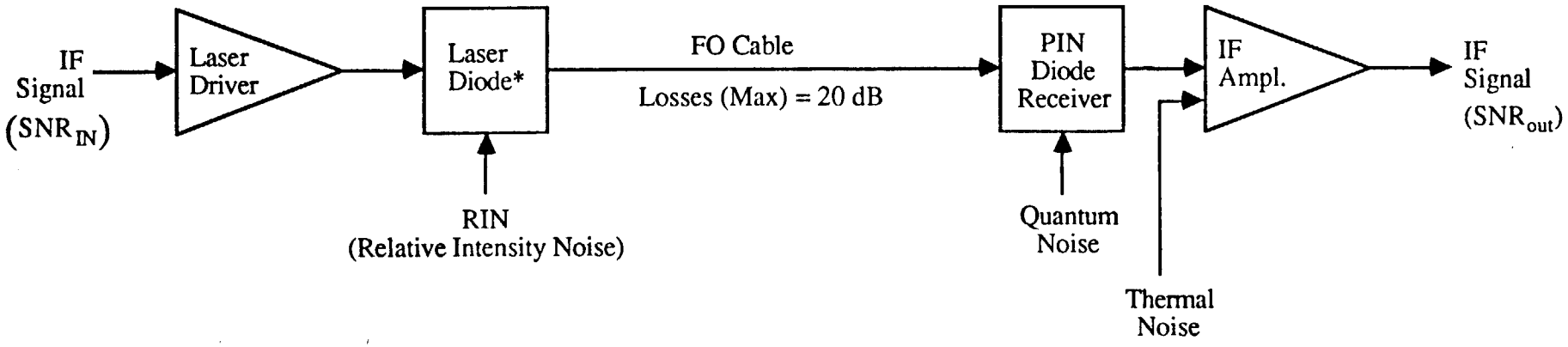

Figure A-1. FO Cable Link Noise Sources.

*General Optronics Corp. GO DIP 1000 Laser Module and/or GO ANA Laser Diode Transmitter are baselined for our analysis.

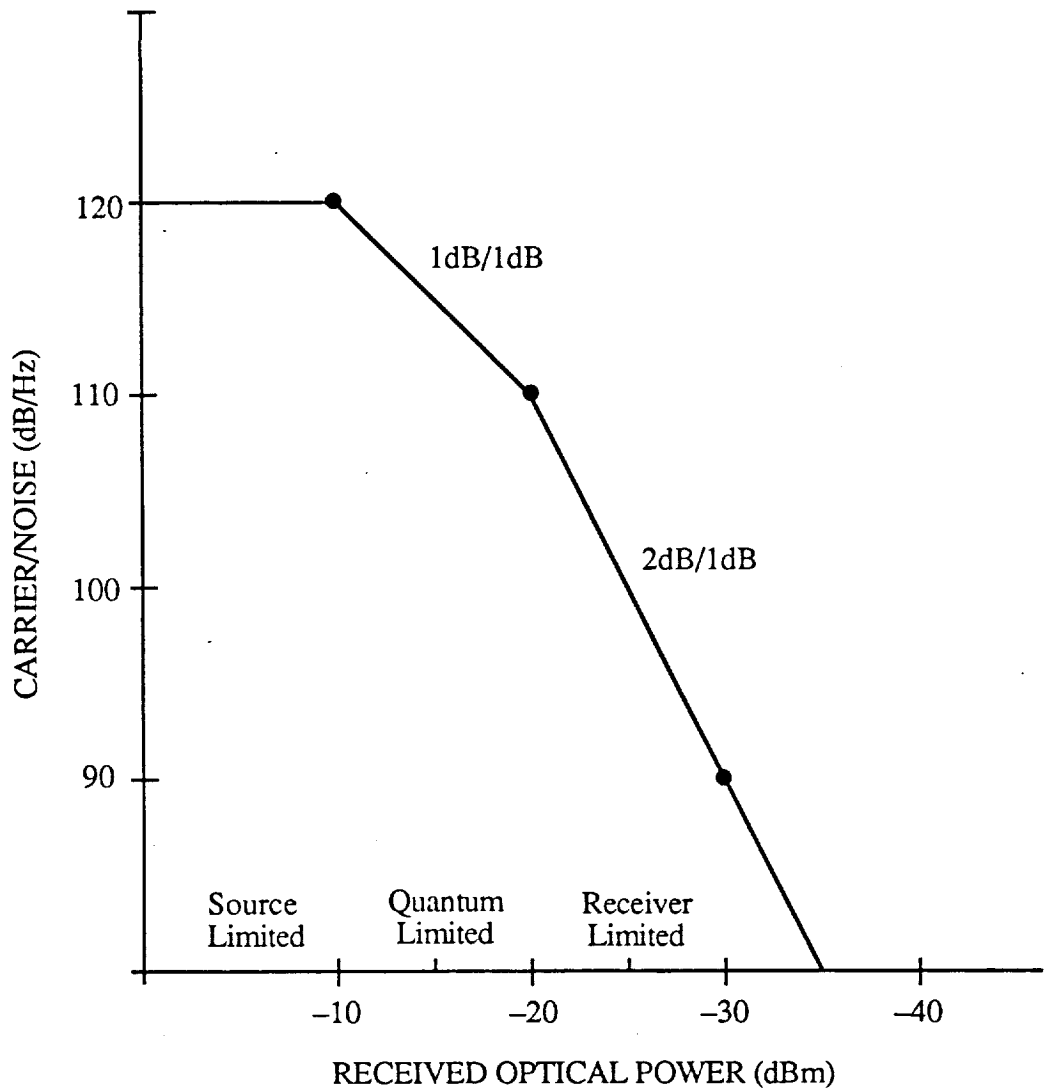

Figure A-2. Carrier/Noise versus Received Optical Power.

The trend shown in Figure A-2 is only a generalized trend. To obtain a more accurate estimate of the performance of our link, we have to make some reasonable quantitative assumptions and perform the required calculations.

For the calculations that follow, we assume that a General Optronics Corp. GO DIP 1000 laser module is used at the transmitting end of the link. This module may be incorporated into the GO ANA analog laser diode transmitter. We also assume that the laser diode, which is rated at 3 mw cw power, is biased at 2.25 mw (i.e. $P_b = 2.25$ mw) and that the total modulation index is 50% for a 5-channel link. We also assume a PIN diode and a transimpedance amplifier with an equivalent resistance of 1kΩ ($R_{eq} = 1k\Omega$) and a noise figure of 3 dB ($F_t = 2$) is used at the receiving end.

Appendix B contains the data sheets on the General Optronics Corp. laser transmitter units.

2.0 CALCULATIONS

The C/N_0 value at the receiving end of an FO cable link can be expressed by the following equation [1]:

$$C/N_0 = \left(\frac{1}{2N}\right) \frac{(mR_0P_b)^2}{\underbrace{(RIN\ R_0^2\ P_b^2\ B)}_{\text{source}} + \underbrace{2q(R_0\ P_b + I_d)B}_{\text{quantum}} + \underbrace{(4KTB/R_{eq})F_t}_{\text{receiver}}} \qquad \text{(A-1)}$$

where

N	=	number of independent channels
R_0	=	diode responsibility (amperes/watt)
m	=	modulation depth (total, all carriers)
P_b	=	average optical power received (w)
q	=	electron charge (1.6×10^{-19} coulombs)
K	=	Boltzman constant (138×10^{-23} watt-sec/°K)
I_d	=	diode dark current (amperes)
B	=	bandwidth of receiver (Hz)
T	=	temperature (°K)
R_{eq}	=	equivalent resistance of photodiode load and amplifier (ohms)
F_t	=	noise factor of preamplifier
RIN	=	source relative intensity noise (dB/Hz in numeric value)

The three terms in the denominator of equation A-1 identify the aforementioned contributions of the source, the quantum and the receiver noise terms. If we let B = 1 Hz and neglect the effect of the diode dark current (i.e., let $I_d = 0$ amp) we can separate equation A-1 into three separate C/N_0 terms as shown below:

Source Noise:

$$C/N_0 = \frac{1}{2N}\frac{m^2}{RIN} \qquad \text{(A-2)}$$

Quantum Noise:

$$C/N_0 = \frac{1}{2N}(m^2)\frac{(R_0P_b)}{2q} \tag{A-3}$$

Receiver Noise:

$$C/N_0 = \frac{1}{2N}(m^2)\frac{(R_0P_b)^2 R_{eq}}{(4KT)\ F_t} \tag{A-4}$$

For our baseline model we assume the following values:

N	=	5 (five channels)
m	=	0.5 (total for five channels)
RIN	=	−131 dB/Hz (7.94×10^{-14} numeric)
R_0	=	0.5 A/w
P_b	=	0.00225 w (2.25 mw at transmitter)
T	=	290°K
R_{eq}	=	1KΩ
F_t	=	2 (NF = 3 dB)
I_d	=	negligible

Using these values we proceed to calculate the various C/N_0 terms.

Source Noise C/N_0:

$$C/N_0 = \frac{1}{(2)\ (5)} \times (0.5)^2 \times \frac{1}{7.97 \times 10^{-14}} = \frac{0.25}{10 \times 7.94 \times 10^{-14}}$$

$$= 3.147 \times 10^{11} \text{ or } \underline{\underline{115}} \text{ dB/Hz}$$

Quantum Noise C/N_0:

$$q = 1.6 \times 10^{-19} \text{ coulombs}$$

$$C/N_0 = \frac{1}{(2)\ (5)} \times (0.5)^2 \times \frac{(0.5)\ (0.00225)}{(2)\ (1.6) \times 10^{-19}} = \frac{2.81 \times 10^{-4}}{(10)\ (3.2) \times 10^{-19}}$$

$$= 8.19 \times 10 \text{ or } \underline{\underline{139.4}} \text{ dB/Hz}$$

The value above is for no cable loss. For a 20 dB loss the C/N_0 value becomes:

$$C/N_0\,(L = 20\text{ dB}) = 139.4\text{ dB/Hz} - 20\text{ dB} = \underline{\underline{119.4}}\text{ dB/Hz.}$$

Receiver Noise C/N_0:

Assume

$R_{eq} = 1000\ \Omega$

$T = 290°K$

$K = 138 \times 10^{-23}$ watt-sec/°K

$(KT = 4 \times 10^{-21})$

$F = 2\ (NF = 3\text{ dB})$

Then for zero cable loss (i.e., L = 0 dB):

$$C/N_0 = \frac{1}{2N}(m^2)\frac{(R_0\,R_b)^2}{4\ K\ T\ F}R_{eq}$$

$$= \frac{1}{(2)\ (5)}\ (0.5)^2\frac{(0.5)^2\ (2.25 \times 10^{-3})^2}{(4)\ (4 \times 10^{-21})\ (2)} \times 10^3$$

$$= \frac{(0.25)\ (0.25)\ (5.1)\ (10^{-6})\ 10^3}{(10)\ (4)\ (2)\ (4 \times 10^{-21})}$$

$$= 9.96 \times 10^{14} \text{ or } \underline{\underline{150}}\text{ dB/Hz}$$

For L = 20 dB this value will decrease by 40 dB:

$$C/N_0 = (L = 40\text{ dB}) = 150\text{ dB/Hz} - (2 \times 20\text{ dB}) = \underline{\underline{110}}\text{ dB/Hz}$$

Figure A-3 shows the three respective C/N_0 terms as the function of the cable loss. The combined value of the three C/N_0 terms is also plotted in Figure A-3 as the function of the cable loss.

Using the combined C/N_0 value for the optical link, the SNR transfer curves can be plotted as the function of the system input SNR and of the FO cable loss. For this the

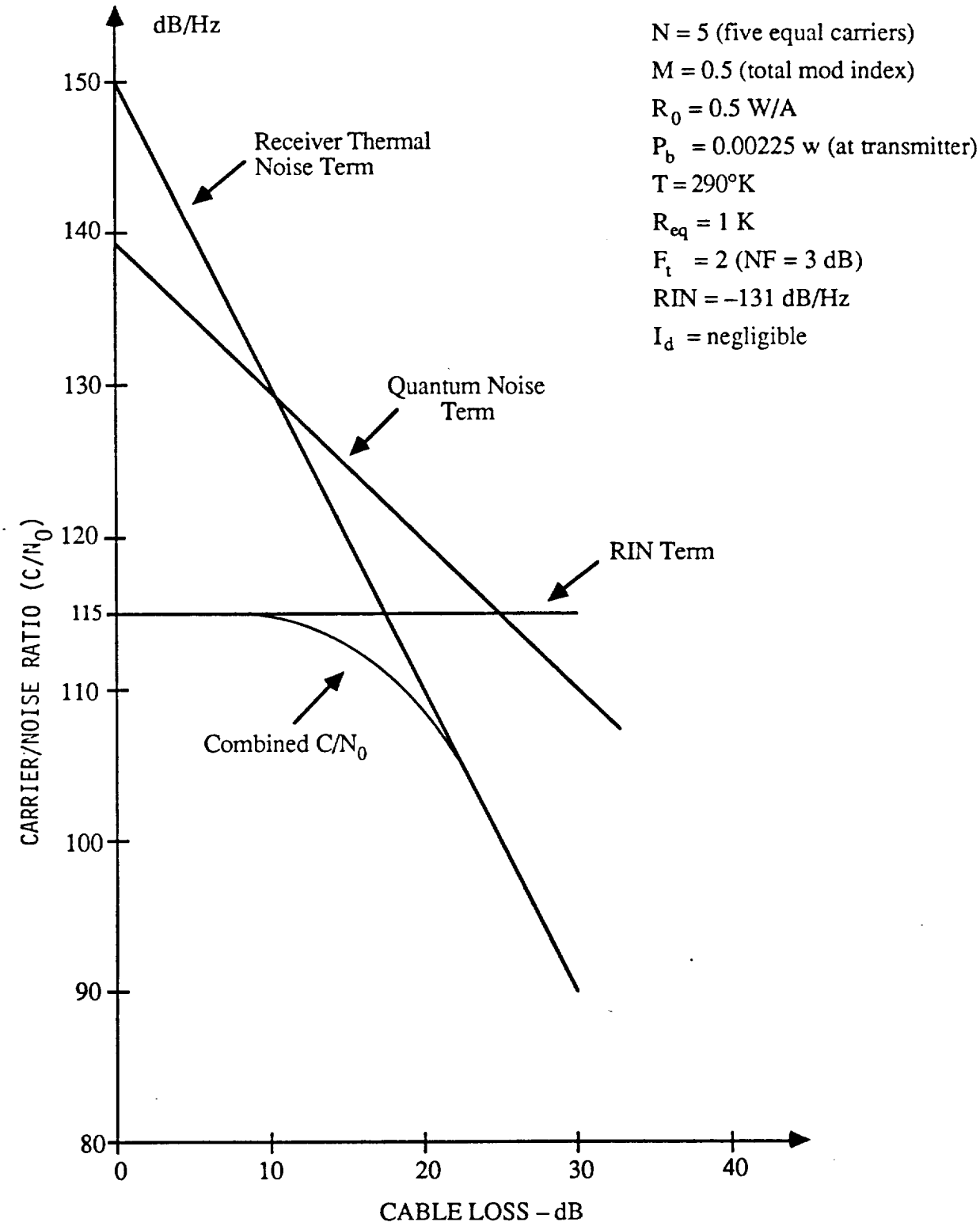

Figure A-3. Carrier/Noise Ratio per Channel as Function of FO Cable Loss.

C/N_0 value is converted to the nominal video link bandwidth of 25 MHz. Figure 2.4.2.3-3 and 2.4.2.3-4 of the report show this conversion.

REFERENCES

(1) J. Koscinsky, "Feasibility of Multi-Channel VSB/AM Transmission on Fiber Optic Links," National Cable Television Association Transactions for 1987.

(2) J. Koscinsky, "Considerations in Transmission of Analog FDM Signals on fiber Optic Links," RF Design, February 1987.

APPENDIX B

DATA SHEETS FOR GENERAL OPTRONICS CORP.
ANALOG LASER DIODE TRANSMITTER UNITS

general optronics corp.

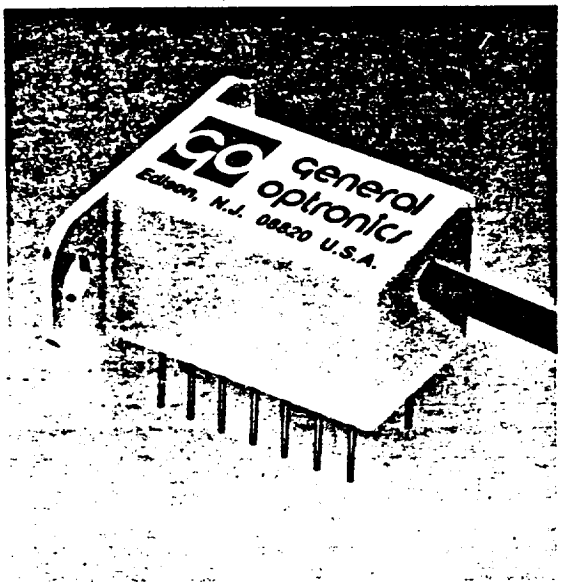

820nm MULTIMODE LASER MODULE GO DIP 1000

FEATURES:
- High power/efficient coupling into fiber
- Temperature and power monitoring
- Low modal noise
- Low self-pulsation noise
- High linearity

DESCRIPTION: The GO DIP 1000 is a 14 PIN dual-in-line package incorporating our GOLS 1000 injection laser diode, coupled to a 50μm core fiber. A photodetector and a thermistor are included for power and laser temperature monitoring. An optional thermo-electric cooler can be used in conjunction with the thermistor for temperature stabilization and control. The entire assembly is hermetically sealed, containing no organic material. Thousands of units are now operating worldwide in analog CATV distribution, digital telephone transmission and high speed data link systems.

SPECIFICATIONS (@ 25°C):

Parameter	Symbol	Min.	Typ.	Max.	Unit	Remarks
Threshold Current	I_{th}		80	100	mA	
Light Output	L	3			mW	out of fiber core
Quantum Efficiency	η	0.08	0.20		mW/mA	in lasing region
Spontaneous Emission	L_{th}		250		μW	L at I_{th}
Wavelength	λ	800	820	850	nm	other λ available
Spectral Width	$\Delta\lambda$	1.0	1.5		nm	30% CW @ 1.5mW
Rise/Fall Time	T		0.5		ns	
Forward Voltage	V_f		1.8	2.0	V	@ L=1.5mW
Monitor Current	I_d	0.4	1.2	2.5	mA	L = 1.5mW
Thermistor Resistance	R_t	9.5	10.0	10.5	kΩ	
Linearity						
2nd harmonic distortion			−35		dB	50% modulation depth
3rd harmonic distortion			−45		dB	50% modulation depth
Fiber Pigtail (1 meter)						
core diameter		47	50	53	μm	customer supplied fiber can be pigtailed on request
cladding diameter		122	125	128	μm	
jacket diameter			950		μm	
numerical aperture		0.18	0.20	0.22		
Cooler Capacity	ΔT_{max}	40			°C	optional
Cooler Current	I_c		0.9	1.1	A	at ΔT_{max}

ABSOLUTE MAXIMUM RATINGS:
- Storage Temperature: −20°C to +60°C
- Operating Temperature: −20°C to +60°C
- Soldering Time: 10 seconds at 260°C
- Reverse Voltage: 5V
- Photodetector Reverse Voltage: 30V
- Light Output: 5mW

ORDERING INFORMATION:
Model Number: GO DIP 1000
Wavelength Specifications: Typical range is 800nm to 850nm. Specify if you require: a) wavelengths outside this range; b) tight tolerance on wavelength.
Options: a) customer supplied fiber; b) thermo-electric cooler (TEC).

ORIGINAL PAGE IS OF POOR QUALITY

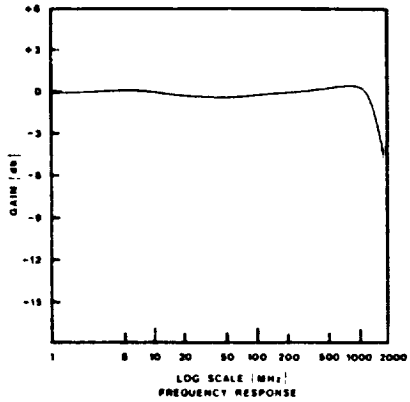

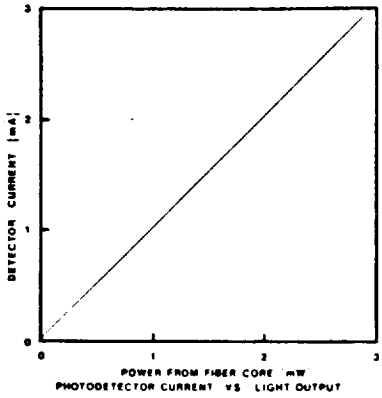

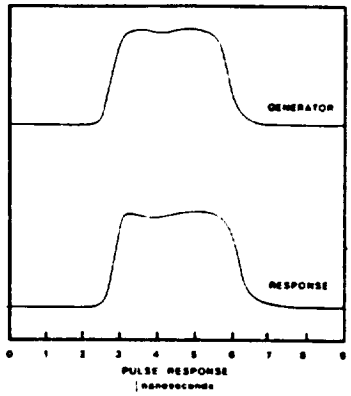

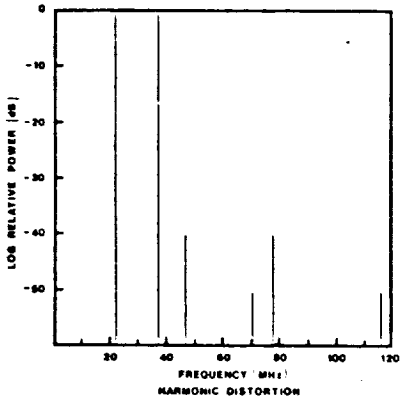

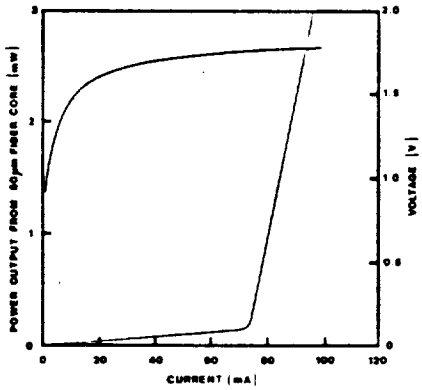

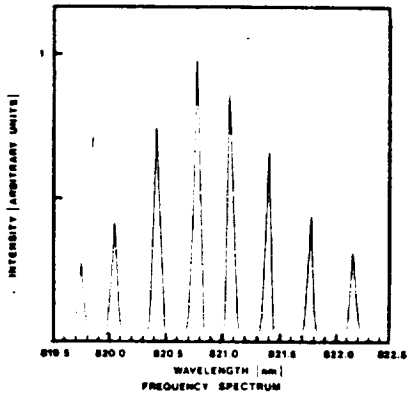

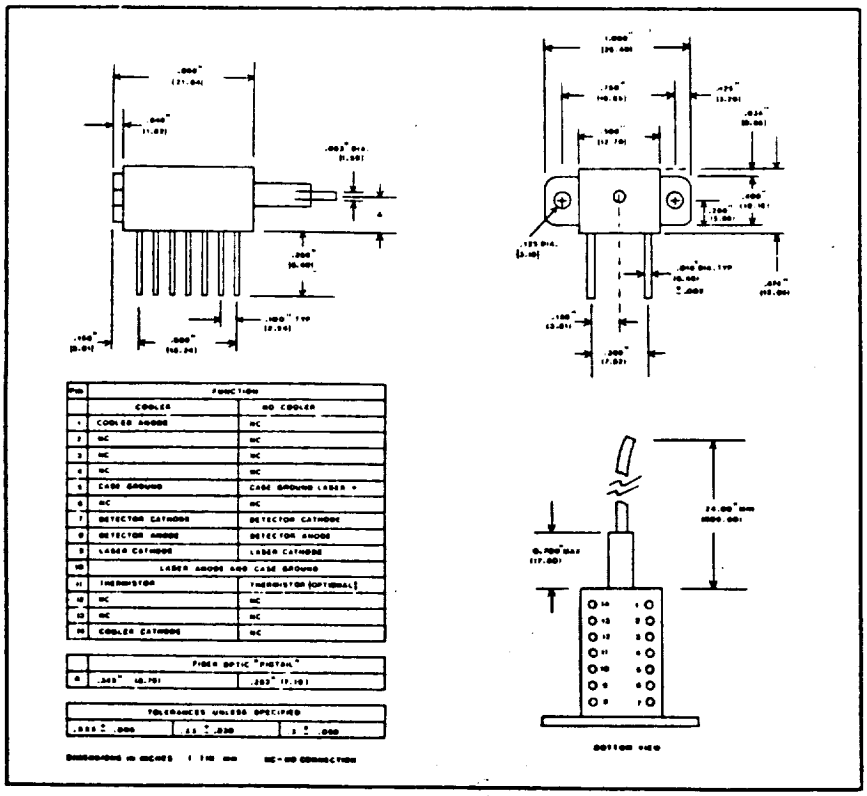

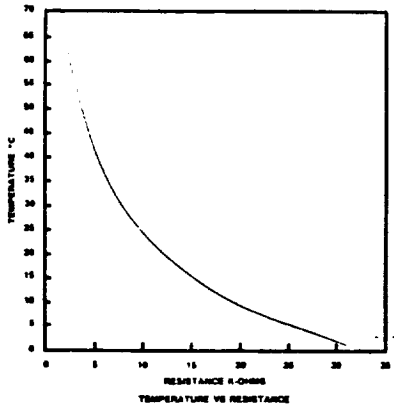

DANGER

INVISIBLE LASER RADIATION.
AVOID DIRECT EXPOSURE TO BEAM.

Aluminum Gallium
Arsenide Laser 50mW
Maximum Output at 760 nm to 890 nm.
Class IIIb Laser Product
Product complies with 21 CFR
1040.10 and 1040.11.

general optronics corp.
Two Olsen Avenue, Edison, NJ 08820
(201) 549-9000 TWX 710-997-9556

GENERAL OPTRONICS reserves the right, without notice, to make changes in equipment design or specifications. Information supplied by GENERAL OPTRONICS is believed to be accurate and reliable. However, no responsibility is assumed by GENERAL OPTRONICS for its use nor for any infringement of patents or other rights of third parties which may result from its use. No license is granted by implication or otherwise under any patent or patent right of GENERAL OPTRONICS

#015-0686-5

general optronics corp.

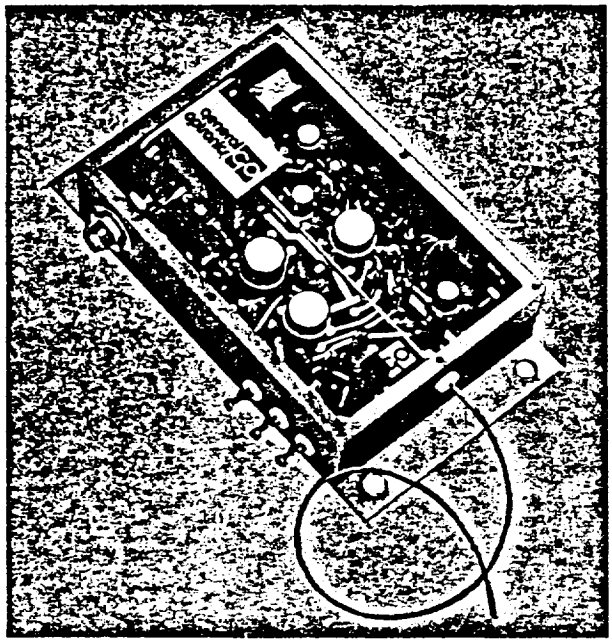

ANALOG LASER DIODE TRANSMITTER GO ANA

FEATURES:
- Wide electrical Bandwidth
- Power and Temperature Control
- Alarm Circuitry
- Uses Hermetic DIP Package, GO DIP Series

DESCRIPTION: This general purpose analog driver can be ordered with any of our DIP packaged laser diodes. The circuit incorporates all functions in order to monitor the optical power bias and the operating temperature. The transmitter can accommodate all types of analog or digital signals (with 50% duty cycle). Power and temperature are factory set depending on the laser module used inside the transmitter.

A detector circuit enables an alarm and monitors the operation of the device.

ABSOLUTE MAXIMUM RATINGS:
- Input Signal: 1Vp-p.
- Supply Voltage: −7V
- Storage Temperature: −50°C to +80°C
- Operating Temperature: −40°C to +65°C

SPECIFICATIONS (@ 20°C):
- Power Supply: −5V, +/−5%, 1.2A max.
- Input Impedance: 50-75Ω
- Stability = 1% at 25°C, 3% over temperature range
- RF Input: SMA

ORDERING INFORMATION:
GO ANA XXXX
XXXX suffix from GO DIP light source 1000, 1300, 3000, 4000, 6300

Temperature setting is 25°C for transmitters incorporating GO DIP 1000, 3000 and 4000, and 20°C for transmitters incorporating GO DIP 1300 and 6300. Power bias is 1.5mW for multimode fiber pigtail, 500μW for 9μm single mode pigtail, 300μW to 1mW for 5μm single mode pigtails.

ORIGINAL PAGE IS
OF POOR QUALITY

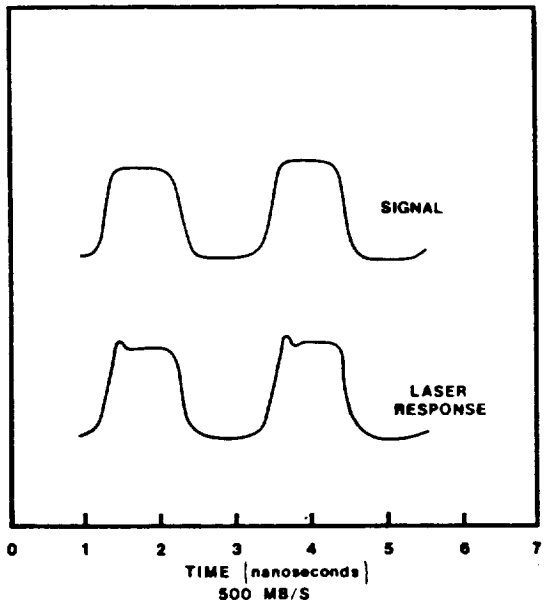

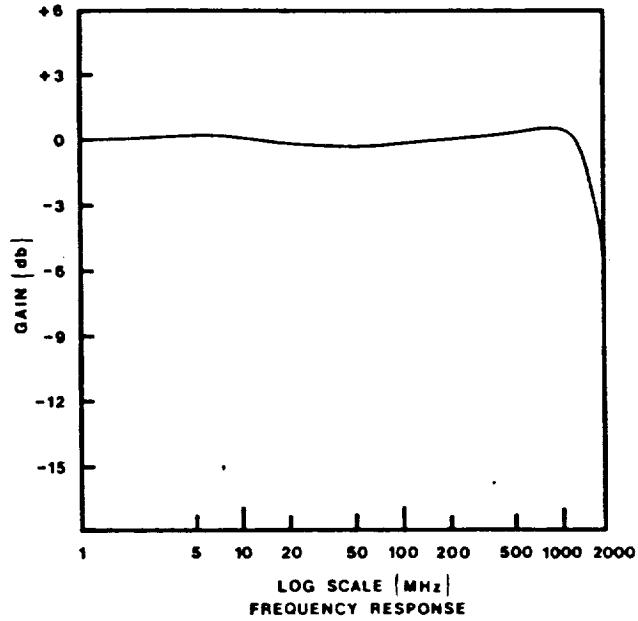

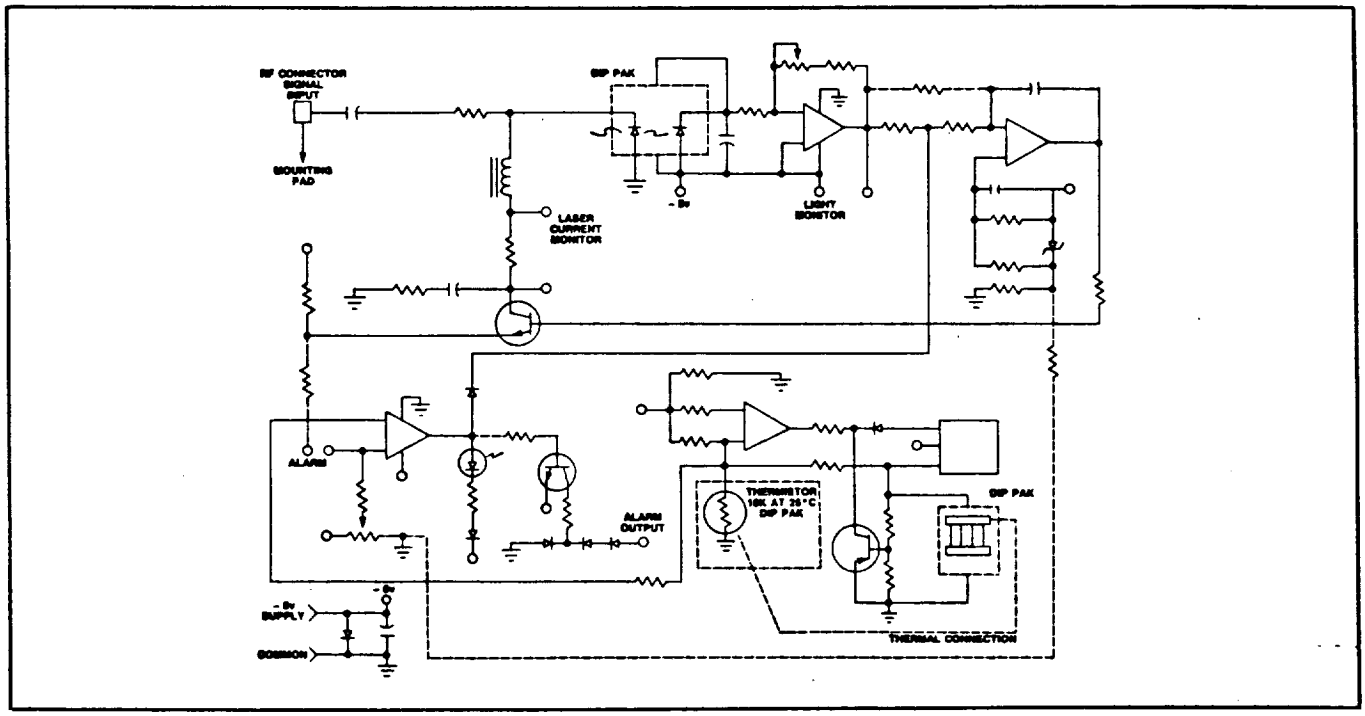

DANGER

INVISIBLE LASER RADIATION.
AVOID DIRECT EXPOSURE TO BEAM.

Aluminum Gallium
Arsenide Laser 50mW
Maximum Output at 760 nm to 890 nm.
Class IIIb Laser Product
Product complies with 21 CFR
1040.10 and 1040.11.

DANGER

INVISIBLE LASER RADIATION
AVOID DIRECT EXPOSURE TO BEAM.

Indium Phosphide Gallium Arsenide
Laser 50 mW Maximum Output at 1250 nm
to 1350 nm.
Class IIIb Laser Product
Product complies with 21 CFR
1040.10 and 1040.11

DANGER

INVISIBLE LASER RADIATION.
AVOID DIRECT EXPOSURE TO BEAM.

Indium Phosphide Gallium Arsenide
Laser 50 mW Maximum Output at
1475 nm to 1575 nm.
Class IIIb Laser Product
Product complies with 21 CFR
1040.10 and 1040.11.

general optronics corp.
Two Olsen Avenue, Edison, NJ 08820
(201) 549-9000 TWX 710-997-9556

GENERAL OPTRONICS reserves the right, without notice, to make changes in equipment design or specifications. Information supplied by GENERAL OPTRONICS is believed to be accurate and reliable. However, no responsibility is assumed by GENERAL OPTRONICS for its use nor for any infringement of patents or other rights of third parties which may result from its use. No license is granted by implication or otherwise under any patent or patent right of GENERAL OPTRONICS.

APPENDIX C

POWER/IERP CONTROL FOR KU-BAND MA SYSTEM USER'S TRANSMITTERS

TECHNICAL MEMORANDUM TM 8706-2

TO: Sergei Udalov

FROM: Richard Austin

SUBJECT: Power/IERP Control for Ku-Band MA System User's Transmitters

DATE: June 9, 1987

1.0 INTRODUCTION

The purpose of this memo is address the issue of power/EIRP control for the Space Station (SS) Ku-Band multiple access (MA) system users. Due to wide variations in user ranges and antenna gains, the dynamic range of the received signal strength could be quite large. This may necessitate the implementation of a system for controlling the users transmitted power or EIRP. This memo examines an approach to the problem from both a system and hardware perspective.

2.0 PROBLEM STATEMENT

Users of the Ku-Band MA system fall into one of four categories. They are listed here along with the approximate gain of their antennas:

(1) Free Fliers (FF) — 30.3 dB

(2) Orbital Maneuvering Vehicle (OMV) — 13.3 dB

(3) Extravehicular Mobility Unit (EMU) — 3 dB

(4) Mobile Service Center (MSC) — 3 dB

Additionally, they will have a transmitted output power baselined at 1 watt cw (BPSK, QPSK, or 8-PSK*) and an operating frequency range of 14.5 – 14.76 or 14.6 – 14.9 GHz. The difference in the transmitted EIRP of these users along with the wide variation in range will result in a large dynamic range of received signal strength at the SS receiver front end. Since a single receiver must accommodate all MA users, gain control at the receiver is ineffective when signals are received from more than one user at the same time.** As a result, some means must be employed to control user EIRP. This may take the form of a reduction in transmitter output power, switching to a lower gain antenna, or both. A quantitative analysis of the problem has shown that at least 30 – 40 dB of power/EIRP control may be required to maintain received signal strength levels within an acceptable range.

3.0 SYSTEM APPROACH

Switching between antennas as a means of reducing EIRP results in abrupt changes in the received signal power. Additionally, if only two antennas are employed, only two EIRP values are obtainable resulting in coarse power control. Coupled with the expense of engineering multiple antennas, it makes this approach the least attractive. The 30 – 40 dB reduction in EIRP is most easily obtained by varying the transmitter output power.

An approach to this solution is shown in Figure C-1. The user transmitter output power is controlled by varying the driver signal to the solid state amplifier with a PIN diode attenuator. A measurement of the received signal strength for a particular user is made by the SS signal processor. If the signal strength falls below or rises above some predetermined value, a command to change the transmitter output power accordingly is generated and modulated onto the SS to user command link. The signal processor in the user decoders the command and sends the appropriate control signals to the attenuator. The

* May require 2.5 watts
** This statement applies to a non-channelized, wideband receiver.

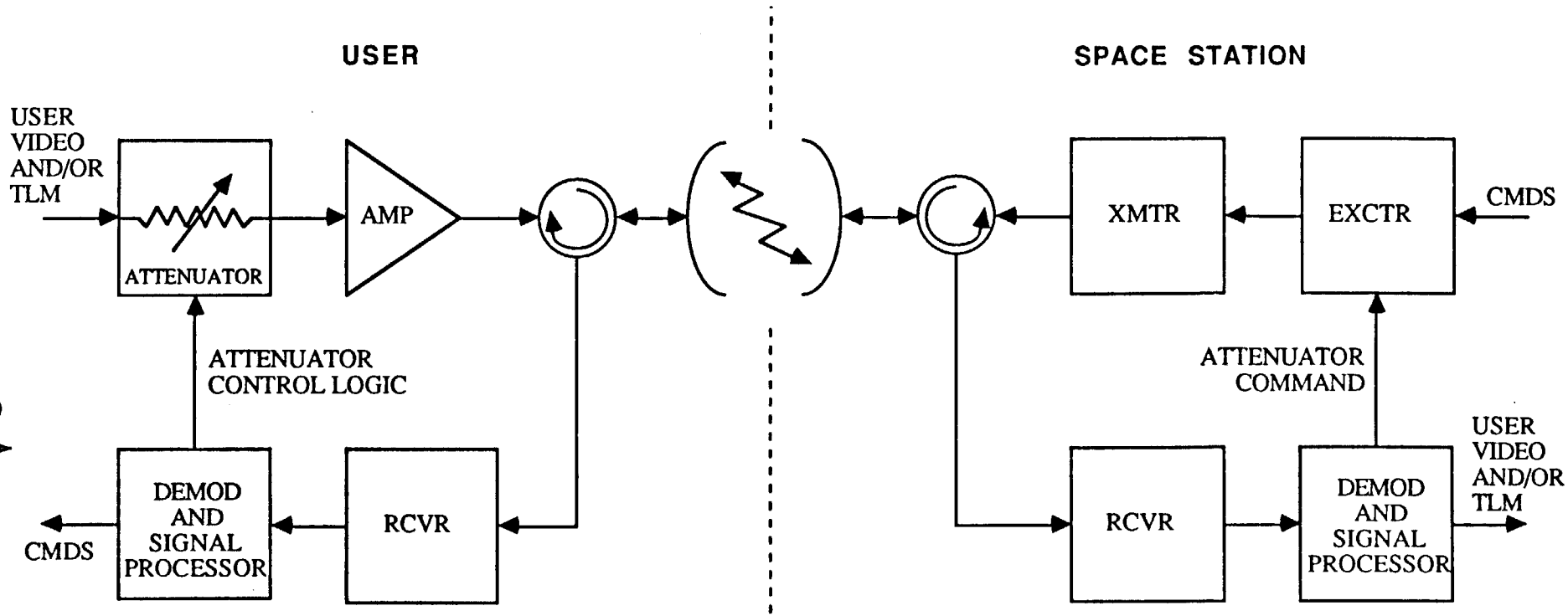

AMPLIFIER:

- Solid State
- 1 watt @ 14.5 — 15 GHz
- Gain = 30 dB
- NF = 10 dB
- SNR_{max} = 77 dB
- SNR_{min} = 17 dB

ATTENUATOR:

- PIN Diode
- 0 — 60 dB
- Continuous

Figure C-1. Functional Block Diagram for User Power Control.

result is similar, a closed loop AGC system. How often the attenuator must be updated and with what granularity would have to be determined based on a study of the rate of change of signal strength due to user motion.

4.0 HARDWARE CONSIDERATIONS

It is worthwhile to examine current device technology and identify possible components that would allow control of the user transmitter output power. A quick review of the requirements shows:

(1) User Output Power = 1 watt cw

(2) Operating Frequency Range = 14.5 – 14.76 or 14.6 – 14.9 GHz

(3) 30 to 40 dB of EIRP/power control

In addition, we require that the 30 – 40 dB of EIRP/power control be achieved by varying the input power to the power amplifier in a linear or quasi-linear manner.

The input-output characteristics of current solid state amplifiers follow the traditional "S" curve found with tube and other types of amplifier, i.e,. a thermal noise floor transitioning to a linear region transitioning into a saturated region. The linear region extends from the noise floor to the 1 dB compression point. This is the point where a 10 dB increase in input signal power results in only a 9 dB increase in output signal power. The dynamic range of the linear region can be quite large – often greater than 70 dB.

It's instructive to look at a specific example. Avantek makes a series of communication satellite uplink driver amplifiers (see attachment) that are typical of devices on the market whose performance characteristics closely match the stated requirements. Model #AWP 145101 has the following characteristics:

Frequency Range:	14.0 – 14.5 GHz
Output Power:	30 dBm (1 watt)
Gain:	30 dB

Noise Figure: 10 dB

The thermal noise floor of this device is determined by the following:

$$P_T = NF - 114 \text{ dBm} + 10 \log Bw$$

where

P_T = noise power in dBm

NF = noise figure = 10 dB

Bw = operating bandwidth in MHz = 300 (14.9 – 14.6 GHz)

$$P_T = 10 \text{ dB} - 114 \text{ dBm} + 10 \log 300$$

$$= 10 \text{ dB} - 114 \text{ dBm} + 24.8 \text{ dB}$$

$$P_T = -79.2 \text{ dBm}$$

If the 1 dB compressed gain maximum output power of the device is 30 dBm and the gain 30 dB, then the maximum input signal power is 0 dBm. Hence, the dynamic operating range of the linear region is approximately 79 dB (0 dBm – 79.2 dBm)

While step attenuators could be used to vary the input (and hence the output) power of the signal, given the linear characteristics of the amplifier, the use of continuous attenuators such as PIN diodes is more appropriate. The use of step attenuators can result in phase discontinuities in the signal when switched. Avantek packages many of their amplifiers with a PIN diode attenuator as part of the first stage of the amplifier. Control of the amount of attenuation is obtained by varying the bias voltage to the diode. This can be done mechanically by means of a potential meter mounted on the case, or electrically by means of a gain control circuit. Depending on the frequency, a single PIN diode stage can yield 30 dB of attenuation. If more attenuation is required, additional stages may be connected in series. For example, General Microwave Corporation's Model 3250 digitally

controlled PIN diode attenuator provides up to 60 dB variable attenuation within the band of interest (see attachment).

An alternative, but generally less desirable method of changing the output power is to vary the DC bias voltage to the output stage of the amplifier. This has the adverse effect of changing many of the parameters of the amplifier which, depending on the specific application, may or may not be a problem. Typical changes that result in varying the DC bias voltage are an increase in the noise figure, lowered gain, reduced linear operating region, and degradation of the AM–PM conversion characteristics.

It will be noted that the communications satellite uplink driver amplifiers listed in the attached sheet and used as an example in the section have an operating frequency range of 14.0 to 14.5 GHz while the requirements specify 14.5 to 14.9 GHz operating range. Discussions with manufacturer representatives have verified that the performance characteristics listed would just as easily be obtained for devices in the required operating band. As the attached sheet shows, the amplifies listed are all designed to meet an existing application. The lack of devices in the 14.5 to 14.9 GHz range is only a reflection of the lack of a demand for such a product and not of any technical difficulties in achieving them.

5.0 CONCLUSIONS

We have presented a variable approach to the user power/EIRP control problem. While effective, it has the drawback of adding additional complexity to the system design of both the user and the SS. A simpler alternative might be to have the users control their output power based solely on their range to the SS. This would result in a simplified open loop system not involving the SS.

MEDIUM POWER, COMMERCIAL COMMUNICATIONS BAND AMPLIFIERS

Guaranteed Specifications @ 25°C Case Temperature

PC5

Model	Frequency Response (MHz) Minimum	Power Output for 1 dB Gain Compression (dBm/Watts) Minimum	Gain (dB) Minimum	Gain Flatness (± dB) Maximum	Typical Intercept Point for IM Products (dBm)	Noise Figure (dB) Maximum	VSWR (50 ohms) Maximum In	VSWR (50 ohms) Maximum Out	Input Power Voltage (VDC ± 3%)	Input Power Current (mA) Typical
3700 to 4200 MHz Point-to-Point Communications Amplifiers										
AWP-42107	3700-4200	+25/.3	26	2	+35	10	1.2	1.2	+15	500
AWP-42108	3700-4200	+32/1.5	33	2	+40	10	1.2	1.2	+15	1200
AWP-42109	3700-4200	+40/10	41	2	+47	10	1.2	1.2	+15	6000
5925 to 6425 MHz Point-to-Point Communications or Satellite Uplink Amplifiers										
AWP-64107	5925-6425	+25/.3	26	2	+34	10	1.2	1.2	+15	500
AWP-64108	5925-6425	+32/1.5	33	2	+40	10	1.2	1.2	+15	1200
AWP-64109	5925-6425	+40/10	41	2	+46	10	1.2	1.2	+15	6000
6425 to 7125 MHz Point-to-Point Communications Amplifiers										
AWP-71107	6425-7125	+25/.3	26	2	+34	10	1.2	1.2	+15	500
AWP-71108	6425-7125	+32/1.5	33	2	+40	10	1.2	1.2	+15	1200
AWP-71109	6425-7125	+40/10	41	2	+46	10	1.2	1.2	+15	6000
7125 to 7725 MHz Point-to-Point Communications Amplifiers										
AWP-77107	7125-7725	+25/.3	26	2	+34	10	1.2	1.2	+15	500
AWP-77108	7125-7725	+32/1.5	33	2	+40	10	1.2	1.2	+15	1200
AWP-77109	7125-7725	+40/10	41	2	+46	10	1.2	1.2	+15	6000
7725 to 8500 MHz Point-to-Point Communications Amplifiers										
AWP-85107	7725-8500	+25/.3	26	2	+34	10	1.2	1.2	+15	500
AWP-85108	7725-8500	+32/1.5	33	2	+40	10	1.2	1.2	+15	1200
AWP-85109	7725-8500	+40/10	41	2	+47	10	1.2	1.2	+15	6000
7725 to 8275 MHz Point-to-Point Communications Amplifiers										
AWP-83107	7725-8275	+25/.3	26	2	+34	10	1.2	1.2	+15	500
AWP-83108	7725-8275	+32/1.5	33	2	+40	10	1.2	1.2	+15	1200
AWP-83109	7725-8275	+40/10	41	2	+47	10	1.2	1.2	+15	6000
10.7 to 11.7 GHz Point-to-Point Communications Amplifiers										
AWP-117107	10.7-11.7	+25/.3	26	2	+32	10	1.2	1.2	+15	500
AWP-117108	10.7-11.7	+32/1.5	33	2	+39	10	1.2	1.2	+15	1200
AWP-117109	10.7-11.7	+37/5	38	2	+43	10	1.2	1.2	+15	6000
14.0 to 14.5 GHz Communications Satellite Uplink Drivers										
AWP-145001	14.0-14.5	+24/.25	20	.25/40 MHz	+30	10	1.2	1.2	+15	400
AWP-145001	14.0-14.5	+27/.5	20	.25/40 MHz	+33	10	1.2	1.2	+15	900
AWP-145101	14.0-14.5	+30/1.0	30	.25/40 MHz	+36	10	1.2	1.2	+15	1000
AWP-145102	14.0-14.5	+33/2	30	.25/40 MHz	+39	10	1.2	1.2	+15	4500
AWP-145103	14.0-14.5	+34/3	30	.25/40 MHz	+40	10	1.2	1.2	+15	4500
AWP-145503	14.0-14.5	+34/3	40	.25/40 MHz	+40	10	1.2	1.2	+15	4500
AWP-145504	14.0-14.5	+36/4	40	.25/40 MHz	+41	10	1.2	1.2	+15	6000
AWP-145505	14.0-14.5	+37/5	40	.25/40 MHz	+42	10	1.2	1.2	+15	6000

For case drawings, contact Avantek, Inc., 180 Blue Ravine Road, Folsom, CA 95630 - Phone (916) 985-1201.

Note 1: Units are available with or without top and/or bottom heatsinks.

Model 3250 Ultra-Broadband Digitally-Programmable PIN Diode Attenuator

- **Frequency range: 0.2 to 18 GHz**
- **Attenuation range: Up to 60 dB**
- **Binary or BCD programming**
- **Absorptive**
- **Guaranteed Monotonicity**

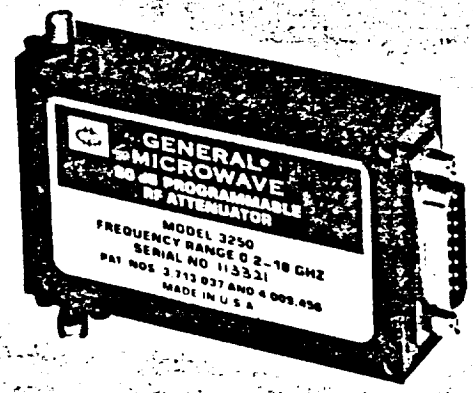

The Model 3250 digitally programmable attenuator provides excellent performance characteristics over the frequency range of 0.2 to 18 GHz. Attenuation levels up to 60 dB are programmable in increments of 1 dB.

The unit is an integrated assembly of a dual T-pad PIN diode attenuator and a driver consisting of a D/A and a V/I Converter. See figures 1 and 2.

The Model 3250 operates as a bilaterally-matched device at all attenuation levels. It is supplied in a compact rugged package well-suited to military applications.

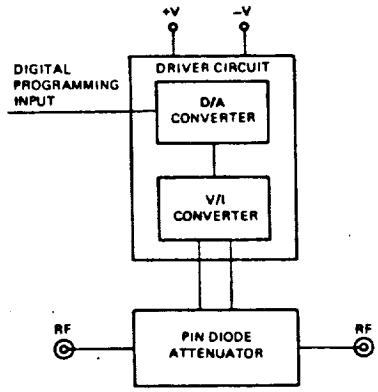

Fig. 1-Model 3250, block diagram

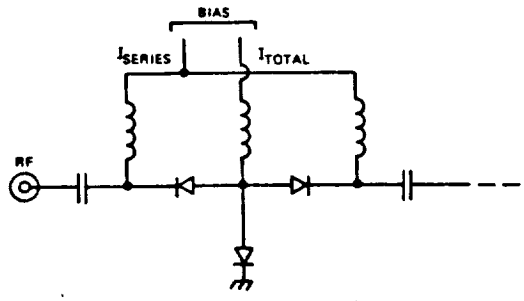

Fig. 2-Model 3250, rf schematic diagram (unit consists of two such sections)

PERFORMANCE CHARACTERISTICS

Frequency Range . . . . . 0.2 to 18 GHz

Mean Attenuation Range
0.2 to 12.4 GHz . . . . . 60 dB
12.4 to 18 GHz . . . . . 50 dB

Insertion Loss (max.)
0.2 to 8 GHz . . . . . 2.5 dB
8 to 12.4 GHz . . . . . 3.0 dB
12.4 to 18 GHz . . . . . 5.0 dB

VSWR (max.)
0.2 to 8 GHz 1.75
8 to 12.4 GHz 2.0
12.4 to 18 GHz 3.0

Accuracy of Attenuation(1) . ±0.3 dB

Temperature Coefficient . . . 0.02 dB/°C max.

Power Handling Capability
Without Performance Degradation . . . . . From 0.4 to 100 mW cw or peak (see Figure 3 below)

Power Handling Capability (con't)
Survival Power (from −65°C to +25°C; see power derating curve, Figure 4 below, for higher temperatures) . . . . . 2W average or peak (1 μsec max pulse width)

Switching Time . . . . . 20 μsec max.

Programming . . . . . Positive true binary (standard) or BCD (option 1). For complementary code, specify Option 2.

Minimum Attenuation Step . 1.0 dB

Logic Input
Logic 0 . . . . . −0.3 to +0.7V
Logic 1 . . . . . +2.5 to +5.0V

Power Supply Requirements . . . . . +5V ±5%, 310 mA
+15V ±5%, 100 mA
−15V ±5%, 100 mA

Power Supply Rejection . . . Less than 0.1 dB/volt change in any supply

FLATNESS (±dB)			
	Frequency (GHz)		
ATTEN. (dB)	0.2 to 8.0	0.2 to 12.4	12.4 to 18.0
10	0.5	0.7	1.0
20	0.5	1.0	1.0
30	0.7	1.5	1.5
40	1.0	1.5	1.5
50	1.0	1.5	1.5
60	1.0	1.5	1.5

(1) *At calibration frequency. All units are calibrated at 4 GHz. Calibration at other frequencies within the band is available upon request.*

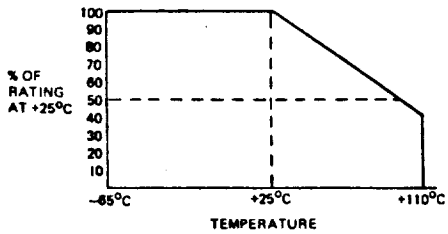

Fig. 3-Model 3250, maximum peak and average operating power without performance degradation.

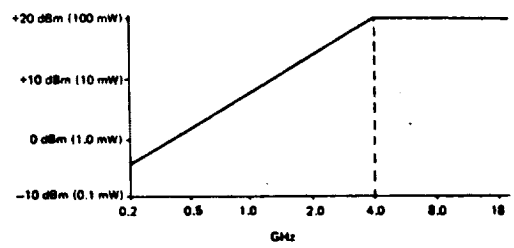

Fig. 4-Model 3250, survival power derating factors.

Model 3250 Specifications

ENVIRONMENTAL RATINGS

Operating Temperature Range ..... −54°C to +110°C
Non-Operating Temperature Range .... −65°C to +125°C
Humidity ..... MIL-STD-202F, Method 103B, Cond. B (96 hrs. at 95%)

Shock ..... MIL-STD-202F, Method 213B, Cond. B (75G, 6 msec)

Vibration ..... MIL-STD-202F, Method 204D, Cond. B (.06" double amplitude or 15G, whichever is less)

Altitude ..... MIL-STD-202F, Method 105C, Cond. B (50,000 ft.)

Temp. Cycling ..... MIL-STD-202F, Method 107D, Cond. A, 5 cycles

AVAILABLE OPTIONS

Option No.	Description
1	BCD programming (Binary is standard
2	Complementary programming (positive true is standard)
7	Two SMA male rf connectors
10	One SMA male and one SMA female rf connector

PIN FUNCTIONS

PIN NO.	BINARY	BCD (Opt. 1)
1	SPARE	SPARE
2	SPARE	SPARE
3	+5V	+5V
4	DIGITAL & POWER GND	DIGITAL & POWER GND
5	GND	1 dB
6	GND	2 dB
7	1 dB	4 dB
8	2 dB	8 dB
9	4 dB	10 dB
10	8 dB	20 dB
11	16 dB	40 dB
12	32 dB	OPEN (NO CONNECTION)
13	+15V	+15V
14	−15V	−15V
15	SPARE	SPARE

ACCESSORY FURNISHED

Mating power/logic connector

DIMENSIONS AND WEIGHTS

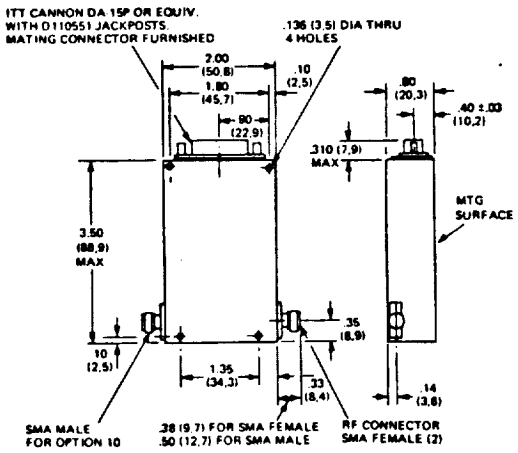

MODEL 3250
Wt: 4 oz. (113 gm) approx.

Dimensional Tolerances, unless otherwise indicated: .XX ± .02; .XXX ± .005

APPENDIX O

DESIGN CONSIDERATIONS FOR A UNIVERSAL MULTI-CHANNEL MODEM FOR SPACE STATION KU-BAND LINKS

DESIGN CONSIDERATIONS FOR A UNIVERSAL MULTI-CHANNEL MODEM FOR SPACE STATION KU-BAND LINKS

Interim Report

Contract No. NAS9-17414

Prepared for

NASA Lyndon B. Johnson Space Center
Houston, TX 77058

Technical Monitor: Dean Bratton

Prepared by

Sergei Udalov
James Dodds

Axiomatix
9841 Airport Boulevard
Suite 912
Los Angeles, CA 90045

Axiomatix Report No. R8702-2
February 28, 1987

TABLE OF CONTENTS

	PAGE
List of Figures	i
List of Tables	iii
1.0 INTRODUCTION AND OVERVIEW	1
2.0 MODEM REQUIREMENTS	2
3.0 MODEM IMPLEMENTATION	7
3.1 Modulator Configurations	7
3.1.1 Configuration for 4/8-PSK with Two Quadrature Modulators	7
3.1.2 Configuration for 4/8-PSK with Two AM Modulators	14
3.2 Demodulator	18
3.2.1 Block Diagram Description	18
3.2.2 Carrier Tracking Error Circuit	21
3.2.3 Data Recovery Circuitry	23
3.2.3.1 Data Recovery for 8-PSK Mode	23
3.2.3.1 Data Recovery for 4-PSK Mode	26
3.3 Design Considerations	29
3.3.1 Channel BER	29
3.3.1.1 General	29
3.3.1.2 Effect of Data Angle Imbalance on Channel BER	31
3.3.2 Tolerance to RF Circuitry Impairments	34
3.3.2.1 Amplitude and Delay	36
3.3.2.2 Carrier Phase Jitter	36
3.3.3 Implementation Philosophy	38

4.0 CONCLUSIONS 40

REFERENCES 41

APPENDIX A 42

A-1 Introduction 43

A-2 Analysis 45

LIST OF FIGURES

		PAGE
Figure 2.1	Functional Diagram of a Multi-Channel 4/8-PSK Modem System	4
Figure 2-2	Functional Hardware Partitioning for the 4/8-PSK Modulator and Demodulator	5
Figure 3.1.1-1	Quadrature Modulator Implementation with Two Bi-Phase Modulators	8
Figure 3.1.1-2	Functional Block Diagram of 4/8-PSK Modem Implemented with Two Quadrature Modulators	9
Figure 3.1.1-3	Generation of an 8-PSK Signal by Means of Two Quadrature Modulators Shifted by 45 Degrees	11
Figure 3.1.1-4	Octal Mapper for 3-Channel 8-PSK Modulator Implementation with Two Quadrature Modulators	12
Figure 3.1.1-5	Octal Mapper Logic Implementation	13
Figure 3.1.2-1	Signal Constellation and Coordinate Definition for 8-PSK Modulation	15
Figure 3.1.2-2	Functional Block Diagram of 4/8-PSK Modem Implemented with Two AM Modulators in Quadrature	16
Figure 3.2.1-1	Block Diagram for an 4/8-PSK Demodulator	19
Figure 3.2.1-2	Phase Relationship between Phase Detector Pairs A/B and C/D and an 8-PSK Signal	20
Figure 3.2.2-1	Carrier Tracking Error Circuit	22
Figure 3.2.2-2	Carrier Tracking Error for 8-PSK and for 4-PSK Modulation	24
Figure 3.2.3-1	Data Recovery Circuitry and Decoding Algorithm for an 8-PSK Demodulator	25
Figure 3.2.3-2	Data Demodulation Circuit for 8-PSK Demodulator	28
Figure 3.3.1.1-1	BER vs. PSK Modulation Level and Symbol-to-Noise Ratio E_s/E_N	30
Figure 3.3.1.2-1	Effect of Imbalance on Channel BER vs. E_s/E_N Ratio	32

Figure 3.3.1.2-2	Channels 1 & 2 vs. Channel 3 Imbalance (α)	33
Figure 3.3.1.2-3	Effect of Imbalance on Average BER of Channels 1, 2, and 3	35
Figure 3.3.2.1-1	Power Penalties Due to Amplitude and Delay Distortion at BER = 10^{-6}	37
Figure 3.3.2.2-1	Power Penalties Due to Carrier Phase Jitter at BER = 10^{-6}	37
Figure 3.3.3-1	Block Diagram of a Digitally Implemented Demodulator	39
Figure A-1	Demodulator for 4-PSK (QPSK) Mode	44

LIST OF TABLES

		PAGE
Table 2-1	Return Link Requirements for Ku-band MA-Users	3
Table 3.2.3-1	Demodulator Output Signals for an 8-PSK Demodulator	27

1.0 INTRODUCTION AND OVERVIEW

This report presents a baseline design of a universal 4/8-PSK modem for potential utilization by the Space Station Ku-band, multiple-access system users. Although the present concept of the return links can be satisfied by a conventional 4-PSK (i.e., QPSK) modulation providing either two independent channels, or one channel coded at rate 1/2, the motivation to consider the 8-PSK mode results from the MSC requirement for 3 digital television channels. Thus, the idea expressed in this report is that a 4-PSK modem design baselined for the major portion of users can be expanded to include an 8-PSK capability at a reasonable cost in increased complexity. In other words, the intent here is to assume a 4-PSK design as a baseline which is easily expanded to include an 8-PSK capability. Ideally, the component partitioning would be such that a major portion of the modem will consist of the 4-PSK capability, with the 8-PSK capability provided in the form of plug-in modules for the MSC user as well as for other users which may require 3 digital TV channels in the future.

The design considerations presented in this report are driven by the requirement to transmit and receive digital TV signals at rates up to 22 Mbps – 25 Mbps per channel. Thus, circuit configurations which can be implemented by high speed circuitry are given primary consideration.

The requirements for the modem in terms of data rates are summarized briefly in Section 2. Modem implementation is outlined in Section 3. In Section 3.1 modulator configurations are presented. Section 3.2 then describes a design for a corresponding demodulator. Section 4 presents conclusions. Appendix A contains a simplified analysis of modem operation in the 4-PSK mode.

2.0 MODEM REQUIREMENTS

The return link requirements for Ku-band MA users are summarized in Table 2-1. From the table, it can be seen that there are basically two return rates; one at about 100 kbps and the other at about 22 Mbps. Although, as shown in the table, the two Phase B contractors established slightly different requirements for these two rates, the implementation driver for the modem is still the upper rate which may be as high as 25 Mbps according the RI estimate.

The functional goals which are the motivators for considering an 8-PSK modem to meet the MSC requirement for 3 simultaneous digital TV channels are as follows:

1) Addition of the three-channel capability must not increase RF channel bandwidth significantly beyond that for the two-channel mode.

2) Modulation method should not change drastically when the modem switches from 2-channel to 3-channel mode.

3) The modem must have as much hardware commonality as possible between the 2-channel and the 3-channel modes.

Figure 2-1 shows a functional diagram of a 4/8-PSK multi-channel modem utilization within the Ku-band MA system. As indicated, the 4-PSK (i.e., QPSK) mode is the baseline, and the 8-PSK mode is considered as a multi-channel capability. This diagram is responsive to the goals stated above. One of the salient features of the concept shown in Figure 2-1 is that a constant envelope signal is provided by the 8-PSK operation making it fully compatible with the RF amplification equipment used with the 4-PSK mode.

Figure 2-2 shows a functional hardware partitioning for the proposed 4/8-PSK modulator and the corresponding demodulator. The main idea expressed in Figure 2-2 is that the 4-PSK mode is the baseline mode for the modem and that the 8-PSK mode is a hardware "add-on" to be utilized by such users as the MSC. Such partitioning requirement determines the modem implementation/configuration design described in the subsequent section of this report.

User	Requirement Rates				Comments
	TLM/Voice (kbps)		Video (Mbps)		
	MCDD	RI	MCDD	RI	
MSC	160	128	22	25	Three simultaneous video signals are required.
EVA	100	128	22	25	
NSTS	100	128	N/A	N/A	
OMV/OTV	100	128	22	25	
FF/COP	100	128	22	25	

MCCD = Requirement established by McDonnell Douglas Corp. team [1].
RI = Requirement established by Rockwell International team [2].

Table 2-1. Return Link Requirements for Ku-band MA-Users.

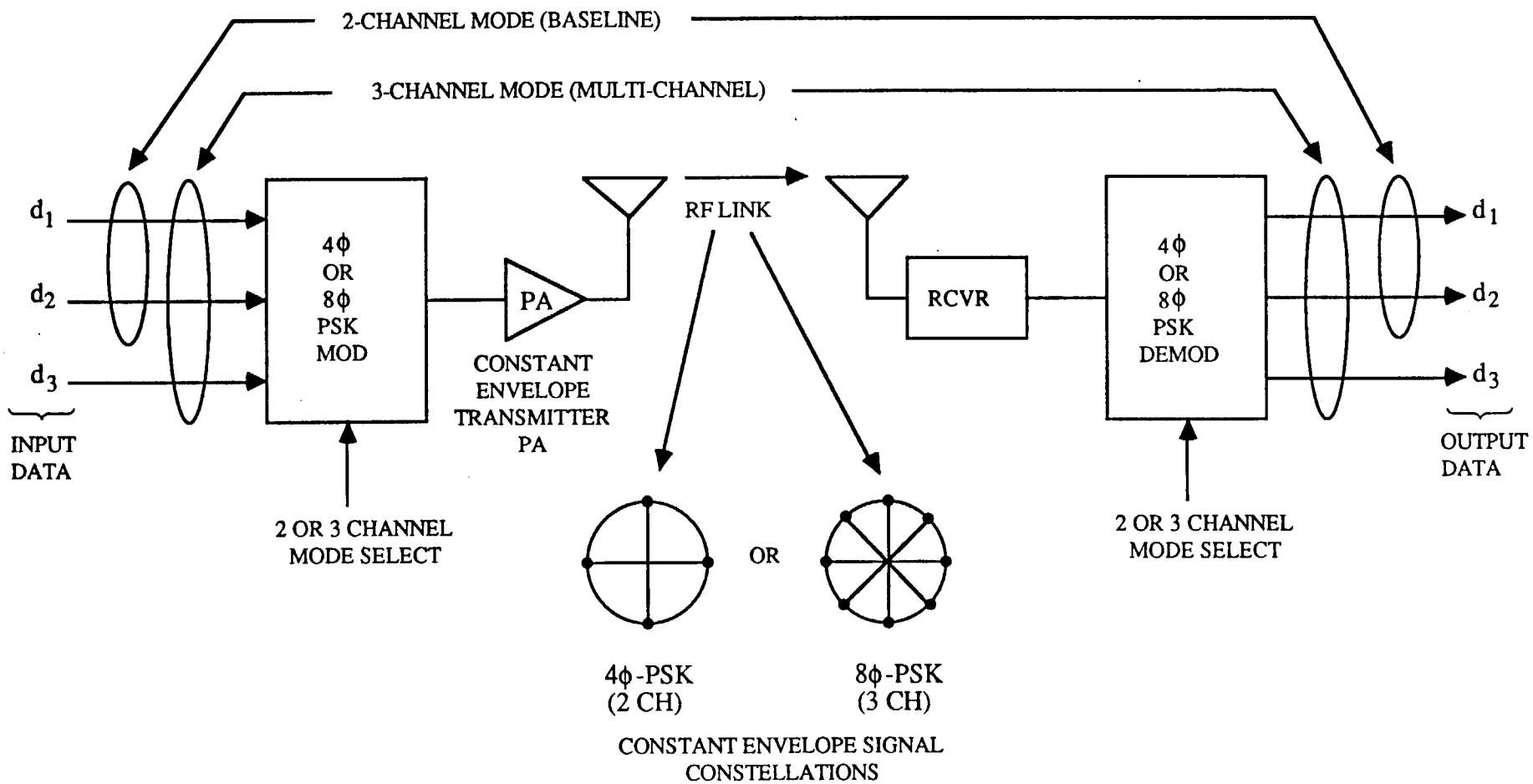

Figure 2-1. Functional Diagram of a Multi-Channel 4/8-PSK Modem System.

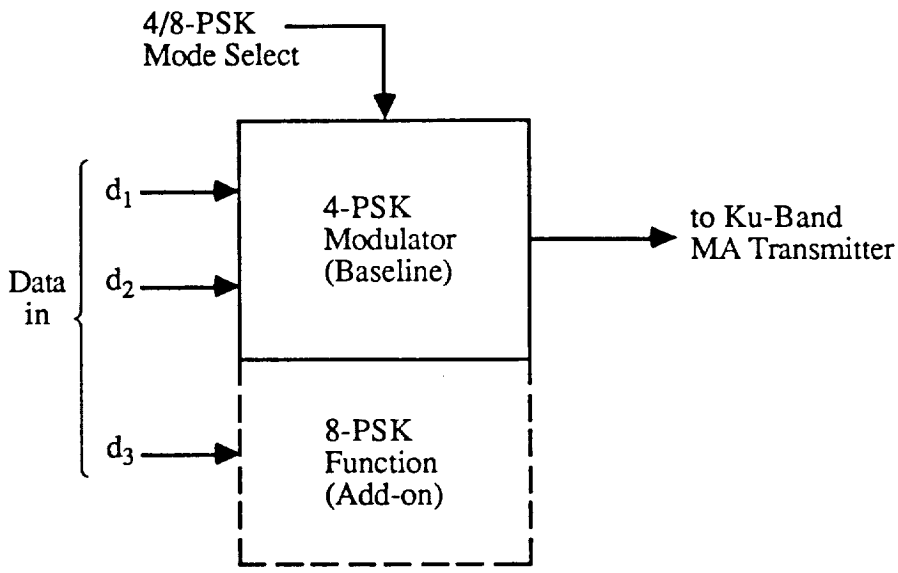

(a) Modulator

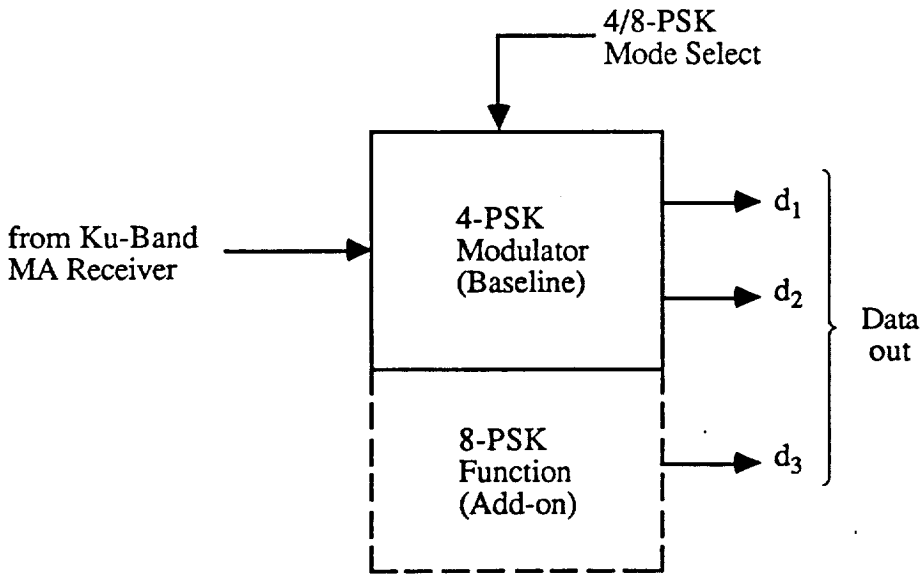

(b) Demodulator

Figure 2-2. Functional Hardware Partitioning for the 4/8 PSK Modulator (a) and Demodulator (b).

Because the subject matter of this report deals mainly with the implementation of the modulation/demodulation functions of the proposed modem, we do not address the issues of an IF frequency at which the actual modem implementation should take place. It suffices to state, however, than an IF frequency in the range of 150 MHz to 700 MHz is envisioned. The final selection of the IF frequency will be determined by the frequency plan of a particular Ku-band MA system selected for the Space Station/user application.

3.0 MODEM IMPLEMENTATION

3.1 Modulator Configurations

3.1.1 Configuration for 4/8-PSK with Two Quadrature Modulators

Because the main idea for a universal modem is to provide a maximum amount of component commonality between the 4-PSK and 8-PSK modes, let us consider first an implementation which uses two quadrature modulators to extend a 4-PSK capability to that of an 8-PSK. For this we first consider a single 4-PSK (i.e., QPSK) modulator implemented with two orthogonal bi-phase modulators.

Part (a) of Figure 3.1.1-1 shows the configuration for such a quadrature modulator implemented with two bi-phase modulators whose phases are orthogonal to each other. As shown in part (a), the bi-phase modulator #1 is driven by baseband data stream a(t), and bi-phase modulator #2 is driven by baseband data b(t). The resultant signal constellation is shown in part (b) of Figure 3.1.1-1.

The positions of the resultant QPSK vectors shown in (b) have been arranged according to the Gray coding technique. With this technique a 90° phase error in the demodulator output results in only a one-bit output error at the time of the error. With other coding schemes both output bits will be in error when a 90° wrong decision is made at the demodulator. This is an important point, because in the subsequent implementation of an 8-PSK modulator, the phase constellation representing positions of 3-bit symbols will be also encoded with Gray code.

Figure 3.1.1-2 shows a functional diagram of 4/8-PSK modem implemented with two quadrature modulators. Each of these modulators is like the quadrature modulator shown in (a) of Figure 3.1.1-1. Thus when the modem is in the 4-PSK mode, only modulator #1 is operational. In this mode it accomodates two baseband channels a(t) and b(t). These can be either two independent channels or two components of rate 1/2 encoded single data stream.

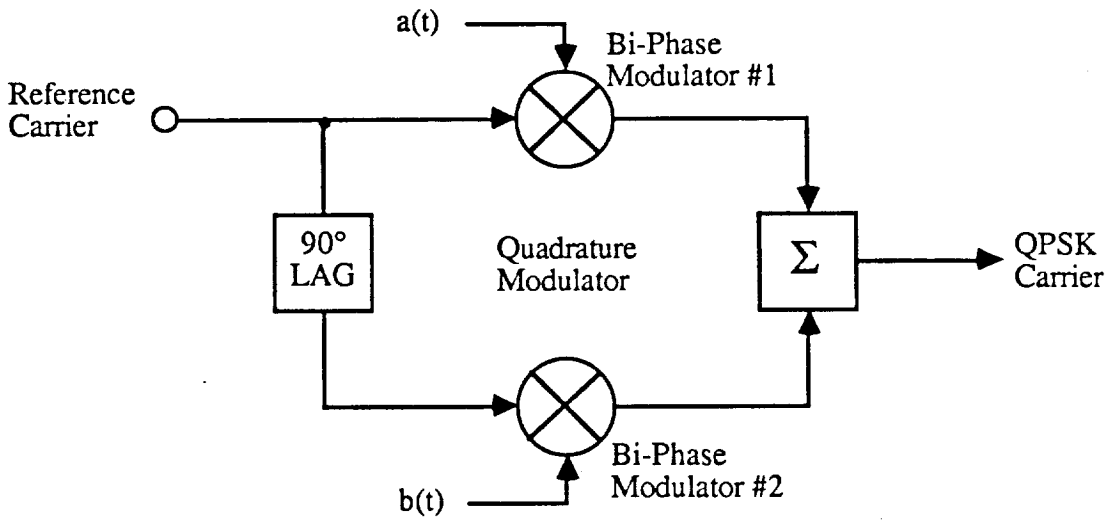

(a) Generic Diagram

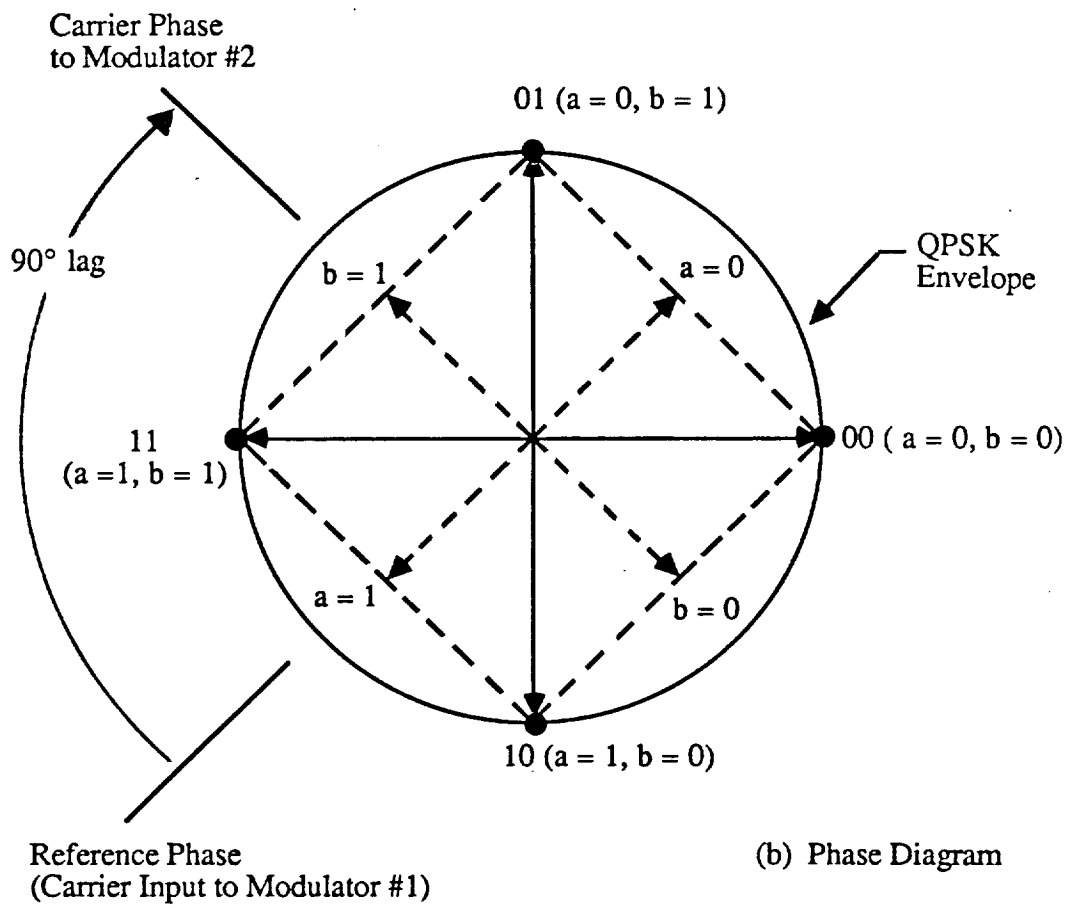

(b) Phase Diagram

Figure 3.1.1-1. Quadrature Modulator Implementation with Two Bi-Phase Modulators

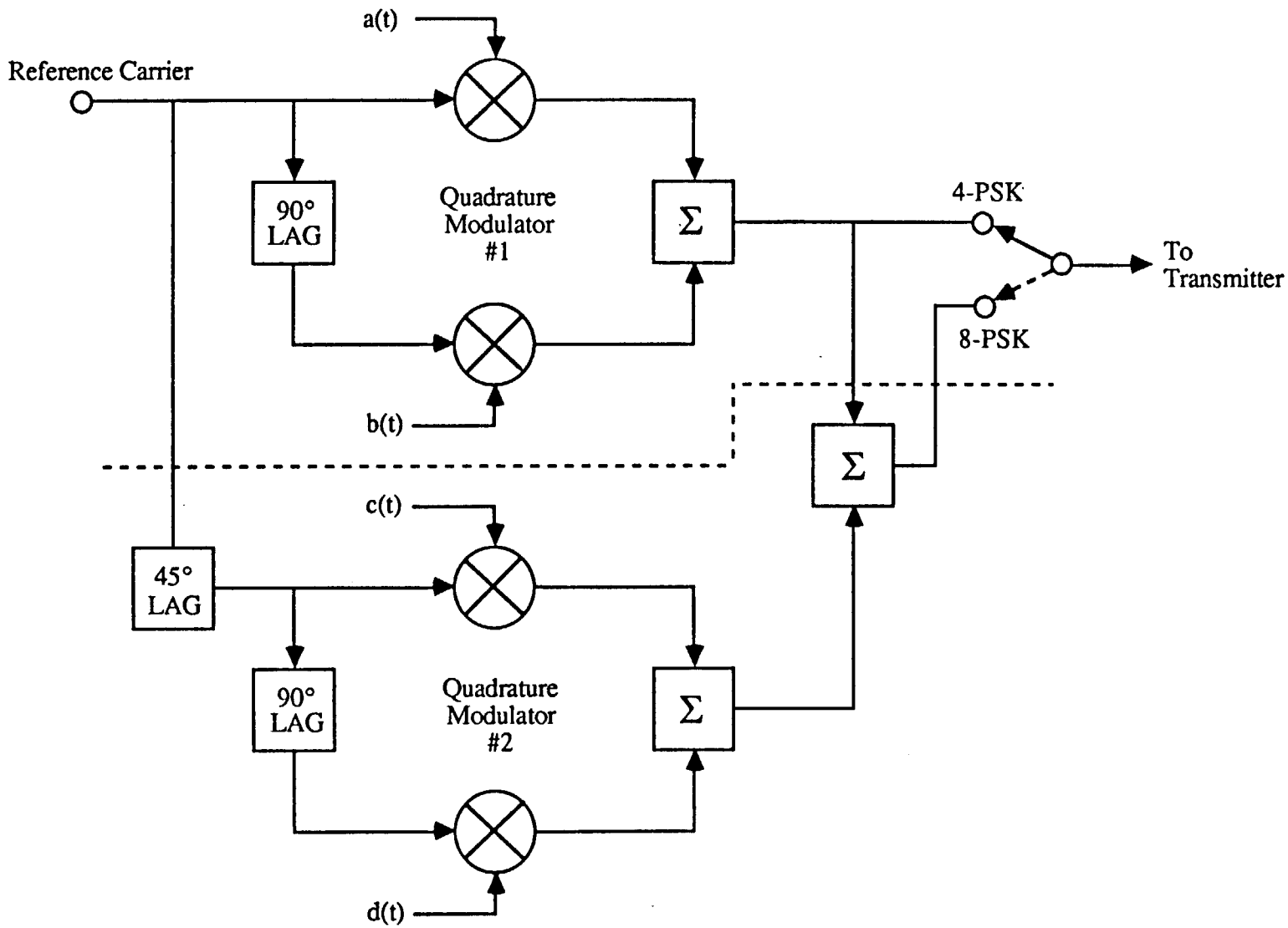

Figure 3.1.1-2. Functional Block Diagram of 4/8-PSK Modem Implemented with Two Quadrature Modulators.

For the 8-PSK mode quadrature modulator #2 is activated in addition to modulator #1 and the outputs of the two modulators are added together to provide an 8-PSK signal. The resultant signal constellation is shown in Figure 3.1.1-3. As can be seen from this constellation, as well as from Figure 3.1.1-2, the outputs of the two quadrature modulators are shifted by 45° with respect to each other. This phase shift permits the two modulators to generate eight vectors which are positioned at multiples of 45° along the constellation locus circle. These vectors, labeled 0 through 7, are encoded in Gray code as indicated in the corresponding parethesis.

It is important to note that use of two quadrature modulators requires two pairs of binary numbers each number consisting of two bits. These bit pairs are labeled a,b and c,d for modulators #1 and #2, respectively. The data inputs a,b and c,d are also indicated in the block diagram of Figure 3.1.1-2.

However, the maximum number of baseband data streams applied to the modem in 8-PSK mode is three. Thus, a method for generating four data streams to drive two quadrature modulators is required. This method is provided by an octal mapper shown in Figure 3.1.1-4. In that figure the logic equations which relate the three binary input data streams $d_1(t)$, $d_2(t)$, and $d_3(t)$ to the required binary pairs a,b and c,d are indicated. These equations provide for Gray code mapping of the three input data streams by means of two quadrature generators.

Figure 3.1.1-5 shows logic implementation for the octal mapper. Because of relatively high clock rates used by the modem (≈25 MHz), it is important that proper timing is maintained between signals a, b, c, and d. As can be seen in Figure 3.1.1-5, signals c and d have no logic elements in their paths, while signals a and b have traveled through logic gates. Thus, a simple way to compensate for this would be insert similar gates into paths d_1 to c and d_2 to d. These gates should be identical to the type of gates used for generating signals a and b. Typically, these may be spare gates in the same IC package as

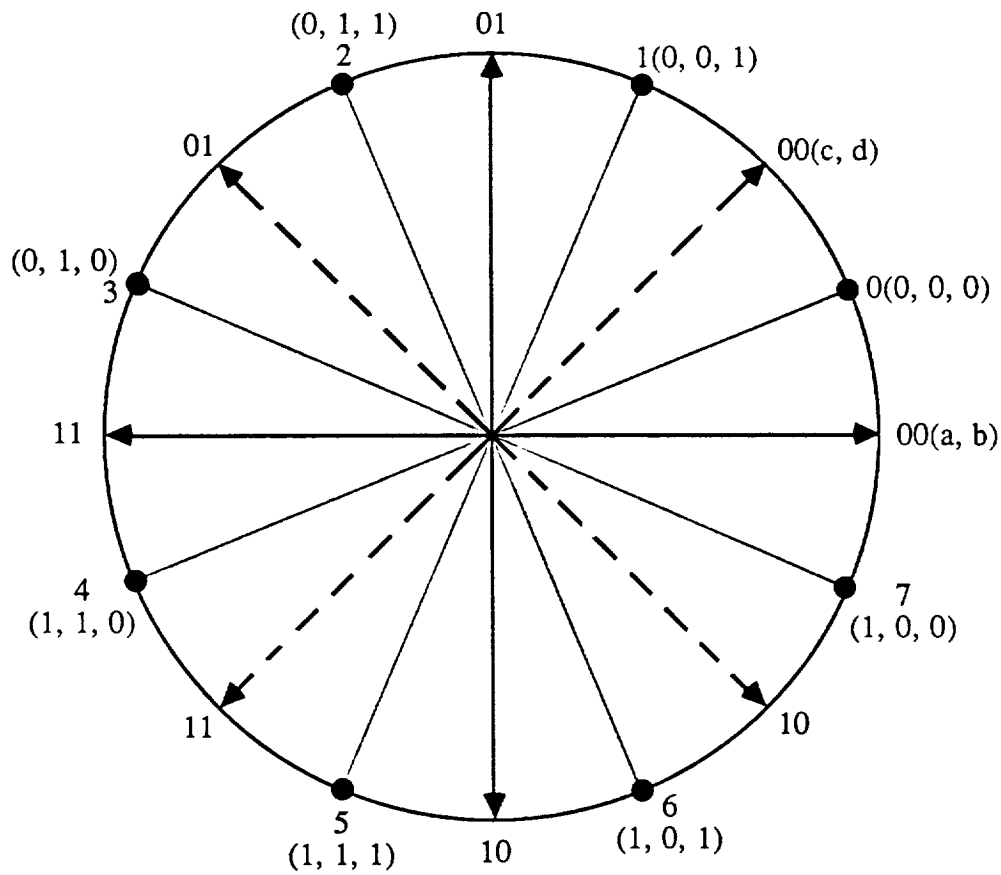

a, b = Quadrature Modulator # 1 Code
c, d = Quadrature Modulator # 2 Code

Figure 3.1.1-3. Generation of an 8-PSK Signal by Means of Two Quadrature Modulators Shifted by 45 Degrees.

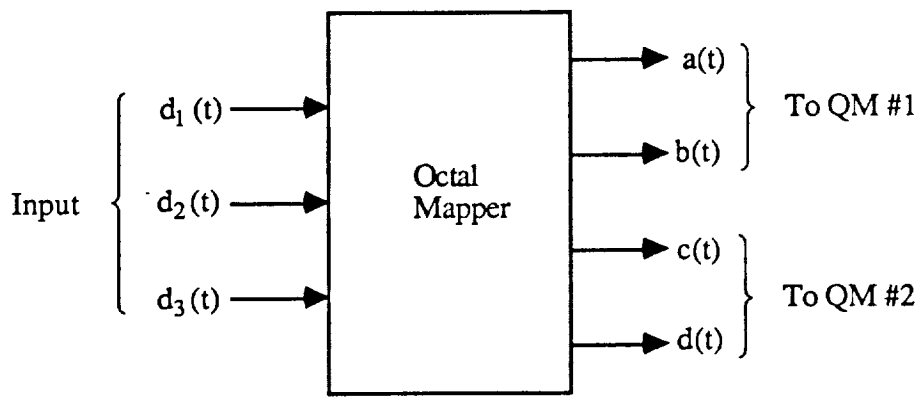

Input	Ouput
$d_1(t)$	$a(t) = d_1(t) \cdot d_3(t) + d_2(t) \cdot \overline{d}_3(t)$
$d_2(t)$	$b(t) = \overline{d}_1(t) \cdot d_3(t) + d_2(t) \cdot \overline{d}_3(t)$
$d_3(t)$	$c(t) = d_1(t)$
	$d(t) = d_2(t)$

Figure 3.1.1-4. Octal Mapper for 3-Channel 8 PSK Modulator Implementation with Two Quadrature Modulators.

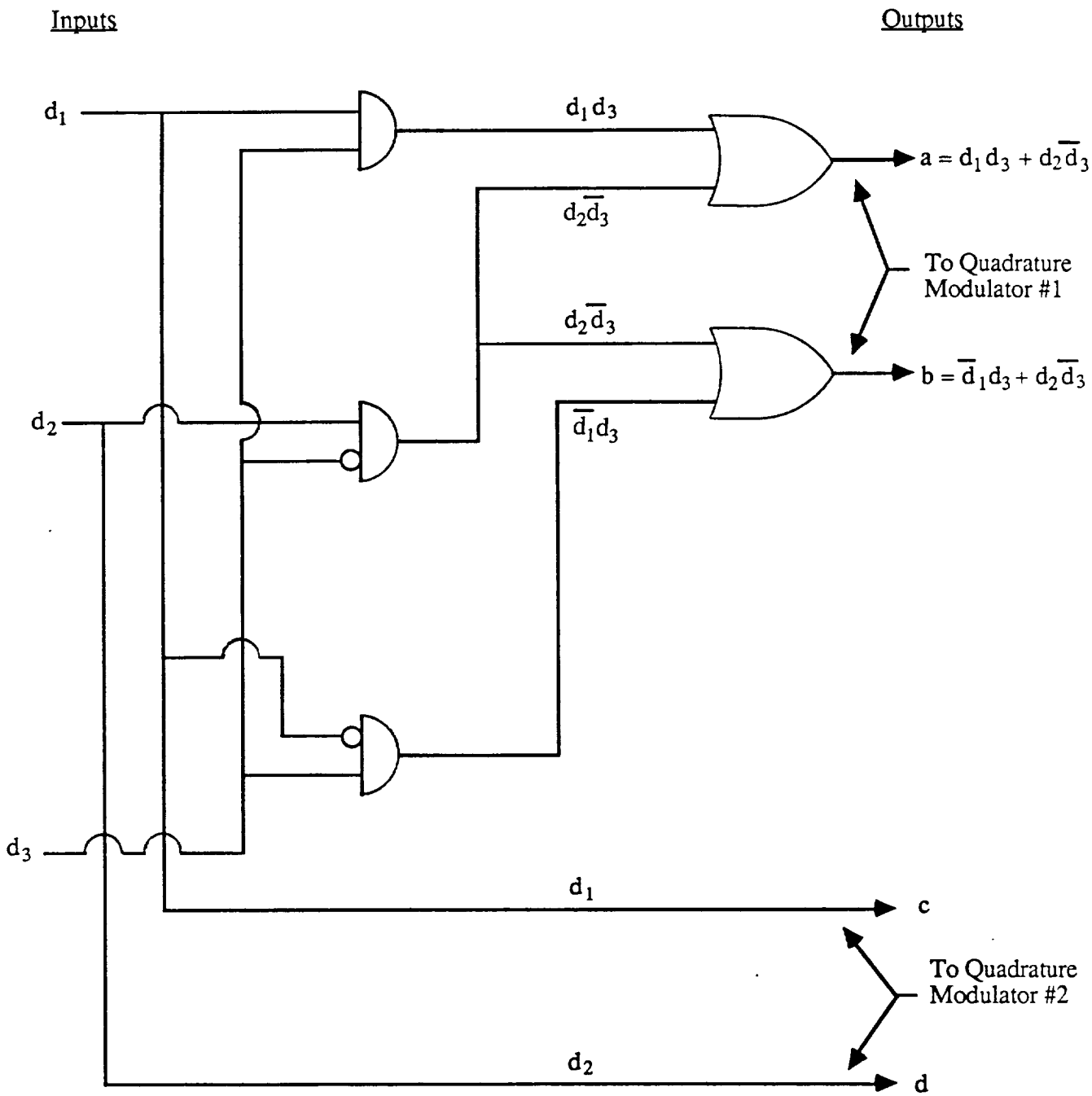

Figure 3.1.1-5. Octal Mapper Logic Implementation.

the "functional" gates. It is also recommended that emitter-coupled logic (ECL) elements be considered for modem implementation.

3.1.2 Configuration for 4/8-PSK with Two AM Modulators

An alternate approach to using two quadrature modulators for generation of 8-PSK signal would be to synthesize the eight phases of the constellation by using the appropriate in-phase (I) and quadrature (Q) components of each constellation point. This is illustrated in part (a) of Figure 3.1.2-1. As shown there, signal 0 (Gray code 0, 0, 0) consists of an I-component of 0.924 and a Q-component of 0.383 for a normalized RF envelope of unity. Part (b) of Figure 3.1.2-1 gives the I and Q values of all of the sixteen components required to form the 8-PSK constellation. Figure 3.1.2-2 shows the block diagram for implementing this approach. As shown in the figure the Quad/Octal Mapper selects the proper digital equivalents of the I and Q components based on the required mapping of the input data bits $d_1(t)$, $d_2(t)$, and $d_3(t)$ into the Gray code.

These digital components are applied to two digital/analog (D/A) converters which, in turn, feed the analog I and Q signals to the corresponding amplitude (AM) modulators. The AM modulators are driven by RF carriers which are orthogonal to each other and, consequently, the summed outputs of these modulators represents the correct phase of resultant vector.

The number of bits (n) used for D/A conversion must be a compromise between accuracy and the speed, the latter being determined by the settling time of the D/A converters. Our preliminary analysis indicates that an 8-bit accuracy is sufficient for this application. Fast settling D/A converters are available with current ECL technology which is recommended for this application.

For the 4-PSK mode, the mapper puts out digital words which result in I and Q components of ± 1.000. Based on combination of input bits $d_1(t)$ and $d_2(t)$, the appropriate quadrature coding is generated as was shown in Figure 3.1.1-1, part (b).

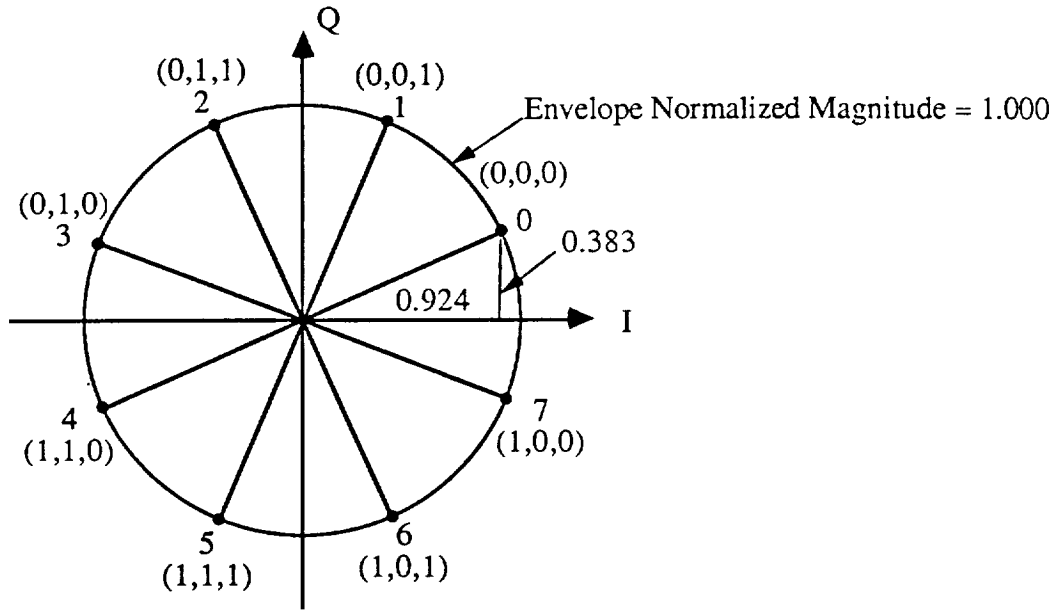

(a) 8-PSK Signal Constellation with Gray Code Mapping of Coded Binary 3-Tuple

Octal Symbol	Phase (deg.)	Magnitude of Quadrature Components	
		I	Q
0	+22.5	+0.924	+0.383
1	+67.5	+0.383	+0.924
2	+112.5	–0.383	+0.924
3	+157.5	–0.924	+0.383
4	–157.5	–0.924	–0.383
5	–112.5	–0.383	–0.924
6	–67.5	+0.383	–0.924
7	–22.5	+0.924	–0.383

(b) Signal Definition for 8-PSK

Figure 3.1.2-1. Signal Constellation (a) and Coordinate Definition (b) for 8-PSK Modulation

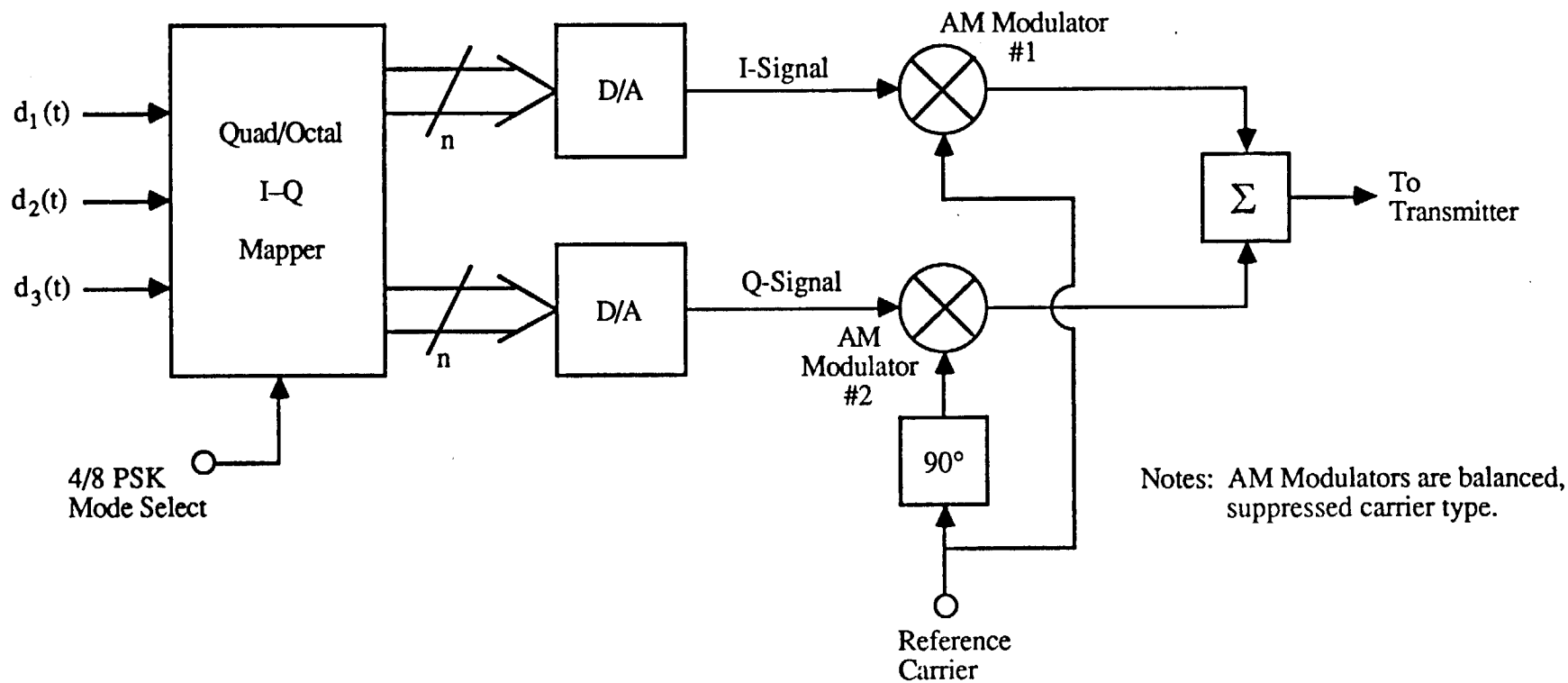

Figure 3.1.2-2. Functional Block Diagram of 4/8 PSK Modern Implemented with Two AM Modulators in Quadrature

It is important to note that only one of the AM modulators is actuated at any one time when the 4-PSK mode is being used and each of the AM modulators is putting out a carrier of unity magnitude and of phase either 0° or 180°. Thus, in designing the balanced modulators attention must be paid to switching speeds and other factors which determine the transient behavior of the modulators. An alternate approach to implementing the 4-PSK mode with two AM modulators is generate a set of I and Q components corresponding to 90° constellation spacing (i.e., I, Q = ±0.707) and use two modulators simultaneously, with only the RF phase changing to generate the required QPSK vectors. There may be some implementation advantage with this alternate approach.

At this point, however, we believe that the details of the implementation and hardware trade-offs are better left to the modem designers. Also, some breadboard tests may be required to experimentally determine the finer points of the design trade-offs.

3.2 Demodulator

3.2.1 Block Diagram Description

The block diagram for a 4/8-PSK demodulator is shown in Figure 3.2.1-1. As shown in the figure, there are four phase detectors. Phase detectors PD-A and PD-B comprise one orthogonal pair. Detectors PD-C and PD-D comprise the second orthogonal pair. Both detector pairs are driven by the local reference carrier VCO, but the VCO signal to the second pair (PD-C and PD-D) is shifted by 45 degrees with respect to the first pair (PD-A and PD-B). This relationship is shown in Figure 3.2.1-2.

It must be noted that for demodulation of a 4-PSK signal only phase detectors A and B are sufficient. However, for an 8-PSK demodulation scheme described here, all four phase detectors are required to develop the carrier tracking error and to recover the data. Thus, in all subsequent discussions, the 8-PSK mode will be emphasized due to the fact that the 4-PSK mode is only a smaller subset of the 8-PSK mode.

As indicated in Figure 3.2.1-1, the baseband outputs of the phase detectors A through D are applied to a unit labled Data Demodulation and Carrier Error Detector Circuitry. In this unit the outputs of the phase detectors are processed to generate the carrier phase tracking error θ. Also, the output data streams $d_1(t)$, $d_2(t)$, and $d_3(t)$ are recovered and applied to their respective destinations.

The bandwidth of the lowpass filters (LPFs) must be optimized to the incoming data rate. Thus, a bandwidth selection feature is also indicated in the block diagram. For example, for telemetry only mode the "low" rate is about 100 kbps. On the other hand, for digital TV and telemetry, the "high" data rate is in the order of 22 Mbps to 25 Mbps. The requirement for the modem to accommodate the high data rate is the primary driver which determines the implementation tradeoffs at the circuit design level.

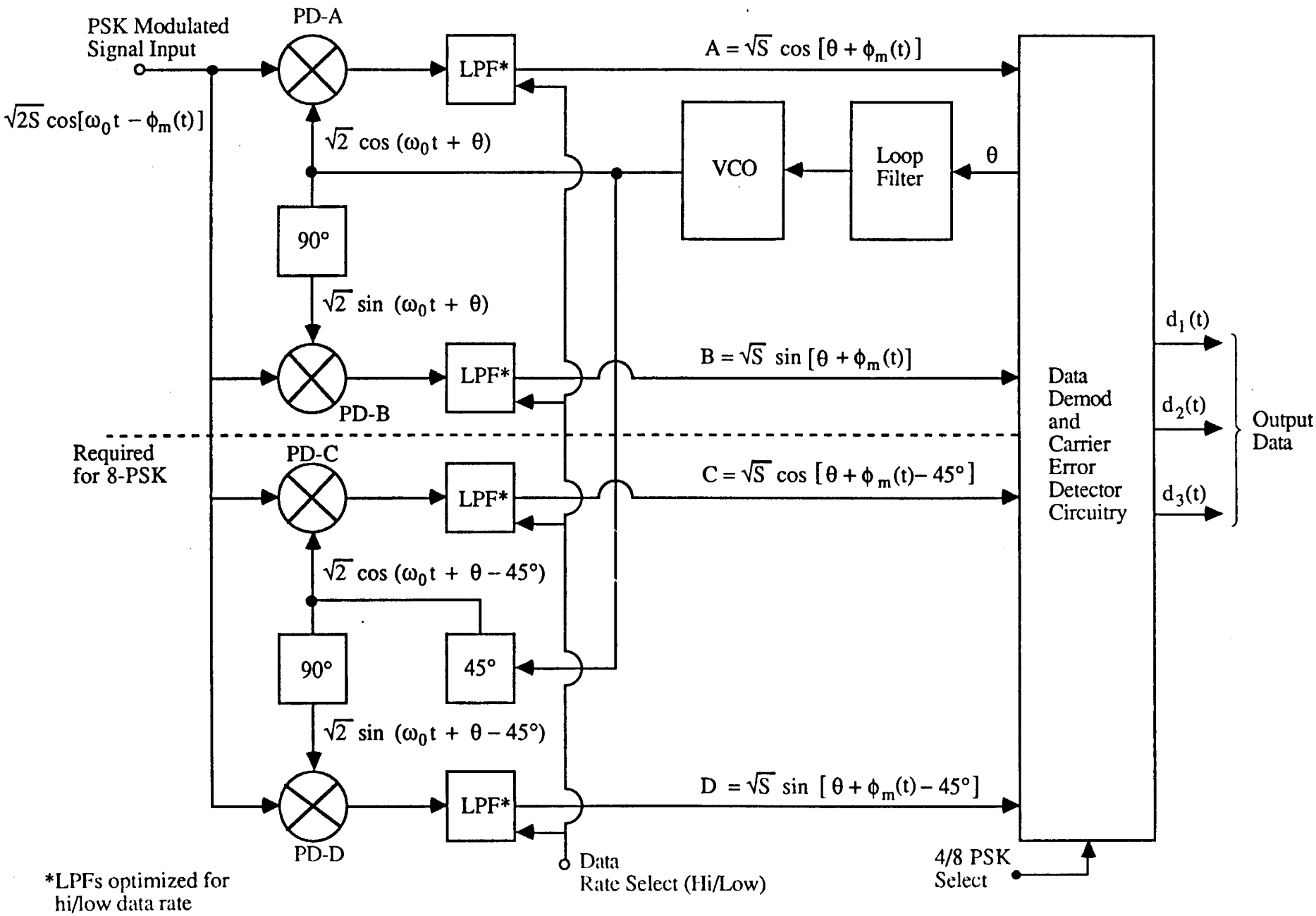

Figure 3.2.1-1. Block Diagram for an 4/8-PSK Demodulator

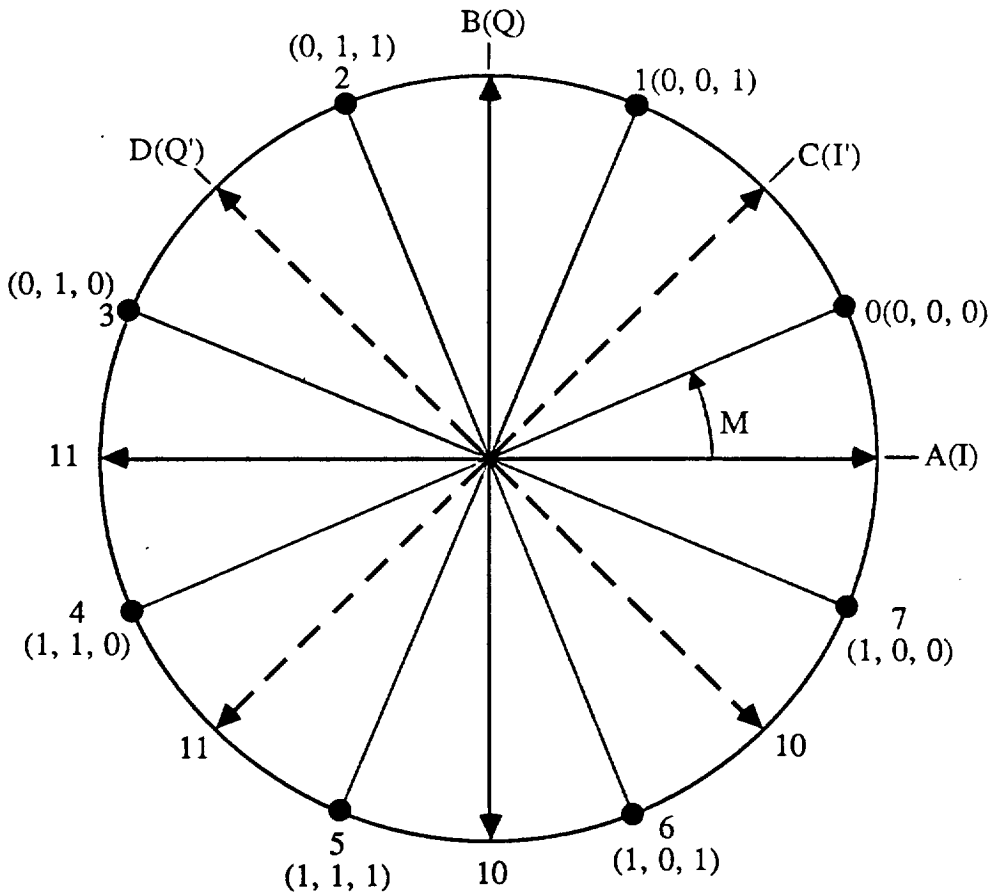

Lengend:

$$\left.\begin{matrix} d_1 \\ d_2 \\ d_3 \end{matrix}\right\} (d_1, d_2, d_3)$$

$$M = \frac{2k+1}{8} (\pi)$$

k = octal symbol

0, 1, 2, ..., 7 are octal symbols for phase codes

Figure 3.2.1-2. Phase Relationship between Phase Detector Pairs A/B and C/D and an 8-PSK Signal.

3.2.2 Carrier Tracking Error Circuit

Figure 3.2.2-1 depicts a block diagram of the carrier tracking error circuit. The circuit consists of four baseband multipliers, BM-A through BM-D, four hard limiter circuits and several analog adders/subtractors. Similar to the demodulator, only the upper portion of the circuit is required for the 4-PSK mode. However, since the uniqueness of this modem is defined by its 8-PSK capability, we will concentrate on that aspect of the circuit.

The specific requirement of the carrier tracking circuit, whether it is in the 4-PSK or in the 8-PSK modes, is to develop some sort of an "S-curve" which will provide a stable lock point, i.e., a point at which the carrier tracking error θ goes to zero. Providing such a curve for suppressed carrier, data-modulated systems is complicated by the fact that the carrier tracking signal, in addition to being proportional to the carrier, tracking error also contains data modulation. This modulation has to be removed from the carrier error signal to make it useable for its intended function. For the antipodal biphase modulation the "third multiplier" in the Costas loop provides the function of removing the data modulation from the carrier tracking error developed in the "Q-channel" of the loop. As the modulation complexity expands to 4-PSK and 8-PSK, the implementation of the carrier tracking loop also increases in complexity.

Using the nomenclature of Figure 3.2.2-1, the carier tracking error e_θ for the 8-PSK mode is:

$$
\begin{aligned}
e_\theta = \; & -A \operatorname{sgn} B + B \operatorname{sgn} A - C \operatorname{sgn} D + D \operatorname{sgn} C \\
= \; & -\sqrt{S} \cos[\theta + \phi_m(t)] \operatorname{sgn} \sqrt{S} \sin[\theta + \phi_m(t)] \\
& +\sqrt{S} \sin[\theta + \phi_m(t)] \operatorname{sgn} \sqrt{S} \cos[\theta + \phi_m(t)] \\
& -\sqrt{S} \cos[\theta + \phi_m(t) - 45°] \operatorname{sgn} \sqrt{S} \sin[\theta + \phi_m(t) - 45°] \\
& +\sqrt{S} \sin[\theta + \phi_m(t) - 45°] \operatorname{sgn} \sqrt{S} \cos[\theta + \phi_m(t) - 45°]
\end{aligned}
\tag{1}
$$

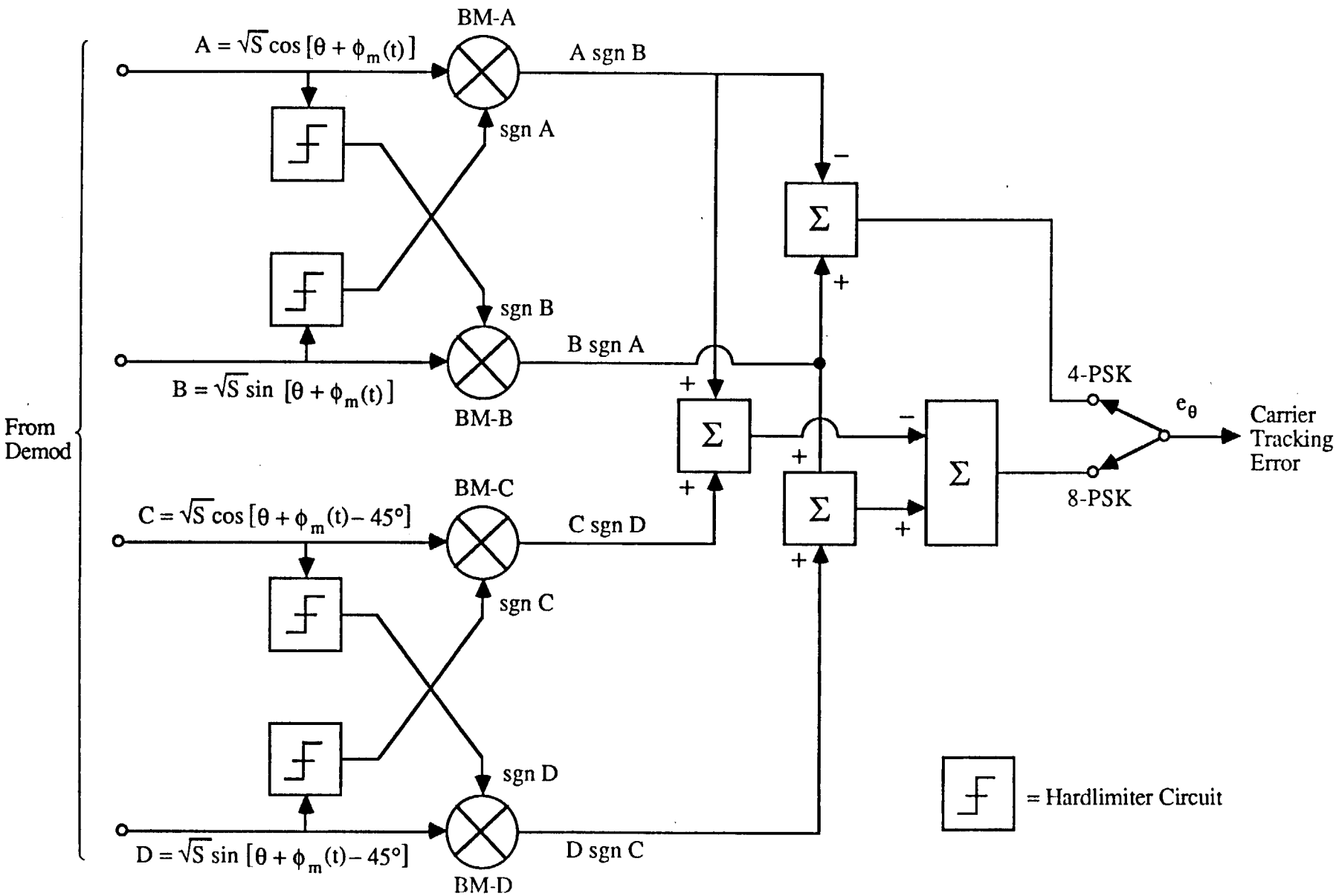

Figure 3.2.2-1. Carrier Tracking Error Circuit

Part (a) of Figure 3.2.2-2 shows the plot of the carrier error voltage e_θ versus carrier tracking error in degrees for an 8-PSK demodulator. The plot shown there is the plot of Equation (1) above. Note that this plot is independent of the phase modulation function $\phi_m(t)$ as long as $\phi_m(t)$ is defined as $(2k + 1)\pi/8$ where k=0,1,2,...,7 for the 8-PSK modulation. It must be also noted that the S-curve "tracks" linearly only within an interval defined by ±22.5° which is the spacing between the phases of an 8-PSK signal (see Figure 3.2.1-2).

Part (b) of Figure 3.2.2-2 shows an S-curve for the 4/8-PSK demodulator in the 4-PSK mode.* As can be seen from this curve, the stable lock points for the 4-PSK mode are spaced by 90° and the linear tracking range extends over the range of ±45°. This is consistent with the QPSK modulation.

3.2.3 Data Recovery Circuitry

3.2.3.1 Data Recovery for 8-PSK Mode

The function of the data recovery circuitry in the 8-PSK mode is to convert the four outputs (A, B, C, and D) of the four respective phase detectors (PD-A, PD-B, PD-C, and PD-D) into three independent data streams defined by $d_1(t)$, $d_2(t)$, and $d_3(t)$. Part (a) of Figure 3.2.3-1 provides a functional representation of this requirement. This "four into three" conversion is an inverse operation of the octal mapper shown in Figure 3.1.1-4.

To provide for better physical understanding of the demodulator action in the 8-PSK mode we have identified axes A and B as I and Q, and axes C and D as I' and Q', respectively. Based on the polarity of the I, Q, I', and Q' signals, the bits d_1, d_2, and d_3 is 0 if Q-output is positive. Conversely, $d_1 = 1$ if Q = output is negative. Similarly, from Figure 3.2.1-2, we note that $d_2 = 1$ when I-output is negative and $d_2 = 0$ when it is positive.

*For derivation of the 4-PSK carrier phase error term, see Appendix A.

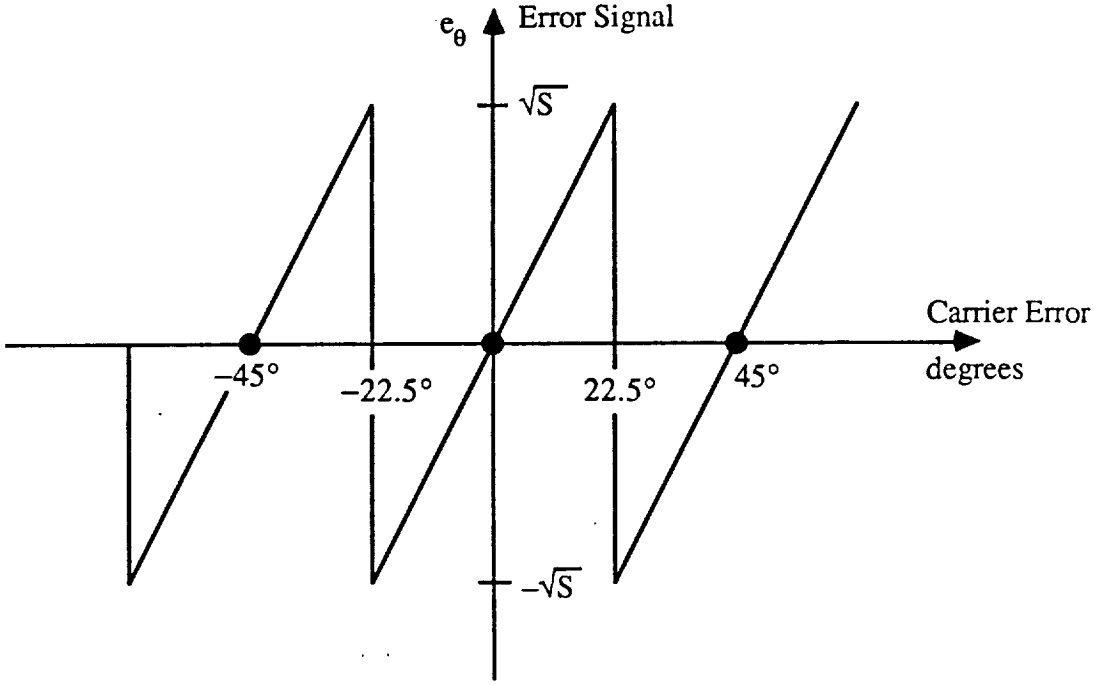

(a) Carrier Error for 8-PSK Demodulator

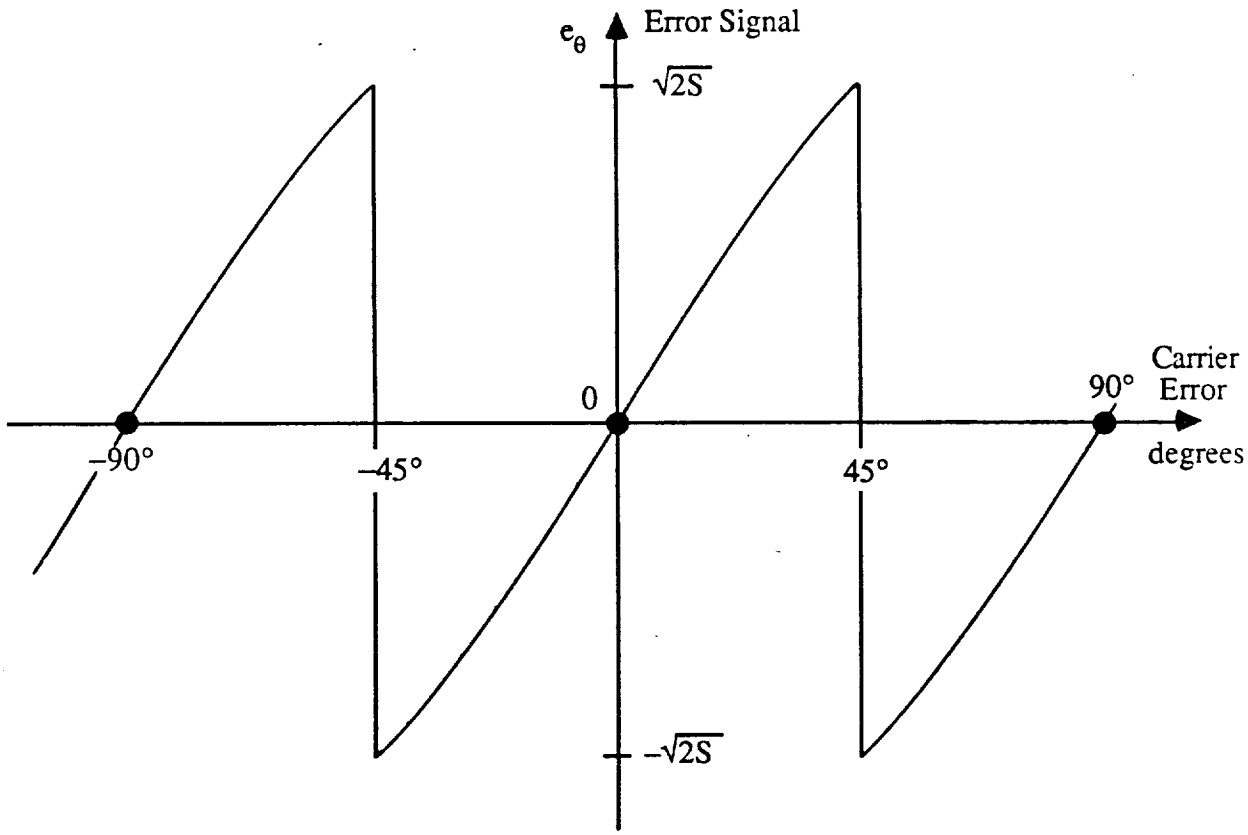

(b) Carrier Error for 4-PSK Demodulator

Figure 3.2.2-2. Carrier Tracking Error (a) for 8-PSK and (b) for 4-PSK Modulation.

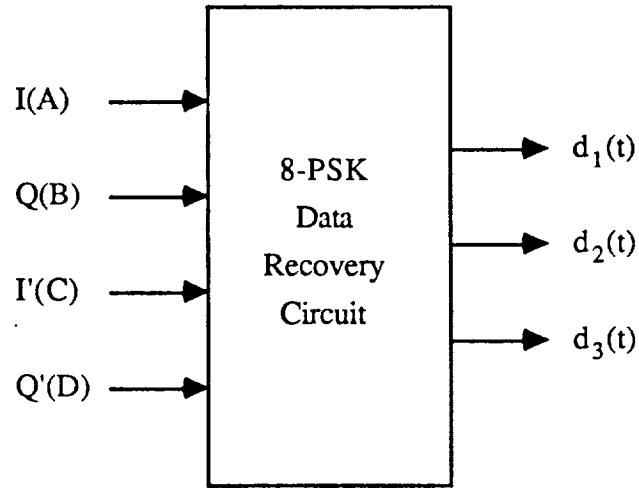

(a) Functional diagram of data recovery circuit.

d_1	Q
0	+
1	–

d_2	I
0	+
1	–

d_3	I'	Q'
1	+	+
0	+	–
0	–	+
1	–	–

(b) Data recovery algorithm for an 8-PSK demodulator.

Figure 3.2.3-1. Data Recovery Circuitry (a) and Decoding Algorithm (b) for an 8-PSK Demodulator.

The decoding of the last bit, d_3, is somewhat more complicated. Observation of the phase diagram in Figure 3.2.1-2 indicates that $d_3 = 1$ for two cases. One is when both I' and Q' are positive, thus representing octal numbers 1 and 2. The second case for $d_3 = 1$ is when both I' and Q' are both negative, i.e., octal numbers 5 and 6 are received. The condition $d_3 = 0$ occurs when I' and Q' have different polarities. This occurs for octal symbols 3, 4, 0, and 7. Table 3.2.3-1 supports the above-presented arguments in terms of the actual magnitudes and polarities of the outputs of an 8-PSK demodulator.

Figure 3.2.3-2 shows an 8-PSK data demodulation circuit which implements the data recovery algorithm given in part (b) of Figure 3.2.3-1. As shown in Figure 3.2.3-2, the I/Q and I'/Q' signals are applied to four threshold circuits. The threshold circuits convert the analog signals into the digital (binary 1 or 0) formats according to the decoding algorithm chosen. The operation of convertin the four baseband signal outputs of an 8-PSK demodulator into three data streams, i.e., d_1, d_2, and d_3, is thus accomplished.

3.2.3.2 Data Recovery for the 4-PSK Mode

For the 4-PSK mode, i.e., a conventional QPSK modulation, the demodulator is reconfigured to use only the upper half of the circuitry shown in Figures 3.2.1-1 and 3.2.2-1. The details of the demodulator operation in the QPSK mode is given in Appendix A. A different labeling is used in the Appendix, but functionally a(t) in the Appendix is d_1 and b(t) is d_2.

		Output Axis*			
Octal Symbol	Modulation Angle M Degrees	I = cos M	Q = sin M	I'=cos(M – 45°)	Q'=sin(M – 45°)
0	22.5	0.924	0.383	0.924	– 0.383
1	67.5	0.383	0.924	0.924	0.383
2	112.5	– 0.383	0.924	0.383	0.924
3	157.5	– 0.924	0.383	– 0.383	0.924
4	202.5	– 0.924	– 0.383	– 0.924	0.383
5	247.5	– 0.383	– 0.924	– 0.924	– 0.383
6	292.5	0.383	– 0.924	– 0.383	– 0.924
7	337.5	0.924	– 0.383	0.383	– 0.924

$M = (2d - 1)\pi/8 \qquad d = 0, 1, 2, \ldots, 7$

*Output signals normalized to a maximum value of unity.

Table 3.2.3-1. Demodulator Output Signals for an 8-PSK Demodulator.

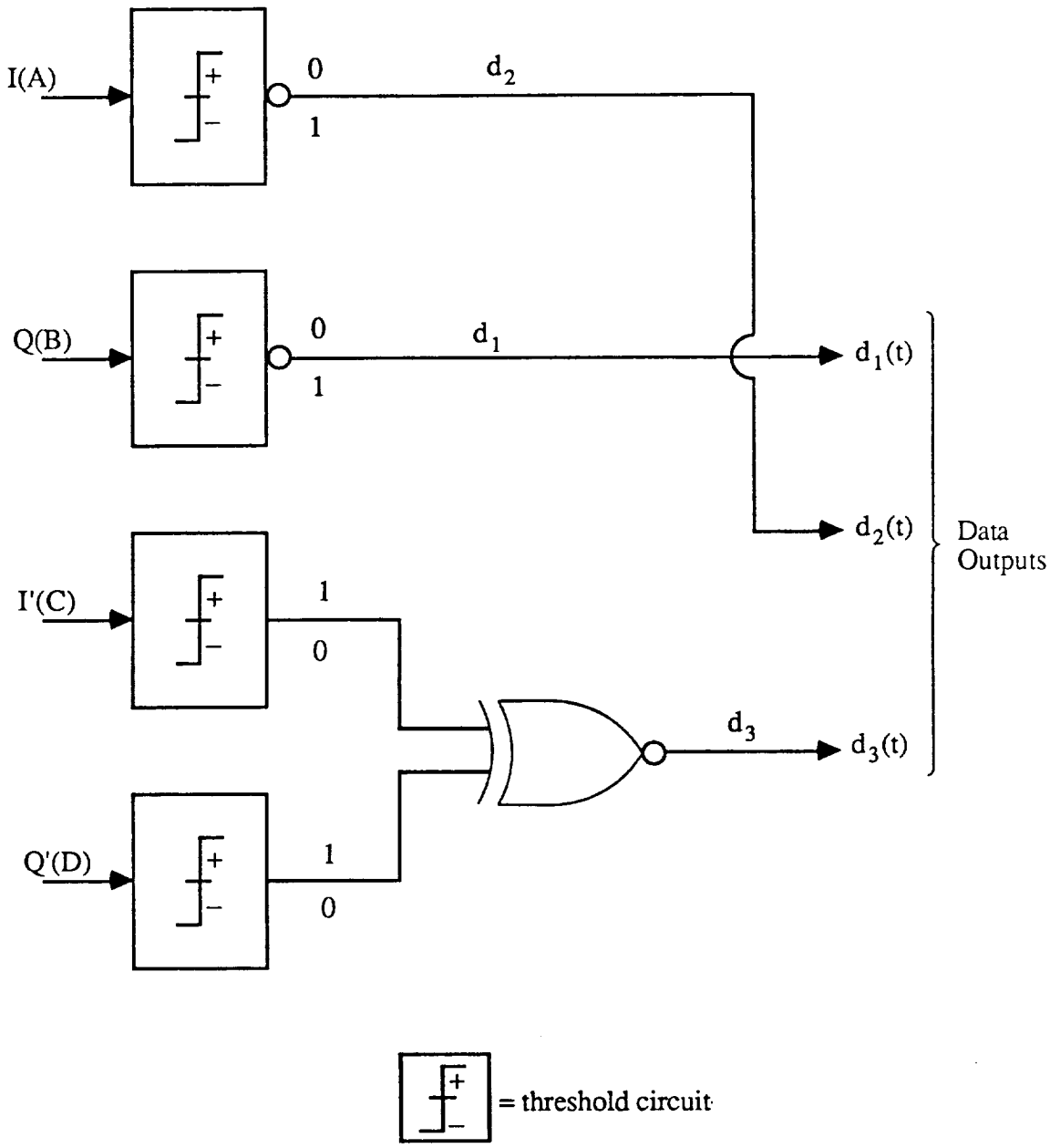

Figure 3.2.3-2. Data Demodulation Circuit for 8-PSK Demodulator.

3.3 Design Considerations

The addition of an 8-PSK capability to the baseline 4-PSK mode imposes certain design considerations not only on the modulator and the demodulator units but also on the transmitter and the receiver units of the MA link as well. In this section, we address some of these considerations particularly from the standpoint of how they affect the performance of the 8-PSK mode.

3.3.1 Channel BER

3.3.1.1 General

Throughout this report we have been referring either to two data streams, identified as d_1 and d_2, for the 4-PSK mode or to three data streams, identified as d_1, d_2, and d_3, for the 8-PSK mode. Operationally, this means that we have either a two-channel capability (d_1 and d_2 in the 4-PSK mode) or a three-channel capability (d_1, d_2, and d_3 in the 8-PSK mode). Because the on-going discussion concerns the 8-PSK mode, we will refer to the independent channels available in this mode as channels 1, 2, and 3.

Consider first the BER behavior of the 8-PSK mode. Figure 3.3.1.1-1 shows the BER performance comparison of the 8-PSK mode with that of the baseline 4-PSK and the 2-PSK modes which are included in the figure for purpose. An interesting feature of the 8-PSK curve is that channels 1 and 2 provide a slightly better BER performance than channel 3. This is due to the fact that, as was shown in Figure 3.2.3-1, the recovery of the data streams d_1 and d_2 is based on the hard discisions in I and Q half-planes, but the decision for the d_3 data stream is based on narrower regions of several quarter-planes. In terms of the penalty in the E_s/E_N ratio, this difference between channels 1, 2 and channel 3 is only about 0.3 dB at BER of 10^{-5}, which is the specified BER for the digital video transmission. The advantage, however, is the simplicity of the data demodulation circuitry as was illustrated in Figure 3.2.3-2.

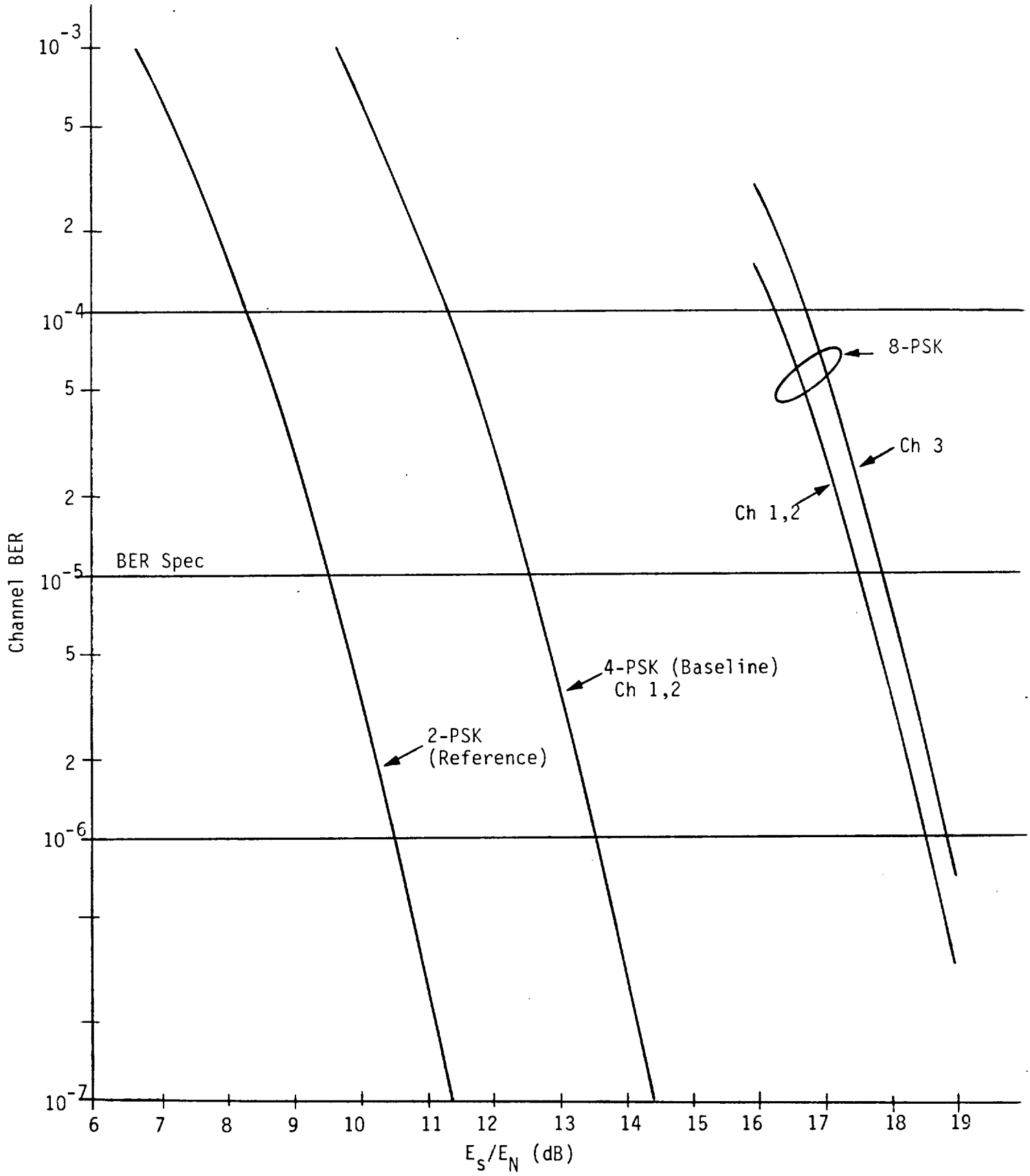

Figure 3.3.1.1-1. BER vs. PSK Modulation Level and Symbol-to-noise Ratio E_S/E_N.

An alternate method of recovering the data streams d_1, d_2 , and d_3 would be to use only the I and Q axes and solve for the modulation angle M using the I and Q components recovered by the I and Q-axis demodulators. This would be an optimum symbol detection method, but for the Gray incoding, it would still make channel 3 BER somewhat worse than channels 1 and 2.

We at Axiomatix have also explored a data decision algorithm which equalizes the BER in all three channels. However, such an equalization results in a BER which is equal to that of channel 3 as shown in Figure 3.3.1-1. Thus, the conclusion is that the RF link which uses an 8-PSK modulation would be designed to achieve BER of 10^{-5} in channel 3 based on curves in Figure 3.3.1-1. In this case channels 1 and 2 would simply have an additional margin of 0.3 dB.

3.3.1.2 Effect of Data Angle Imbalance on Channel BER

As explained in Section 3.2, the data demodulation boundaries are defined by two sets of orthogonal axes I/Q and I'/Q'. An examination of the phase relationship shown in Figure 3.2.1-2 indicates that for an ideal implementation all eight phases of the 8-PSK signal are never more than 22.5 degrees from either one of the orthogonal axes defined by the I/Q and I'/Q' pairs. With a practical implementation of the modulator/demodulator, a question arises in regards to the angular (i.e., phase) tolerance, or imbalance, with which the 8-PSK data is generated at the transmitter and demodulated at the receiver. Imbalance is defined as per Figure 3.3.1.2-2. Figure 3.3.1.2-1 shows the effect of imbalance on the BER of the channel 1, 2, and the channel 3 data outputs. From this figure it is evident that at E_s/E_N of 18 dB, there is very little angular tolerance allowed for imbalance. This, in turn, translates into a very "tight" angular tolerance on the angular relationship between the I, Q, I', and Q' axes. For E_s/E_N = 18.5 dB the allowed tolerance increases, and for E_s/E_N = 19 dB the allowed tolerance falls within the limits ($90° \pm 2°$) of the practical quadrature hybrids. Such hybrids would be used for implementing both the modulator and the

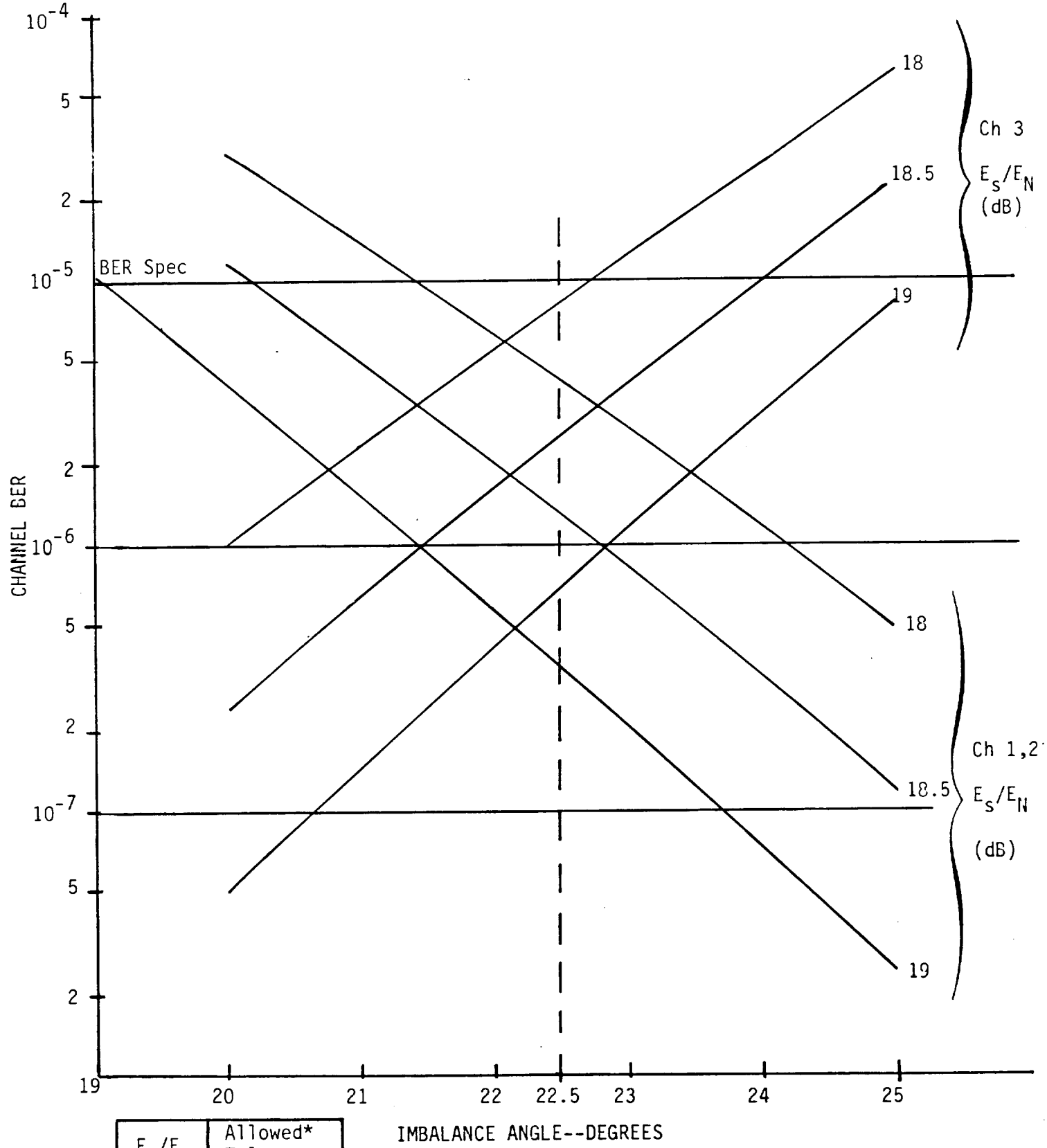

E_s/E_N (dB)	Allowed* Tolerance	
	- deg	+ deg
18	1.1	0.3
18.5	2.3	1.5
19	3.4	2.6

*For BER less than 10^{-5}

Figure 3.3.1.2-1. Effect of Imbalance on Channel BER vs. E_s/E_N Ratio.

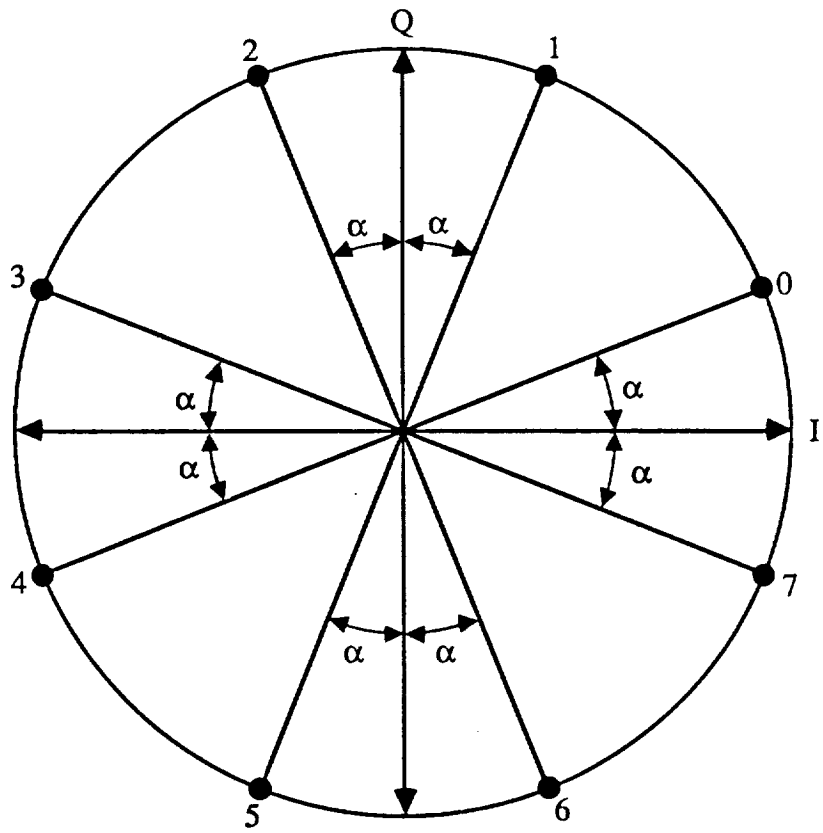

Figure 3.3.1.2-2. Channels 1 & 2 vs. Channel 3 Imbalance (α)

demodulator units. This increase of E_s/E_N from 18 to 19 dB can be attributed in a link budget to what is generally referred to as an "implementation loss" of 1 dB.

It must be noted in Figure 3.3.1.2-1 that the equal BER values for channel 1,2 and channel 3 appear at an angle which is approximately 22.2° rater than the "nominal" angle of 22.5°. This is due to the fact that we are considering each channel individually rather than treating the average rate of all three channels. If we consider the BER value averaged over all of the three channels, we obtain curves shown in Figure 3.3.1.2-3. From these curves it is evident that the minimum in average BER value does occur at the nominal value of 22.5°.

The significance of this discussion is that for application on hand, i.e., providing a capability to transmit three independent channels, one must analyze the performance of each channel individually rather than treat the performance of an 8-PSK modem on an "average" basis.

3.3.2 Tolerance to RF Circuitry Impairments

When utilizing higher order modulation techniques, such as 8-PSK, 16-PSK, 16 QAM, etc., one must pay attention to the effect of the RF circuitry impairments on the performance of the modulation technique. This, of course, is also true for the bi-phase (2-PSK) and the quadriphase (4-PSK) modulations. But, because we are introducing an 8-PSK technique here, our primary concern is the relative sensitivity of the 8-PSK technique to such impairments as compared to a 4-PSK modulation.

Our consideration, therefore, focuses specifically on such impairments as (1) amplitude distortion, (2) delay distortion, and (3) carrier phase jitter. Although, at this point in time, it is difficult to determine the exact location of these impairments in the RF chain extending from the transmitter to the receiver, the purpose of this discussion is to make the potential users of the 8-PSK aware of the effect of these impairments.

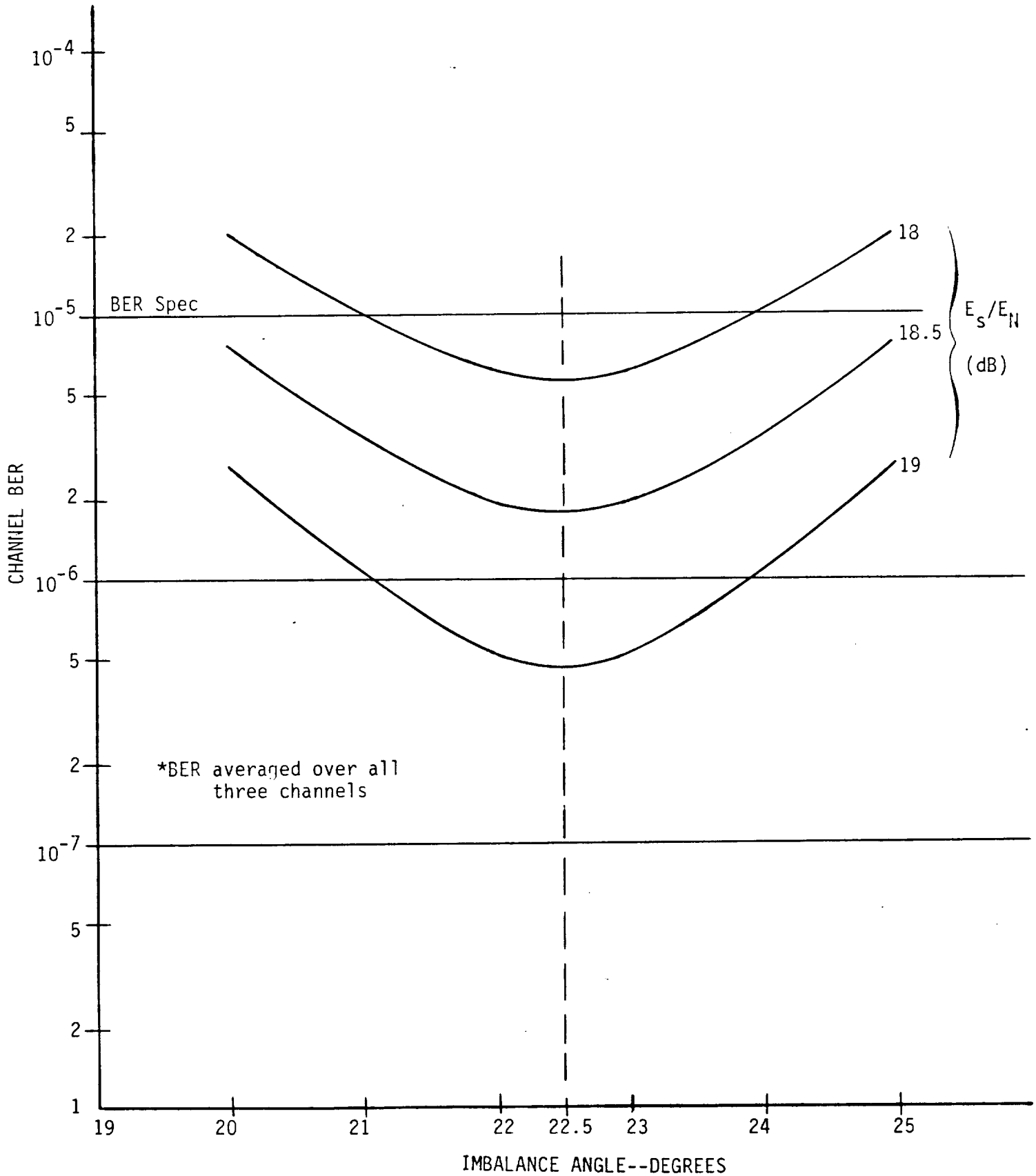

Figure 3.3.1.2-3. Effect of Imbalance on Average* BER of Channels 1, 2 and 3.

3.3.2.1 Amplitude and Delay

Figure 3.3.2.1-1 shows the power penalties due to amplitude and delay distortion for several high order modulation schemes. For both the amplitude and the delay, there are two terms: (1) a symmetrical term and (2) an asymmetrical term. These terms are referred to, respectively, as "linear" and "quadratic" terms. Also, these terms are defined by their respective coefficients, i.e., A_1 and A_2 for the amplitude response and d_1 and d_2 for the delay response.

An example of using the information in Figure 3.3.2.1-1 may be as follows. Suppose we are considering a symbol rate of 22 Msps, the duration of each symbol is about 45 nsec. If the attenuation of the bandpass filters preceeding the demodulator is 1 dB at ±11 MHz (i.e., A_2 = 1dB), the power penalty will be about 0.7 dB for the 8-PSK mode and about 0.3 dB for the 4-PSK mode. Similarly, if d_1 = 9 nsec then the power penalty paid for this distortion alone will be about 0.9 dB for the 8-PSK mode and about 0.2 dB for the 4-PSK mode. These penalties define an increase in E_s/E_N required to maintain BER of 10^{-6} if each of these distortions is taken separately.

In an actual system, there will be all four distortions present, each claiming its own power penalty. Thus, from the standpoint of the RF system design, the impact of using the 8-PSK has to be reflected in the "baseline" specification (i.e., the 4-PSK spec). If this is not done, then the 8-PSK mode has to be provided with sufficient amount of additional RF power to work over the channels baselined for the 4-PSK.

3.3.2.2 Carrier Phase Jitter

The effect of carrier phase jitter on the power penalty is shown in Figure 3.3.2.2-1. For example, a phase jitter of 2 degrees RMS would result in power penalty of about 0.4 dB for the 8-PSK system and about 0.1 dB for the 4-PSK system.

The information provided in Figure 3.3.2.2-1 is useful for determining whether the phase noise characteristics of the local oscillators, synthesizers and other frequency

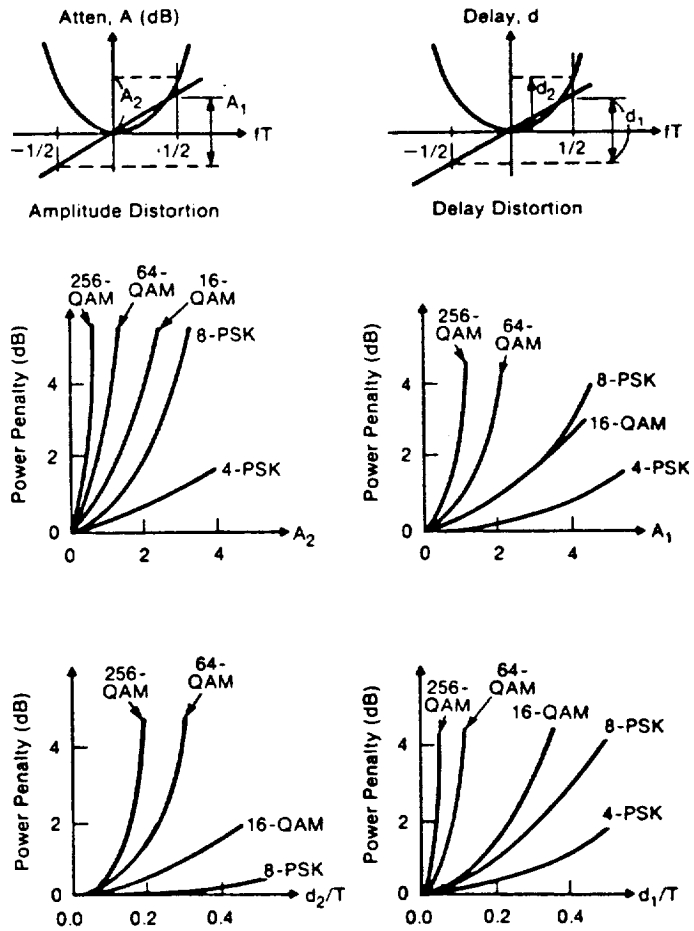

Figure 3.3.2.1-1. Power Penalties Due to Amplitude and Delay Distortion at BER = 10^{-6} (Ref. [3]).

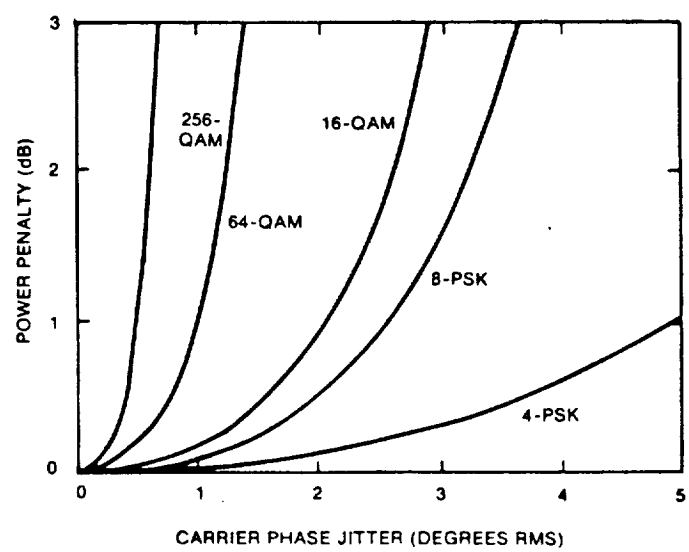

Figure 3.3.2.2-1. Power Penalties Due to Carrier Phase Jitter at BER = 10^{-6} (Ref. [3]).

sources used by the Ku-band MA system have a significant impact on the power required to establish an 8-MSK link. Conversely, if the phase noise level is established by factors other than the 8-MSK operation, then the designers of the 8-PSK link must consider means within the framework of the modulator/demodulator design to reduce the effect of the phase noise on link performance. One parameter, for example, which determines the carrier phase jitter is the bandwidth of the carrier tracking loop for the 8-MSK demodulator. For an MSC application the doppler shift may not be a problem because of small relative motion between the transmitter and the receiver units. Thus, the trade off is then between making the carrier tracking loop wide enough to maintain lock despite the carrier phase noise or to make it narrow enough to minimize the effect of the thermal noise.

It must be also stated here that the power penalties indicated for the impairments are for BER of 10^{-6}. For BER of 10^{-5}, which is a baseline requirement for the digital TV links, these penalties will be less.

3.3.3 Implementation Philosophy

Digital implementation is recommended, wherever applicable, for the design of both the modulator and the demodulator units. Digital implementation of the modulator unit was discussed briefly in Section 3.1.2. For the demodulator design, the digital implementation will particularly be of great benefit. Figure 3.3.3-1 shows a block diagram of a digitally implemented demodulator. As shown, the baseband signals from phase detectors A, B, C, and D are converted to digital format and applied to a digital processor.

The processor performs the functions of (1) carrier tracking, (2) data demodulation, and (3) data clock recovery. For the low data rate (≈ 100 kps), several microprocessors may be used to achieve to desired processing speed. However, for the video data rates (≈25 Mbps) special purpose, high speed processor circuitry has to be used.

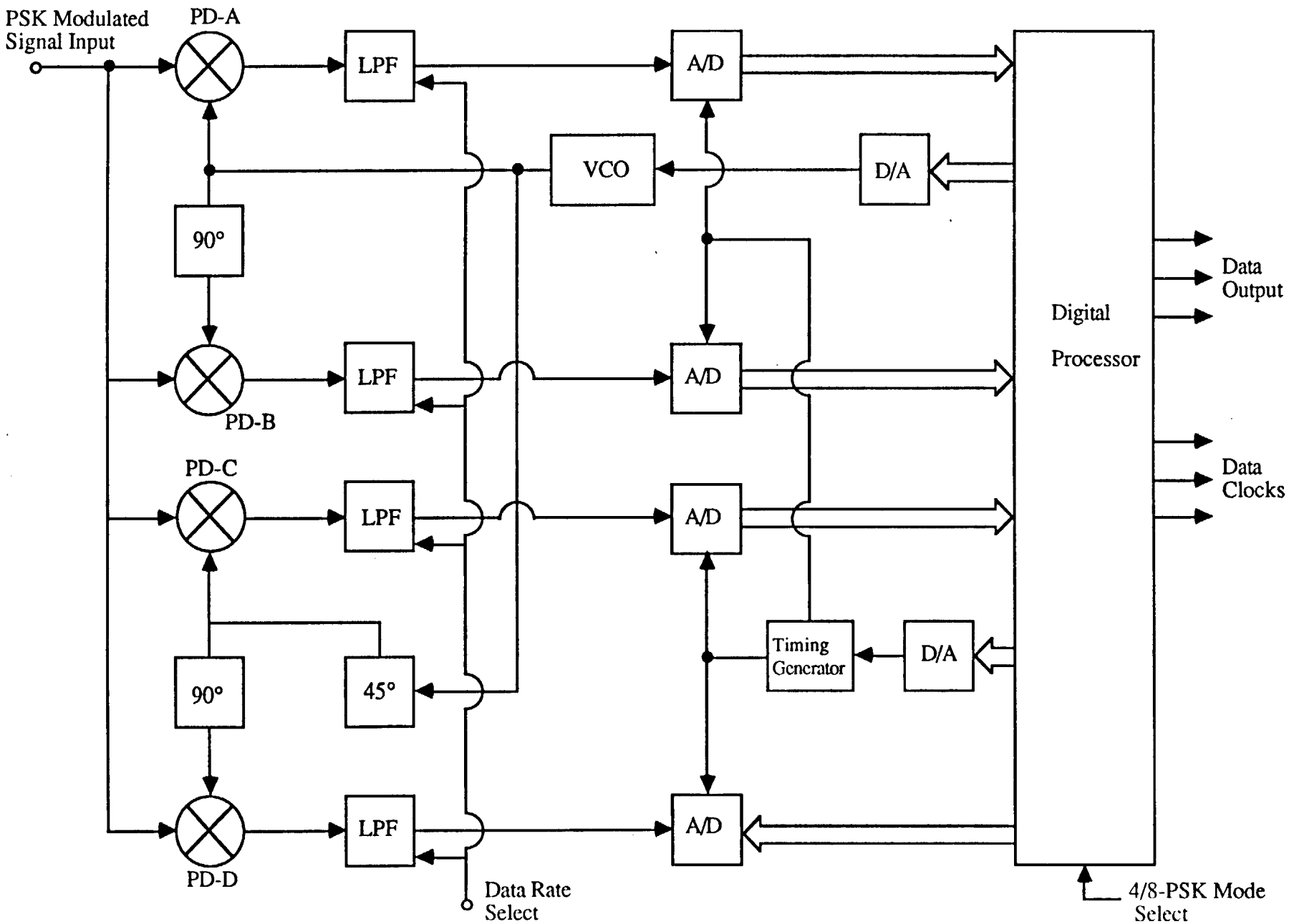

Figure 3.3.3-1. Block Diagram of a Digitally Implemented Demodulator.

4.0 CONCLUSIONS

It has been shown that the baseline 4-PSK capability of the Space Station's Ku-band MA system can be expanded for some users to provide three simultaneous digital TV channels by using 8-PSK modulation. The encorporation of the 8-PSK capability can be provided by designing what is referred to in this report as a "multi-channel" modulator/demodulator. The design philosophy is to provide the 8-PSK capability as a selectable "add-on" capability to the baseline 4-PSK mode. In this manner only those users who require the three channel capability will have to carry the additional circuitry. This circuitry may be either on a "plug in" card or in some other form of a plug-in module.

This report presented a conceptual design for a 4/8-PSK modulator/demodulator unit. The design concept described here can be used as a starting point for a more detailed engineering design. The selection of an IF frequency still remains an open issue. But, the impact of the IF frequency value will be primarily on the circuit design of the modulator/demodulator rather than on the conceptual design.

The subject of the clock recovery is not addressed in this report. We feel that it is a separate topic. However, there are techniques reported in literature which provide for a relatively easily implementable means of recovering the clock information from an 8-PSK signal [4]. For example, the technique described in [4] uses narrow-band filtering of the 8-PSK IF signal to recover the clock component which is present in the RF envelope of an 8-PSK modulated signal.

REFERENCES

[1] McDonnel Douglas Corp., "Space Station Definition and Preliminary Design," Work Package #2, Preliminary Analysis and Design Document, Book 12; Communication Tracking, MDC H2028A, June 1986.

[2] Rockwell International, "Space Station, Work Package 2, Definition and Preliminary Design Phase," Communications and Tracking Report, Volume 12, SSS 86-0073, June 6, 1986.

[3] T. Noguchi, Y. Daido, and J. A. Nassek, "Modulation Techniques for Microwave Digital Radio," IEEE Communications Magazine, Vol. 25, No. 10, October 1986, pp. 21-30.

[4] C. R. Hogge, "Carrier and Clock Recovery for 8-PSK Synchronous Demodulation," IEEE Trans Comm., Vol COM-26, pp. 528-533, May 1978.

APPENDIX A

DEMODULATOR FUNCTION IN THE 4-PSK MODE

DEMODULATOR FUNCTION IN 4-PSK MODE

A-1 INTRODUCTION

This appendix presents a simple analysis of the demodulator operation in the 4-PSK mode, which is generally referred to as the QPSK mode.

Figure A-1 shows the block of a QPSK demodulator. As shown, the demodulator consists of two orthogonal phase detectors PD-A and PD-B. For carrier error generation, the outputs of these detectors are cross-coupled via two hard limiters and baseband multipliers BM-A and BM-B.

An analysis of the method of the carrier error generation is given below.

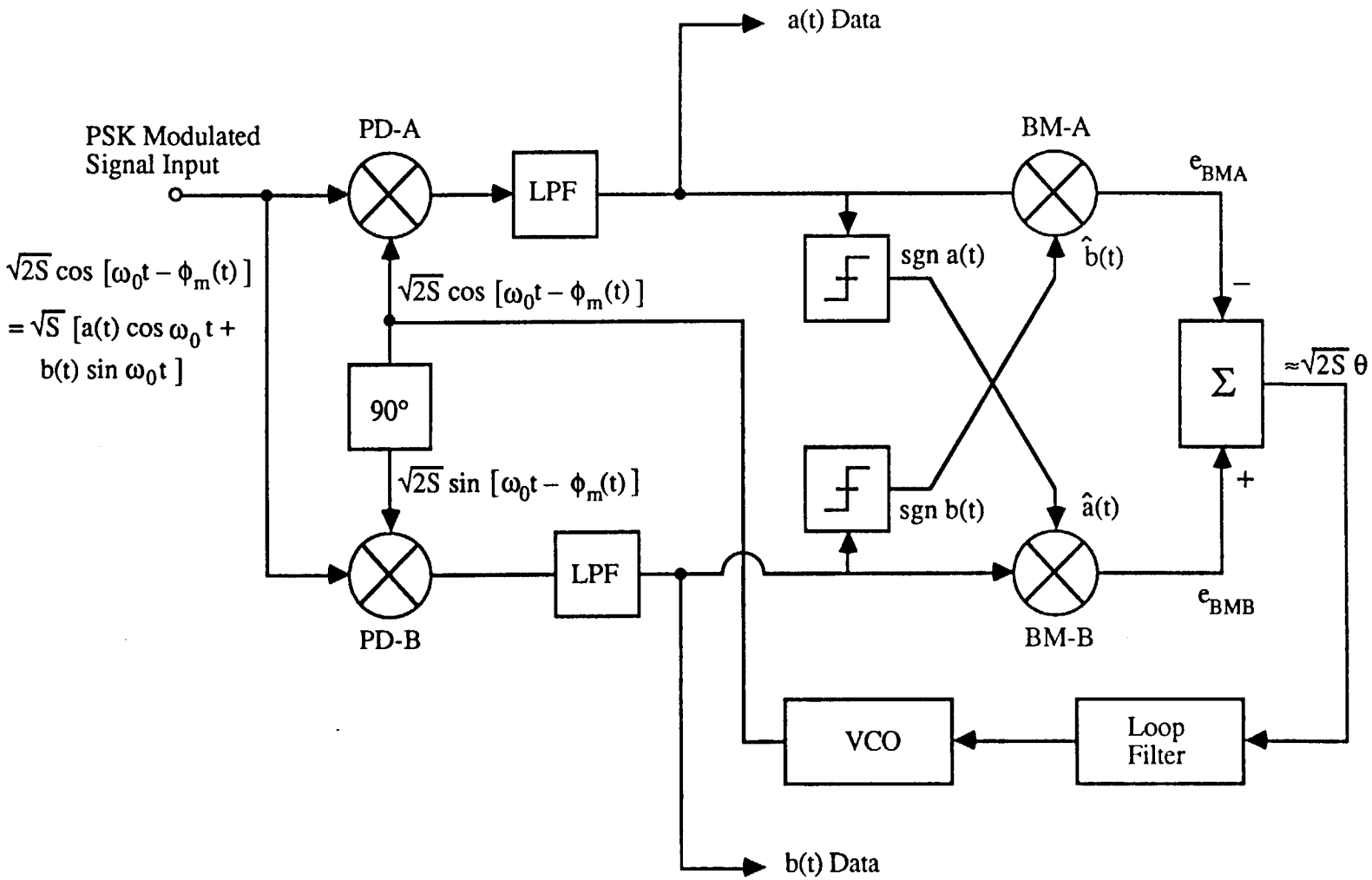

Figure A-1. Demodulator for 4-PSK (QPSK) Mode.

A-2 ANALYSIS

To simplify analysis, we will represent the input signal to the QPSK demodulator in terms of two in-phase and quadrature components. These components are labeled a(t) and b(t), respectively. Figure A-2 shows the idea. The input signal to the demodulator can, therefore, be written as:

$$e_{in} = \sqrt{S}\,[a(t)\cos\omega_0 t + b(t)\sin\omega_0 t\,]\,, \tag{1}$$

where a(t) = ±1 and b(t) = ±1, depending on the data patterns of the respective data streams. The output of phase detector PD-A is

$$\begin{aligned} e_{PDA} &= \sqrt{S}\,[a(t)\cos\omega_0 t + b(t)\sin\omega_0 t]\,\sqrt{2}\cos(\omega_0 t + \theta) \\ &= \sqrt{S/2}\,[a(t)\cos\theta - b(t)\sin\theta]\ . \end{aligned} \tag{2a}$$

Similarly, the output of phase detector PD-B can be obtained

$$\begin{aligned} e_{PDB} &= \sqrt{S}\,[a(t)\cos\omega_0 t + b(t)\sin\omega_0 t]\,\sqrt{2}\sin(\omega_0 t + \theta) \\ &= \sqrt{S/2}\,[a(t)\sin\theta - b(t)\cos\theta]\ . \end{aligned} \tag{2b}$$

As shown in Figure A-1, the outputs of the phase detectors are, after low pass filtering, applied to baseband multipliers BM-A and BM-B. The outputs also are applied to two threshold detectors which not only determine the polarity of the appropriate signals, but also "clean up" the signals a(t) and b(t) making them look more or less like square waves. Thus, for a resonably high SNR in the LPFs, we can assume that

$$\begin{aligned} \text{sgn}\ a(t) &= \hat{a}(t)\ , \\ \text{sgn}\ b(t) &= \hat{b}(t)\,. \end{aligned} \tag{3}$$

Using the relationship in (3) above, we proceed to find the expressions for the outputs of the baseband multipliers BM-A and BM-B:

$$
\begin{aligned}
e_{BMA} &= \sqrt{S/2}\,[a(t)\cos\theta - b(t)\sin\theta]\,\hat{b}(t) \\
&= \sqrt{S/2}\,[a(t)\,\hat{b}(t)\cos\theta - b(t)\,\hat{b}(t)\sin\theta] \qquad (4a) \\
&= \sqrt{S/2}\,[a(t)\,\hat{b}(t)\cos\theta - \sin\theta]
\end{aligned}
$$

and

$$
\begin{aligned}
e_{BMB} &= \sqrt{S/2}\,[a(t)\sin\theta + b(t)\cos\theta]\,\hat{a}(t) \\
&= \sqrt{S/2}\,[\hat{a}(t)\,a(t)\cos\theta + \hat{a}(t)\,b(t)\cos\theta] \qquad (4b) \\
&= \sqrt{S/2}\,[\sin\theta + \hat{a}(t)\,b(t)\cos\theta]\,.
\end{aligned}
$$

It must be noted that in (4a) and (4b), we have made a valid assumption that $a(t)\,\hat{a}(t) = 1$ and $b(t)\,\hat{b}(t) = 1$. For the next step, we will make a further resonable assumption, specially that

$$\hat{a}(t)\,b(t) = a(t)\,\hat{b}(t)\,. \qquad (5)$$

Using this assumption we will show that the carrier tracking error out of the summer is

$$
\begin{aligned}
e_\theta &= e_{BMB} - e_{BMA} \\
&= \sqrt{2S}\,\sin\theta\,, \qquad (6)
\end{aligned}
$$

which for $\theta \approx$ small becomes

$$e_\theta = \sqrt{2S}\,\theta\,.$$

The tracking capability of the QPSK demodulator extends only to $\pm 45°$ because, as can be seen from Figure A-2, when $\theta \geq 45°$ the output of PD-A becomes b(t) and the output of PD-B becomes a(t). Thus, the data streams "flip."

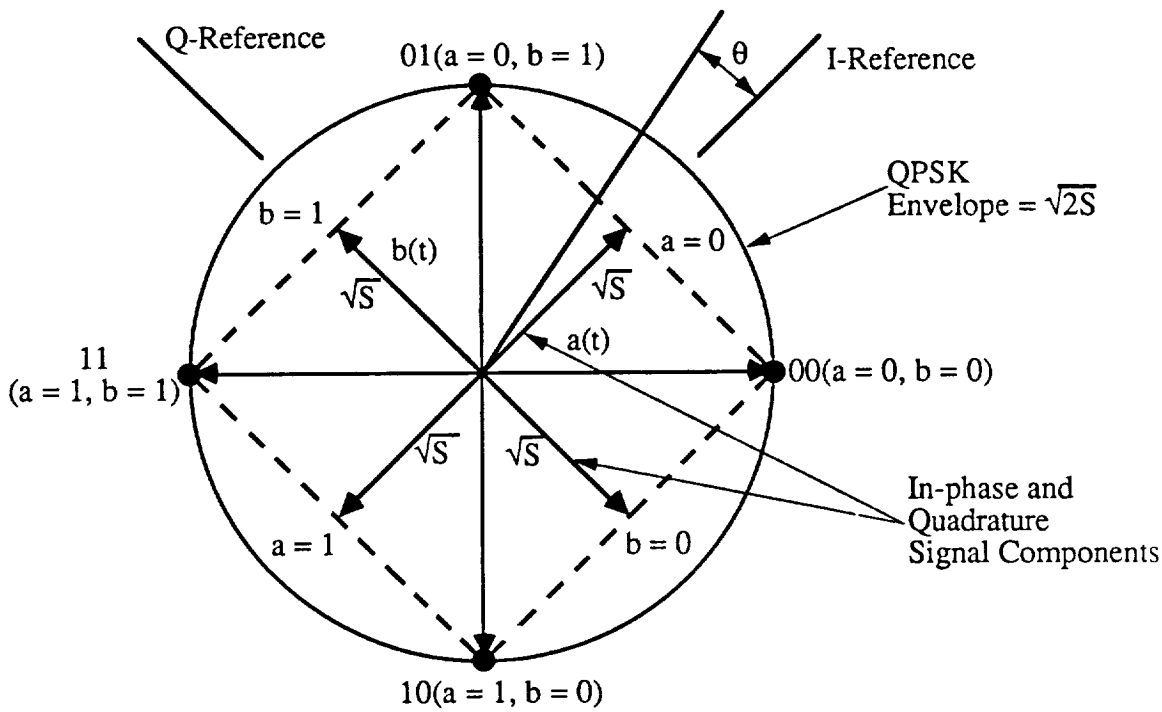

Figure A-2. Phase Diagram for DPSK Demodulation.

APPENDIX P

CODING FOR THE SPACE STATION INFORMATION SYSTEM

CODING FOR THE SPACE STATION INFORMATION SYSTEM

1.0 INTRODUCTION

The Space Station Information System (SSIS) is intended to provide reliable information flow between SSIS users. In order to provide the quality of service required, forward error correction (FEC) and forward error detection (FED) codes will be used. Axiomatix was tasked to examine several candidate codes, and propose alternatives as deemed necessary. In this memo, we discuss the performance of the candidate block codes for the SSIS transfer frame and transfer frame header. Performance is determined by analysis or simulation, as appropriate. Details of the performance assessment are covered in this memo.

1.1 Transfer Frame Requirements

The SSIS transfer frame will consist of a header field and a data field. An error detection code may be included in the header field to provide the required header reliability, which we understand to be on the order of 10^{-12} bit error rate, as per [Ref 1]. In addition, an error correcting code will be added to the transfer frame to mitigate the channel errors and improve message throughput. The required output bit error rate of the decoded transfer frame depends on the grade of service: grade 1 is 10^{-12}, grade 2 is 10^{-8} and grade 3 is 10^{-5}. However, a more relevant measure of message fidelity is the overall probability of transfer frame error or header error. In terms of random bit error rate, the probability of correct message is the probability that all the constituent bits in the message are correct, and the probability of message error is given as:

$$P_{ME} = 1 - (1 - BER)^N,$$

with BER the bit error rate, P_{ME} the message (codeword) error rate, and N the length of the coded message, in bits. Thus, for a 64 bit transfer frame header, a bit error rate of 10^{-12}

corresponds to a header error rate of 6.4×10^{-11}, and for a 2040 bit transfer frame codeword, a bit error rate of 10^{-12} corresponds to a frame codeword error rate of 2×10^{-9}. If the transfer frame is encoded using a Reed-Solomon code, as proposed in [Ref 2], and error correction is performed, the resultant output will either contain no errors, or will contain several bursts of errors since the received sequence will be transformed to a codeword differing in at least 33 symbols of 8 bits each. The point behind the preceding discussion in that average bit error rate out is not the appropriate statistic to specify, but rather the average frame error rate should be considered. In the following discussion, the error detection and correction performance of the codes will be presented in terms of frame or frame header error rate, as the transformation to bit error rate is somewhat of an artifact.

1.2 General Code Consideration

We have examined the performance of the two codes proposed in [Ref 2]. The performance of the (255, 223) Reed-Solomon code proposed for transfer frame error correction was investigated using analytical techniques. The codeword weight structure of Reed-Solomon codes is well known, and the message error rate and throughput can be calculated explicitly, based on the channel symbol error rate. At this point, we need to make a distinction between channel symbol error rate and channel bit error rate. The weight structure of the Reed-Solomon codes is based on symbols, with each non-zero symbol consisting of one or more non-zero bits. Thus, the weights given by the formula of Section 2 are independent of the number of non-zero bits, so the the weight in bits cannot be derived from this result. As a consequence, the probability of undetected error as a function of bit error rate, rather than symbol error rate, cannot be derived in closed form from the symbol weight structure. Even though symbols for the code can be reconstructed from bits transmitted over a binary channel, the codeword errors induced by bit errors have a different probability measure than the same errors induced by symbol errors. That is, in an M-ary symbol channel, with $n = \log_2 M$ bits, a received sequence with w errors has

maximum probability of $\left(\frac{1}{2^n - 1}\right)^w \left(1 - \frac{1}{2^n - 1}\right)^{N-w}$ in a code of length N. However, the same codeword, if it were to consist of symbols with one bit error each, would have a maximum probability of $\left(\frac{1}{n}\right)^w \left(1 - \frac{1}{n}\right)^{N-w}$. The latter probability is considerably larger than the former, and the potential for undetected errors using a binary channel could be higher than with a non-binary channel using the same Reed-Solomon code. Simulation with a shorter code, discussed in Section 3, indicates that there are not enough codewords with low binary weight symbols to cause this to be a problem for the Reed-Solomon code tested. The (255,223) code proposed for the transfer frame has enough distance, even after correcting sixteen errors, to provide a probability of undetected error less than 10^{-13} using a non-binary channel. However, simulation will probably be needed to verify that this code will perform as well with a binary channel. In fact, a rather lengthy simulation will be required to verify a 10^{-13} error rate, but it will be worthwhile if this one code can provide both error correction and error detection with the required probability of false message. The simulation may be expedited by testing codewords with a low binary weight. We discuss this issue in more detail in Section 2.

The frame header code candidates are examined using a simulation, thereby making it possible to verify the code performance with a binary channel. Since the error rates involved are higher, this simulation is possible on a personal computer. We have run an extensive simulation involving three potential header codes, a Hamming code, a binary BCH code, and a Reed-Solomon Code. All three codes are 64 bits long with 16 check bits, which gives an undetected error rate bound of 2^{-16}, or 1.5×10^{-5} at an input error rate of 0.5. Results of this simulation are discussed in Section 3.

2.0 TRANSFER FRAME ERROR CORRECTION CODE

We have evaluated the performance of the (255,223) 8-bit per symbol Reed-Solomon code proposed by Miller and Morakis [Ref 2]. Results from this paper, reproduced as Figure 2.0-1, show a probability of undetected bit error exceeding 10^{-3} at low signal-to-noise ratio. We believe that these results are based on a weak upper bound, or based on a maximum likelihood decoding algorithm, as our results indicate a probability of undetected error of less than 10^{-13} at all signal-to-noise ratios for a non-binary channel, and we will argue that the same result may apply to a binary channel. Our results assume that we correct a maximum of 16 errors, the guaranteed capability of the code.

We examine the error detection performance of the code using two techniques. First, we calculate the total number of codewords in the received signal space. Then, assuming we are going to correct a maximum of 16 errors, we calculate the number of codeword neighbors within distance 16. An erroneous codeword will be accepted if more than 16 errors occur, and the received sequence lands within 16 symbols of another codeword, which we call a neighbor. Thus, under the condition that landing on a codeword or a neighbor is no more or less likely than landing on any other possible received sequence at the same distance, the probability of error is upper bounded by the ratio of codewords and nearest neighbors to the total possible number of received sequences.

We can calculate the number of codewords in an (N,k) code over GF(q) as q^k, which in this case is 256^{223}. The number of sequences within distance 16 of any given codeword is equal to the number of sequences of weight less than 17, which is

$$\sum_{i=1}^{16} \binom{N}{i} (q-1)^i = .302 \times 10^{64}$$

for the code in question. The total number of sequences is $q^N = 256^{255}$. Thus, the ratio of codewords and neighbors to the total calculates out to 0.26×10^{-13}. This is the worst case

PRECEDING PAGE BLANK NOT FILMED

probability of landing within 16 symbols of another codeword.

A more rigorous expression which relates undetected codeword error to channel error rate can be derived based on a formula from Forney [Ref 3]. The number $N_{d,w}$ of codewords of weight w for a code of minimum distance d is

$$N_{d,w} = \binom{N}{w}(q-1)\sum_{i=1}^{w-d}(-1)^i\binom{w-1}{i}q^{w-d-i} \quad ,$$

and the probability of error, i.e., the probability of receiving a sequence within distance 16 of another codeword is given as

$$P_e = \sum_{w=d}^{N}\sum_{k=0}^{16}\sum_{i=0}^{k}\sum_{\ell=0}^{m} N_w \times \frac{(N-w)!\,w!\,(q-1)^{k-w-i-\ell}(q-2)^i\,P^{w+2\ell+i-k}\,(1-p)^{N-w-2\ell-i+k}}{!(N-w-\ell)!\,i!\,(k-i-\ell)!\,(w-k+\ell)!}$$

with m = min (k–i, N–w), and p the channel symbol error rate. This expression is corrected from [Ref 3], which has an error in the upper limit of the inner sum. This expression was evaluated using double precision Fortran, and the results are plotted in Figure 2.0-2. Note that, as expected, the maximum undetected error rate is equal to 0.26×10^{-13}.

The use of a decoder that corrects a fixed maximum number of errors, 16 in this case, will result in rejection of transfer frames with more than 16 errors. The probability of accepting a correct message, which is the probability of 16 or fewer errors, is a function of the channel error rate. The correct message rate is plotted in Figure 2.0-3. The use of a decoder that corrects to some codeword regardless of the number of errors will result in a slightly higher probability of accepting a correct message since there are some error patterns of 17 or greater that will still be closer to the true codeword than any other codeword. However, the probability of undetected error goes to one as the channel error rate deteriorates since all detection capability is lost. Since the frame header code does not provide the required error rate, as we will show in the next section, it would be advisable to

REED-SOLOMON (255,223) 16-ERROR CORRECTION CODE

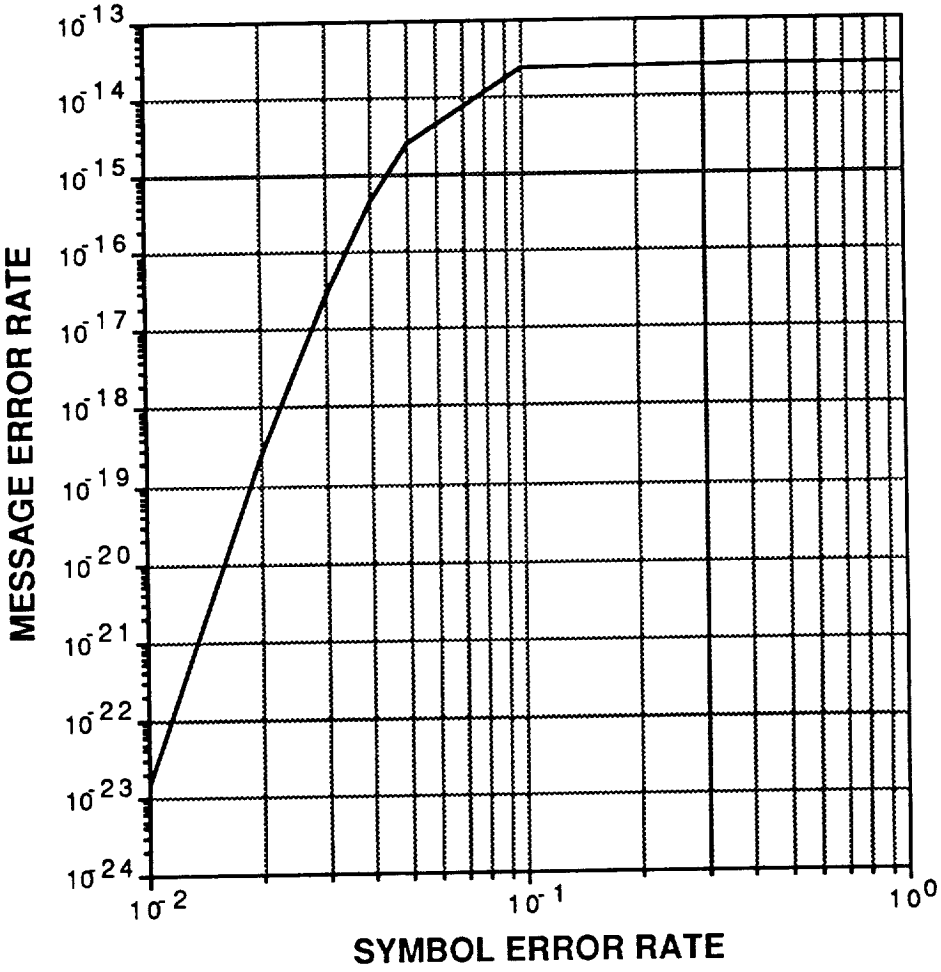

FIGURE 2.0-2

REED-SOLOMON (255,223) 16-ERROR CORRECTION CODE

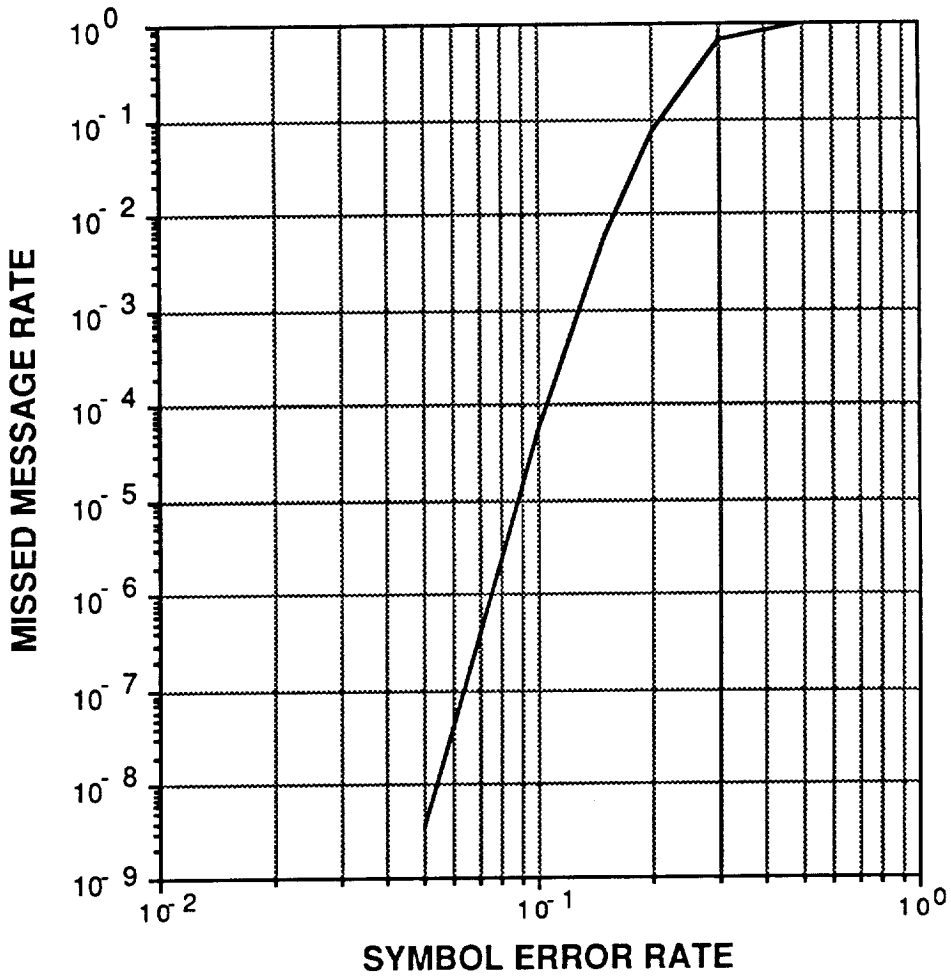

FIGURE 2.0-3

use algebraic decoding with a maximum error correction of 16 symbols rather than maximum likelihood decoding with arbitrary error correction.

2.1 Reed-Solomon Code Performance over a Binary Channel

The previous results cover Reed-Solomon code performance over a non-binary channel, or a channel with equi-probable symbol errors, as depicted in Figure 2.0-2. The worst case error detection performance using this channel can be heuristically bounded by noting that, regardless of the error pattern affecting the k information symbols, the errors affecting the N-k check symbols must cause perfect agreement between every computed check symbol and every received check symbol. Note that with a Reed-Solomon code, any change in one information symbol affects each and every computed check symbol. The worst case probability of receiving a check symbol that agrees with an erroneous computed check symbol is $P_e / (q-1)$, which is less than $(q-1)^{-1}$. The probability that all check symbols agree is $(q-1)^{-(N-k)}$ with error detection only, and no error correction. With $q = 256$ and $N-k = 32$, this gives a $P_e < 10^{-77}$.

By comparison, with a binary channel, low binary weight error patterns are more likely than error patterns with a large number of bit changes. The concern is that a codeword differing from the transmitted codeword by N–k+1 symbols may only differ by N–k+1 bits, one bit per symbol. In a manner analogues to the non-binary channel, we can calculate the probability of match for a set of N–k check symbols consisting of n bits each, and each with one bit error. The probability of one check symbol matching is pq^{n-1} with one bit error in the symbol. This is maximized with $p = \frac{1}{n}$, so that the probability of N–k check symbols matching with one error each is $P_e \leq \left(\frac{1}{n}\right)^{N-k}\left(1 - \frac{1}{n}\right)^{(n-1)(N-k)}$. For our example, this is $P_e \leq \left(\frac{1}{8}\right)^{32} \cdot \left(\frac{7}{8}\right)^{7x32} = 10^{-42}$ for one specific sequence of check symbols given that the appropriate information symbols have been received. The overall probability of error is much less since the overall probability of receiving the information

symbols as well as the check symbols must be factored in. The question that we can't answer at this point is how many low binary weight codewords exist relative to the total number of codewords. In all likelihood, the density of binary weight check sequences is uniform for a given binary weight of the information sequence, in which case we can argue that the error detection performance over a binary channel is equivalent to the performance over a non-binary channel. Recall that a Reed-Solomon code has the property that a change in any one information symbol changes each and every check symbol. Thus, each check symbol can be written as a linear combination of the information symbols as shown below

$$C_0 = \alpha_{0,0} I_0 + \alpha_{0,1} I_1 + \cdots + \alpha_{0,k-1} I_{k-1}$$

$$C_1 = \alpha_{1,0} I_0 + \alpha_{1,1} I_1 + \cdots + \alpha_{1,k-1} I_{k-1}$$

$$\vdots$$

$$C_{31} = \alpha_{31,0} I_0 + \alpha_{31,1} I_1 + \cdots + \alpha_{31,k-1} I_{k-1}$$

with all the coefficients $\alpha_{i,j}$ non-zero. Now, the next step is to argue that is a column of the coefficient matrix of the α's is not a constant, each change of an information symbol will result in every check symbol changing by a different amount corresponding to a different value of the coefficient. For example, if the all-zero codeword is transmitted and one information symbol is received in error, all the check symbols will be non-zero. At most eight can have binary weight one if all the coefficients in one column are unique, and the remaining check symbols have minimum binary weight two. Thus, under this assumption, the minimum binary weight non-zero codeword is $1 + 8 + 2 \times 24 = 57$. In order to pursue this, the coefficient matrix for a specific code needs to be generated, and the properties examined. Looking at the code from this perspective, however, intimates that a change in one or more information symbols "randomizes" the check symbol sequence.

To lend some credence to these arguments, we examine the performance of a Reed-Solomon code in the next section, and compare it to a binary BCH code and a Hamming code of the same rate. The simulation results will show that the Reed-Solomon code outperforms the other two. While we can't run a full-up simulation of the (255,223) code at all error rates, we can examine areas of concern. That is, we can induce specific numbers of errors, 17, 18, and so on, to bias the simulation to a high error rate and accelerate the statistical reliability of the results.

We feel that this effort will be justified since this code has the potential for simultaneously satisfying both the error correction desired and the false message requirements.

3.0 FRAME HEADER SIMULATION RESULTS

A frame header code to provide protection against acceptance of erroneous headers has been prepared. [Ref 1] specifies a header BER of 10^{-12}. This bit error rate is not possible at all input error rates using the candidate error detection code proposed. The code proposed in [Ref 2] is a (64,48) binary Hamming code. In fact, the best any code with 16 check bits can do is guarantee an error rate of 2^{-16} unless the input, or channel, error rate is small. Fortunately, the results of section 2 indicate that this BER requirement can be met by the channel code. However, should a header code be required, we have simulated the performance of the proposed Hamming code as well as a comparable binary BCH code and a Reed-Solomon code. Al codes were tested with the same binary error pattern to provide consistency.

The Hamming code has a generator polynominal given as

$$g(x) = 1 + x^5 + x^{12} + x^{16} .$$

The BCH code had a generator polynominal given as

$$\begin{aligned} g(x) &= (1 + x^2 + x^3 + x^4 + x^8)(1 + x + x^2 + x^4 + x^5 + x^6 + x^8) \\ &= 1 + x + x^5 + x^6 + x^8 + x^9 + x^{10} + x^{11} + x^{13} + x^{14} + x^{16} \end{aligned}$$

The Reed-Solomon code check symbols consist of the first three symbols, C_0, C_1, and C_2, generated by constraining the first three syndrome equations to zero. The fourth symbol is an overall parity check on the codeword. Header error rates for these three codewords are plotted in Figure 3.0-1. Ultimately, the Reed-Solomon code outperforms the other two.

A listing of the frame header simulation follows. A copy of this program was given to LOCKHEED personnel at JSC for their use. It compiles under LAHEY F77L FORTRAN using a PC with the 8087 coprocessor.

[Ref 1] "Space Station Specification," Section 4.3.2.2, January 5, 1987

[Ref 2] "Channel Coding Performance Analysis," (Private Communication), Warner Miller and James Morakis, February, 1987.

[Ref 3] "Concatenated Codes," Forney, G. David, The MIT Press, 1966.

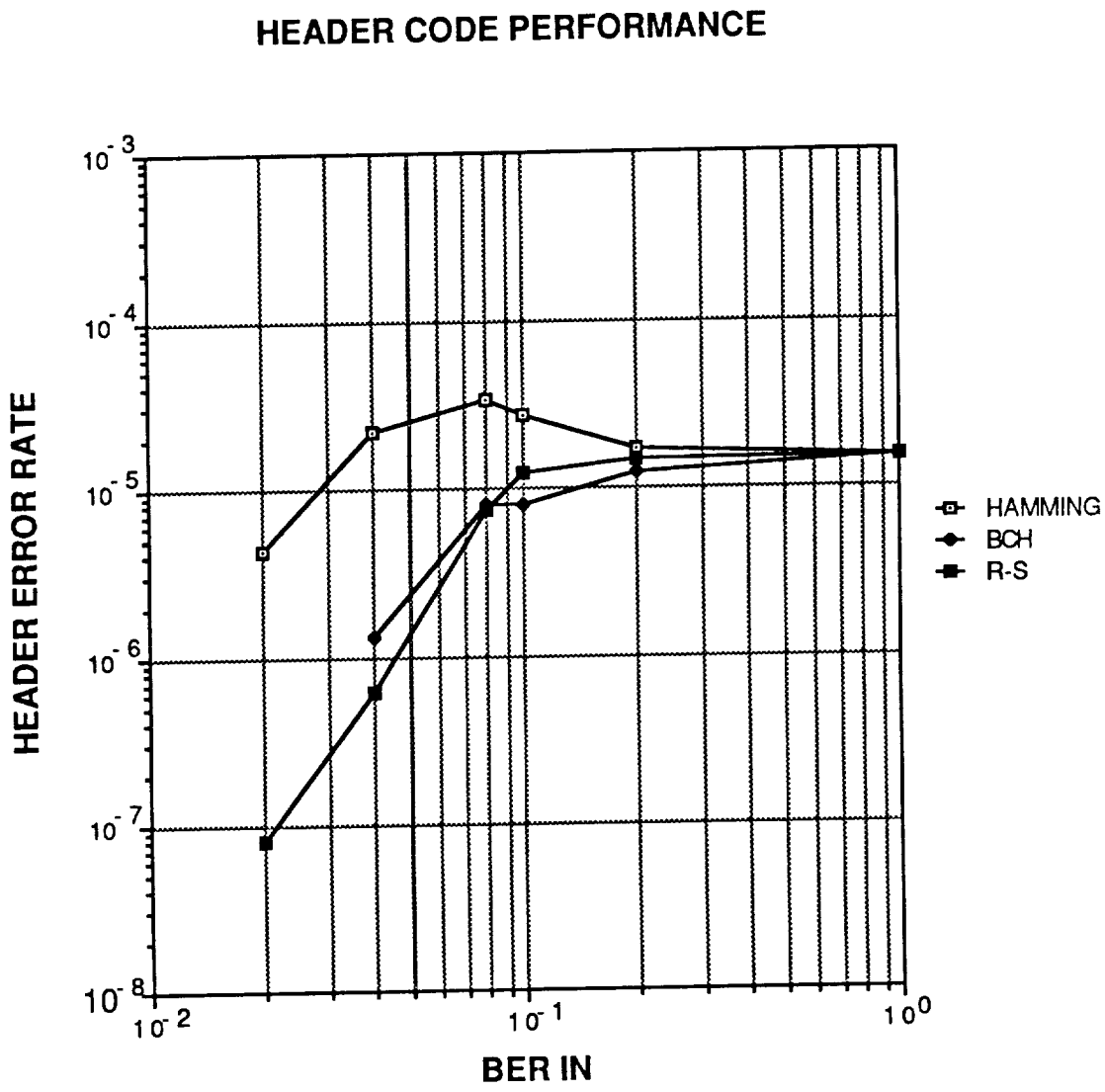
HEADER CODE PERFORMANCE
HEADER ERROR RATE
10^-3
10^-4
10^-5
10^-6
10^-7
10^-8
10^-2
10^-1
10^0
BER IN
HAMMING
BCH
R-S

FIGURE 3.0-1

```
      PROGRAM RS
      INTEGER*2 IC(0:15),IFR,IMUL(0:15),ISUM,IETAR(0:3)
      DIMENSION IETAB(0:31)
* Hamming generator
      DATA IFH/Z'10210000'/
* Reed-Solomon symbol field generator polynomial
      DATA IFR/Z'13'/
* BCH generator
      DATA IFB/Z'6F630000'/
* 8087 Initialization
      CALL INVALOP(I2)
      OPEN(2,FILE="LPT1")
*     Y=RRAND()
      IONE=1
      CWCNT=0.
      CWEH=0
      CWEB=0
      CWER=0
      WRITE(*,*) "INPUT BER"
      READ(*,*) PE
* Initialize PR generator
      CALL DRANSET
      IETAB(0)=1
      DO 10 I=1,31
* 8087 word shift
* IETAB and IETAR are used to add errors to input
      IETAB(I)=ISHFT(IETAB(I-1),IONE)
10    CONTINUE
      IETAR(0)=1
      DO 101 I=1,3
      IETAR(I)=2*IETAR(I-1)
101   CONTINUE
* IMUL is GF(16) multiplication table
      IMUL(0)=0
      IMUL(1)=2
      DO 15 I=2,15
      IMUL(I)=I*2
* IEOR is 8087 XOR
      IF (IMUL(I).GE.16) IMUL(I)=IEOR(IMUL(I),IFR)
15    CONTINUE
* Print BER on screen @ 10K, on printer @ 100k cwords
30    DO 21 I=1,10
      DO 20 IPR=1,10000
* Clear R-S input words
      DO  33 J=0,15
33    IC(J)=0
* Input error counter
      BTMP=0
* Clear BCH input words-Note B is BCH, H is Hamming
      IR1B=0
      IR0B=0
* Clear Hamming input  words
      IR1H=0
      IR0H=0
* Clear decoder syndrome registers (Ref. pg. 150 Vol 1 Peterson)
      ICDH=0
      ICDB=0
      I1=0
* Generate first 32 input bits packed into  IC and IR1B
      DO  50 I2=0,7
      DO 60 I3=0,3
```

```
* Generate PR#
        Y=DRAN(1.)
*       Y=RND()
        IF(Y.LE.PE) THEN
* Set bit to 1 if PR# less than input error rate
                IC(I2)=IOR(IC(I2),IETAR(I3))
                BTMP=BTMP+1
                IR1B=IOR(IR1B,IETAB(I1))
        ENDIF
        I1=I1+1
60      CONTINUE
50      CONTINUE
        I1=0
* Generate second 32 input bits
        DO 501 I2=8,15
        DO 601 I3=0,3
        Y=DRAN(1.)
        IF(Y.LE.PE) THEN
                IC(I2)=IOR(IC(I2),IETAR(I3))
                BTMP=BTMP+1
                IROB=IOR(IROB,IETAB(I1))
        ENDIF
        I1=I1+1
601     CONTINUE
501     CONTINUE
* Copy BCH  input to Hamming input
        IR1H=IR1B
        IROH=IROB
*.Increment cword counter
        CWCNT=CWCNT+1.
* Skip if no input errors
        IF(BTMP.EQ.0) GOTO 20
        BERR=BERR+BTMP
        DO 110 I6=0,63
* Sign bits hold current bit to be processed
* XOR syndrome,input for BCH
        IFLGB=IEOR(ICDB,IR1B)
        ICDB=ISHFT(ICDB,IONE)
* 64-bit left shift
        IR1B=ISHFT(IR1B,IONE)
        IF(IROB.LT.0) IR1B=IOR(IR1B,IONE)
        IROB=ISHFT(IROB,IONE)
* Feedback g(x) if high order bit is 1
* Next do Hamming
        IF(IFLGB.LT.0) ICDB=IEOR(ICDB,IFB)
        IFLGH=IEOR(ICDH,IR1H)
        ICDH=ISHFT(ICDH,IONE)
        IR1H=ISHFT(IR1H,IONE)
        IF(IROH.LT.0) IR1H=IOR(IR1H,IONE)
        IROH=ISHFT(IROH,IONE)
        IF(IFLGH.LT.0) ICDH=IEOR(ICDH,IFH)
110     CONTINUE
* Increment error count if syndrome not zero
        IF (ICDB.EQ.0) THEN
                CWEB=CWEB+1
        ENDIF
        IF (ICDH.EQ.0) THEN
                CWEH=CWEH+1
        ENDIF
* R-S decoder
1004    ISUM=0
```

```
* First do overall parity check
        DO 80  I5=0,15
80      ISUM=IEOR(ISUM,IC(I5))
* Detect error if nonzero, i.e. not UNDETECTED error
        IF(ISUM.NE.0) GOTO  20
* Calc first syndrome=sum(IsubI4*Alpha**I4)
        ISUM=IC(0)
        DO 70 I4=1,14
        ISUM=IMUL(ISUM)
        ISUM=IEOR(ISUM,IC(I4))
70      CONTINUE
* Detect error if nonzero
        IF(ISUM.NE.0) GOTO  20
        ISUM=IC(0)
* Second syndrome=sum(IsubI6*Alpha**(2*I6))
        DO 90 I6=1,14
        ISUM=IMUL(ISUM)
        ISUM=IMUL(ISUM)
        ISUM=IEOR(ISUM,IC(I6))
90      CONTINUE
* Detect error if nonzero
        IF(ISUM.NE.0) GOTO 20
        ISUM=IC(0)
* Third syndrome
        DO 100 I7=1,14
        ISUM=IMUL(ISUM)
        ISUM=IMUL(ISUM)
        ISUM=IMUL(ISUM)
        ISUM=IEOR(ISUM,IC(I7))
100     CONTINUE
* If all syndromes zero, we have undetected error, inc count
        IF (ISUM.EQ.0) THEN
                CWER=CWER+1
        ENDIF
20      CONTINUE
* Calc error rates, PB is check on input  rate
        CWOUTB=CWEB/CWCNT
        CWOUTH=CWEH/CWCNT
        PB=BERR/CWCNT/64
        CWOUTR=CWER/CWCNT
        WRITE(*,*)  PB,CWCNT,CWOUTH,CWOUTB,CWOUTR
21      CONTINUE
        WRITE(2,*)  PB,CWCNT,CWOUTH,CWOUTB,CWOUTR
        GOTO 30
        END
* Big mother PR# generator
        FUNCTION DRAN(X)
        DOUBLE PRECISION M,A,C,RM,Y,XX
        DIMENSION RANT(97)
        J=1.D0+(97.D0*Y)/M
        Y=RANT(J)
        DRAN=Y*RM
        XX=DMOD(A*XX+C,M)
        RANT(J)=XX
        RETURN
* Initialization for PR# gen.
        ENTRY DRANSET
        DRANSET=1
        M=1771875.
        A=2416.
        C=374441.
```

```
      RM=1.D0/M
      XX=DMOD(A*12345.,M)
      DO  10,I=1,97
      XX=DMOD(XX*A+C,M)
      RANT(I)=XX
10    CONTINUE
      XX=DMOD(XX*A+C,M)
      Y=XX
      RETURN
      END
```

APPENDIX Q

SSIS HEADER CODE

Axiomatix

9841 Airport Boulevard • Suite 912 • Los Angeles, California 90045 • Phone (213) 641-8600

TECHNICAL MEMORANDUM **TM8706-4**

TO: Sid Novosad, Henry Chen, NASA/JSC

FROM: James Dodds

SUBJECT: SSIS Header Code

DATE: June 19, 1987

Warner Miller and Henry Chen recently sent me some new material on the use of a binary Kasami code for burst error control with the SSIS frame header. I understand that there is a CCSDS meeting next week (6/22), and that this is one of the topics of consideration. I have a few quick comments prior to a more detailed analysis. The assumptions made by Goddard regarding the error rate into the (85,64) binary code are:

- Probability of burst length greater than 10 bits is zero.
- Input error rate less than 10 – 5.

With these assumptions, they bound the probability of header error as the probability of 2 or more channel errors with no burst errors, or 1 channel error with a burst of length 10 or less. This is certainly a conservative bound, given the assumption. We might want to take a harder look at the burst error statistics, however. A related issue is the performance of the error trapping decoder. Historically (if 20 years in the past can be considered history) the error trapping decoder was considered because of its relative simplicity. However, modern high speed processors allow us to consider the use of other decoding techniques. The reason for bringing this up is that I don't know what the residual error detection capability is with this code in the event that a burst length of 11 or greater occurs, or if it is overloaded with random errors.

I took a quick look at an alternate, a (17,13) Reed Solomon code with 5-bit symbols. This code is 85 bits long, with 20 check bits, 64 address bits and 1 "freebie." It can correct bursts in the range of 6 to 10 bits, with six guaranteed. In addition, the residual error detection capability is estimated to be as follows:

BER_{IN}	$P_{e,header}$
0.5	0.125
0.1	0.25×10^{-1}
0.05	0.50×10^{-2}
0.01	0.59×10^{-4}

A (19,13) Reed-Solomon code, with a length of 95 bits, can correct bursts in the range of 11 to 15 bits, with 11 guaranteed. The residual error detection capability is also better.

I'll call you Monday and we can discuss pursuing this further.

APPENDIX R

SSIS SM CODES

Axiomatix

9841 Airport Boulevard • Suite 912 • Los Angeles, California 90045 • Phone (213) 641-8600

TECHNICAL MEMORANDUM TM8709-1

TO: Sid Novasad, NASA-JSC

FROM: James Dodds

SUBJECT: SSIS SM Codes

DATE: September 22, 1987

1.0 INTRODUCTION

Axiomatix has implemented a nominal rate 1/2 (8 data rows + 8 check rows) SM-8 decoder in order to verify the Schilling/Manela results. This memo describes details of the specific algorithm implemented. We are getting close to the results claimed by Manela in his thesis for the SM-8 code, and in fact, one variation of the decoding algorithm is exceeding his results. The outstanding question is, of course, the complexity of the hardware implementation vis-a-vis a Reed-Solomon code of comparable performance.

The Axiomatix decoder has a checkered history; the initial decoder had performance several orders of magnitude worse than the Manela results. However, after working with the codes, and gleaning incidental pieces of information from David Manela and Don Schilling, we were able to approach, but not duplicate, their results. We have tried several sets of parity check slopes, which are not necessarily optimum. Schilling and Manela are not willing to provide us with the "optimum" slopes, but it appears that we are close enough for practical purposes.

2.0 SM-8 CODE CHARACTERISTICS

The specific code implemented is depicted in Figure 2.0-1. The maximum block size is limited by the maximum allowable storage space of the Fortran compiler object

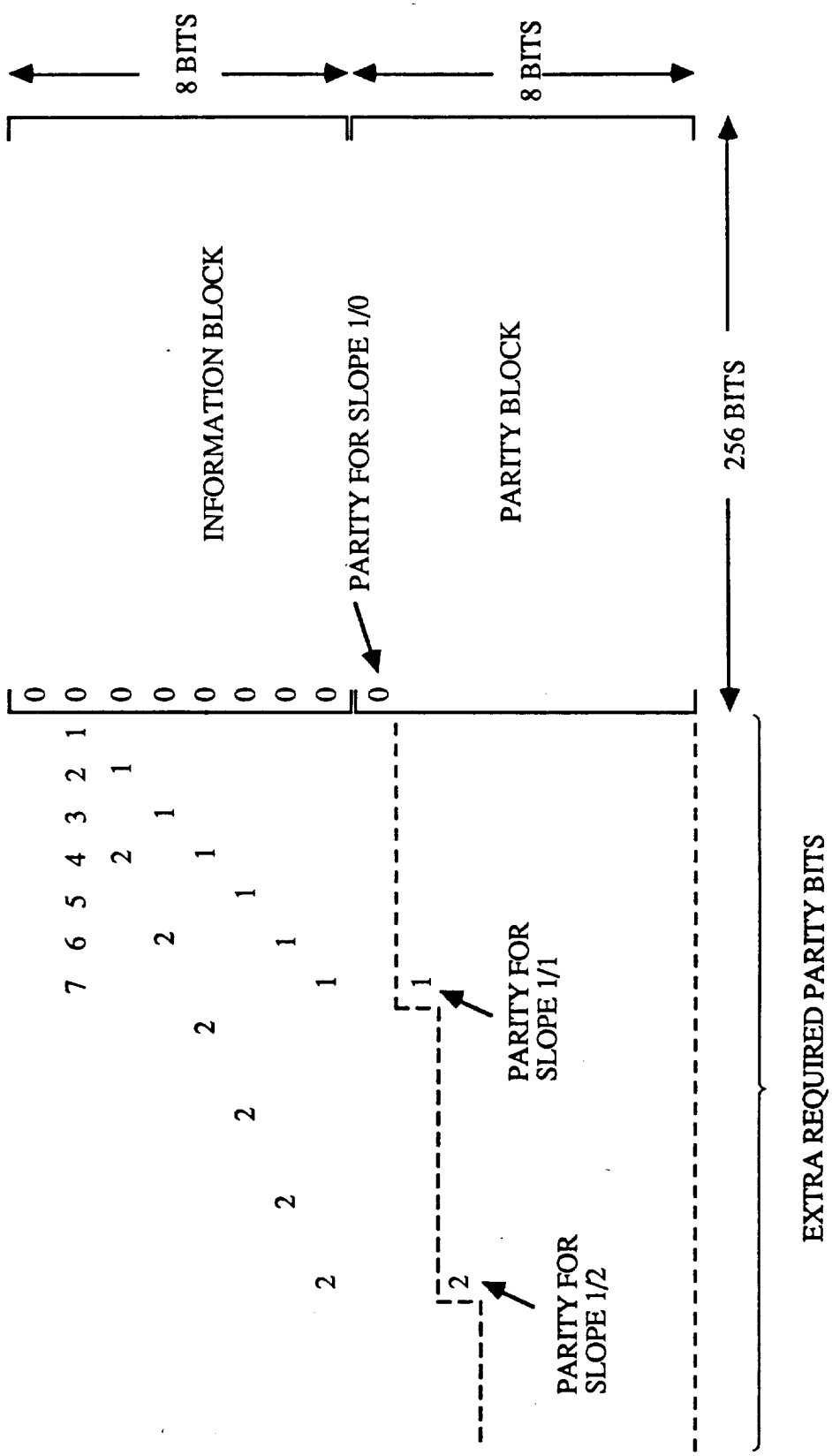

FIGURE 2.0-1. SM-8 CODE BLOCK INCLUDING EXTRA PARITY

modules, 64 K. The code of Figure 2.0-1 has parity slopes of 1/0, 1/1, 1/2,..., 1/7. A code with slopes consisting of the reciprocal of prime numbers was also implemented. The code performance is close to the 1/n slope code, but the block size is necessarily shorter due to the steeper slope. The nominal code rate is 1/2, but the flush bits lower the code rate by a significant factor. The number of flush bits can be calculated as follows: The slope 1/0 parity line requires no flush bits, the slope 1/1 requires 7 flush bits, the 1/2 slope requires 14 flush bits, and the 1/n slope requires 7n flush bits. Thus, the total number of flush bits is

$$F = \sum_{i=1}^{n} 7 * i = 7\frac{(n+1)n}{2} = 196 \text{ bits}$$

The overall code rate for the 1/n code is $R = \frac{2048}{4096 + 196} = 0.477$

The rate of the prime number code is $\frac{1376}{2752 + 294} = 0.45$

One of the ARQ strategys described in the next section lowers the effective code rate. The code rate loss is, of course, a function of input error rate, as the number of retransmissions increases over the noisy channel.

3.0 SM-8 DECODER IMPLEMENTATION

Two variations of an SM-8 decoder have been implemented. The basic decoder decodes a block of data using a single "pass," while the ARQ version decodes a block, checks the cumulative syndrome register against a threshold, and makes an additional pass if any cell is above the threshold. This variation allows us to use a lower threshold and pick up more errors. The number of passes must be limited, both to prevent error propagation, and to prevent infinite decoder loops.

The simulation uses a pseudo-random number (PRN) generator which computes a uniformly distributed PRN, compares the number with the selected input error rate, and

stores a 1 in those bits which have a PRN less than the input error rate. A block diagram of the simulation is shown in Figure 3.0-1. Referencing this figure, one of eight arrays, R1 through R8, are dedicated to each of the eight parity lines. If a parity line has odd parity, all bits on the diagonal line of the appropriate array are set to one. After all array have been set, the contents of each array are added, with the result stored in array ICNT. For example, a single error at row J, column I in the information block will result in 1's being stored at all diagonals of R1 through R8 that intersect at I, J. Thus ICNT (J,I) will contain an 8 after all the R arrays are added together.

The cell corrections are made from bottom (Row 8) to top (Row 1), and the threshold level for correction is initially set to 8, then 7, and so on. Using a higher threshold first, as per a hint by David Manela, corrects the most likely (single) errors first. This strategy gives a significant improvement in decoder performance. Figure 3.0-2, a reproduction of a plot from the Manela thesis, shown the results of the Axiomatix simulation relative to the Manela results.

3.1 Modified SM-8 Decoder

In the course of trying to reconcile the Axiomatix results with the published SM-8 results, a variation of the Manela decoder was implemented. The basic decoding algorithm is unchanged, but the threshold is lowered to a value of 4. If no other changes were made, this would increase the error rate due to a propagation effect. However, once the block is initially decoded, we interate on the block. That is, the cumulative weights are recomputed, and the decoding process repeats. This procedure can lead to an infinite loop at low SNR, so a maximum count of 2 iteration per block is imposed. If, after two interations some cells still contain values equal to or greater than 4, a retransmission is requested. This strategy reduces the code rate, but is a very effective error detection strategy. At an input error rate of 0.02, the unmodified decoder has an output error rate of 3.2×10^{-6}, while the modified decoder has an error rate of 1×10^{-7}. The net code rate is lowered by a factor of 0.98, equivalent to a loss of 0.07 dB.

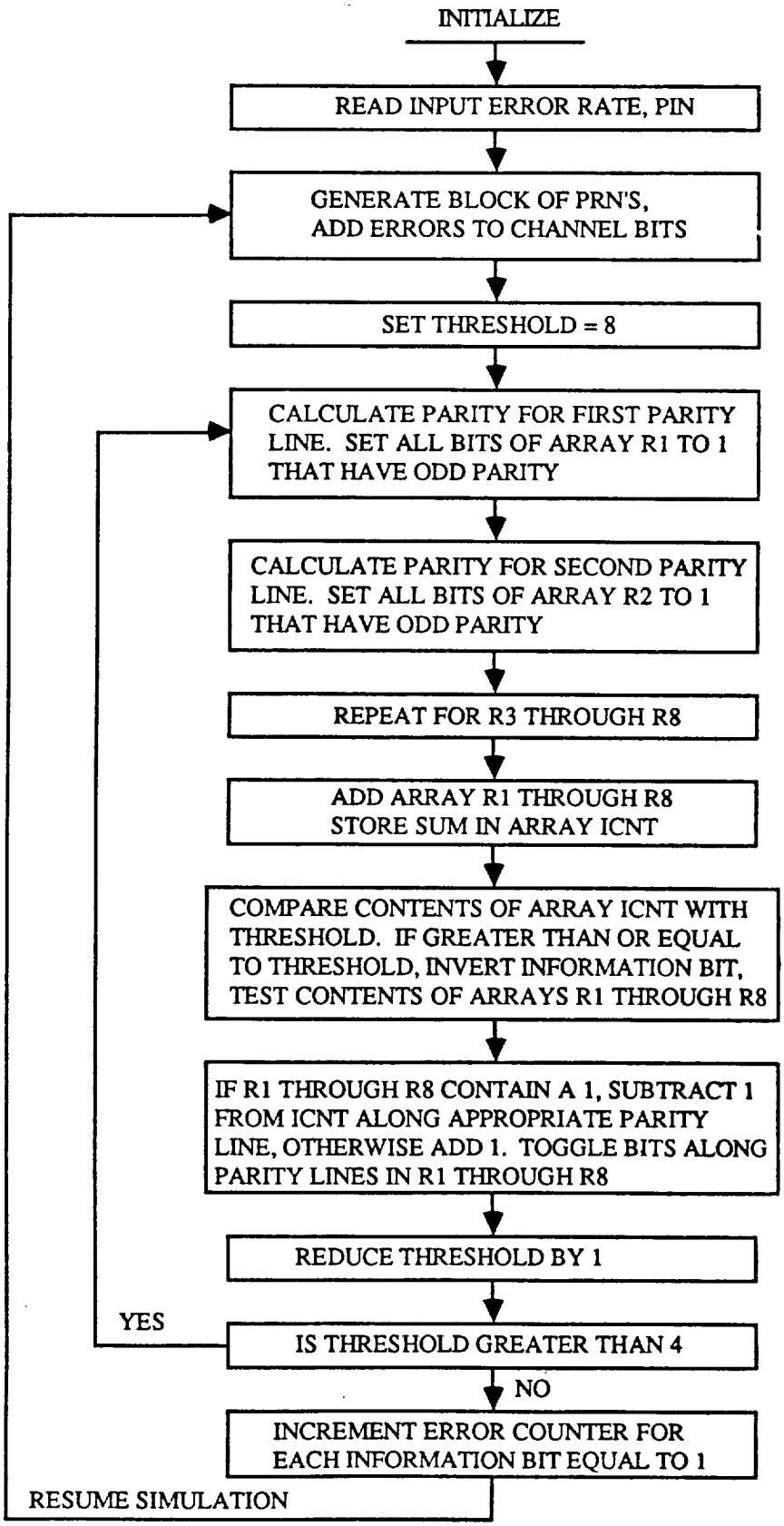
INITIALIZE
READ INPUT ERROR RATE, PIN
GENERATE BLOCK OF PRN'S, ADD ERRORS TO CHANNEL BITS
SET THRESHOLD = 8
CALCULATE PARITY FOR FIRST PARITY LINE. SET ALL BITS OF ARRAY R1 TO 1 THAT HAVE ODD PARITY
CALCULATE PARITY FOR SECOND PARITY LINE. SET ALL BITS OF ARRAY R2 TO 1 THAT HAVE ODD PARITY
REPEAT FOR R3 THROUGH R8
ADD ARRAY R1 THROUGH R8 STORE SUM IN ARRAY ICNT
COMPARE CONTENTS OF ARRAY ICNT WITH THRESHOLD. IF GREATER THAN OR EQUAL TO THRESHOLD, INVERT INFORMATION BIT, TEST CONTENTS OF ARRAYS R1 THROUGH R8
IF R1 THROUGH R8 CONTAIN A 1, SUBTRACT 1 FROM ICNT ALONG APPROPRIATE PARITY LINE, OTHERWISE ADD 1. TOGGLE BITS ALONG PARITY LINES IN R1 THROUGH R8
REDUCE THRESHOLD BY 1
YES
IS THRESHOLD GREATER THAN 4
NO
INCREMENT ERROR COUNTER FOR EACH INFORMATION BIT EQUAL TO 1
RESUME SIMULATION

FIGURE 3.0-1

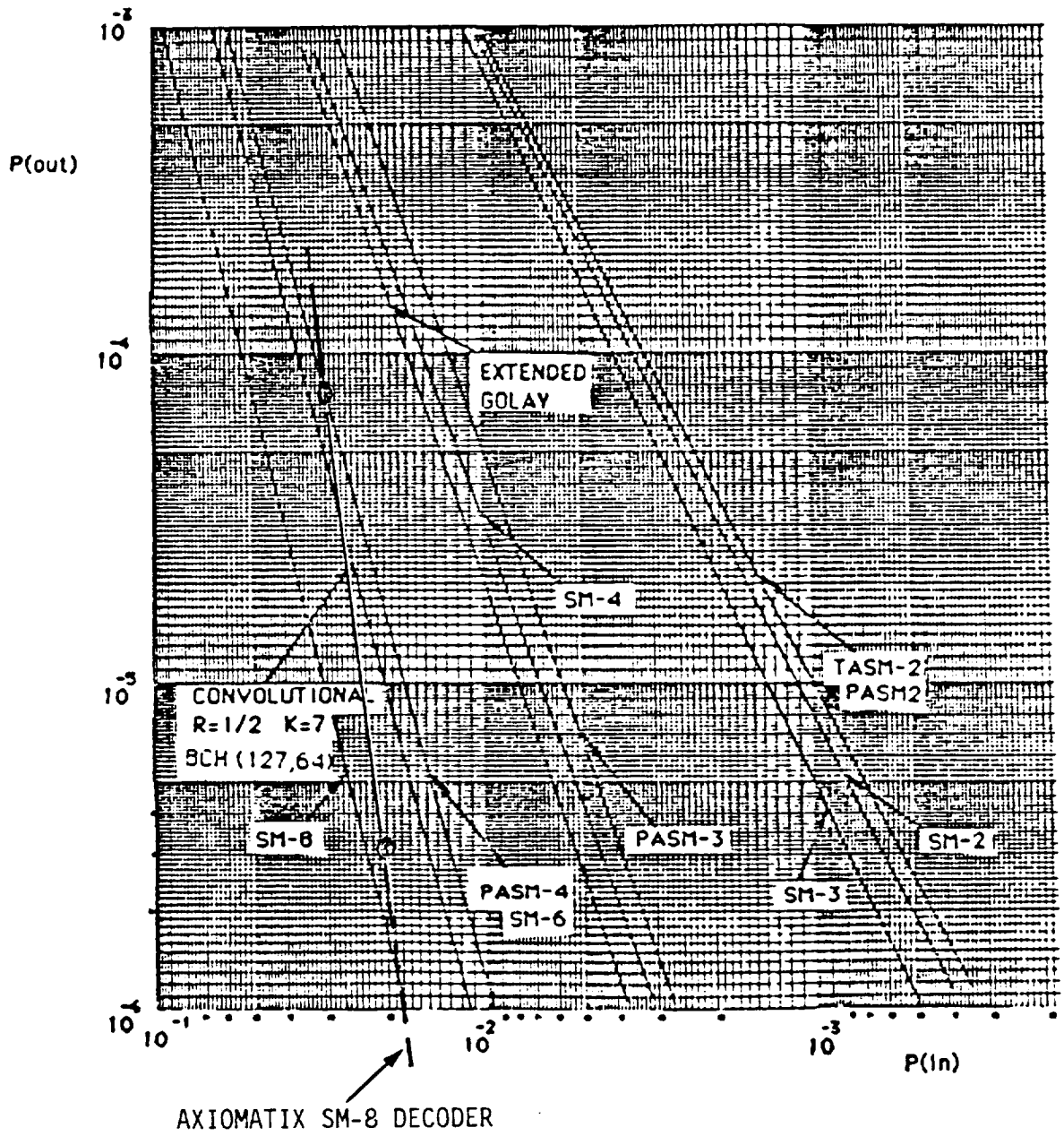

(FIGURE 3.2-5 P(out) versus P(in) R=1/2)

FIGURE 3.0-2. AXIOMATIX SIMULATION RESULTS.

APPENDIX S

A CRITIQUE OF THE SCHILLING-MANELA CODES

Axiomatix

9841 Airport Boulevard • Suite 912 • Los Angeles, California 90045 • Phone (213) 641-8600

TECHNICAL MEMORANDUM TM8710-1

TO: Sid Novosad, NASA/JSC

FROM: James Dodds

SUBJECT: A Critique of the Schilling-Manela Codes

DATE: October 14, 1987

Axiomatix has been evaluating the performance of a subset of the SM codes presented in Dr. Manela's thesis (Ref. 1). In addition, we have reviewed a critique of the thesis by Lin and Costello (Ref. 2) provided by NASA/JSC. In general, we agree with the Lin and Costello review of the codes: the codes are threshold decodable convolutional codes, and the decoding complexity engendered by the iterative decoding technique can cause throughput delay. One advantage claimed for the code proposed for Space Station use, the partially autoconcatenated (PASM) code, is the ARQ strategy permitting transmission of additional parity only. However, this is not unique to the SM codes. Any systematic code can be re-decoded with additional transmitted parity bits. This technique is of dubious advantage in decoding a high rate code as proposed for the Space Station. For example, a rate 0.9 code will, on the average, have 9 out of 10 errors in the information bits. Thus, it may be more efficient to retransmit the whole block rather than just parity for high rate codes. This is particularly true considering that each additional parity line has a shallower slope than the prior line, and the overall rate decreases faster than just the ratio of data rows to the total number of rows.

The probabilistic nature of the decoding process was evidenced in the Axiomatix implementation of the decoder. Each cell of the composite matrix is compared with a

threshold. In the case of the SM-8 code, the threshold starts at 8, since this would be induced by a single error (single errors are more likely than double errors, and so on). If the cell equals the threshold, the appropriate input bit is toggled, and all affected cells are recomputed. This process repeats for each cell. Next, the threshold is lowered to 7 and the whole threshold comparison repeats. Note that the decoding rate will vary as a function of the error patterns. Two widely separated errors will cause two recomputations at the threshold = 8 level, whereas two errors affecting the same composite cell will require only 1 recomputation at the threshold = 7 level. This means that the computational speed of the decoder must be fast enough to handle worst-case error patterns, or data will either be lost or output out-of-order.

The actual computational requirements of the decoder will be governed by a probability distribution function which is a function of channel noise, much like the probability of buffer overflow of a sequential decoder. That is, the probability of computational failure will increase as channel noise increases, and the decoder clock rate must be set fast enough to provide an acceptably low probability of failure. The nature of the computational distribution function may have to be estimated using simulations, since the iterative nature of the decoding process is not deterministic.

The Axiomatix implementation of the proposed rate 0.9 PASM code has been frustrated by the FORTRAN compiler 64K byte memory constraint. If we were to use the same programming shortcuts that allowed us to rapidly implement the SM-8 code, the memory requirement for a single composite matrix would exceed this limit. In lieu of using straightforward programming techniques, we would have to invoke complex bit shuffling algorithm which will slow down the decoder (and the programmer). An alternative is to program the decoder in "C" which is more suitable for this type of problem, but which will cause a delay due to our " learning curve" with the C language, or tie into the TCD VAX with a modem and remote terminal.

In conclusion, barring any new revelations, the SM codes do not appear to offer any significant advantage over other threshold decodable convolutional codes, and the dynamic behavior of the decoder may preclude its use over high-speed links. The proposed (255,223) Reed-Solomon code can provide the required error protection. This code can correct a minimum of 16 bit errors per block, with a residual error detection capability guaranteeing a probability of undetected error less then 10^{-13}. Since the chip set exists to implement this decoder, we feel that it is logical to use the Reed-Solomon code rather than the less mature SM code. On the positive side, the algorithm is simple and easy to understand; this class of codes presents an excellent introduction to multiple error correcting codes without resorting to the use of higher order algebraic fields and could well serve as a first example in a coding course.

REFERENCES

Ref 1. "A New Class of Forward Error Correcting Codes for Burst and Random Errors" by David Manela, Ph.D. Thesis, City University of New York, 1987.

Ref 2. "Review of 'A New Class of Forward Error Correcting Codes for Burst and Random Errors,'" Lin and Costello, Private Correspondence.

APPENDIX T

WANDERER TRACKER PERFORMANCE GOALS

Axiomatix

9841 Airport Boulevard • Suite 912 • Los Angeles, California 90045 • Phone (213) 641-8600

TECHNICAL MEMORANDUM TM8702-1

TO: NASA/JSC
Attn: EE8/S. W. Novasad
EE8/J. Ratliff
EE8/W. Marker
BE2(51)/K. Erickson

CONTRACT NO.: NAS9-17414

EE4/D. Fenner
EE/J. Johnson
EE/D. Bratton

FROM: James Dodds

SUBJECT: WANDERER TRACKER PERFORMANCE GOALS

DATE: February 17, 1987

1.0 INTRODUCTION

This memo addresses two of the significant concerns regarding candidate systems to detect wandering behavior and track a wanderer-cost and effectiveness. We feel that minimum cost can be attained by using devices based wholly or predominantly on commercial products and technology wherever possible. The use of a low cost intrusion alarm as part of the perimeter detection system is discussed in a subsequent paragraph. Effective wanderer tracking forces us to consider conflicting requirements, for example, long range implies high power transmitters, which in turn may require excessive battery power and short battery life. Again, some suggested tradeoffs and possible solutions are discussed in subsequent paragraphs.

2.0 TECHNICAL CONSIDERATION FOR EFFECTIVE WANDERER TRACKING

The following discussion assumes that a potential wanderer will be equiped with a radio-frequency transmitter, a perimeter alarm will detect the presence (or absence) of the

RF signal, and tracking capability will be provided by RF direction finding. Topics considered include:

- Minimization of battery power requirements
- Directionality of signal
- Signal penetration of structures
- Range
- Available technology

The first topic, minimization of power, has lead us to consider a system with a wanderer's transmitter in the "normally off" condition. With this system, depicted in Figure 2.0-1, the transmitter is held in the off state by the presence of an acoustic or electronic field provided, for example, by a commercial intrusion alarm. Such alarm systems can be purchased for under $200 per unit (Ref. 1) and provide an inexpensive source of microwave or acoustic energy. A receiver on the wanderers unit detects the presence of the energy to suppress the wearers transmitter. The wearers unit can also be equipped with a "dead-mans" switch which will trigger the transmitter if the unit is removed by the wanderer. Battery life should be extended substantially, since power is only needed for the receiver during periods of normal activity. This system has the added advantage that only a single, inexpensive transmitter is needed for each area to be monitored, regardless of the number of doors and windows, thus eliminating antennas, loops, or receivers at each portal. The same system can be used to monitor outdoor activity by careful placement of transmitters.

The wearer units can be tested by periodically shutting down the area transmitters. The system can be considered fail-safe, since the failure of any component of the system can be detected automatically. Failure of an area transmitter will cause all wearer units to

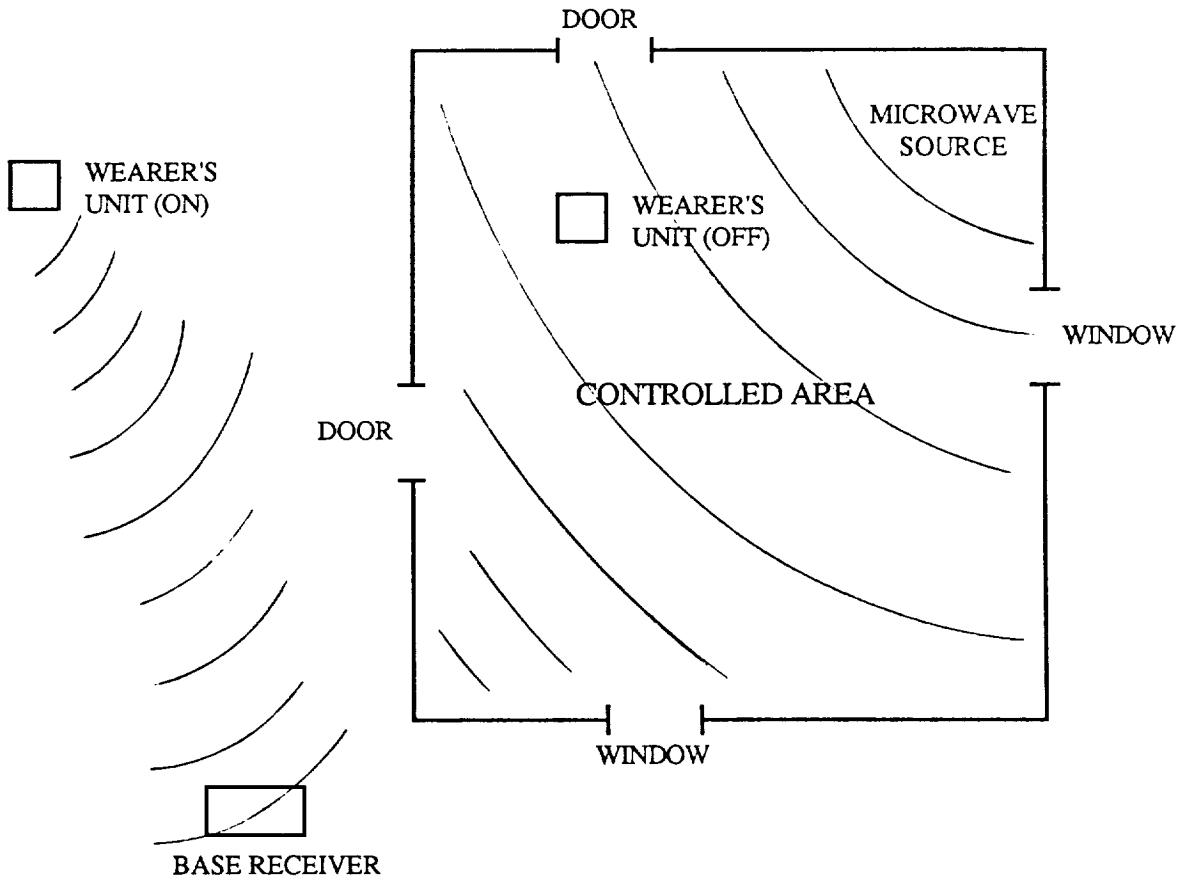
DOOR
MICROWAVE SOURCE
WEARER'S UNIT (ON)
WEARER'S UNIT (OFF)
WINDOW
CONTROLLED AREA
DOOR
WINDOW
BASE RECEIVER

FIGURE 2.0-1

respond, failure of one wearer unit (assuming each has a unique ID) will be evident during periodic checkout, as will failure of the base receiver when all units fail to respond during checkout. However, to distinguish individual wearer units during checkout, we must use a modulation which cannot be jammed by alternate wearers. A baseline modulation for consideration is a pulse-position modulator with time division multiplex pulse timing unique to each wearer. The wearer-unique code provides identification as well as low mutual interference.

In addition to the three components disscussed, the energy source, the wearer unit and the base receiver, a fourth component is needed for direction finding. For simplicity, we assume the direction finding unit is not required to identify a specific wearer unit once identification is made at the base receiver, but rather it is sufficient to track the energy of the wearer unit. Thus, the portable unit can be consideraly simplified. At this point we need to examine another tradeoff area, that of the frequency band utilized by the wearers unit. As depicted in Figure 2.0-2; two types of direction finding can be employed: (1) locate peak of pattern and (2) locate null of pattern. The requirement for a portable, hand-held receiver dictates that a horn antenna at EHF be used for the peak-of-pattern method, while a loop or ferrite antenna can be used at HF to locate with a null-of-pattern. Direction finding on a null is much less satisfactory for an inexpenrienced operator, particularly with the broad nulls at HF using a loop or ferrite. In addition, it is difficult to distinguish the 180° directional ambiguity, as shown in Figure 2.0-2; at EHF, a highly directional beam can be formed with a moderately sized antenna. Thus, it would seem that frequencies at K_a band and above would be prime candidates for the wanderer system if the low cost technology is available. However, these frequencies are easily blocked by structures and foliage, whereas HF energy is not attenuated as readily by obstacles. A hybrid approach would be

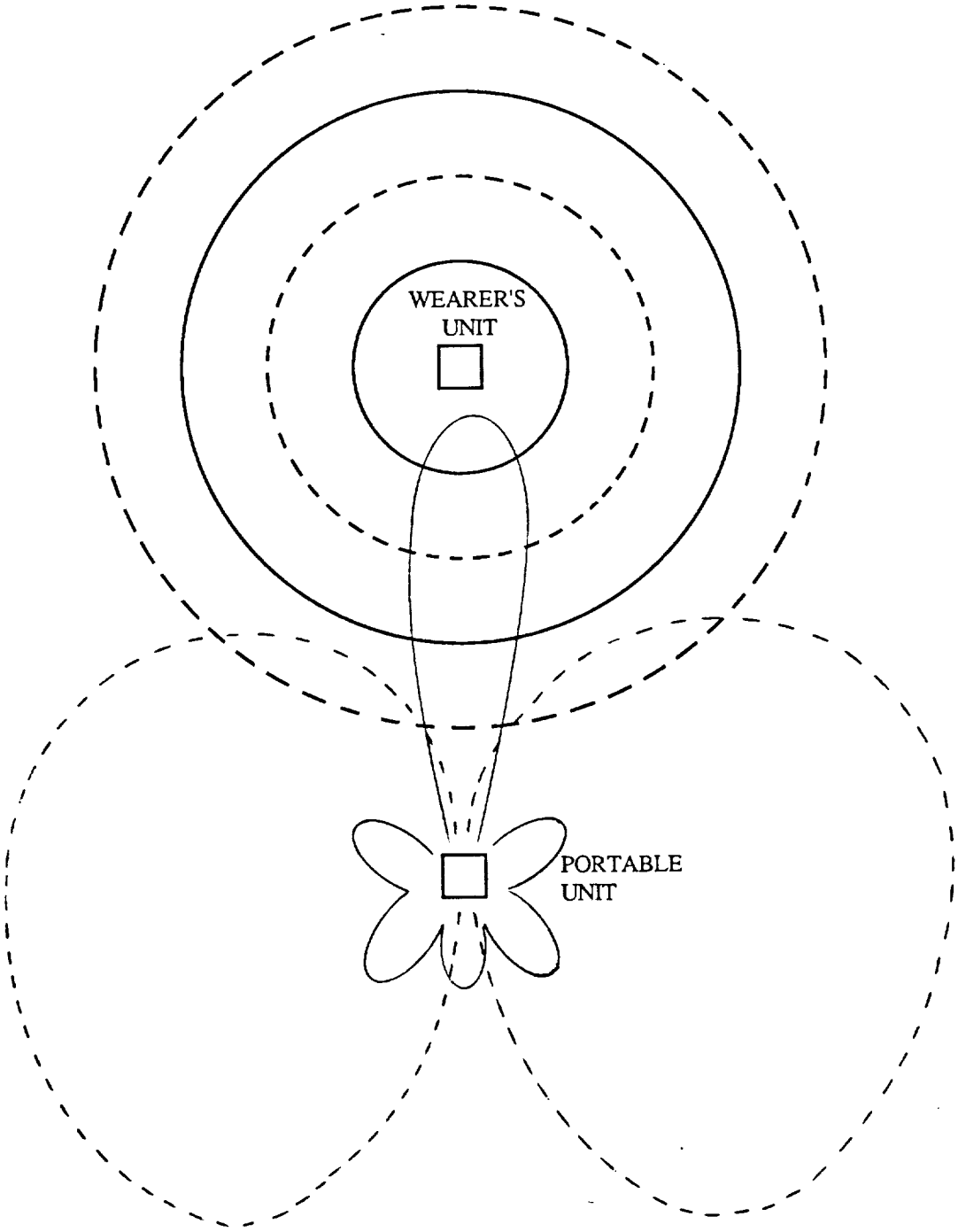

EHF PATTERN

HF PATTERN

FIGURE 2.0-2

to use a dual frequency system with coarse direction finding at HF in the presence of obstacles, and accurate direction finding at EHF. One frequency band could be implemented as a simple CW source, with modulation on the other band to provide the wearer ID. The complexity of the wearer unit would be slightly increased, with the worst impact on the portable direction-finding receiver which would probably need to accommodate both peak and null detection capability.

2.1 Wearer Identification

The problem of discriminating between different wanderers is exacerbated when, during self test, all wearer untis are turned on as the area transmitter is turned off. Some form of orthogonal modulation must be used to prevent mutual interference, overloading of the area receiver's front end, and suppression of weak signals from more distant wearers.

An example of a modulation scheme with a relatively simple demodulation, not requiring sophisticated spread spectrum demodulation or correlation receivers, would have the wearer units time synchronized to the area receiver clock. This system is depicted in Figure 2.1-1. Pulses from the area transmitter periodically reset counters in the wearer units and in the area receiver. Each wearer unit clock then counts to a preset value, T_i, different for each unit, before commencing transmission of alarm pulses. The minimum counter period of each wearer unit is greater than the reset pulse period T_r from the area transmitter, thus preventing transmission by wearer units within range of the area transmitter. Once activated, the wearer units transmit at a pulse interval T_r. The stability of the free-running oscillator in the wearer unit need only be good enough to provide adequate time to identify the unit by preventing the pulse epochs from drifting into the time slot

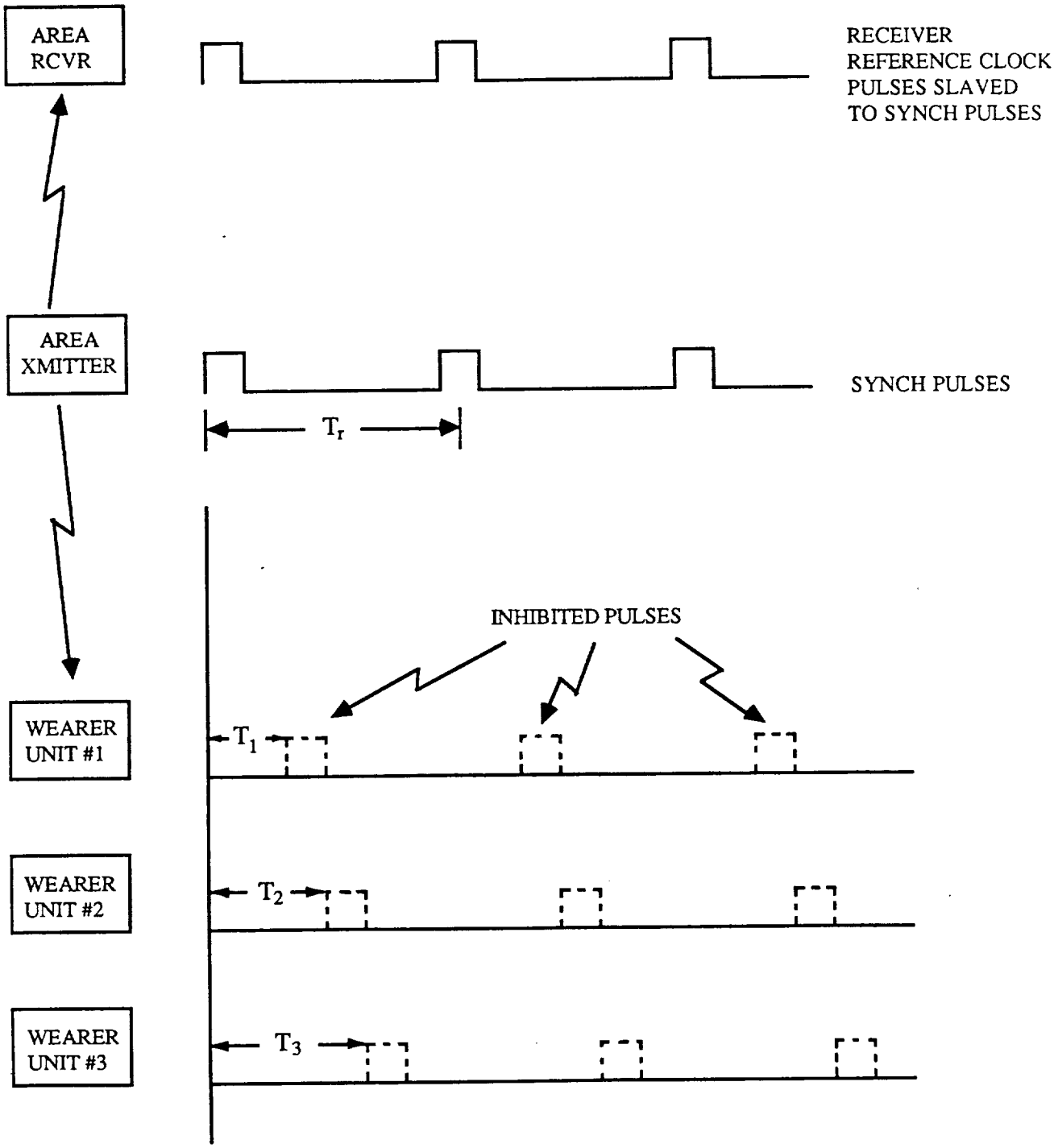
AREA RCVR
RECEIVER REFERENCE CLOCK PULSES SLAVED TO SYNCH PULSES
AREA XMITTER
SYNCH PULSES
T_r
INHIBITED PULSES
WEARER UNIT #1
T_1
WEARER UNIT #2
T_2
WEARER UNIT #3
T_3

FIGURE 2.1-1

corresponding to another wearer. For example, a system capable of accommodating 50 wearer units might have the following parameters:

Pulse duration	:	10 μsec
Guard time	:	10 μsec
Repetition	:	1 KHz
Number of time slots	:	50

If we assume that the receiver can tolerate a 5 μsec drift (1/2 a guard time), and 1second (1 thousand pulses) is an adequate time to identify a wanderer, then the transmitter stability requirement is about 5×10^{-6}, which is not difficut to achieve.

Installation having more than one area transmitter will require that the transmitters be synchronized, since it is assumed that only one area receiver will be needed. The transmitters can be hardwired together, or the synchronization signal can be superimposed on the AC powerline. Note that simplification can be effected for small installations not requiring wearer identification, but the economy of mass production would probably dictate a common wearer unit, whether or not identification is desired.

3.0 CONCLUSIONS

We have proposed a candidate wanderer tracking system with features which provide fail-safe operation, minimizes battery power requirements, and can provide good tracking capability. A more detailed investigation will provide insight into the cost effectiveness of considering a dual-band wearer unit or whether a compromise single frequency system would provide a better cost/performance ratio.

APPENDIX U

SIMULATION MODELS FOR OPTICAL COMMUNICATION SYSTEMS ANALYSIS

TELECOMMUNICATIONS AND INFORMATION SCIENCES LABORATORY
The University of Kansas
Nichols Hall - West Campus
2291 Irving Hill Road
Lawrence, Kansas 66045-6929
(913) 864-4832

SIMULATION MODELS FOR

OPTICAL COMMUNICATION SYSTEMS ANALYSIS

K. Sam Shanmugan
J. K. Townsend

Final Report
Contact #NAS9-17414
(For NASA-Johnson Space Center)

TR-7570-2

June, 1987

TABLE OF CONTENTS

Abstract ii
1. Introduction.....1
2. Laser Module.....2
3. OOK Optical Source.....3
4. Single Mode Fiber Module.....3
5. Avalanche Photodetector.....6
6. PIN Photodetector.....8
7. OOK Semi-Analytic Error Estimator.....9
8. Examples 10
9. References.....12
Appendix A Literature Review - Models for Optical Sources.....54
Appendix B Simulation of Digital Lightwave Communication Links.....65

C-4

SIMULATION MODELS FOR

OPTICAL COMMUNICATION SYSTEMS ANALYSIS

K. Sam Shanmugan

J. K. Townsend

ABSTRACT

Because of the presence of intersymbol interference and non-Gaussian noise sources, the analytical evaluation of the performance of lightwave communicaton links is difficult. Monte-Carlo simulations provide a powerful alternate approach to performance evaluation. This report describes a set of simulation models that can be used as building blocks for simulation based analysis and design of lightwave communication systems including the systems that are being proposed for on-board signal distribution within the Space Station. The simulation models described in this repaort are implemented within the BOSS (Block-Oriented Systems Simulation) framework.

Two appendices are included with this report. Appendix A is a summary of a literature review on models for optical sources that will be useful for simulating analog lightwave communication links. A tutorial on the simulation of digital lightwave links is included in Appendix B.

1. INTRODUCTION

The BOSS Lightwave Module Library contains modules which are useful for analyzing certain single mode fiber digital and analog communication links. The library features a general Single Mode Fiber module, an Avalanche Photodetector module, a PIN Photodetector module, a Semi-Analytic Error Rate Estimator module for digital On-Off Keyed (OOK) systems, and a Power Series Laser module, plus various other lower-level and internal modules (listed below).

In addition, two example systems are included to demonstrate how to use the modules.

The following is a list of the modules in the Lightwave Module Library arranged according to group name:

ANALOG MODULATORS
    LASER (POWER SERIES)

BASIC BULDING BLOCKS *TYPE/UNITS CONVERSION*
    REAL TO DBM

CALIBRATION DEVICES/METERS
    DELAY METER (REAL)
    OPTICAL AVERAGE POWER
    PRINT AVERAGE OPTICAL POWER

CHANNELS
    SINGLE MODE FIBER (LINEAR)

DIGITAL SOURCES
    OOK OPTICAL SOURCE

ESTIMATORS
    NOISE BW IMPULSE INJECT (REAL)
    OOK_ERROR RATE ESTIMATOR

ESTIMATORS *INTERNALS*
    COUNT ERRORS_& GENERATE STOP
    DELAY TX_SIG
    NOISE_BW COMPUTE (REAL)
    OOK ERROR PROB CALCULATE
    OOK PRINT
    OOK_POINT TO_DISTANCE

FILTERS
    BUTWTH FILTER (REAL)

FILTERS *INTERNALS*

2ND ORDER IIR SECTION (REAL)
TAPPED DELAY LINE CELL (REAL)

NOISE AND INTERFERENCE
AVALANCHE PHOTO-DETECTOR
AVALANCHE PHOTODIODE RAN_GEN
PIN PHOTO-DETECTOR

The top-level modules are discussed in more detail below. Many of the modules in the lightwave database are lower-level internal modules and are not explicitly discussed in detail here. Of course, on-line documentation is available for these modules as well as all other modules in BOSS. On-line documentation for the modules discussed below is provided in the Appendix.

It should be pointed out that in general, modeling of lightwave systems is rather problem dependent. It is difficult to separate the functionality of the various components of lightwave systems into modules which are totally independent of other modules in the system. This is the reason why modules for other lightwave system degradations are not currently available in the Lightwave Module Library.

2. LASER MODULE

This module models the input current to optical power output characteristic for a laser diode above threshold using a power series nonlinearity. The module is intended for modeling analog lightwave communication systems where the nonlinearity of the laser is the predominate degredation (in the laser). The maximum order of the polynomial is five, and is specified either by harmonic levels (in decibels relative to the fundamental) or by direct entry of the polynomial coefficients themselves.

The parameters of the module are:

HARM/COEF
TEST TONE MAGNITUDE
5TH HARMONIC LEVEL
4TH HARNOMIC LEVEL
3RD HARMONIC LEVEL
2ND HARMONIC LEVEL
EFFICIENCY
BIAS POWER
BIAS CURRENT

3. OOK OPTICAL SOURCE

This module outputs an On-Off Keyed (OOK) non-return-to-zero signal used to drive a lightwave fiber module. The random binary data on-amplitude is controlled by the value of the parameter "AVG OPTICAL POWER", which has units of decibel milliwatts (dbm). Initialization code reads in this value and computes the on-amplitude assuming that the off-amplitude is zero.

4. SINGLE MODE FIBER MODULE

The Single Mode Fiber modules provided in the BOSS lightwave Module Library is an implementation of a model given by Duff [1]. The baseband transfer function of a single mode fiber used in this module is given by the following equation:

$$H(f) = \int_{-\infty}^{\infty} S(\lambda)L(\lambda)\, e^{-j\omega LT(\lambda)} d\lambda \qquad (1)$$

where

ω = $2\pi f$
L = fiber length
$S(\lambda)$ = optical source spectrum vs wavelength
$L(\lambda)$ = 1/(fiber loss) vs wavelength
$T(\lambda)$ = fiber group delay vs wavelength
(antiderivative of dispersion vs wavelength)

In the BOSS module, an initialization subroutine calculates the transfer function given in Equation 1, takes the inverse FFT, and truncates the resulting impulse response. The impulse response is then convolved with the incoming signal using a tapped delay-line, implemented in block diagrams.

The integral in Equation 1 is implemented using Simpson's rule. The interval specified by the lower and upper limits of integration should be large enough to include insignificant portions of the source spectral envelope, $S(\lambda)$.

The module has three "modes" of operation:

1. Both source spectral envelope and fiber chromatic dispersion specified by closed form approximate functions;

2. Source spectral envelope specified by tabular data file, and closed form approximation for chromatic dispersion;

3. Both source spectral envelope and chromatic dispersion specified by tabular data files.

In all three modes, the fiber loss per kilometer is specified by tabular data files.

The closed form approximation for the source spectrum as a function of wavelength is given by

$$S(\lambda) = \frac{1}{\sigma_2 \sqrt{2\pi}} \exp\left(-\frac{(\lambda - \lambda_s)^2}{2\,\sigma_s^2}\right) \qquad (2)$$

where

σ_s = rms spectral width

λ_s = source center wavelength

The chromatic dispersion closed form approximation as a function of wavelength is (assuming a silica fiber)

$$\frac{dT(\lambda)}{d\lambda} = (s/c)\left(\frac{\lambda - \lambda_0}{\lambda^2}\right) \qquad (3)$$

where

s = a unitless constant

c = speed of light

λ_0 = zero-dispersion wavelength

The group delay is then

$$T(\lambda) = (s/c)\left[\ln\left(\frac{\lambda}{\lambda_0}\right) + \frac{\lambda_0 - \lambda}{\lambda}\right] \qquad (4)$$

Some of the parameters only apply to the closed form approximation, while others only apply to functions specified by tabular data files. Although BOSS always requires a valid entry for each parameter, the value for the parameter may be ignored by the module if it does not apply to the given module mode of operation.

The following parameters are read only when the closed form approximation for chromatic dispersion is used:

DISPERSION ADJUSTMENT CONSTANT
ZERO DISPERSION WAVELENGTH

Parameters read only when the closed form approximation for the source spectrum is used are:

RMS SOURCE SPECTRAL WIDTH
SOURCE CENTER WAVELENGTH

The following parameters apply only when chromatic dispersion as a function of wavelength is specified in a tabular data file:

GROUP DELAY POINT (WAVELENGTH)
GROUP DELAY POINT (DELAY)
DISPERSION FILENAME

The following parameter is read only when the source spectral envelope is specified by a tabular data file:

SOURCE SPECTRAL ENVELOPE FILENAME

The remainder of the parameters are used regardless of the mode of operation of the fiber module, and are as follows:

FIBER LENGTH
OF POINTS IN FIBER H(F)
OF PARTITIONS FOR INTEGRATION
INTEGRATION UPPER LIMIT
INTEGRATION LOWER LIMIT
FIBER H(T) SAVE FILENAME
FIBER LOSS FILENAME

RECALCULATE FIBER H(T)
MODE OF OPERATION

Computing the fiber impulse response for a given set of parameters can require from five to forty-five minutes of cpu time. In many applications, the same fiber characteristics may be used from one simulation to the next. To prevent wasting time recalculating the fiber impulse response in these cases, the module writes the calculated impulse response to the "FIBER H(T) SAVE FILENAME" when the value of the parameter "RECALCULATE FIBER H(T)" is set to TRUE. In subsequent simulation runs, the value would be set to FALSE, which causes the program to read the impulse response from the file specified by the parameter "FIBER H(T) SAVE FILENAME."

To insure that the parameters passed to the fiber module in a given simulation run are the same as the ones used to calculate the fiber impulse response in the save file, the module writes out a "verification record" (explained in the BOSS user's manual) at the bottom of the file. This verification record contains the numeric values for all parameters which were required to generate the fiber impulse response. Before the fiber module will successfully read the verification record, all of the parameters of the verification record must agree with the parameters passed into the fiber module. This prevents reading from a fiber impulse response file which was generated with parameters different from those values shown on the simulation parameter list.

5. AVALANCHE PHOTODETECTOR

This module is an implementation of an Avalanche PhotoDetector (APD) based on the Poisson and McIntyre distributions [2].

The number of primary charge carries (hole-electron pairs) in an APD is modeled by a Poisson process, with the average number per Δt given by

$$\overline{N} = \frac{\eta}{h\upsilon} P_{inc}(t) \cdot \Delta t + n_d \cdot \Delta t \qquad (5)$$

where

$P_{inc}(t)$ = incident optical power

η = quantum efficiency

h = Plank's constant

υ = optical frequency

n_d = number of dark charge carriers/second

The exact number of primary carriers, np, is drawn from this Poisson. Each primary charge carrier pair generates secondary charge carriers (providing the gain) in a random way. The discrete probability density of the number of secondary charge carriers plus the original primary charge carrier was found by McIntyre to be

$$P(n_i = m) = \frac{(1-k)^{m-1}\ \Gamma(\frac{m}{1-k})\ [\frac{1+k(g-1)}{G}]^{[\frac{1+k(m-1)}{1-k}]}}{[1+k(m-1)]\ (m-1)!\ \Gamma\ [\frac{1+k(m-1)}{(1-k)}]} \cdot [\frac{G-1}{G}]^{(m-1)} \qquad (6)$$

Hence for a given Δt, the output current of the APD is

$$i(t) = \frac{C_e}{\Delta t} \sum_{i=1}^{np} n_i \qquad (7)$$

where

C_e = the charge of an electron

n_i = number of secondary charge carries plus the primary generated in Δt seconds

The actual random number generation is done by the primitive module AVALANCHE PHOTODIODE RAN_GEN. The McIntyre distribution is implemented using the table lookup method. The following parameters to the APD module are related to the distribution:

AVG APD GAIN
APD "K" PARAMETER
MAX CDF PROBABILITY
CDF TABLE SIZE

The cumulative distribution function (cdf) is generated once at the beginning of the simulation from values given in the above parameters. A binary search is used to produce variates from the table during the simulation. "MAX CDF PROBABILITY" and "CDF TABLE SIZE" control the accuracy as explained in the on-line documentation in the Appendix.

Note that usage of this module in shot noise limited cases where the error rate however, is low (e.g., 10^{-9}) require to much simulation time to be practical. It does accurately model the APD, and could be useful for waveform analysis.

The Poisson random number generator uses the acceptance-rejection method to output a deviate for the given mean [3].

The remaining module parameters are:

APD INITIAL SEED
DARK CURRENT (NANOAMPS)
QUANTUM EFFICIENCY
SOURCE CENTER WAVELENGTH

These parameters are further discussed in the on-line documentation given in the Appendix.

6. PIN PHOTODETECTOR

A PIN photodetector module is also provided, and is the same as the APD module, except that there is no secondary charge carrier generation. Hence, for the PIN, the number of primary charge carriers is the same as in Equation (5). The output current is given by

$$i(t) = \frac{C_e \cdot np}{\Delta t}$$

where

C_e = the charge of an electron
np = the number of primary charge carriers generated in Δt seconds

The parameters are the same as the APD, except there are no parameters pertaining to the McIntyre distribution.

7. OOK SEMI-ANALYTIC ERROR ESTIMATOR

This module uses the combined analytic-simulation technique for estimating the bit error rate of digital OOK systems [4]. This module is used in conjunction with the NOISE BW IMPULSE INJECT (REAL) module which is inserted in the block diagram at the point where the additive white Gaussian noise enters the system. The Error Estimator can be used only if the modules downstream of the point where additive white Gaussian noise enters the system are linear.

When set up properly, this module automatically determines the equivalent noise bandwidth of the cascade of modules downstream from the additive white Gaussian noise source, and estimates the amount of delay between the transmitted and received bitstreams. Results from the calibration phase are available for viewing in the Postprocessor using the View Printed Output option.

After the module has finished the calibration phase, it begins the error estimation phase. For each received sample, the distance to the decision threshold is measured (the decision threshold is a parameter to the module). The estimated noise bandwidth and the user specified value of noise power spectral density are used to determine the variance of the Gaussian noise at the input to the estimator. The measured distance to the threshold is divided by the square root of this variance and a Gaussian tail probability (Q function) lookup is performed. The resulting error probability for this received sample is averaged with the error probability for the corresponding sample in all the bits in the estimation phase of the simulation.

The results are plotted in a multi-dimensional plot for viewing in the Postprocessor. If the BOSS Parameter Iteration option is NOT used, the only independent axis for the plot is NORMALIZED BIT TIME (MICROSECONDS). This plot is useful for determining the sensitivity of the error rate to timing errors in the sample and decide portion of the receiver.

If Parameter Iteration is used, the extra independent axis can be used to plot the variation of a parameter (where each iterated value is used in a

separate simulation) on the same multi-dimensional error rate plot (see the BOSS user's manual for a more detailed description of Parameter Iteration).

This Estimator module has an option which allows it to count actual errors which occur due to shot noise or severe ISI and store these in a multi-dimensional plot with NORMALIZED BIT TIME (MICROSECONDS) as the independent axis. The user can input the minimum number of errors which must be counted for every sample in the bit interval. When this number of errors has been exceeded for all samples in the bit interval, the Estimator module outputs a signal which can be used to drive a TERMINATE SIMULATION module. This module shuts down the simulation by setting time equal to STOP TIME. This feature allows the Estimator to be used in situations where there is a significant amount of shot noise (enough to cause the sample to cross the decision threshold) in addition to thermal noise.

From 10 to 100 errors should be counted to obtain reasonable confidence in the error probability estimate, so for extremely low error rates direct simulation is impractical. In these cases, an alternate simulation technique such as Importance Sampling should be used [4].

The parameters for the Error Estimator module are:

CALIBRATION START TIME
NOISE BW CALC DURATION
OF SAMPLES IN CORR SUB SEQ
MAX DELAY TO CALCULATE
OF SYMBOLS FOR ERROR EST
OF SAMPLES/SYMBOL
THERMAL NOISE PSD
DECISION THRESHOLD
MINIMUM # OF ERRORS
PROB OF ERROR AXIS LABEL
INDEPENDENT AXIS #2 LABEL
INDEPENDENT AXIS #2 VALUE

8. EXAMPLES

Two examples are presented in this section which use most of the modules in the Lightwave Module Library. The examples are mainly for illustration, and are not intended to show the only valid usage of the modules.

The first example is an end to end single mode fiber system with on-off keying (block diagram shown in Figure 1). The simulation parameters are shown in Figure 2. In this example, the fiber module uses the closed form approximations for both source spectral envelope and dispersion given in Equation 2 and Equation 3 (hence the parameter value CLOCLO). Since the parameter "RECALCULATE FIBER H(T)" is FALSE, the module will read the fiber impulse response from the file HIGHRES.SAV. The decision threshold value of 0.125 was determined from a previous simulation run.

The system level parameter values for the error estimator, PIN photodetector, fiber, and source modules are shown respectively in Figure 3. The INDEPENDENT AXIS #2 parameters are not used in this example, but are available for Parameter Iteration if desired. Notice that the three tabular filenames in the fiber module are all exported to the same filename. Since the fiber module is using closed form approximations for source spectrum and dispersion, it ignores the file name given for the respective tabular file parameters.

Data written out into the Postprocessor by the error rate estimator and PRINT AVERAGE OPTICAL POWER modules is shown in Figure 4 (this data can be read by selecting the View Printed Output option). The estimator writes out the beginning and ending times for calculating the noise bandwidth of the receiver and the start time for measuring the delay between the transmitted and received bitstreams. Also, the time which the actual error rate estimation begins is printed along with the minimum value of STOP TIME required to process the requested number of bits. The calculated delay in samples is displayed along with the single sided noise bandwidth in Megahertz. This information is useful when initially setting up a run with the error rate estimator module. The PRINT AVERAGE OPTICAL POWER module writes out the optical power in both dBm and Watts, as seen in Figure 4.

A plot of Log (Probability of Bit Error) versus normalized symbol time for this example is shown in Figure 5. From the plot, sensitivity to timing errors in the receiver can be easily seen. If the independent axis # 2 parameters had been used with Parameter Iteration, this plot would have had an additional dimension (the additional dimension would be orthogonal to the plane of the page).

The block diagram for the second example is shown in Figure 6. In this example, the three QPSK channels are Frequency Division Multiplexed and the composite signal used to intensity modulate a laser. The QPSK portion of the system is simulated using complex envelope representation. A Pseudocarrier is introduced to interface this complex envelope signal to the lightwave portion of the link, which operates on real signals. The pseudocarrier is the removed at the output of the lightwave link. From this point on, the signal is again in complex envelope form.

Figure 7 shows the simulation parameters and the system level parameters for the Laser module. In the example, a normalized baud rate of one is used, with a pseudocarrier frequency of 10. The laser operates with a third harmonic level of 14 dB below the fundamental. Thus when the laser has an input tone with a magnitude of 10, (the test tone magnitude) the output will have a third harmonic value 14 dB below the output at the input tone frequency.

In this particular simulation, the nonlinearity of the laser is the predominate degradation, therefore the fiber module is not used (since it is linear). A gain module is used for scaling in place of the fiber module.

In Figure 8, the magnitude spectrum of the laser output in shown. Figure 9 displays a scatter plot and a time plot of the receive filter output.

It is hoped that the examples provide some assistance in using the Lightwave Module Library. The Block diagrams and parameter listings should provide a starting point for using the modules to analyze other lightwave system configurations.

9. REFERENCES

[1] D. G. Duff, "Computer-Aided Design of Digital Lightwave Systems," IEEE Journal on Selected Areas in Communications, Vol. SAC-2, No. 1, pp. 171-185, January 1984.

[2] R. J. McIntyre, "The distribution of Gains in Uniformly Multiplying Avalanche Photodiodes: Theory," IEEE Transactions on Electron Devices, Vol. ED-19, pp. 703-718, June 1972.

[3] W. H. Press, B. P. Flannery, S. A. Tukolsky, W. T. Vetterling, "Numerical Recipes: The Art of Scientific Computing," New York, New York, Cambridge University Press, 1986.

[4] M. C. Jeruchim, "Techniques for Estimating the Bit Error Rate in the Simulation of Digital Communication Systems," IEEE Journal on Selected Areas in Communications, Vol. SAC-2, No. 1, pp. 153, 170, January 1984.

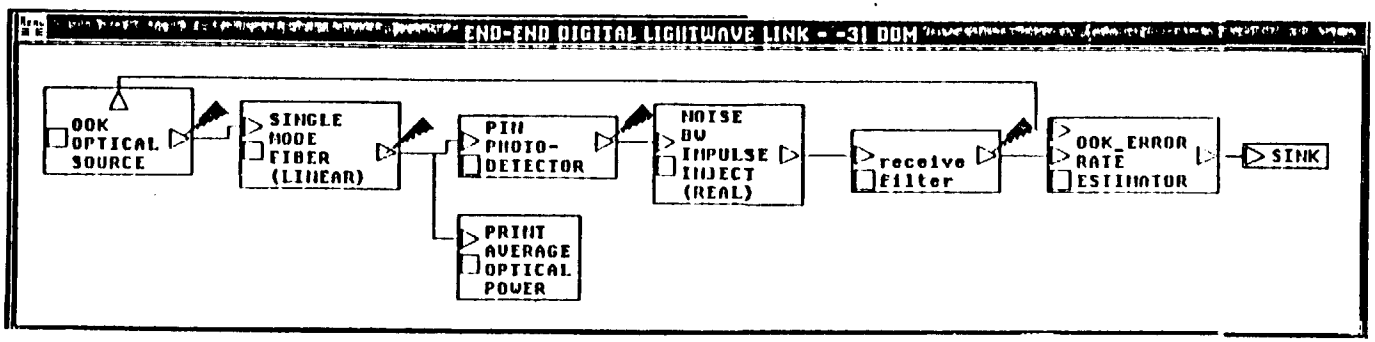

Figure 1. OOK digital lightwave example block diagram.

END-END DIGITAL LIGHTWAVE LINK--31 DDM - Module Help

```
STOP-TIME = 3.3
DT = 4.4643e-4
# OF SAMPLES/SYMBOL = 16
BIT RATE = 140
LAUNCHED OPTICAL POWER = -31
FIBER LOSS FILENAME = BOSS$SYSTEM:[DB.USER_TABDATA]LOSSFILE.DAT
;2
MODE OF OPERATION = cloclo
RECALCULATE FIBER H(T) = .FALSE.
FIBER H(T) SAVE FILENAME = BOSS$SYSTEM:[DB.USER_TABDATA]HIGHRES
.SAV;0
# OF PARTITIONS FOR INTEGRATION = 4000
# OF POINTS IN FIBER H(F) = 2240
PIN INITIAL SEED = 55899921
DARK CURRENT (NANOAMPS) = 21
THERMAL NOISE PSD = 1.88e-6
FILTER ORDER = 3
3 DB BANDWIDTH = 100
DECISION THRESHOLD = 0.125
NOISE BW CALC DURATION = 0.0714
# OF SAMPLES IN CORR SUB SEQ = 160
MAX DELAY TO CALCULATE = 40
# OF SYMBOLS FOR ERROR EST = 384
```

Figure 2. Simulation parameters for digital lightwave example.

```
Module/System Parameters>                                   KB
CALIBRATION START TIME          ::0
NOISE BW CALC DURATION          ::$NOISE BW CALC DURATION
# OF SAMPLES IN CORR SUB SEQ:: $# OF SAMPLES IN CORR SUB
MAX DELAY TO CALCULATE          ::$MAX DELAY TO CALCULATE
# OF SYMBOLS FOR ERROR EST     ::$# OF SYMBOLS FOR ERROR E
# OF SAMPLES/SYMBOL             ::$# OF SAMPLES/SYMBOL
THERMAL NOISE PSD               ::$THERMAL NOISE PSD
DECISION THRESHOLD              ::$DECISION THRESHOLD
MINIMUM # OF ERRORS             ::1000
PROB OF ERROR AXIS LABEL        ::Prob of Bit Error
INDEPENDENT AXIS #2 LABEL       ::*NOT USED*
INDEPENDENT AXIS #2 VALUE       ::0.0
EXIT

Module/System Parameters>                                   KB
DARK CURRENT (NANOAMPS)  ::0DARK CURRENT (NANOAMPS)
INITIAL SEED             ::$PIN INITIAL SEED
QUANTUM EFFICIENCY       ::0.75
SOURCE CENTER WAVELENGTH::1.28
EXIT

Module/System Parameters>                                   KB
DISPERSION ADJUSTMENT CONSTANT    ::0.0412
RMS SOURCE SPECTRAL WIDTH         ::0.03
SOURCE CENTER WAVELENGTH          ::1.28
ZERO DISPERSION WAVELENGTH        ::1.31
GROUP DELAY POINT (DELAY)         ::0
GROUP DELAY POINT (WAVELENGTH)    ::1.31
FIBER LENGTH                      ::15
# OF POINTS IN FIBER H(F)         ::$# OF POINTS IN FIBER H(F)
# OF PARTITIONS FOR INTEGRATION   ::$# OF PARTITIONS FOR INTEGRATION
INTEGRATION UPPER LIMIT           ::1.49
INTEGRATION LOWER LIMIT           ::1.07
FIBER H(T) SAVE FILENAME          ::$FIBER H(T) SAVE FILENAME
DISPERSION FILENAME               ::$FIBER LOSS FILENAME
SOURCE SPECTRAL ENVELOPE FILENAME::$FIBER LOSS FILENAME
FIBER LOSS FILENAME               ::$FIBER LOSS FILENAME
RECALCULATE FIBER H(T)            ::$RECALCULATE FIBER H(T)
MODE OF OPERATION                 ::$MODE OF OPERATION
EXIT

Module/System Parameters>                                   KB
AVG OPTICAL POWER::0LAUNCHED OPTICAL POWER
BIT RATE          ::$BIT RATE
ISEED             ::8967899
EXIT
```

Figure 3. Parameter values at the system level for: Error Rate Estimator, PIN Photodetector, Single Mode Fiber, and OOK Source.

```
Your choice of parameters for the
OOK_ERROR ESTIMATOR result in the
following computed times:
noise bw start time, noise bw stop time
 :   7.1400002E-02  0.1428000
delay est start time, error est start time
 :   0.2142000      0.3213432
error est minimum stop time :    3.071352

On-Off keyed error est tx to rx delay          25 (samples)
On-Off keyed error est noise bw   104.3952     (single sided, Hertz)
There were          384 bits used in ook error estimation.
Incident average optical power  -38.98030    Decibel milliwatts
Incident average optical power  1.2646481E-07 watts
```

Figure 4. Postprocessor printed output for digital lightwave example.

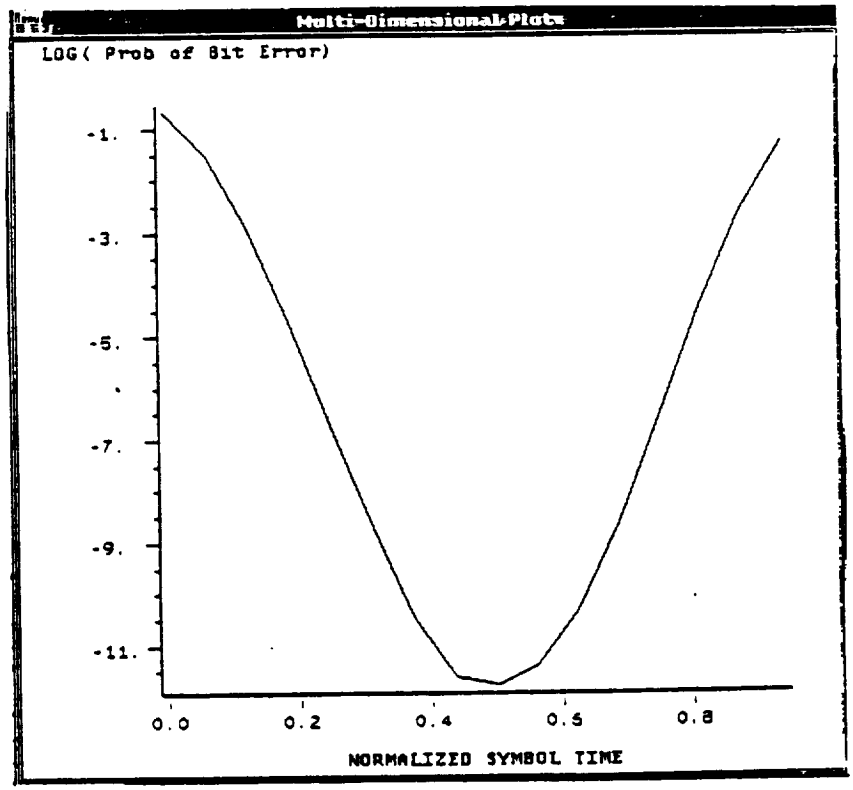

Figure 5. Bit error rate plot for digital example.

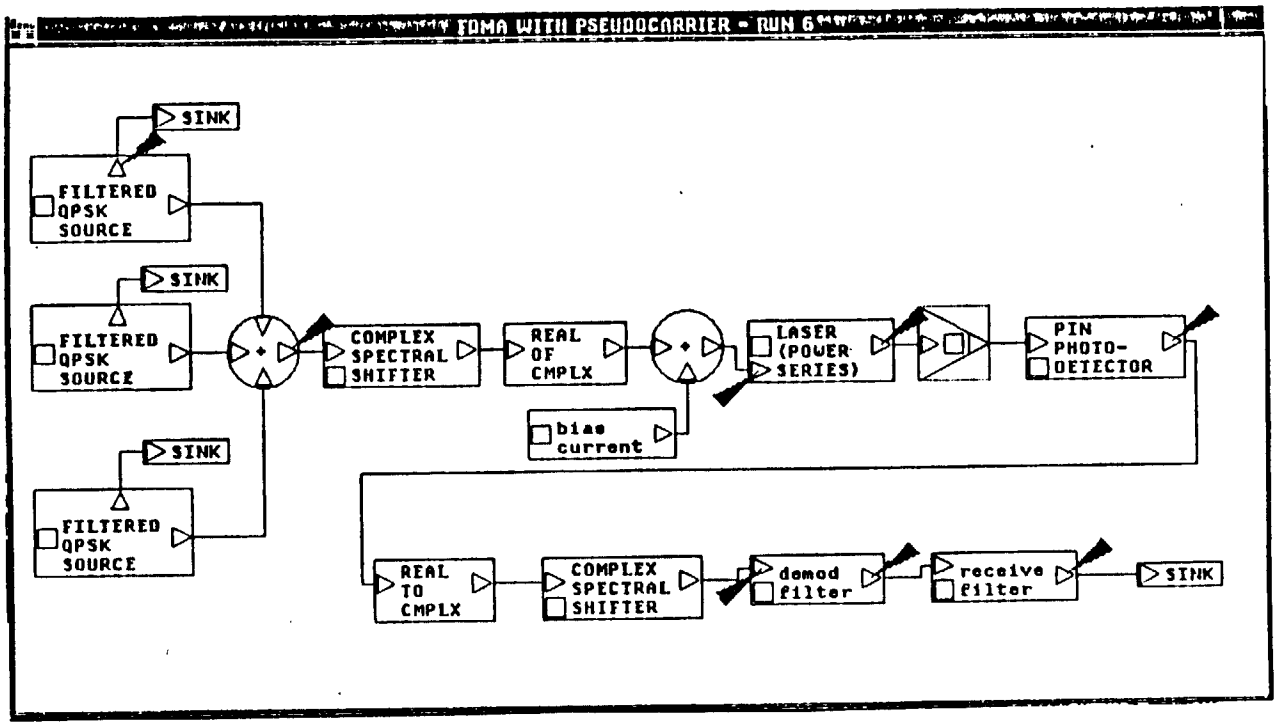

Figure 6. Intensity modulation example block diagram.

```
FDMA-WITH-PSEUDOCARRIER-RUN-6 - Module Help
STOP-TIME = 82
DT = 0.01
PIN INITIAL SEED = 992335
DARK CURRENT (NANOAMPS) = 30
QUANTUM EFFICIENCY = 0.7
FIBER GAIN = 1.0e-7
RX FILTER BW = 0.8
RX FILTER ORDER = 5
DEMOD FILTER BW = 5
NEGATIVE PSEUDOCARRIER FREQ = -10
SOURCE CENTER WAVELENGTH = 1.3
BIAS POWER = 5
BIAS CURRENT = 20
EFFICIENCY = 0.5
3RD HARMONIC LEVEL = -14
5TH HARMONIC LEVEL = -100
PSEUDOCARRIER FREQ = 10
TX FILTER ORDER = 5
3 DB BANDWIDTH = 1
BAUD RATE = 1
```

```
Module/SystemParameters                    K8
HARM/COEF              ::TRUE.
TEST TONE MAGNITUDE::10
5TH HARMONIC LEVEL ::$5TH HARMONIC LEVEL
4TH HARMONIC LEVEL ::-100
3RD HARMONIC LEVEL ::$3RD HARMONIC LEVEL
2ND HARMONIC LEVEL ::-100
EFFICIENCY             ::$EFFICIENCY
BIAS POWER             ::$BIAS POWER
BIAS CURRENT           ::$BIAS CURRENT
EXIT
```

Figure 7. Simulation parameters for FDMA example and the system level parameters for the Laser module.

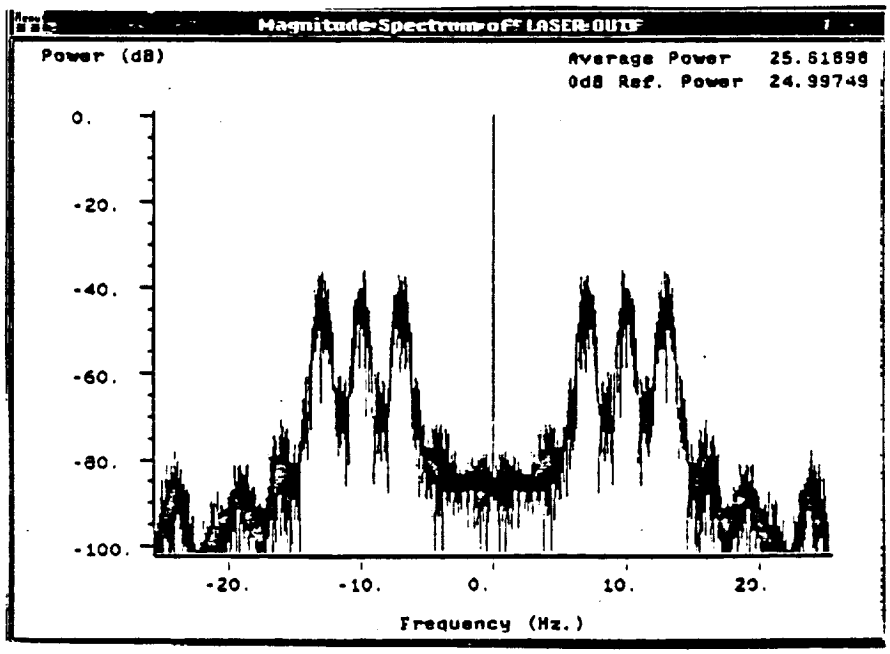

Figure 8. Laser module output spectrum for the FDMA example.

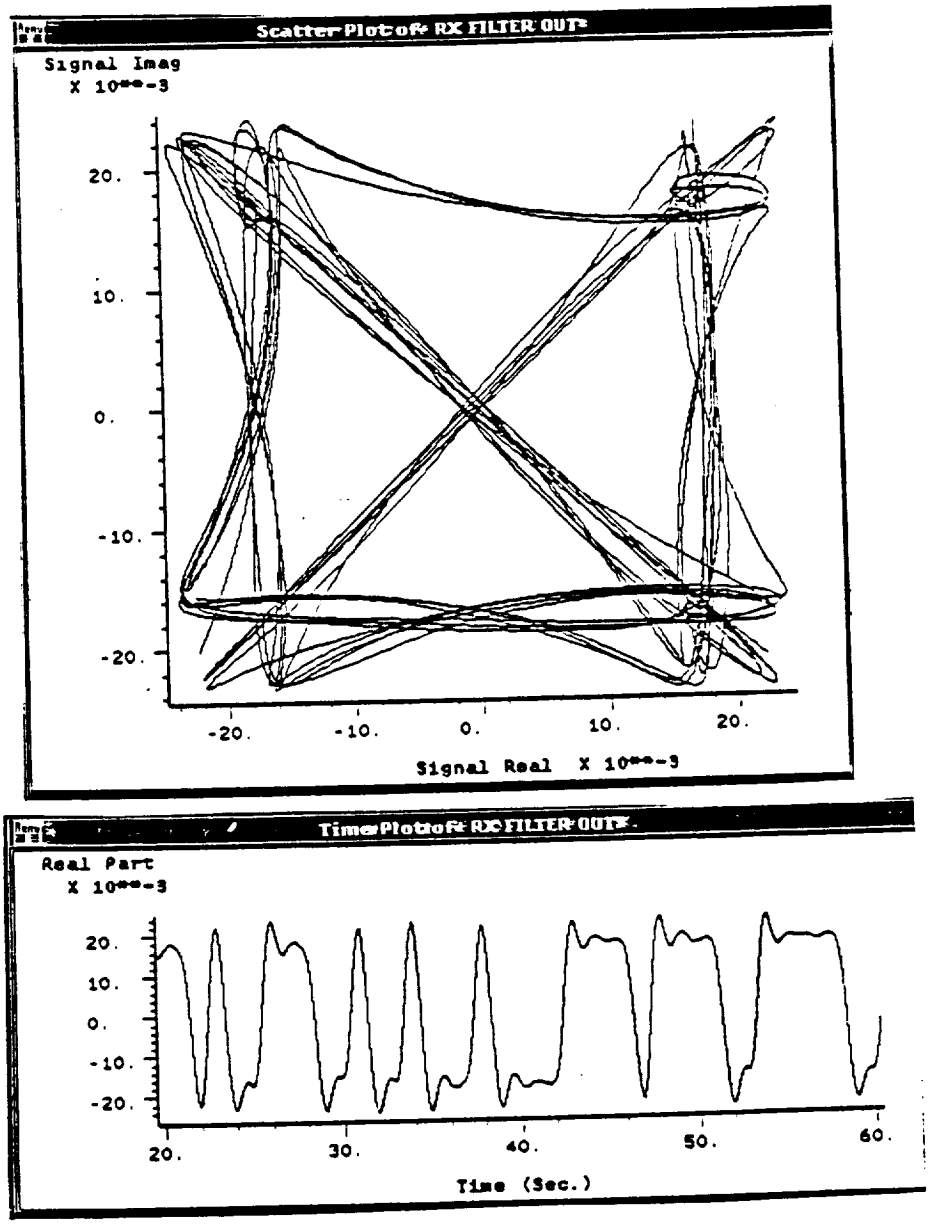

Figure 9. Scatter plot and time plot of receive filter output.

11. APPENDIX

This Appendix contains the on-line documentation for the following top-level lightwave modules:

AVALANCHE PHOTO-DETECTOR

LASER (POWER SERIES)

OOK OPTICAL SOURCE

OOK_ERROR RATE ESTIMATOR

PIN PHOTO-DETECTOR

SINGLE MODE FIBER (LINEAR)

MODULE NAME: AVALANCHE PHOTO-DETECTOR
GROUP: NOISE AND INTERFERENCE
DATABASE: DUAO:[BOSS.ADD_DB.LIGHT]
AUTHOR: TOWNSEND
CREATION DATE: 18-May-1987 16:41:03

DESCRIPTION:

This module implements an avalanche diode photo detector. The input signal should be an optical power signal (Watts). Any small amount of negative power on this input will be ignored by the module (this may occur in an FFT filter, for example). Shot noise effects are simulated using an AVALANCE PHOTODIODE RAN_GEN module.. The output current is in units of microamps.

REVISIONS:

Author : SYSADMIN
Date : 6-Jun-1987 1:50:40
Description:

Module RECOMPILED by CONVERTER.

Author : SYSADMIN
Date : 18-May-1987 16:41:03
Description:

Module RECOMPILED by CONVERTER.

INPUT SIGNALS:

OPTICAL POWER IN — Type: REAL
Lower Limit: -1.7e38
Upper Limit: 1.7e38

The incident optical power in watts.

OUTPUT SIGNALS:

OUTPUT CURRENT — Type: REAL
Lower Limit: 0.0
Upper Limit: 1.7e38

The avalanche photo diode output current in MICROAMPS.

PARAMETERS:

APD INITIAL SEED — Type: INTEGER
Lower Limit: 1

Upper Limit: 2147483647

Initial seed for random number generator. Should be a large odd integer.

AVG APD GAIN Type: REAL
Lower Limit: 3.0e-39
Upper Limit: 1.7e38

The gain of the apd (average number of total charge carriers for each primary charge carrier).

APD "K" PARAMETER Type: REAL
Lower Limit: 0
Upper Limit: 0.99999

The apd "k" parameter (ionization ratio).

DARK CURRENT (NANOAMPS) Type: REAL
Lower Limit: 0.0
Upper Limit: 1.7e38

The PIN dark current in nanoamps.

QUANTUM EFFICIENCY Type: REAL
Lower Limit: 0.0
Upper Limit: 1.0

The quantum efficiency of the pin diode.

SOURCE CENTER WAVELENGTH Type: REAL
Lower Limit: 0.0
Upper Limit: 1.7e38

Center wavelength of the source in micrometers. This is used to determine the optical frequency.

MAX CDF PROBABILITY Type: REAL
Lower Limit: 0.8
Upper Limit: 0.999999

This parameter specifies the maximum probability used when generating the discrete cumulative distribution function. Ie, this is the maximum probability accumulated during the generation of the cdf (the probability is set to 1 at this point in the cdf). A typical number for this parameter is 0.9999. If this number is set too close to 1, the routine may never finish generating the cdf due to roundoff error, hence it is usually best not to exceed 0.9999.

CDF TABLE SIZE Type: INTEGER
Lower Limit: 1
Upper Limit: 5000

This parameter defines the number of elements in the cumulative distribution function (cdf) for the McIntyre (internal) random number gen. This number should be as large as the largest number in the internally generated cdf lookup table, up to a maximum of around 1000. Note: 1000 is always a reasonable value. So, if for example, the average apd gain is 10, an the "k" parameter is equal to .2, the largest number used in the cdf table is around 20 to get "max probability" equal to 0.9999. So a cdf table size of 20 would be large enough in this example. The largest number used in generating the cdf is read using the POST PROCESSOR VIEW PRINTED OUTPUT option. If the cdf table size is larger than necessary, the random number generator will be slower (because of the larger table to search).
For situations where the cdf table requires values >1000 or so, the size should be fixed at 1000, since the table will do a linear interpolation if necessary.

COMPUTED PARAMETERS:

ELECTRON CONST Type: REAL
Lower Limit: 0.0
Upper Limit: 1.7e38

Electron constant, computed.

DARK CONST Type: REAL
Lower Limit: 0.0
Upper Limit: 1.7e38

Dark constant, computed.

POWER CONST Type: REAL
Lower Limit: 0.0
Upper Limit: 1.7e38

Power constant, computed.

MODULES USED IN BLOCK DIAGRAM:

SELECT
>= REAL
ADDER
MULTIPLIER

CONST GEN
AVALANCHE PHOTODIODE RAN_GEN

INITIALIZATION CODE:

Subroutine: avalanche_photo_detector
Arguments:
QUANTUM EFFICIENCY
SOURCE CENTER WAVELENGTH
DARK CURRENT (NANOAMPS)
POWER CONST
DARK CONST
ELECTRON CONST

Description:

This routine calculates 3 constants: "power const", "dark const", and "electron const". "Power const" equals the product of "source center wavelength", "quantum efficiency", and "dt", divided by 1.989e-13. "Power const" converts the input optical power units to average number of charge carriers. "Dark const" is the number of dark charge carriers in delta t seconds. "Electron const" converts charge into current in microamps.

AVALANCHE PHOTO-DETECTOR

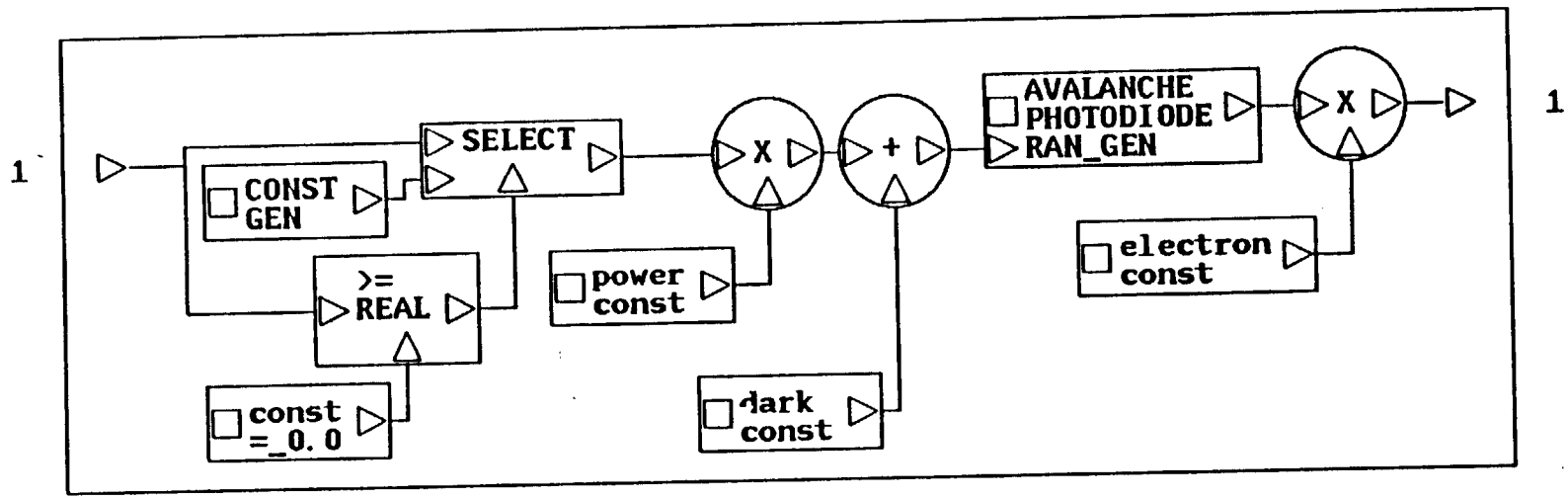

I# 1 OPTICAL POWER IN

O# 1 OUTPUT CURRENT

MODULE NAME: LASER (POWER SERIES)
GROUP: ANALOG MODULATORS
DATABASE: DUAO:[BOSS.ADD_DB.LIGHT]
AUTHOR: TOWNSEND
CREATION DATE: 26-Mar-1987 9:56:13

DESCRIPTION:

This module models the optical power output vs current input characteristic for a laser diode above threshold. The laser is represented by an AM-AM, memoryless non-linearity which is approximated by a fifth order polynomial. Laser diodes are biased for analog applications above the threshold (lasing region). The input current, output optical power, and slope of the characteristic (the output efficiency) at the bias point must be given. The coefficients of the remaining terms in the polynomial approximation may be entered directly (if "harm/coef" is .false.) or as the levels of the 2nd through 5th harmonics (if ""harm/coef" is .true.), measured relative to the fundamental with a test tone of peak magnitude "test tone magnitude".

The polynomial approximation assumes that the input current remains above the threshold current. If the input drops below this, the calculated output power may be <0. In this case, the output power is set to 0, since power output cannot be negative. In this case, the results will not be accurate for samples near or below threshold.

REVISIONS:

Author : SYSADMIN
Date : 6-Jun-1987 2:04:28
Description:

Module RECOMPILED by CONVERTER.

Author : SYSADMIN
Date : 26-Mar-1987 9:56:13
Description:

Module RECOMPILED by CONVERTER.

INPUT SIGNALS:

INPUT CURRENT Type: REAL
Lower Limit: 0.0
Upper Limit: 1.7e38

Laser input current. Should always be greater than the

threshold current.

OUTPUT SIGNALS:

OPTICAL PWR OUT Type: REAL
Lower Limit: 0.0
Upper Limit: 1.7e38

Laser optical power output.

PARAMETERS:

HARM/COEF Type: LOGICAL
Lower Limit: NIL
Upper Limit: NIL

When this logical parameter is .true., the values of parameters "XXX harmonic level" are interpreted as harmonic levels. When .false., they are interpreted as coefficents of the 5th order polynomial (efficiency is the first order term).

TEST TONE MAGNITUDE Type: REAL
Lower Limit: 3.0e-39
Upper Limit: 1.7e38

Peak magnitude of sinusoidal input current for which the harmonic levels were determined.
This parameter value is not used if "harm/coef" is .false.

5TH HARMONIC LEVEL Type: REAL
Lower Limit: -1.7e38
Upper Limit: 1.7e38

Level of fifth harmonic (in dB) relative to the fundamental. If the parameter "harm/coef" is .false., this parameter is the coefficient of the fifth order term in the polynomial.

4TH HARMONIC LEVEL Type: REAL
Lower Limit: -1.7e38
Upper Limit: 1.7e38

Level of fourth harmonic (in dB) relative to the fundamental. If the parameter "harm/coef" is .false., this parameter is the coefficient of the fourth order term in the polynomial.

3RD HARMONIC LEVEL Type: REAL
Lower Limit: -1.7e38

Upper Limit: 1.7e38

Level of third harmonic (in dB) relative to the fundamental. If the parameter "harm/coef" is .false., this parameter is the coefficient of the cubed term in the polynomial.

2ND HARMONIC LEVEL Type: REAL
Lower Limit: -1.7e38
Upper Limit: 1.7e38

Level of second harmonic (in dB) relative to the fundamental.
If the parameter "harm/coef" is .false., this parameter is the coefficient of the squared term in the polynomial.

EFFICIENCY Type: REAL
Lower Limit: 3.0e-39
Upper Limit: 1.7e38

Slope of the output power vs input current characteristic at the bias point. The units of this parameter must correspond to the units of the output power/input current.

BIAS POWER Type: REAL
Lower Limit: 3.0e-39
Upper Limit: 1.7e38

Power output at bias point (corresponding current specified by the parameter "bias current"). Units should be same as the output power signal.

BIAS CURRENT Type: REAL
Lower Limit: 3.0e-39
Upper Limit: 1.7e38

The units of this parameter should be the same as the input current, and the parameter "test tone magnitude".

COMPUTED PARAMETERS:

A2 Type: REAL
Lower Limit: -1.7e38
Upper Limit: 1.7e38

Computed.

A3 Type: REAL
Lower Limit: -1.7e38
Upper Limit: 1.7e38

Computed.

A4 Type: REAL
Lower Limit: -1.7e38
Upper Limit: 1.7e38

Computed.

A5 Type: REAL
Lower Limit: -1.7e38
Upper Limit: 1.7e38

Computed.

MODULES USED IN BLOCK DIAGRAM:

SUBTRACTOR
GAIN
MULTIPLIER
ADDER
>= REAL
CONST GEN
SELECT

INITIALIZATION CODE:

Subroutine: laser_pwr_series
Arguments:
EFFICIENCY
2ND HARMONIC LEVEL
3RD HARMONIC LEVEL
4TH HARMONIC LEVEL
5TH HARMONIC LEVEL
TEST TONE MAGNITUDE
HARM/COEF
BIAS POWER
A2
A3
A4
A5

Description:

This subroutine calculates the coefficients of the second through fifth order terms of the polynomial approximation of the power output vs current input characteristic of the laser diode. These values are determined from the levels of the 2nd through 5th harmonics (relative to the fundamental), the magnitude of the test tone, the output efficiency (ie, slope of the characteristic at the

bias point). If "harm/coef" is .false., then the entered harmonic level parameters are used as the polynomial coefficients.

LASER (POWER SERIES)

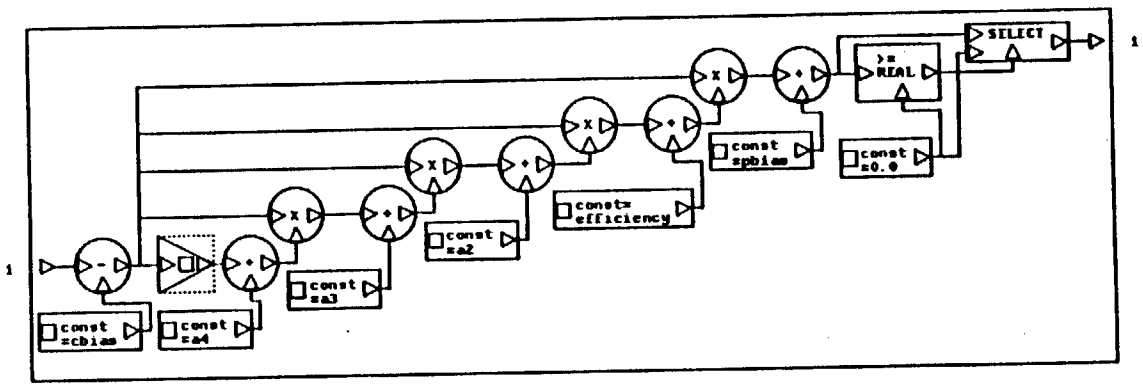

I# 1 INPUT CURRENT

O# 1 OPTICAL PWR OUT

MODULE NAME: OOK OPTICAL SOURCE
GROUP: DIGITAL SOURCES
DATABASE: DUA0:[BOSS.ADD_DB.LIGHT]
AUTHOR: TOWNSEND
CREATION DATE: 3-Mar-1987 8:01:29

DESCRIPTION:

This module outputs an on-off keyed signal used to drive a lightwave fiber module. The user specifies the on level via the value of parameter "avg optical power", which is in units of decibel milliwatts.
The logical transmitted bitstream is also output for useage in an error estimator module.

REVISIONS:

Author : SYSADMIN
Date : 4-Jun-1987 17:43:54
Description:

Module RECOMPILED by CONVERTER.

Author : SYSADMIN
Date : 3-Mar-1987 8:01:29
Description:

Module RECOMPILED by CONVERTER.

INPUT SIGNALS: (none)

OUTPUT SIGNALS:

TRANSMITTED BITSTREAM Type: LOGICAL
Lower Limit: NIL
Upper Limit: NIL

The (logical) transmitted bitstream.

OPTICAL OUTPUT Type: REAL
Lower Limit: 0.0
Upper Limit: 1.7e38

Signal representing the optical power out of a digital lightwave source (for use with the SINGLE MODE FIBER (LINEAR) module).

PARAMETERS:

AVG OPTICAL POWER Type: REAL

Lower Limit: -300
Upper Limit: 300

The average optical power in decibel milliwatts.

BIT RATE Type: REAL
Lower Limit: 3.0e-39
Upper Limit: 1.7e38

Bit rate in Hertz.

ISEED Type: INTEGER
Lower Limit: 1
Upper Limit: 2147483647

Initial seed for the uniform random number generator. Should be a large odd integer.

COMPUTED PARAMETERS:

ON LEVEL Type: REAL
Lower Limit: 0.0
Upper Limit: 1.7e38

Computed by init code, the optical power for the on state.

MODULES USED IN BLOCK DIAGRAM:

RANDOM DATA
LOGICAL TO NUMERIC

INITIALIZATION CODE:

Subroutine: ook_optical_source
Arguments:
AVG OPTICAL POWER
ON LEVEL

Description:

This routine reads in the average optical power in decibel milliwatts, and outputs the on level necessary to produce this amount of optical power.

OOK OPTICAL SOURCE

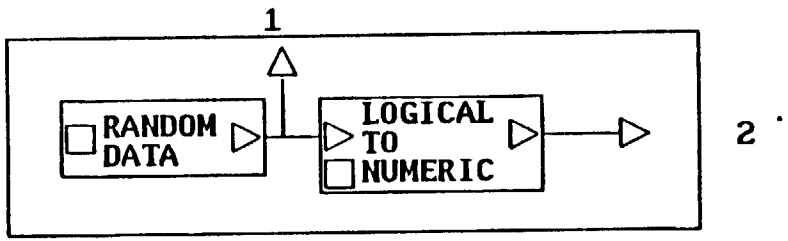

O# 1 TRANSMITTED BITSTREAM
O# 2 OPTICAL OUTPUT

MODULE NAME: OOK_ERROR RATE ESTIMATOR
GROUP: ESTIMATORS
DATABASE: DUA0:[BOSS.ADD_DB.LIGHT]
AUTHOR: TOWNSEND
CREATION DATE: 6-Mar-1987 8:21:22

DESCRIPTION:

This module uses the combined analytic-simulation technique for estimating the probability of error for On-Off Keyed (OOK) systems. This module is used in conjunction with the NOISE BW IMPULSE INJECT (REAL) module, which is used during calibration.
During calibration time, the module calculates the equivalent noise bandwidth of the linear portion of system, estimates the number of samples of delay between the transmitted and received signals. (These numbers are printed out for viewing in the post processor (VIEW PRINTED OUTPUT)).
The simulation stop time must be greater than or equal to est_stop, where est_stop is given by the following formula:

```
est_stop = caltime + 3*nbwdur + (nsseq + 2*maxdel)*dt
                + symtime*(numsym+1)
```

where:

```
caltime = "calibration start time"
nbwdur  = "noise bw calc duration"
nsseq   = "# samples in corr subseq"
maxdel  = "max delay to calculate"
dt      = simulation dt
symtime = the symbol time in seconds
numsym  = "# symbols for error est"
```

This module also counts the number of bit errors which occured during simulation and outputs the number of errors vs normalized symbol time as a multi-dimensional plot in the post processor.
The module provides an additional independent axis for the multi-dimensional error rate plot. This is for use with the BOSS PARAMETER ITERATION option.
Also, this module outputs a signal which can be used to drive a TERMINATE SIMULATION module when a specified number of errors have been counted in the simulation for ALL samples in a bit interval. For further details refer to external documentation.

REVISIONS:

Author : KOMP
Date : 5-Jun-1987 17:17:11
Description:

Module RECOMPILED by CONVERTER.

Author : SYSADMIN
Date : 6-Mar-1987 8:21:22
Description:

Module RECOMPILED by CONVERTER.

INPUT SIGNALS:

TRANSMITTED BITSTREAM Type: LOGICAL
Lower Limit: NIL
Upper Limit: NIL

The (logical) transmitted bitstream input.

RECEIVED SIGNAL Type: REAL
Lower Limit: -1.7e38
Upper Limit: 1.7e38

The received (and degraded) on-off keyed signal.

OUTPUT SIGNALS:

TERMINATE SIMULATION Type: LOGICAL
Lower Limit: NIL
Upper Limit: NIL

This signal becomes .true. when all samples in the symbol have exceeded the user input "max # of errors". This signal is typically connected to a TERMINATE SIMULATION module.

PARAMETERS:

CALIBRATION START TIME Type: REAL
Lower Limit: 0.0
Upper Limit: 1.7e38

Start time (absolute) of error rate estimator calibration in seconds. Nothing is happening in the error estimator before this time.

NOISE BW CALC DURATION Type: REAL
Lower Limit: 0.0
Upper Limit: 1.7e38

Duration of the noise bandwidth calculation time interval in seconds.

OF SAMPLES IN CORR SUB SEQ Type: INTEGER
Lower Limit: 1
Upper Limit: 4096

This parameter specifies the number of samples used to perform the correlation between the 2 input data streams. The trade-off is accuracy of the delay estimate vs the amount of time needed to perform the correlation.

MAX DELAY TO CALCULATE Type: INTEGER
Lower Limit: 1
Upper Limit: 2147483647

The maximum delay which the module can calculate. (Units are in samples).

OF SYMBOLS FOR ERROR EST Type: INTEGER
Lower Limit: 1
Upper Limit: 2147483647

This is the number of symbols which are used in the actual calculation of the probability of error.

OF SAMPLES/SYMBOL Type: INTEGER
Lower Limit: 1
Upper Limit: 10000

The number of samples in a symbol interval.

THERMAL NOISE PSD Type: REAL
Lower Limit: 3.0e-39
Upper Limit: 1.7e38

The power spectral density (SINGLE SIDED) of the analytically handled thermal noise.

DECISION THRESHOLD Type: REAL
Lower Limit: 0.0
Upper Limit: 1.7e38

The decision threshold used to determine whether a 1 or zero was sent.

MINIMUM # OF ERRORS Type: REAL
Lower Limit: 0.0
Upper Limit: 1.7e38

The minimum number of errors which must occur in each sample of the symbol interval before the "terminate simulation" signal toggles .true.

PROB OF ERROR AXIS LABEL Type: CHARACTER
Lower Limit: 1
Upper Limit: 255

Label which will appear on the dependent axis of the plot. This parameter can also be thought of as the title of the plot, and must be unique for multiple instances of multi-dimensional plots in the same simulation.

INDEPENDENT AXIS #2 LABEL Type: CHARACTER
Lower Limit: 1
Upper Limit: 255

(If used) label which will appear on the independent axis of the multi-dimensional error rate plot corresponding to the independent axis #2 values. This parameter and the parameter "independent axis #2 value" provide an additional independent axis for the error rate plot in the post processor, and are typeically used with the BOSS PARAMETER ITERATION option. If not used, the parameter should be set to the default value *NOT USED*.

INDEPENDENT AXIS #2 VALUE Type: REAL
Lower Limit: -1.7e38
Upper Limit: 1.7e38

Value which will appear on the independent axis corresponding to the independent axis #2 label. The value entered for this parameter is ignored if the independent axis #2 label has the value *NOT USED*. This parameter and the parameter "independent axis #2 label" provide an additional independent axis for the error rate plot in the post processor, and are typically used with the BOSS PARAMETER ITERATION option.

COMPUTED PARAMETERS:
SIM STOP TIME Type: REAL
Lower Limit: 0.0
Upper Limit: 1.7e38

The simulation stop time (computed by init code).

DELAY EST START TIME Type: REAL
Lower Limit: 0.0
Upper Limit: 1.7e38

Absolute time (seconds) in which the estimation of delay begins.

NOISE BW START TIME Type: REAL
Lower Limit: 0.0
Upper Limit: 1.0e37

Time (seconds) in which noise bandwidth calculation begins. Computed by init code.

NOISE BW STOP TIME Type: REAL
Lower Limit: 0.0
Upper Limit: 1.0e37

Time (seconds) after which the noise bandwidth calculation ends. Computed by init code.

ERROR EST START TIME Type: REAL
Lower Limit: 0.0
Upper Limit: 1.7e38

Time (seconds) after which actual calculation of the probability of error begins. Computed by init code.

MODULES USED IN BLOCK DIAGRAM:

ERROR ENABLE & SYMBOL COUNTER
SYMBOL SAMPLE NUMBER
T >= T_ON & T <= T_OFF
NOISE_BW COMPUTE (REAL)
DELAY METER (REAL)
OOK PRINT
DELAY TX_SIG
SAMPLE & HOLD
NOT
PRINT SIGNAL
T >= T_ON
OR
LOGICAL TO NUMERIC
COUNT ERRORS & GENERATE STOP
OOK ERROR PROB CALCULATE

INITIALIZATION CODE:

Subroutine: ook_error_est
Arguments:
CALIBRATION START TIME
NOISE BW CALC DURATION
OF SAMPLES IN CORR SUB SEQ
MAX DELAY TO CALCULATE
OF SYMBOLS FOR ERROR EST
OF SAMPLES/SYMBOL

NOISE BW START TIME
NOISE BW STOP TIME
DELAY EST START TIME
ERROR EST START TIME
SIM STOP TIME

Description:

This is rather complicated. The routine computes the various times required by modules in the simulation from more user friendly parameters. Many of the parameters this routine calculates are written into the PRINTED DATA option in the post processor. Refer to external documentation for further details.

OOK_ERROR RATE ESTIMATOR

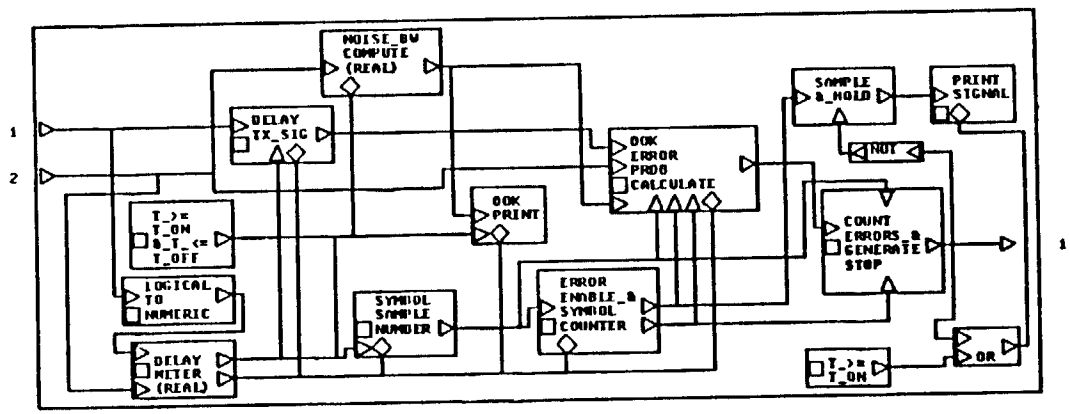

O# 1 TERMINATE SIMULATION

I# 1 TRANSMITTED BITSTREAM
I# 2 RECEIVED SIGNAL

MODULE NAME: PIN PHOTO-DETECTOR
GROUP: NOISE AND INTERFERENCE
DATABASE: DUA0:[BOSS.ADD_DB.LIGHT]
AUTHOR: TOWNSEND
CREATION DATE: 19-Feb-1987 14:17:40

DESCRIPTION:

This module implements a PIN diode photo detector. The input signal should be an optical power signal (Watts). Any small amount of negative power on this input will be ignored by the module (this may occur in an FFT filter, for example). Shot noise effects are simulated using a Poisson random number generator. The output current is in units of microamps.

REVISIONS:

Author : SYSADMIN
Date : 6-Jun-1987 1:53:33
Description:

Module RECOMPILED by CONVERTER.

Author : SYSADMIN
Date : 19-Feb-1987 14:17:40
Description:

Module RECOMPILED by CONVERTER.

INPUT SIGNALS:

OPTICAL POWER IN — Type: REAL
Lower Limit: -1.7e38
Upper Limit: 1.7e38

The incident optical power in watts.

OUTPUT SIGNALS:

OUTPUT CURRENT — Type: REAL
Lower Limit: 0.0
Upper Limit: 1.7e38

The pin diode output current in MICROAMPS.

PARAMETERS:

DARK CURRENT (NANOAMPS) — Type: REAL
Lower Limit: 0.0

Upper Limit: 1.7e38

The PIN dark current in nanoamps.

INITIAL SEED Type: INTEGER
Lower Limit: 1
Upper Limit: 2147483647

Initial seed for Poisson random number generator. Should be large and odd.

QUANTUM EFFICIENCY Type: REAL
Lower Limit: 0.0
Upper Limit: 1.0

The quantum efficiency of the pin diode.

SOURCE CENTER WAVELENGTH Type: REAL
Lower Limit: 0.0
Upper Limit: 1.7e38

Center wavelength of the source in micrometers. This is used to determine the optical frequency.

COMPUTED PARAMETERS:

ELECTRON CONST Type: REAL
Lower Limit: 0.0
Upper Limit: 1.7e38

Electron constant, computed.

DARK CONST Type: REAL
Lower Limit: 0.0
Upper Limit: 1.7e38

Dark constant, computed.

POWER CONST Type: REAL
Lower Limit: 0.0
Upper Limit: 1.7e38

Power constant, computed.

MODULES USED IN BLOCK DIAGRAM:

SELECT
>= REAL
ADDER
MULTIPLIER

CONST GEN
POISSON RAN_GEN

INITIALIZATION CODE:

Subroutine: pin_photo_detector
Arguments:
QUANTUM EFFICIENCY
SOURCE CENTER WAVELENGTH
DARK CURRENT (NANOAMPS)
POWER CONST
DARK CONST
ELECTRON CONST

Description:

This routine calculates 3 constants: "power const", "dark const", and "electron const". "Power const" equals the product of "source center wavelength", "quantum efficiency", and "dt", divided by 1.989e-13. "Power const" converts the input optical power units to average number of charge carriers. "Dark const" is the number of dark charge carriers in delta t seconds. "Electron const" converts charge into current in microamps.

PIN PHOTO-DETECTOR

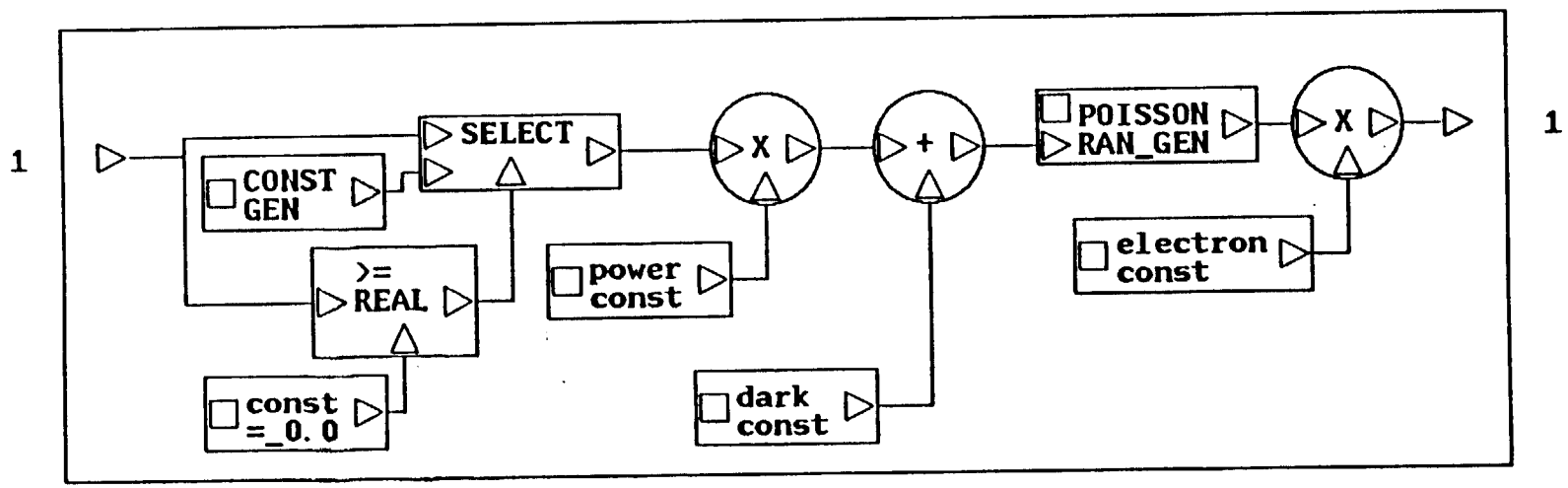

I# 1 OPTICAL POWER IN

O# 1 OUTPUT CURRENT

MODULE NAME: SINGLE MODE FIBER (LINEAR)
GROUP: CHANNELS *
DATABASE: DUAO:[BOSS.ADD_DB.LIGHT]
AUTHOR: TOWNSEND
CREATION DATE: 10-Feb-1987 10:33:43

DESCRIPTION:

This module implements one model of a single mode fiber. The initialization code reads in the parameters which describe the fiber and source characteristics, and generates from these the transfer function H(f) of the fiber. The init code then takes the inverse FFT of H(f), and truncates the insignificant portions from the resulting impulse response. This impulse response is written to a save file so that in subsequent runs it doesn't have to be recalculated (this is controlled by a parameter). The model is linear since it relys of FFT relationships.

The model is discussed in "IEEE Journal on Selected Areas in Communications", January 1984, VOL SAC-2, NO 1, on pages 171 thru 184, by Don G. Duff. The details of this model are to complicated to describe here, please refer to external documentation for a more complete description of this module.

REVISIONS:

Author : SYSADMIN
Date : 4-Jun-1987 17:44:54
Description:

Module RECOMPILED by CONVERTER.

Author : SYSADMIN
Date : 10-Feb-1987 10:33:43
Description:

Module RECOMPILED by CONVERTER.

INPUT SIGNALS:

INPUT — Type: REAL
Lower Limit: 0.0
Upper Limit: 1.7e38

Fiber input signal. This signal is proportional to the optical power of the fiber input.

OUTPUT SIGNALS:

OUTPUT Type: REAL
Lower Limit: 0.0
Upper Limit: 1.7e38

Fiber output signal (optical power signal).

PARAMETERS:

DISPERSION ADJUSTMENT CONSTANT Type: REAL
Lower Limit: 3.0e-39
Upper Limit: 1.7e38

When the internal closed form approximation for dispersion is used, this constant is multiplied by the dispersion function. A typical value is 0.0412.

RMS SOURCE SPECTRAL WIDTH Type: REAL
Lower Limit: 3.0e-39
Upper Limit: 1.7e38

The rms source spectral envelope width (standard deviation) of the closed form internal Gaussian approximation to source spectral envelope. This parameter is ignored if tabular source spectral envelope is used. Units are micrometers.

SOURCE CENTER WAVELENGTH Type: REAL
Lower Limit: 3.0e-39
Upper Limit: 1.7e38

The center wavelength of the source (micrometers). This parameter is used only when the closed form Gaussian approximation to the source spectral envelope is used. The parameter is ignored in all other cases.

ZERO DISPERSION WAVELENGTH Type: REAL
Lower Limit: 3.0e-39
Upper Limit: 1.7e38

The fiber zero dispersion wavelength (micrometers). This value is used only when the "mode of operation" is set to require closed form internal approximation of dispersion, and is otherwise ignored.

GROUP DELAY POINT (DELAY) Type: REAL
Lower Limit: -1.7e38
Upper Limit: 1.7e38

The group delay value (picoseconds/Kilometer) for the point which the tabular group delay finction is forced to pass

thru. (This function is obtained by integrating the tabular dispersion). This value is not used if the internal closed form function for dispersion is used. In this case, the group delay equals zero at the zero dispersion wavelength.

GROUP DELAY POINT (WAVELENGTH) Type: REAL
Lower Limit: 3.0e-39
Upper Limit: 1.7e38

The wavelength value (micrometers) for the point which the tabular group delay function is forced to pass thru. (This function is obtained by integrating the tabular dispersion). This value is not used if the internal closed form function for dispersion is used. In this case, the delay is zero at the zero dispersion wavelength.
form function for dispersion is used.

FIBER LENGTH Type: REAL
Lower Limit: 0.0
Upper Limit: 1.7e38

The length of the fiber in Kilometers.

OF POINTS IN FIBER H(F) Type: INTEGER
Lower Limit: 2
Upper Limit: 10000

The number of points in the fiber transfer function. This number sets the resolution of the transfer function and specifies the number of times that the integration over wavelength is performed. Must be EVEN.

OF PARTITIONS FOR INTEGRATION Type: INTEGER
Lower Limit: 4
Upper Limit: 10000

The number of partitions used in the Simpson's rule numerical integration over wavelength. There are several considerations in choosing this number. First, it must be an EVEN number. The larger this number, the more accurate the integration but the longer it will take to generate the fiber impulse response. Also, if this number is no chosen large enough, the integrand will not be sampled often enough and errors due to undersampling will result. Many times these errors will show up as a transfer function with many large bumps (it won't look anything like a Gaussian shaped spectrum).

INTEGRATION UPPER LIMIT Type: REAL

Lower Limit: 3.0e-39
Upper Limit: 1.7e38

Upper limit of integration which generates a sample of the fiber transfer function. Units are in micrometers. See external documentation for further info.

INTEGRATION LOWER LIMIT Type: REAL
Lower Limit: 3.0e-39
Upper Limit: 1.7e38

Lower limit of integration which generates one sample of the fiber transfer function. The units of this value are micrometers (this integration is with respect to wavelength). See external documentation for further info.

FIBER H(T) SAVE FILENAME Type: NEW-FILE
Lower Limit: NIL
Upper Limit: NIL

Filename of file containing the impulse response of the fiber. A new version of this file is written out each time the parameter "recalculate fiber h(t)" is .true. When this parameter is set to .false., the module READS the impulse response from this file.

This file is required because calculation of the fiber impulse response can require a reletively large amount of cpu time. This file allows the user to generate an impulse response for a given set of fiber parameters, then for subsequent simulation runs, read from this file (assuming the fiber parameters are not changed in these subsequent runs).

DISPERSION FILENAME Type: OLD-FILE
Lower Limit: NIL
Upper Limit: NIL

Filename of file containing a tabular specification of fiber dispersion (picoseconds/kilometer/micrometer) vs wavelength (micrometers). This file must be in the BOSS preferred file format. Data from this file is only used if the mode is either CLOTAB or TABTAB, but a valid old filename must be entered in any case. This function must span the range of integration specified by the parameters "integration lower limit" and "integration upper limit".

The antiderivitive of this function is calculated to get the group delay function for the fiber. This group delay function is then raised to the power e and multiplied by the fiber length in kilometers.

The resulting group delay function is required to pass

thru the point specified by the parameters "group delay point (wavelength)" and "group delay point (delay)" (this evaluates the constant of integration).
The maximum number of entries is 10,000.

SOURCE SPECTRAL ENVELOPE FILENAME Type: OLD-FILE
Lower Limit: NIL
Upper Limit: NIL

Filename of file containing the tabular specification of source spectral envelope vs wavelength (micrometers). For the overall gain to be correct, the source spectral envelope function MUST be normalized so that the area under this function equals unity. The BOSS preferred file format must be used, and wavelength values must be in the first column, with source spectral envelope values in the second. This function does not have to span the range of integration specified by the parameters "integration lower limit" and "integration upper limit", but the function will be assumed to be zero outside the values given. Since this function is a factor in the integrand, it should approach zero within the range of integration.
This file is not required if the mode is either CLOCLO or CLOTAB, BUT a valid old filename must still be entered in any case (the fiber loss filename could be used in these cases).
The maximum number of entries is 10,000.

FIBER LOSS FILENAME Type: OLD-FILE
Lower Limit: NIL
Upper Limit: NIL

Name of file containing the tabular values of fiber loss (dB/Kilometer) vs wavelength (micrometers). (Note that the loss is 1/gain).The file MUST be in the BOSS prefered file format, with wavelength in the first column and loss in the second column. This file is required in ALL modes of operation. The minimum and maximum values of wavelength MUST span the range of integration specified by the parameters "integration lower limit" and "integration upper limit".
The maximum number of entries is 10,000.

RECALCULATE FIBER H(T) Type: LOGICAL
Lower Limit: NIL
Upper Limit: NIL

If this logical variable is .true., the current parameter values are used to recalculate a new fiber impulse response and write it to the save file. If .false., the

impulse response is read from the save file. This parameter is needed because the calculation of the fiber impulse response takes a long time (up to 1 cpu hour). So the first time a simulation is run with new parameter values, this parameter should be set to .true. For all subsequent runs using the same parameters, the value should be .false. THEREFORE, THIS PARAMETER SHOULD BE EXPORTED TO THE HIGHEST (SIMULATION) LEVEL!

MODE OF OPERATION Type: CHARACTER
Lower Limit: 1
Upper Limit: 6

This parameter specifies how the module will compute the fiber impulse response. There are 4 legal character entries (case INsensitive):

cloclo - Closed form internal approximation for source spectral envelope and dispersion.
clotab - Closed form internal approximation for source spectral envelope and tabular dispersion data supplied from a file.
tabclo - Tabular source spectral envelope data from a file and closed form internal approximation for dispersion.
tabtab - Both source spectral envelope AND dispersion are supplied as tabular inputs from 2 separate files.

For further information about the tabular data files or the approximations see the respective help info.

COMPUTED PARAMETERS:

TAP GAIN Type: REAL
Lower Limit: -1.7e38
Upper Limit: 1.7e38
Vector Length: (# OF TAPS)

Tap gain for this cell.

OF TAPS Type: INTEGER
Lower Limit: 1
Upper Limit: 4096

The number of taps in the fiber impulse response. (Computed by initialization code).

MODULES USED IN BLOCK DIAGRAM:

TAPPED DELAY LINE CELL (REAL)
SINK
CONST GEN

INITIALIZATION CODE:

Subroutine: single_mode_fiber
Arguments:
- MODE OF OPERATION
- RECALCULATE FIBER H(T)
- FIBER LOSS FILENAME
- SOURCE SPECTRAL ENVELOPE FILENAME
- DISPERSION FILENAME
- FIBER H(T) SAVE FILENAME
- INTEGRATION LOWER LIMIT
- INTEGRATION UPPER LIMIT
- # OF PARTITIONS FOR INTEGRATION
- # OF POINTS IN FIBER H(F)
- ZERO DISPERSION WAVELENGTH
- FIBER LENGTH
- SOURCE CENTER WAVELENGTH
- RMS SOURCE SPECTRAL WIDTH
- DISPERSION ADJUSTMENT CONSTANT
- GROUP DELAY POINT (DELAY)
- GROUP DELAY POINT (WAVELENGTH)
- # OF TAPS
- TAP GAIN

Description:

Most of the work in this module is performed here. The routine reads in all parameters required to calculate the fiber impulse response. Description of the module describes this routine, so we will not be redundant here.

SINGLE MODE FIBER (LINEAR)

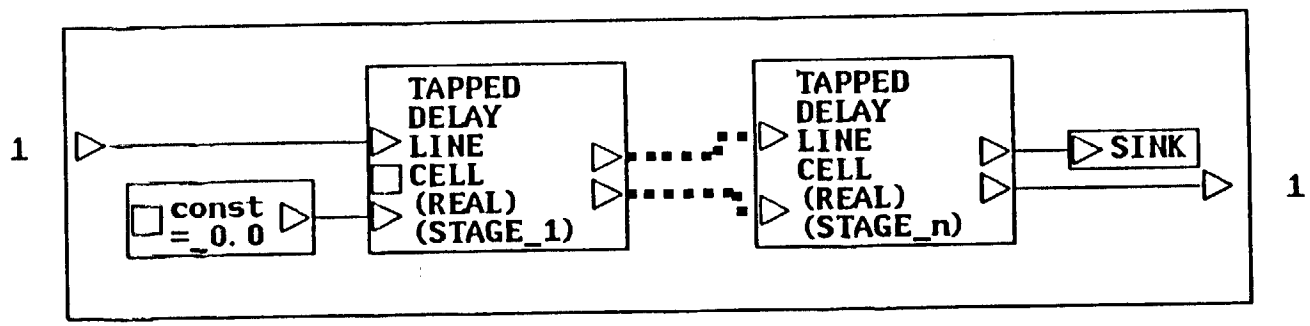

I# 1 INPUT

O# 1 OUTPUT

APPENDIX A

Literature Review - Models for Optical Sources

LASER DIODE MODELS

Fiber optic system sources and detectors are generally composed of direct bandgap semiconductor materials such as Gallium Arsenic which have an energy gap approximately equal to the energy in a photon of light of the desired wavelength. In photodetectors, most received photons cause ionization of a lattice atom creating a hole-electron pair (which can then create more hole-electron pairs in an avalanche photodiode). In optical sources, a forward biased junction is used to inject minority carriers, which create photons when they recombine.

Optical sources are of two types; light emitting diodes (LED's) and laser diodes. In LED's, recombination of injected minority carriers causes emission of light with a relatively broad wavelength range. The optical power emitted is approximately proportional to the LED current, but relatively little power may be coupled into an optical fiber. Also, the frequency response of LED's limit the frequencies at which they can be modulated.

Laser diodes have a better frequency response and can be modulated at frequencies up to several gigahertz, and more power can be coupled into a fiber over a narrower wavelength range. These properties make lasers preferable to LED's for applications which require high power or high frequency modulation.

However, lasers also have disadvantages, one of which is their nonlinearity. At low input currents, laser diodes act essentially as LED's, producing light by spontaneous emission. When the current is increased to a value called the threshold current, stimulated emission (lasing) begins and causes the power output to increase much faster with increasing current than it did below threshold. In stimulated emission, a photon striking a lattice atom in the active region can either be absorbed in ionizing the atom, or can cause a photon of the same wavelength to be released. Conditions are created so that the latter occurs more frequently, so that the light is amplified. Reflecting facets are placed at the ends of the active region so that light may continue to be amplified. It is this positive feedback which causes the power to be increased over that due to spontaneous emission. The initial photons to start this process come from spontaneous emission.

The power output versus current input curve (the laser's L-I characteristic) rises sharply above threshold due to the higher power output with stimulated emission than with spontaneous emission alone. This makes the laser diode an inherently nonlinear device, and therefore it is essential in analog applications that the laser remain above threshold for all values of the input. The laser is thus biased with a current which is about halfway between the threshold current and the highest laser current (in the middle of the lasing region). Because of the steepness of the L-I characteristic above threshold, the bias current is generally a small fraction above the threshold current. This makes temperature stability of the laser crucial, since the threshold current varies with temperature.

Since lasers are generally kept above threshold, it is the output in this region that it is most important to model. In this region, the slope of the L-I characteristic for all early and many current laser diodes exhibit prominent nonlinearities called "kinks," making them unsuitable for analog use. These kinks have several proposed explanations, such as the excitation of higher order transverse modes [1] (the active region of a laser diode is a resonant cavity). Newer lasers, such as narrow stripe lasers, have decreased the active region width so that these modes do not occur at normal current levels, and so these lasers can have a very linear characteristic above threshold. Third order intermodulation signals (the most important if signal frequencies are kept within an octave) can be as much as 60 to 80 dB below the fundamental [2], so for some lasers a linear model (requiring only the bias point and slope of the L-I characteristic at the bias point) may be fairly accurate.

If the L-I relationship is not considered to be linear, the most straightforward way to model it is as a polynomial

$$L = aI + bI^2 + cI^3 + \cdots$$

where L is the power output and I is the current input relative to their bias values. The coefficient of the I term (a) is the slope of the L-I characteristic at the bias point (the efficiency), and the other coefficients may be determined from measured harmonic magnitudes, along with the input currents for which they were measured.

Nonlinearities are also sometimes described by measured values of AM to AM and AM to PM characteristics, which indicate the effect of variations in the input signal amplitude on the output magnitude and phase, respectively. Measurements on some lasers have shown [3] that below resonance, most of the intermodulation terms are due to AM to AM characteristics, while at the laser's resonant frequency, AM to PM characteristics may become significant due to increased reflection noise.

There are many models based on the physics of laser diodes, some of which are reviewed by Buus [4]. Some of these [5, 6, 7] allow the calculation of points on the L-I characteristic, which can then be used directly, or to determine the coefficients of a polynomial approximation. However, these models require values of many laser parameters, many of which would not be accurately known, and they require iterative solution. Although these models agree fairly well with measured threshold currents and efficiencies, the degree to which they model the nonlinearity is unknown.

There is another source of nonlinearity which may be as significant as the nonlinearity of the L-I characteristic. Most laser diodes do not emit a single wavelength of light, but rather a narrow spectrum of discrete wavelengths. The active regions of many lasers (such as stripe geometry lasers) have one dimension (the length) which is much greater than the other two. The active region is a resonant cavity, and the output wavelengths correspond to different longitudinal modes (normally, only the lowest order transverse modes are permitted). The spacing between the output wavelengths thus depends on the cavity length, and the relative magnitudes depend on the spontaneous emission and the optical gain of the different wavelengths. The shape of the output spectrum is generally modeled as Gaussian or Lorentzian [8], but the center wavelength and width of the spectrum are both functions of the output power level.

The shift in the center wavelength, when combined with a fiber with dispersion (different wavelengths propagate at different speeds) give rise to harmonics for a sinusoidal input current, and thus is a source of nonlinearity [9, 10]. This shift in center frequency may be on the order of the spacing between modes (or less) and still give rise to a possibly significant effect [9]. Published spectra [6, 11, 12] sometimes show a greater shift than

this. The width of the output spectrum has been shown to be approximately inversely proportional to the output power, so that as the output power increases, the spectrum shifts to longer wavelengths and narrows [6].

The model of the laser output spectrum may also need to account for modal partition noise. Although for a given constant input current, the total power output is nearly constant, the power in each mode may vary greatly. If the light then travels through a dispersive fiber, different wavelengths will travel at different velocities, so the power reaching the receiver will vary with time. Since the partitioning is random, this will have the effect of producing noise (unlike the shift in wavelengths above, which occurs synchronously with modulation and appears as a nonlinearity). Given the center wavelength, modal spacing, a measure of the spectral width and the total output power, the time averaged spectrum can be calculated using a Gaussian or Lorentzian envelope. Then, a random component can be added to each mode since the exact partitioning of the output power is random. Since the total output power is nearly constant, the power in the different modes must be negatively correlated, and the covariance between modes can be approximated by [8]

$$C(i, j) = -K^2 A(i) A(j)$$

$$C(i, i) = K^2 A(i) [1 - A(i)]$$

where C(i, j) is the covariance between modes i and j, C(i, i) is the variance of the power in mode i, A(i) is the fraction of the total power in mode i, and K is a partition coefficient which has been measured and determined to be between 0.3 or 0.4 and 0.6 [8, 13].

So a complete model of the output spectrum would require that first the total output power be determined based on the input current and information about the L-I characteristic, and from this average power the spectral width and center wavelength could be calculated. From this and the mode spacing, the number of modes with significant power could be determined along with the wavelength and average power for each. Then, a random component with the above covariances could be added to each. Since modal partition noise is more of a problem when there are few modes, it may be reasonable to ignore this factor when there are many modes since the effect is reduced while the calculations required are increased.

This would be required for each sample of the input current, which may make the model impractical to use without further simplification. The complication is that the nonlinearity associated with the spectral shift and the modal partition noise are both effects due to both the laser source and dispersion in the optical fiber, so to model the laser alone so that when combined with any fiber model these effects will be observed seems to require calculating an output spectrum for each current level.

The discussion so far has assumed that the laser is memoryless, so that the output at any time depends only on the input at that time. The measured frequency response of laser diodes is generally flat a low frequencies, then has a resonant peak, after which the power output decreases with increasing frequency at 40 dB/decade[2]. As long as the modulation frequency is in the flat region of the frequency response (below the resonant frequency) this is a reasonable assumption. If it is modulated above this region, then the frequency response might be inserted as a filter placed after the input current but before the output power is calculated. However, the frequency response is often flat up to several gigahertz, and it is generally desirable to use the laser in this region, so the frequency response can probably be neglected most of the time.

REFERENCES

1. Shen, T. M., "Effects of TE-TM Kinks on the Performance of Semiconductor Lasers in Lightwave Communication Systems," Journal of Lightwave Technology, Vol. LT-4, No. 9, September 1986, pp. 1420-1424.

2. Channin, D. J., "Optoelectronic Performance Issues in Fiber-Optic Communications," RCA Review, Vol. 46, December 1985.

3. Way, W. I., and A. Afrashteh, "Linearity Characterization of Connectorized Laser Diodes Under Microwave Intensity Modulation by AM/AM and AM/PM Measurements," 1986 IEEE MTT-S International Microwave Symposium Digest, pp. 659-662.

4. Buus, J., "Principles of Semiconductor Laser Modelling," IEE Proceedings, Vol. 132, Pt. J., No. 1, February 1985, pp. 42-51.

5. Streifer, W. D., R. Scifres and R. D. Burnham, "Analysis of Diode Laser Properties," IEEE Journal of Quantum Electronics, Vol. QE-18, No. 11, November 1982, pp. 1918-1929.

6. Streifer, W. D., R. Scifres and R. D. Burnham, "Longitudinal Mode Spectra of Diode Lasers," Applied Physics Letters, Vol. 40, No. 4, February 15, 1982, pp. 305-307.

7. Streifer, W. D., R. Scifres and R. D. Burnham, "Analysis of Spontaneous Emission Effects on Spectra and L vs. I Characteristics of Diode Lasers," Japanese Journal of Applied Physics, Vol. 21, No. 5, May 1982, pp. L282-L284.

8. Laughton, A. K., "Mode Partition Noise in Gain-Guided Lasers and Its Effect on a Multimode Fibre-Optic System," IEE Proceedings, Vol. 132, Pt. J., No. 6, December 1985, pp. 359-363.

9. Lyons, P. B., S. D. Personick and G. A. Hayward, "Applications of Optical Fibers to Analog Telemetry Delay Lines and Sensing Systems," IEEE Journal on Selected Areas in Communications, Vol. SAC-1, No. 3, April 1983, pp. 555-561.

10. Personick, S. D., Fiber Optics, Plenum Press, 1985, pp. 123-125.

11. Wada, M., K. Hamada, T. Shibutani, H. Shimizu, M. Kums, K. Itoh, G. Kano and I. Teramoto, "A New Chemical Etching Technique for Formation of Cavity Facets of (GaAl) As Lasers," IEEE Journal of Quantum Electronics, Vol. QE-21, No. 6, June 1985, pp. 658-662.

12. Burkhard, H., and E. Kuphal, "Three- and Four-Layer LPE InGaAs(P) Mushroom Stripe Lasers for λ = 1.38, 1.54 and 1.66 μm," IEEE Journal of Quantum Electronics, Vol. QE-21, No. 6, June 1985, pp. 650-657.

13. Duff, D. G., "Computer-Aided Design of Digital Lightwave Systems," IEEE Journal on Selected Topics in Communications, Vol. SAC-2, No. 1, January 1984, pp.171-185.

BIBLIOGRAPHY

Multiple Topics

The following books and articles each discuss most of the important characteristics of laser diodes, such as their nonlinearity, frequency response, modal noise and mode partition noise. Duff also discusses modeling of many laser characteristics that show up in digital applications, such as turn-on and turn-off response, pattern dependence and oscillations (also discussed by Channin). The linearity of some current laser diodes are quite good (Channin) and the frequency response of some allows them to be modulated above 1 GHz.

1. Channin, D. J., "Optoelectronic Performance Issues in Fiber-Optic Communications, RCA Review, Fol. 46, December 1985.

2. Daly, J. C., (Ed.), Fiber Optics, CRC Press, 1984.

3. Duff, D. G., "Computer Aided Design of Digital Lightwave Systems," IEEE Journal on Selected Topics in Communications, Vol. SAC-2, No. 1, January 1984, pp. 171-185.

4. Gowar, J., Optical Communications Systems, Prentice-Hall International Series in Optoelectronics, 1984.

5. Personick, S. D., Fiber Optics, Plenum Press, 1985.

Quantum Physical Models

The following articles and books are concerned with modeling the physical operation of laser diodes. Buus is a review of the relevant equations used and of the various published models based on these. The articles by Streifer, Scifres and Burnham give a model which can be used to calculate the L-I characteristic of a laser diode given a number of its physical parameters. Many of these would be hard to determine, the model requires an iterative solution, and the results do not necessarily accurately describe the characteristics we are interested in. However, these articles also model the spectral width, which appears to be inversely proportional to the output power, which may be useful in modeling the output spectrum.

6. Buus, J., "Principles of Semiconductor Laser Modeling," IEE Proceedings, Vol. 142, Pt. J., No. 1, February 1985, pp. 42-51.

7. Streifer, W. D., R. Scifres and R. D. Burnham, "Analysis of Diode Laser Properties," IEEE Journal of Quantum Electronics, Vol. QE-18, No. 11, November 1982, pp. 1918-1929.

8. Streifer, W. D., R. Scifres and R. D. Burnham, "Longitudinal Mode Spectra of Diode Lasers," Applied Physics Letters, Vol. 40, No. 4, February 15, 1982, pp. 305-307.

9. Streifer, W. D., R. Scifres and R. D. Burnham, "Analysis of Spontaneous Emission Effects on Spectra and L vs. I Characteristics of Diode Lasers," Japanese Journal of Applied Physics, Vol. 21, No. 5, May 1982, pp. L282-L284.

10. Thompson, G. H. B., Physics of Semiconductor Laser Devices, Wiley, 1980.

Nonlinearity

These articles are concerned with the nonlinearities of laser diodes. Shen discusses the kinks found in the above threshold region of many laser diodes and the effects of these on digital communication systems. Way and Afrashteh measured the AM/AM and AM/PM characteristics of laser diodes for modulation frequencies above 1 GHz, and conclude that below the resonant frequency, the AM/AM characteristic is most important. Lyons, Personick and Hayward discuss a nonlinearity due to the variation of the center wavelength synchronously with modulation and dispersion in the optical fiber. This is also discussed in Reference 5 above.

11. Lyons, P. B., S. D. Personick, and G. A. Hayward, "Applications of Optical Fibers to Analog Telemetry Delay Lines and Sensing Systems," IEEE Journal on Selected Areas in Communications, Vol. SAC-1, No. 3, April 1983, pp. 555-561.

12. Shen, T. M., "Effects of TE-TM Kinks on the performance of Semiconductor Lasers in Lightwave Communication Systems," Journal of Lightwave Technology, Vol. LT-4, No. 9, September 1986, pp. 1420-1424.

13. Way, W. I., and A. Afrashteh, "Linearity Characterization of Connectorized Laser Diodes Under Microwave Intensity Modulation by AM/AM and AM/PM Measurements," 1986 IEEE MTT-S International Microwave Symposium Digest, pp. 659-662.

Some Published L-I Characteristics and Spectra

Although there seems to be little published quantitative data on the nonlinearity of laser diodes or on the magnitude of shift of the center wavelength described above, there are very many published L-I characteristics and output spectra at different power levels which show the shift in the center wavelength (and the narrowing described in an earlier section). Below are listed a few articles containing one or both of these types of data.

14. Burkhard, H., and E. Kuphal, "Three- and Four-Layer LPE InGaAs(P) Mushroom Stripe Lasers for λ = 1.38, 1.54 and 1.66 μm," IEEE Journal of Quantum Electronics, Vol. QE-21, No. 6, June 1985, pp. 650-657.

15. Dolginov, L. M., A. E. Drakin, P. G. Eliseer, B. N. Sverdlov and E. G. Shevchenko, "CW InGaAsP/InP Injection Lasers with Very Low Threshold Current Density at Room Temperature," IEEE Journal of Quantum Electronics, Vol. QE-21, No. 6, June 1985, pp. 646-649.

16. Dutta, N. D., R. B. Wilson, D. P. Wilt, P. Besoni, R. L. Brown, R. J. Nelson and R. W. Dixon, "Performance Comparison of InGaAsP Lasers Emitting at 1.3 μm and 1.55 μm for Lightwave Systems Applications," AT&T Technical Journal, Vol. 64, No. 8, October 1985, pp. 1857-1884.

17. Haupt, H. and O. Hildebrand, "Lasers and Photodetectors in Europe," IEEE Journal on Selected Areas in Communications, Vol. SAC-4, No. 4, July 1986, pp. 444-455.

18. Wada, M., K. Hamada, H. Shimizu, M. Kume, F. Tajiri, K. Itoh and G. Kano, "High Power Lasers of the Twin-Ridge-Substrate Type," IEE Proceedings, Vol. 132, Pt. J.. No. 1, February 1985, pp. 3-8.

Noise

The power output of a laser diode is almost constant for a constant current input, but there can be significant noise due to two mechanisms. One is reflections, in which the laser's output characteristic changes when light is reflected back into the laser, which is discussed in Garvey and Quinn, and which would probably be difficult to model since it depends on the connections outside the laser source. The other type of noise is mode partition noise, which is caused by random variations in the power output of each mode (wavelength) which causes noise when passed through a dispersive fiber. To model this and the nonlinearity associated with the wavelength shift, it would probably be necessary to model the output spectrum. Laughton discusses the

characteristics of partition noise, and the shape of the output spectrum (approximated by a Gaussian or Lorentzian envelope).

19. Garvey, M. J. and S. W. Quinn, "Sources of Intensity Noise in Wideband UHF Analog Optical Communications Systems: Their Elimination and Reduction," Journal of Lightwave Technology, Vol. LT-4, No. 9, September 1986, pp. 1285-1293.

20. Laughton, A. K., "Mode Partition Noise in Gain-Guided Lasers and its Effect on a Multimode Fiber-Optic System," IEE Proceedings, Vol. 132, Pt. J., No. 6, December 1985, pp. 359-363.

APPENDIX B

Simulation of Digital lightwave Communication Links

SIMULATION OF DIGITAL LIGHTWAVE COMMUNICATION LINKS USING SYSTID

K. Sam Shanmugan, Ed E. Komp, J. Keith Townsend
ST*AR Corporation and University of Kansas
Lawrence, Kansas 66044

Aly E. Elrefaie, Malcolm B. Romeiser
Bell Communications Research
Red Bank, New Jersey 07701-7020

ABSTRACT

Because of the presence of intersymbol interference and non-Gaussian noise sources, the evaluation of the performance of digital lightwave communication links is difficult. Direct Monte Carlo type simulations are impractical because of the long run times required to estimate low bit error rates. In this paper, techniques that combine analysis and simulation in modeling and implementing the functional blocks of a single-mode lightwave system using the SYSTID simulation package are discussed. A simulation example is presented which illustrates the capabilities of the semi-analytic approach to digital single-mode lightwave system analysis.

I. INTRODUCTION

The rapid pace in the research and development of improved and economical fiber cable, devices, and systems technology has resulted in large-scale deployment of lightwave communication systems. Early lightwave communication systems utilized multimode fibers which allowed only limited information bandwidth and repeater spacing [1]. As technology advanced, emphasis shifted away from multi-mode lightwave systems, in favor of the higher bandwidths and lower losses available with single-mode systems. This growth has increased the range of potential applications and led to lightwave systems being used more and more in highly competitive commercial applications. As a result, lightwave systems engineers require more detailed information on the possible tradeoffs available when designing or deploying a system. Analytical methods alone are becoming insufficient because of many necessary simplifying assumptions. The lightwave system designer is often forced to evaluate design alternatives by constructing prototypes; an approach which can be costly - especially in a research or early design phase.

In a recent paper [2], Duff presented models and analysis methods for computer-aided design of digital lightwave systems. Duff's approach was based primarily on analytical approximations to compute performance measures such as error rates, eye diagrams, and power penalties. In contrast, the approach presented here is based on detailed simulation models for functional blocks in lightwave communication links. Computer simulation of digital lightwave systems is an alternative to both hardware evaluation and pure analytical methods of analysis. An important advantage of computer simulation is the flexibility available to the designer. Simulation packages such as SYSTID [3] offer the user the capability to study the effects various parameters have on total link performance via bit error rate (BER) estimates, eye diagrams, spectral plots, time plots, etc. In general, computer simulation involves performing a series of transformations on a data structure (i.e., a signal) and analyzing the effects of these transformations using the performance measures mentioned above. The transformations are between and within the time and frequency domains, and model the behavior of cascaded or single components in the system being simulated.

Three important approaches to computer simulation are as follows: a) direct or brute-force Monte Carlo simulation, b) modified Monte Carlo simulation (importance sampling), and c) semi-analytic Monte Carlo simulation. Digital lightwave systems of interest typically operate with bit error probabilities from 10^{-6} to 10^{-9}. For the brute-force Monte Carlo approach to be accurate, a large number of errors must be observed which at these low error rates require on the order of several million simulated bits. Generating and processing this number of bits requires too much computer time to be practical. Importance sampling and semi-analytic approaches reduce the number of bits simulated to a more reasonable value.

Modeling lightwave system functional blocks and using these in a semi-analytic simulation framework are discussed in this paper. Lightwave systems are ideally suited for the semi-analytic approach. The effects of intersymbol interference (ISI) introduced by the optical source and the fiber, in addition to the quantum noise introduced by the photodetector are simulated. Thermal noise (assumed to be white Gaussian) enters the simulation only in the receiver which is downstream of any non-linearities introduced by the optical source or photodetector. Hence the effects of thermal noise are handled analytically. Typically, short PN sequences (on the order of hundreds of bits) can be used to evaluate the effects of the non-Gaussian degradations, which greatly reduce the computer time required as compared to the brute-force approach.

The contents of this paper are divided into

four sections. Section II is a brief discussion of the SYSTID simulation package. Section III presents the models for the lightwave functional blocks considered here. Discussed in this section are the single-mode optical fiber models featuring versions which allow tabular input of fiber parameters, and a choice between time domain or frequency domain signal processing. A PIN diode model and two BER estimator models are also discussed.

Section IV presents an example lightwave system simulation which illustrates the capabilities of SYSTID as a tool for lightwave systems analysis. Results from more detailed simulation studies are presented in [4]. The simulated system is a single-mode 140 Mb/s, 1.28 μm LED link with a fiber length of 15 Km. Waveform plots are shown at various points throughout the system, along with a plot of probability of bit error versus received optical power. Concluding remarks are presented in Section V.

II. THE SYSTID SIMULATION PACKAGE

The SYSTID simulation package (developed originally by the Hughes Aircraft Corporation) is a powerful tool for analyzing and designing communication systems [3]. SYSTID features a flexible topology format with an input language which corresponds closely to system level block diagrams. This minimizes the amount of time a user spends translating the block diagram of the system under analysis into the simulation source program. Although the user can easily construct new blocks, the SYSTID Model Library contains many commonly used functional blocks such as signal generators, filters, modems, and source encoders. Results of simulations are analyzed using the SYSTID postprocessor RIP. RIP is menu-driven with a large number of commands available such as spectral plots, time plots, eye diagrams, histograms, correlation, covariance and others. To decrease the amount of time a user spends answering questions in a given menu, standard default values are provided when possible.

The structure of SYSTID makes it easy for the user to construct and use models which require tabular data input. This feature was used in the single-mode fiber models to allow laboratory hardware measurements to be used in simulating the fiber, as discussed in Section III.

III. MODELING FUNCTIONAL BLOCKS IN A LIGHTWAVE COMMUNICATIONS LINK

Optical Sources

Depending upon the application, optical sources under consideration for lightwave communication systems are either semiconductor light emitting diodes (LED) or laser diodes [5, 6]. Both types of optical sources tend to degrade the input bit stream, although incoherent LEDs are more well behaved (and therefore easier to model) than semi-coherent laser sources. Lasers, however, are capable of providing higher values of launched optical power and are widely used in long distance single-mode fiber systems. LEDs are finding increasing application with single-mode fibers for the shorter distance distribution plant [7].

The spectrum of the optical source plays an important role in determining the effects of dispersion on a single-mode fiber communication system. When using one of the four single-mode fiber models discussed below, the user can either input an arbitrary source spectral density curve in tabular form, or supply the needed parameters to specify a built-in Gaussian approximation to the source spectrum. If the source spectrum were very narrow, it could be approximated as an impulse and the effects of the single-mode fiber could be handled analytically. This is not a realistic assumption, however, and simulation techniques are required to evaluate the effects of a non-ideal source spectrum on system performance.

Single-Mode Fiber

The baseband transfer function of a single-mode fiber can be modeled by the following equation [8]:

$$H(f) = \int_{-\infty}^{\infty} S(\lambda)L(\lambda)e^{-j\omega LT(\lambda)}d\lambda \qquad (1)$$

where

ω = $2\pi f$
L = fiber length
$S(\lambda)$ = optical source spectrum vs wavelength
$L(\lambda)$ = 1/(fiber loss) vs wavelength
$T(\lambda)$ = fiber group delay vs wavelength

The two major physical characteristics which influence the performance of the single-mode fiber are fiber loss and chromatic dispersion. In eq. (1), $L(\lambda)$ is the reciprocal of loss (gain) as a function of wavelength. The fiber group delay term, $T(\lambda)$, is actually the antiderivative of the dispersion characteristic. The degrading effects of chromatic dispersion are related to the spectral purity of the optical source. Real optical sources contain a distribution of energy around the source center wavelength λ_s. An optical source with a broad spectrum of optical energy results in a narrowing of the information bandwidth of the fiber. This can be easily noted from eq. (1) if we approximate $L(\lambda)$ by a constant, and $T(\lambda)$ by a linear function of λ. Now the source spectrum $S(\lambda)$ and the fiber transfer function $H(f)$ can be visualized as Fourier transform pairs (except for a scale constant). Hence, a broad $S(\lambda)$ versus λ corresponds to a narrow $H(f)$ versus f, and vice versa.

If the optical source spectrum is narrow enough to be approximated by an impulse, the fiber transfer function is given by

$$H(f) = L(\lambda_s)\, e^{-j\omega LT(\lambda_s)} \qquad (2)$$

which results in a delayed and attenuated version of the input signal. Although this case is not interesting in itself, this approach was used to verify the fiber models implemented in SYSTID.

The source spectrum can sometimes be approx-

imated by a Gaussian as follows [2, 8],

$$S(\lambda) = \frac{1}{\sigma_s\sqrt{2\pi}} \exp\left(-\frac{(\lambda - \lambda_s)^2}{2\,\sigma_s^2}\right) \qquad (3)$$

where

σ_s = rms spectral width

λ_s = source center wavelength

Chromatic dispersion for silica fibers is sometimes approximated by [2, 8],

$$\frac{dT(\lambda)}{d\lambda} = (s/c)\left(\frac{\lambda - \lambda_0}{\lambda^2}\right) \qquad (4)$$

where

s = a unitless constant

c = speed of light

λ_0 = zero-dispersion wavelength

The group delay is then

$$T(\lambda) = (s/c)\left[\ln\left(\frac{\lambda}{\lambda_0}\right) + \frac{\lambda_0 - \lambda}{\lambda}\right] \qquad (5)$$

These closed-form approximations to the source spectrum and chromatic dispersion are not adequate when it is desired to simulate a single-mode fiber and optical source which have characteristics that deviate drastically from those in eqs. (3) and (5). In addition, no reasonable closed-form expression exists for fiber loss. Hence, some means for arbitrary entry of the various functions is required for a single-mode fiber model to be general enough to handle arbitrary dispersion, loss and source spectrum characteristics.

Four different models of the single-mode fiber have been implemented in SYSTID. All four models use eq. (1) to calculate the fiber transfer function. Two of the models use frequency domain signal processing methods, while the other two perform signal processing in the time domain via the convolution sum. One of the frequency and one of the time domain models use the closed form approximations to the source spectrum and chromatic dispersion curves given in eqs. (3) and (4) respectively. The other set of models allows the user to input either the source spectrum or dispersion, (or both) as tabular functions. The advantage of using the "closed-form" models is that they are easier to use and require less computer time to calculate the transfer function. All models require fiber loss data to be input in tabular form.

The integral in eq. (1) is implemented using Simpson's rule. Euler's identity is used to break the integrand into real and imaginary parts yielding

$$H(f) = \int_{-\infty}^{\infty} S(\lambda)L(\lambda)\cos(\omega LT(\lambda))d\lambda - j\int_{-\infty}^{\infty} S(\lambda)L(\lambda)\sin(\omega LT(\lambda))d\lambda \qquad (6)$$

To save computer time when calculating H(f), the values of $S(\lambda)\cdot L(\lambda)$ and $2\cdot\pi\cdot L\cdot T(\lambda)$ are calculated during the first integration (i.e., the first value of baseband frequency, f) and stored in arrays for future integrations. The upper and lower limits of integration are parameters to the model, and are chosen to include the significant non-zero values of $S(\lambda)$. One additional constraint on the function $S(\lambda)$ is that $\int S(\lambda)d\lambda = 1$, otherwise the attenuation of the fiber will be incorrectly biased.

It is important to use sufficient resolution in the discrete integration to provide an accurate approximation to the continuous integration. It was found that if the resolution of the integrations in eq. (6) was inadequate, the fiber transfer function at higher frequencies would be incorrect. It was determined that double precision arithmetic is required to eliminate roundoff errors which occur under some circumstances. Double precision is only required when calculating the fiber transfer function and not when performing the signal processing, so the speed penalty for using double precision arithmetic is not proportional to the number of samples processed by the simulation.

To help reduce the amount of computer time required during execution of a lightwave simulation, all four fiber models can be configured to either write the calculated transfer function to a save file, or read from this save file. This feature is useful when it is desirable to hold the single-mode fiber parameters constant and study the effects of varying parameters of other models in the simulation.

The group delay function, $T(\lambda)$ is obtained as follows. The antiderivative of the user-input tabular dispersion data is automatically calculated yielding group delay plus an arbitrary constant versus wavelength. Next, the arbitrary constant of integration is evaluated by biasing the group delay function to force it to pass through a user-specified point. There is no restriction on what type of function the user specifies for dispersion, loss, or source spectral density, as long as adequate resolution is used.

The calculated transfer function of the single-mode fiber is used directly in the two models which perform the signal processing in the frequency domain. The FFT of the fiber input signal is multiplied by the transfer function and the inverse FFT of the result is calculated. To preserve a modular program structure, these frequency domain signal processing operations are performed by a SYSTID library model. Use of frequency domain signal processing requires the input signal to be periodic, and introduces an artificial delay equal to the size of the FFT. This approach offers the advantage of very fast execution time when compared to the time domain convolution approach.

The two models which use time domain signal processing implement the discrete convolution sum using a tapped delay line algorithm. In these models the calculated transfer function is inverse transformed to obtain the sampled impulse response of the single-mode fiber. Each sample of the impulse response is a tap gain in the

tapped delay line. It is not uncommon to have on the order of 2000 points to accurately characterize the impulse response. Hence, this method is slower than the FFT approach but has the advantages of neither requiring periodic data nor introducing an artificial delay.

PIN Diode Photodetector

The PIN diode photodetector is a semiconductor device that produces an electrical current which is approximately proportional to the incident optical power and is a potential source of degradation in a lightwave communication system link. In practical PIN receivers the effects of quantum or shot noise are overshadowed by the thermal noise of succeeding receiver stages. In this analysis, however, quantum noise has been added because of the need to eventually model an APD receiver, where the photodetector noise becomes more important.

The number of charge carriers (electron-hole pairs) in a PIN diode can be modeled mathematically as a Poisson process, with a mean (and variance) proportional to the incident optical power [2, 9]. The average number of charge carriers N generated in a time Δt is given by

$$\overline{N} = \frac{\eta}{h\nu} P_{inc}(t) \cdot \Delta t + n_d \cdot \Delta t \qquad (8)$$

where

$P_{inc}(t)$ = incident optical power
η = quantum efficiency
h = Plank's constant
ν = optical frequency
n_d = number of dark charge carriers/ second

The probability that exactly k electron-hole pairs is generated in a time Δt can be written as

$$P(n = k) = \frac{(\overline{N})^k (e)^{-\overline{N}}}{k!} \qquad (9)$$

which is simply the Poisson probability mass function. The PIN diode output current is proportional to the number of carriers, and is given by

$$i(t) = \frac{c_e n}{\Delta t} \qquad (10)$$

where

c_e = the charge of an electron
n = the number of charge carriers generated in Δt seconds

Implementation of the mathematical model of the PIN detector shot noise in SYSTID is relatively straight-forward. The majority of the programming effort was involved in generating the Poisson random numbers, and providing the parameters necessary to allow the user some flexibility in controlling the trade-off between simulation run-time and accuracy.

Several methods for generating the Poisson random numbers are available, but the model we implemented utilizes the fact that in a Poisson process the interarrival time between events is exponentially distributed. The mean of the interarrival time random variable is equal to the reciprocal of the mean of the Poisson process (for an observation time interval equal to unity). For each sample in the simulation, the PIN diode model produces the Poisson distributed random number using the above relationship. If the average number of carriers, $\overline{N}$, given in eq. (8) is large, then a Gaussian random number is generated with mean and variance equal to $\overline{N}$. This is an extremely good approximation for $\overline{N}$ larger than 50, and requires much less computer time.

Bit Error Estimator Models

There are currently two bit error rate (BER) estimation models implemented in SYSTID which are designed for lightwave communication system simulation. Both employ the semi-analytic approach to reduce the amount of simulation time required to obtain accurate estimates of link BER. The primary difference between the two is that one assumes thermal noise (additive white Gaussian) is added at a single point in the receiver, while the other model assumes two different thermal noise sources.

It was necessary to modify a BER estimator model which already existed in SYSTID library so that it could be used with the on-off keying modulation scheme used in lightwave systems. These models automatically calculate the noise equivalent bandwidth of the portion of the system which lies downstream of the point where thermal noise enters the system. This is accomplished by injecting an impulse into this portion of the system (which is assumed linear) and summing the magnitude squared of the impulse response. The signal power at the point where noise enters the system is also measured and input to the BER estimator model.

The BER estimator models measure the distance from the received sample to the threshold, and calculate the probability of error for the values of signal power to noise power ratio requested by the user. This calculation is repeated for the corresponding sample in each bit, and the results averaged. For example, if there are 16 samples per bit then there are 16 different average error probabilities calculated. If sampling were assumed to occur at the optimum instant during each bit interval, the overall BER would be the minimum of the 16 (for example) different BER estimates. Because it is not always reasonable to assume that the receiver timing recovery is accurate enough to provide optimum sampling, the BER models discussed here provide the user with tables of the probability of error estimate for each of the samples in the bit interval, making it easier to evaluate the effects of timing errors on system performance.

IV. LIGHTWAVE SYSTEM SIMULATION EXAMPLE

To help demonstrate the capabilities of computer simulation of lightwave communication systems, a simple SYSTID simulation example is

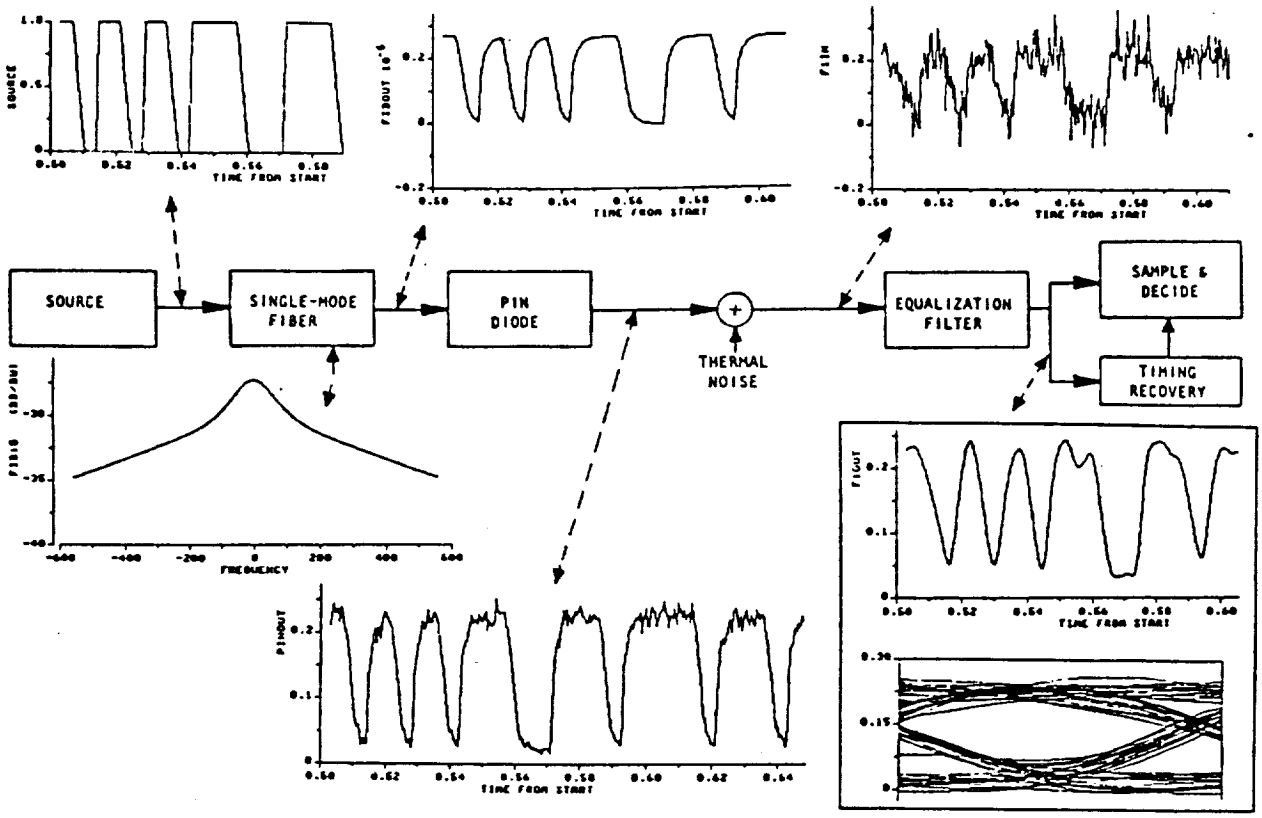

Figure 1. Digitial lightwave communications system block diagram with waveforms generated by SYSTID. Shown are time plots of source output, fiber output, PIN diode output, equalization filter input (including thermal noise), and equalization filter output; equalization filter output eye diagram; and fiber transfer function magnitude (MHz). The received optical power is -40 dBm.

presented which employs the lightwave models previously discussed (LED source, single-mode fiber, PIN photodiode, BER estimator). The example is not intended to show any new advances in lightwave system technology. The purpose of the example is to demonstrate the potential usefulness of simulation in analyzing lightwave systems.

Figure 1 shows a digital lightwave communications system block diagram with RIP postprocessor plots of the signals at various points. In Figure 1, the actual thermal noise samples are generated and shown for illustration. In the actual semi-analytic simulation, the effects of thermal noise are determined analytically - no thermal noise samples are generated, and the sample and decide block is replaced with a BER estimator model.

The information source is modeled using an NRZ PN sequence generator, which in these examples produces 128 bit PN sequences with 16 samples per bit. The bit rate is 140 Mb/s. The PN generator selected for this example allows the user to specify the rise and fall times independently, and is therefore useful for modeling the fact that most optical sources have turn-on and turn-off characteristics which are not equal. The Gaussian approximation to the optical source spectral density curve is used in the example. The source operates with a center wavelength of 1.28 micrometers and an RMS spectral width of 30 nanometers.

The single-mode fiber in the example simulation uses the dispersion curve given in eq. (5), with a zero-dispersion wavelength equal to 1.31 micrometers. A tabular fiber loss function was used with a fiber loss of approximately 0.5 dB/Km at 1.31 micrometers. The single-mode fiber model also includes optical source power level scaling, which in this example corresponds to a launched optical power of -28 dBm. Four thousand subintervals were used in the discrete implementation of the integral in eq. (1) to evaluate the fiber transfer function. The resulting transfer function was calculated over the entire simulation bandwidth (-1120 to +1120 MHz) and contained 2240 frequency samples.

The remainder of the functional blocks in the example simulation model the various mechanisms of a lightwave receiver. The number of dark charge carriers generated by the PIN diode photodetector was set equal to 1.34×10^{11} carriers/second (21 nanoamperes). The PIN diode photodetector represents the only non-linearity in the lightwave communications link.

Thermal noise enters the receiver in the circuitry following the PIN diode as shown in

Figure 1. When using the semi-analytic simulation approach in SYSTID, the ENBSIG model is inserted into the simulation at the point where the Gaussian noise enters the system. For the BER estimates to be correct, the portion of the system from the ENBSIG model to the end of the signal path must be linear. This turns out to be a very realistic assumption - this section of actual lightwave receivers is always linear. For purposes of illustration, the third order, 100 MHz Butterworth filter is used to simulate the equalization filter in a lightwave system receiver. However, a variety of SYSTID library models are available to simulate the equalization filter.

To keep the example simple, a single thermal noise source was used. Inputs to the BER estimator model include the receiver filter output signal, the input bitstream, the decision threshold value, and the thermal noise power spectral density. For each value of received optical power, the BER estimator model produces a table which lists probability of error versus S/N for each of the 16 samples in a simulation bit. The table includes probability of error estimates for each sample in the bit interval so that the effects of non-optimum sampling due to timing errors can be evaluated.

A plot of probability of bit error versus received optical power is given for this example simulation in Figure 2. The plot in Figure 2 assumes ideal sampling.

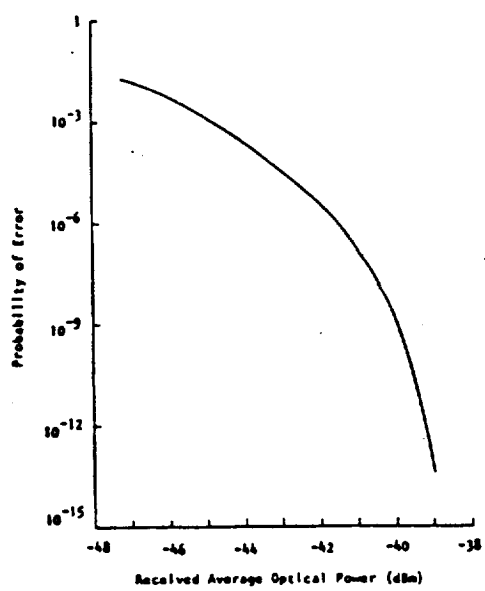

Figure 2. Probibility of bit error vs received average optical power for the SYSTID example.

V. CONCLUSIONS

Techniques for modeling lightwave system functional blocks in SYSTID have been presented, along with examples of their usage in an end-to-end lightwave system simulation. Flexible-topology simulation packages such as SYSTID can be used to analyze different types of communications links (i.e., satellite and lightwave). Future trends in simulation package design are leading toward combining this flexibility with more user-friendly graphics editing capabilities.

REFERENCES

[1] T. Li, "Advances in optical fiber communications: An historical perspective," IEEE Journal on Selected Areas in Communications, Vol. SAC-1, No. 3, April 1983.

[2] D. G. Duff, "Computer-aided design of digital lightwave systems," IEEE Journal on Selected Areas in Communications, Vol. SAC-2, No. 1, pp. 171-185, January 1984.

[3] M. Fashano, A. L. Strodtbeck, "Communication systems simulation and analysis with SYSTID," i.b.i.d., pp. 8-28, January 1984.

[4] A. Elrefaie et al., "Lightwave systems simulation in the time and frequency domain," Manuscript in preparation.

[5] A. A. Bergh, J. A. Copeland, "Optical sources for fiber transmission systems," Proceedings of the IEEE, pp. 1240-1247, October 1980.

[6] E. E. Basch, T. G. Brown, "Introduction to coherent optical fiber transmission," IEEE Communications Magazine, Vol. 23, No. 5, pp. 23-30, May 1985.

[7] P. W. Shumate, J. L. Gimlett, M. Stern, M. B. Romeiser, N. K. Cheung, "Transmission of 140 Mbit/s signals over single-mode fiber using surface and edge emitting 1.3 μm LED's," Electronics Letters, pp. 522-524, June 6, 1985.

[8] A. E. Elrefaie, "Computer simulation of single-mode fiber transmission characteristics," Submitted to Electronics Letters.

[9] R. G. Smith, "Photodetectors for fiber transmission systems," Proceedings of the IEEE, pp. 1247-1253, October 1980.